The Coseismicity and Morphology of the Acheron Rock Avalanche Deposit in the Red Hill Valley, New Zealand.

A thesis submitted in fulfillment of the requirements
for the degree of
Master of Science in Engineering Geology
at the University of Canterbury
by

Guyon Matthew Smith

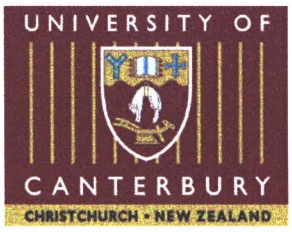

Department of Geological Sciences
University of Canterbury, Christchurch, New Zealand

September 2003

THE RED HILL VALLEY

A view of the Red Hill valley looking north toward the source of the Acheron rock avalanche (identifiable by the grey scree covered peak facing eastward in the centre of the picture). The trail of morning mist conveniently traces the position of the Porters Pass Fault as it crosses westward beneath the rock avalanche deposit.

ABSTRACT

The Acheron rock avalanche is located in the Red Hill valley almost 80 km west of Christchurch and is one of 42 greywacke-derived rock avalanches identified in the central Southern Alps. It overlies the Holocene active Porters Pass Fault; a component of the Porters Pass-Amberley Fault Zone which extends from the Rakaia River to beyond the Waimakariri River. The Porters Pass Fault is a dextral strike-slip fault system viewed as a series of discontinuous fault scarps. The location of the fault trace beneath the deposit suggests it may represent a possible source of seismic shaking resulting in the formation of the Acheron rock avalanche.

The rock mass composition of the rock avalanche source scar is Torlesse Supergroup greywacke consisting of massive sandstone and thinly bedded mudstone sequences dipping steeply north into the centre of the source basin. A stability analysis identified potential instability along shallow north dipping planar defects, and steep south dipping toppling failure planes. The interaction of the defects with bedding is considered to have formed conditions for potential instability most likely triggered by a seismic event.

The depositional area of the rock avalanche covers 7.2×10^5 m^2 with an estimated volume of 9×10^6 m^3. The mobilised rock mass volume was calculated at 7.5×10^6 m^3. Run out of the debris from the top of the source scar to the distal limit reached 3500m, descending over a vertical fall of almost 700m with an estimated *Fahrböschung* of 0.2. The run out of the rock avalanche displayed moderate to high mobility, travelling at an estimated maximum velocity of 140-160 km/hour. The rapid emplacement of the deposit is confirmed by highly fragmented internal composition and burial of forest vegetation

New radiocarbon ages from buried wood retrieved from the base of Acheron rock avalanche deposit represents an emplacement age closely post-dating (Wk 12094) 1152 ± 51 years B.P. This differs significantly from a previous radiocarbon age of (NZ547) 500 ± 69 years B.P. and modal lichenometry and weathering-rind thickness ages of approximately 460 ± 10 yrs and 490 ± 50 years B.P. The new age shows no resemblance to an earthquake event around 700-500 years B.P. on the Porters Pass-Amberley Fault Zone.

The DAN run out simulation using a friction model rheology successfully replicated the long run out and velocity of the Acheron rock avalanche using a friction angle of 27° and high earth pressure coefficients of 5.5, 5.2, and 5.9. The elevated earth pressure coefficients represent dispersive pressures derived from dynamic fragmentation of the debris within the mobile rock avalanche, supporting the hypothesis of Davies and McSaveney (2002). The DAN model has potential applications for areas prone to large-scale instability in the elevated slopes and steep waterways of the Southern Alps.

A paleoseismic investigation of a newly identified scarp of the Porters Pass Fault partially buried by the rock avalanche was conducted to identify any evidence of a coseismic relationship to the Acheron rock avalanche. This identified three-four fault traces striking at 078°, and a sag pond displaying a sequence of overbank deposits containing two buried soils

representing an earthquake event horizon. A 40cm vertical offset of the ponded sediment and lower buried soil horizon was recorded, which was dated to (Wk 13112 charcoal in palosol) 653 ± 54 years B.P. and (Wk 13034 palosol) 661 ± 34 years B.P. The evidence indicates a fault rupture occurred along the Porters Pass Fault, west of Porters Pass most likely extending to the Red Lakes terraces, post-dating 700 years B.P., resulting in 40cm of vertical displacement and an unknown component of dextral strike slip movement. This event post-dates the event one (1000 ± 100 years B.P) at Porters Pass previously considered to represent the most recent rupture along the fault line.

This points to a probable source for resetting of the modal weathering-rind thicknesses and lichen size populations in the Red Hill valley and possibly the Red Lakes terraces. These results suggest careful consideration must be given to the geomorphic and paleoseismic history of a specific site when applying surface dating techniques and furthermore the origin of dates used in literature and their useful range should be verified.

An event at 700-500 years B.P did not trigger the Acheron rock avalanche as previously assumed supporting Howard's conclusions. The lack of similar aged rupture evidence in either of the Porters Pass and Coleridge trenches supports Howard's hypothesis of segmentation of the Porters Pass Fault; where rupture occurs along one fault segment but not along another.

The new rock avalanche age closely post-dating 1200-1100 years B.P. resembles the poorly constrained event one rupture age of 1700-800 years B.P for the Porters Pass Fault and the tighter constrained Round Top event of 1010 ± 50 years B.P. on the Alpine Fault. Eight other rock avalanche deposits spread across the central Southern Alps also resemble the new ages however are unable to be assigned specific earthquake events due to the large associated error bars of ± 270 years. This clustering of ages does represent compelling lines of evidence for large magnitude earthquake events occurring over the central Southern Alps.

The presence of a rock avalanche deposit does not signify an earthquake based on the historical evidence in the Southern Alps however clustering of ages does suggest that large Mw >7 earthquakes occurred across the Southern Alps between 1200-900 years BP.

Acknowledgments

This project has benefited immensely from the time and contributions of many people. I am especially grateful for the supervision of Dave Bell and Tim Davies, and invaluable assistance and enthusiasm from Mauri McSaveney, Jocelyn Campbell, David Nobes and Harry Jol. I am particularly appreciative of the Mason Trust for funding this project

To John Southward, Cathy Knight, Rob Spiers, Jane Guise and Julie-Ann Hale thank you for your help and good humour over the last years particularly with the no-warning requests for equipment and help.

I would also like to express thanks to Alan Hogg from Waikato Radiocarbon Laboratory. Richard Holdaway for the lessons on radiocarbon calibration, Matt Howard for freely sharing his figures and information on the Porters Pass Fault. Brooksdale Station Ltd for generous access to their land

Big thank you to Peter and Edith for their unwavering "ask no questions" policy and support over these last years.

Claire thanks for all your help and support at home and in the field

To Tim, Anekant and Tania who helped me in my hour(s) of need (sprint to the finish), thank you.

Finally at university you meet marvelous people James, Matt, Terry, Grim, Verne, Eric the Bird thanks for making it a fun place to be.

TABLE OF CONTENTS

CHAPTER 2. GEOLOGY AND GEOMORPHOLOGY OF THE RED HILL VALLEY

CHAPTER 3. THE MECHANISMS AND MORPHOLOGY OF ROCK AVALANCHES

CHAPTER 4. DESCRIPTION AND MORPHOMETRIC ANALYSIS OF THE ACHERON ROCK AVALANCHE

LIST OF FIGURES

CHAPTER 1

CHAPTER 2

CHAPTER 3

CHAPTER 4

CHAPTER 5

CHAPTER 6

ATTACHED MAPS (in pocket)

LIST OF TABLES

CHAPTER 2

CHAPTER 3

CHAPTER 4

CHAPTER ONE

INTRODUCTION

1.1. BACKGROUND TO STUDY

Rock avalanches are large gravity driven landslides which fail suddenly and begin to fragment, undergoing changes to the internal energy enabling the debris to travel extended distances at extremely high velocities. In New Zealand, the rock avalanche process is typically confined to granitic and gneissic rock of the western South Island and to low-grade metamorphosed sedimentary rocks of the central Southern Alps (Whitehouse, 1981). Greywacke sandstone and mudstone of the Torlesse Supergroup are the dominant rock type of the central Southern Alps and evidences of ancient large-scale slope failures are common (Whitehouse and Griffith, 1983). Whitehouse and Griffith (1983) identified 46 Holocene rock avalanche deposits between Mount Cook and Arthur's Pass, with volumes ranging from about 1 x 10^6 m^3 to 500 x 10^6 m^3. The presence of these large landslides represents enormous sources of sediment flux into the South Island's fluvial systems and it has been estimated that within the last 2000 years 19 large rock avalanches have moved 1, 000 x 10^6 m^3 of material (Whitehouse, 1983). The volume of debris displaced during a rock avalanche represents a significant hazard within the South Island of New Zealand.

The Acheron rock avalanche deposit is found in a small northwest to southeast trending vale called Red Hill valley approximately 82 km west of Christchurch off State Highway 73 (see Fig.1.1, Fig. 1.2). The Acheron deposit is one of the rock avalanches identified by Whitehouse and Griffith (1983) in the central Southern Alps, and extends 3.4 km in length (from the top of the source scar to its distal end) with a vertical fall of 700m (this study). The deposit volume of 7-10 x10^6 m^3 covers approximately 720 000m^2 (this study). The trigger for the failure is considered to be of seismic origin based on the tendency for large rock avalanches to occur during earthquakes. This is a trend worldwide and was recorded during the historical 1929 South Island Arthur's Pass earthquake forming the Falling Mountain deposit (Hancox et al. 1994).

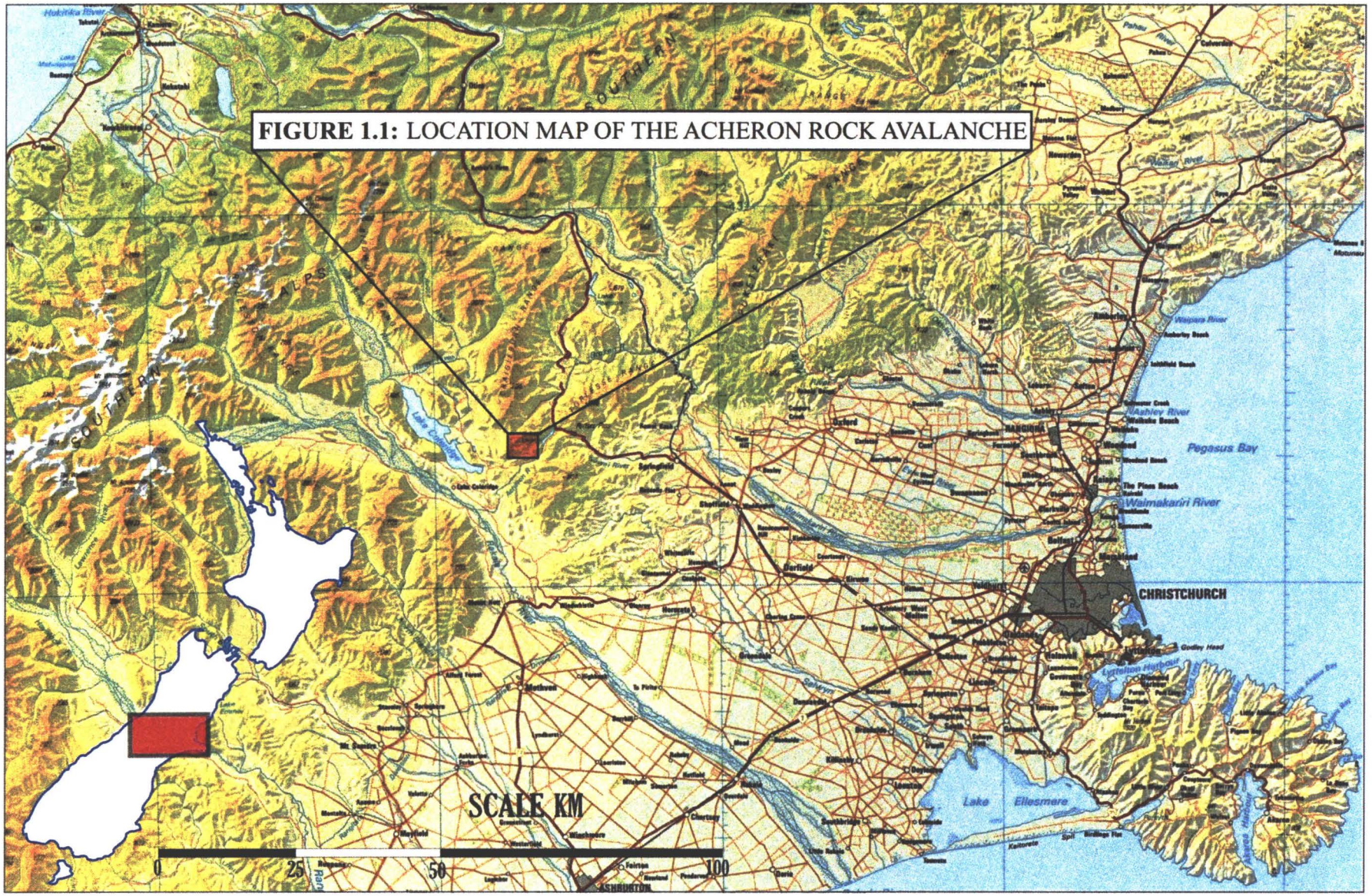

FIGURE 1.1: LOCATION MAP OF THE ACHERON ROCK AVALANCHE

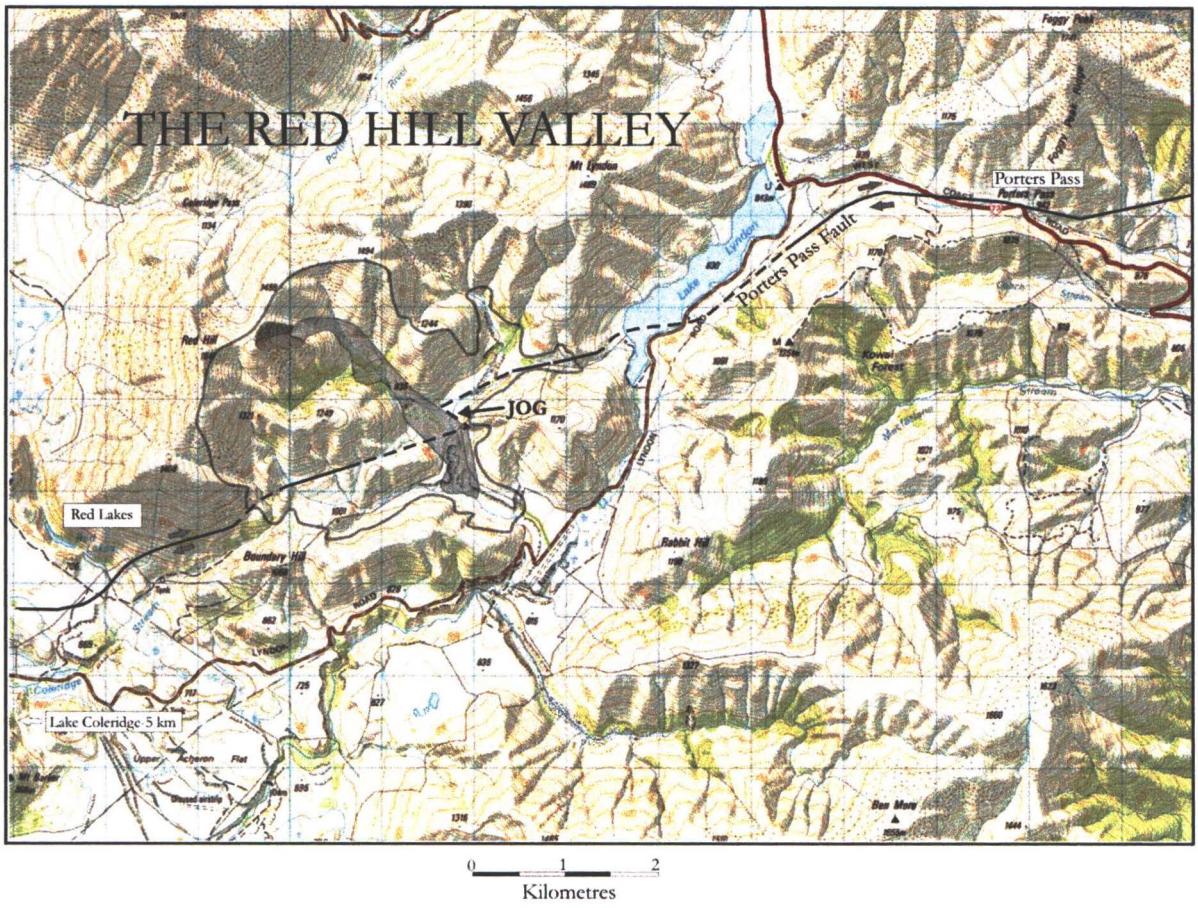

Figure 1.2: Map of the Red Hill valley study area (grey outline) showing the site of the Acheron rock avalanche deposit and source scar (shaded grey). The approximate position of the Porters Pass Fault (as defined in Howard, 2001) is shown as a discontinuous black line where the fault trace is identified and a dashed line where its path is inferred. The sense of displacement is right lateral or dextral strike slip with a small component of normal faulting. (1: 50 000 topographic map K35 Ed1 1989 rev 1998 NZMG)

The Acheron rock avalanche is found in close proximity to a series of thrust structures bounding the Castle Hill basin and an active zone of faulting called the Porters Pass-Amberley Fault Zone, and buries the Holocene active Porters Pass Fault trace (see Fig. 1.3) (Cowen, 1992; Cowan et al. 1996).

The Porters Pass–Amberley Fault Zone (here called PP-AFZ) is ca 100 km long northeast trending zone of deformation thought to be associated with the Marlborough Fault Zone (here called MFZ) (Fig. 1.3, Howard, 2001). The MFZ is the extensive fault zone which absorbs part of the stress of the converging Australian and Pacific plates in North Canterbury (Pettinga et al. 2001). The Porters Pass Fault a component of the PP-AFZ is defined by a ca 40-km discontinuous trace, however within the Red Hill valley the fault is not distinguishable though inferred to cross beneath the rock avalanche (Fig. 1.2, Howard, 2001). Howard (2001) has suggested that the fault strikes laterally across the valley in a northeast direction, forming a 700m jog in the valley centre (Fig. 1.2). The rock avalanche was considered to display no surface representation of the trace implying that it postdates the last rupture at this site (Howard, 2001).

Previous studies of the Acheron rock avalanche used a variety of dating techniques to assign an age of emplacement. These included lichenometry, radiocarbon ^{14}C dating, and two greywacke rock weathering-rind ages. Burrows (1975) obtained a single radiocarbon date from a buried wood sample which gave a conventional age of (NZ547) 500 ± 69 years B.P. The lichen study conducted by Bull (Bull and Brandon, 1996) looking for evidence of earthquakes on the Alpine Fault, used a polymodal distribution of maximum diameters of lichen, to produce an age of 460 ± 10 years B.P. for the surface of the Acheron deposit with minor lichen population extending back to around 1030 years B.P. (Bull and Brandon, 1996, 1998; Howard, 2001). Weathering–rind thickness measurements identified slightly differing modal peak thicknesses of 0.66mm from Whitehouse (1983) and 0.83mm from Howard (2001) of which represented an age of 490 ± 55 years B.P. The average of the combined ages from the different dating techniques equated to an age for the deposit of 464 ± 79 years B.P. (Howard, 2001; Bull and Brandon, 1996; Whitehouse, 1983; Burrows 1975). However based on radiocarbon dating presented later in this study, this appears too young.

Along the length of the PP-AFZ, Cowan et al. (1996) identified six landslides including the Acheron deposit dated between 700-500 years B.P (based on ages from earlier studies

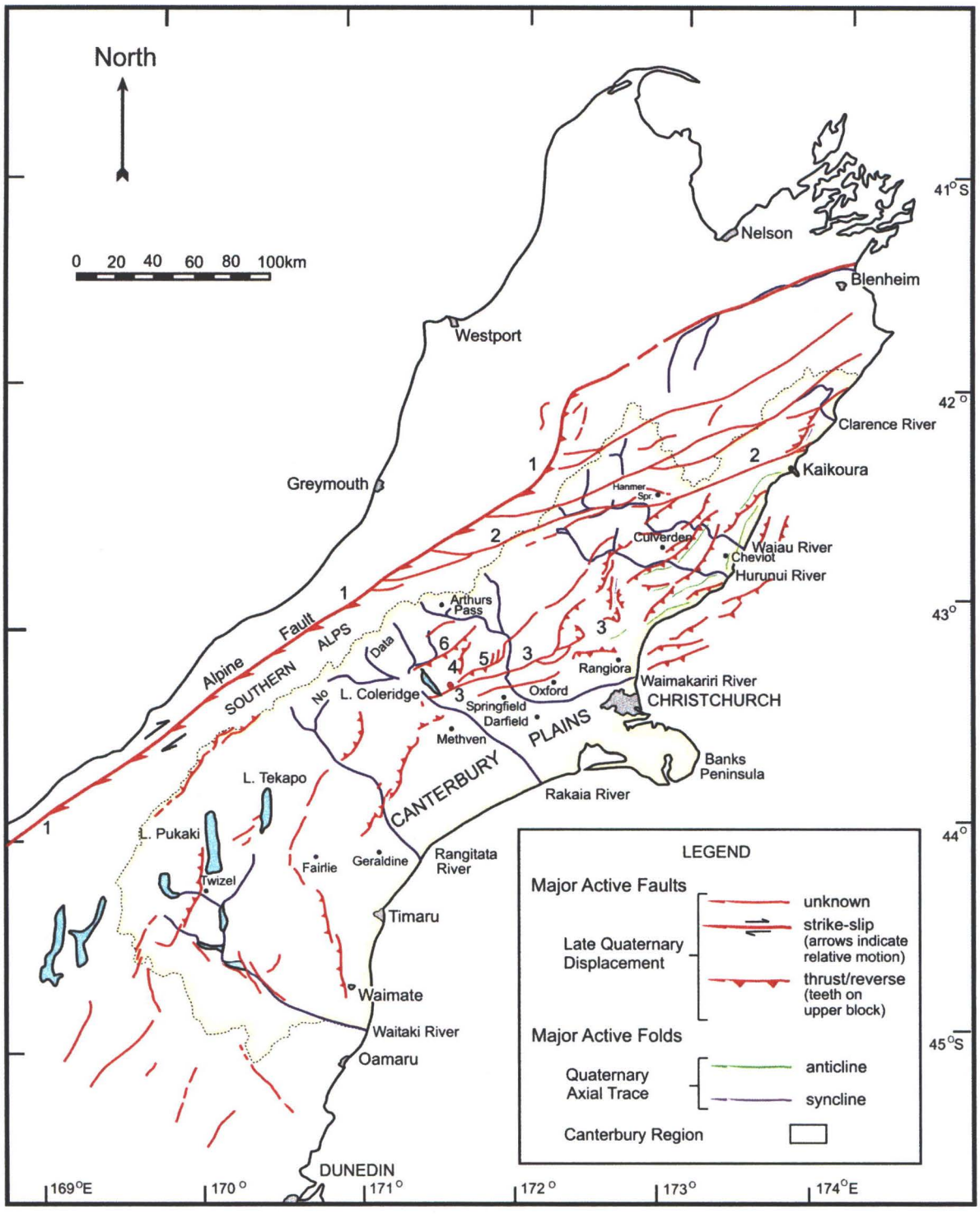

Figure 1.3: Map of the South Island illustrating the position of major active faults . The Porters Pass-Amberley Fault Zone is numbered (3) with the Porters Pass Fault segment trending south -west between the Waimakariri and Rakaia Rivers immediately south of Lake Coleridge. The Acheron rock avalanche is identified by a red circle east of Lake Coleridge.

Other important faults adjacent to the Acheron deposit are the Craigieburn Fault (4), the Torlesse Fault (5), the Harper Fault (6). The Alpine Fault (1) is northwest of the rock avalanche and the Hope Fault (2) of the MFZ is to the north. (Figure adapted from Pettinga, 1998).

outlined above) all within 1 km of an active trace of PP-AFZ. Assuming that the trigger for the instability was from a single seismic episode, then Cowan et al. (1996) suggests the landslides may represent an earthquake event between 700-500 years B.P. A recent study of earthquake induced instability in the central and northern Southern Alps identified that concentrations of landslides, triggered by historical earthquakes broadly defined the zone of causative fault rupture (Hancox et al. 1994). Considering those observations it is reasonable to assume that the concentration of landsliding between 700-500 years B.P. does delineate the source of the earthquake.

To compare regional slope instability with the landslides along the PP-AFZ, Cowan et al. (1996) looked at the largest source of rock avalanche information for the central Southern Alps compiled by Whitehouse and Griffith (1983; Whitehouse, 1983; Whitehouse, 1981). Only two landslides coincided with the ages of the PP-AFZ landslides. The lack of overlap of rock avalanche ages in the central Southern Alps between 700-500 years B.P. encourages the inference that any earthquake rupture at that time was from a local source probably the PP-AFZ (Cowan et al. 1996).

Further evidence was obtained from several augur holes and four trench excavations across the Porter Pass Fault (Howard, 2001). Using this information Howard (2001) identified Holocene rupture ages of 8500 ±200, 5300 ±700, 2500 ±200 and 1000 ±100 years B.P. This failed to show a fault rupture coinciding with 700-500 year B.P. age but instead inferred the youngest earthquake event at 1000 ± 100 years B.P.

The differences of age for the dates of the Acheron deposit and other landslides along the PP-AFZ compared with the trench observations of Howard (2001), creates a quandary between the stratigraphic evidence and geomorphologic dating techniques. This questions the reliability of the interpretation of paleo-indicators as signals of earthquake events. It has been reiterated in two earlier studies that inferences of a rupture age based wholly on landslides ages are to be regarded with caution (Cowan et al. 1996; Howard, 2001). However, the seismic hazard posed by the Porters Pass Fault and potential impact of associated catastrophic collapses to Canterbury highlights the need for further investigation to accurately identify the implications of the hazard.

1.2. PURPOSE AND SCOPE OF THESIS

1.2.1. RELEVANCE OF RESEARCH

The ongoing uplift of the Southern Alps is the result of the oblique collision of the opposite dipping Australian and Pacific plates (Fig. 1.4). This zone of compression results in the formation of a series of fault systems along which ongoing displacement occurs and energy is released in the form of high magnitude earthquakes (Howard, 2001).

Historically large rock avalanches have been shown to occur above a moment magnitude of Mw 6.5 (Hancox et al. 1994). The moment magnitude compares the seismic moment (Mo) or energy released from an earthquake source to a relation developed by Hanks and Kanamori (1977). This calculates a moment magnitude or Mw and is typically used to estimate paleo-earthquake events.

Hancock et al. (1994) applied Keefer's (1984) relationship between earthquake magnitudes to distribution of landslides to the Southern Alps. This investigation concluded that larger landslides with volumes exceeding 1×10^6 m^3 (which is the minimum volume described for forming rock avalanches) can occur during earthquakes of Mw 6-8 over distances up to 100-200 km from the earthquake epicenter. This suggests it is probable that a large rock mass failure forming a rock avalanches could occur in the central and eastern Southern Alps during an $Mw > 6.5$ earthquake.

The principal rock type of the eastern Southern Alps is the well-indurated sandstones and mudstones of the Torlesse Supergroup. This terrain is typically highly fractured and prone to large rock mass collapse particularly in steepened valley topography (Yetton, 1999). The persistent joint planes and bedding contacts offer abundant potential detachment surfaces and the rate of dilation and response to seismic motion is probably a significant influence leading to large-scale mountain collapse.

While there are cases of rock avalanches triggered by non-seismic processes, the forming of rock avalanches during an earthquake is well documented internationally (Voight and Pariseau, 1978). With the threat of an $M > 7$ rupture on faults such as the Alpine Fault and

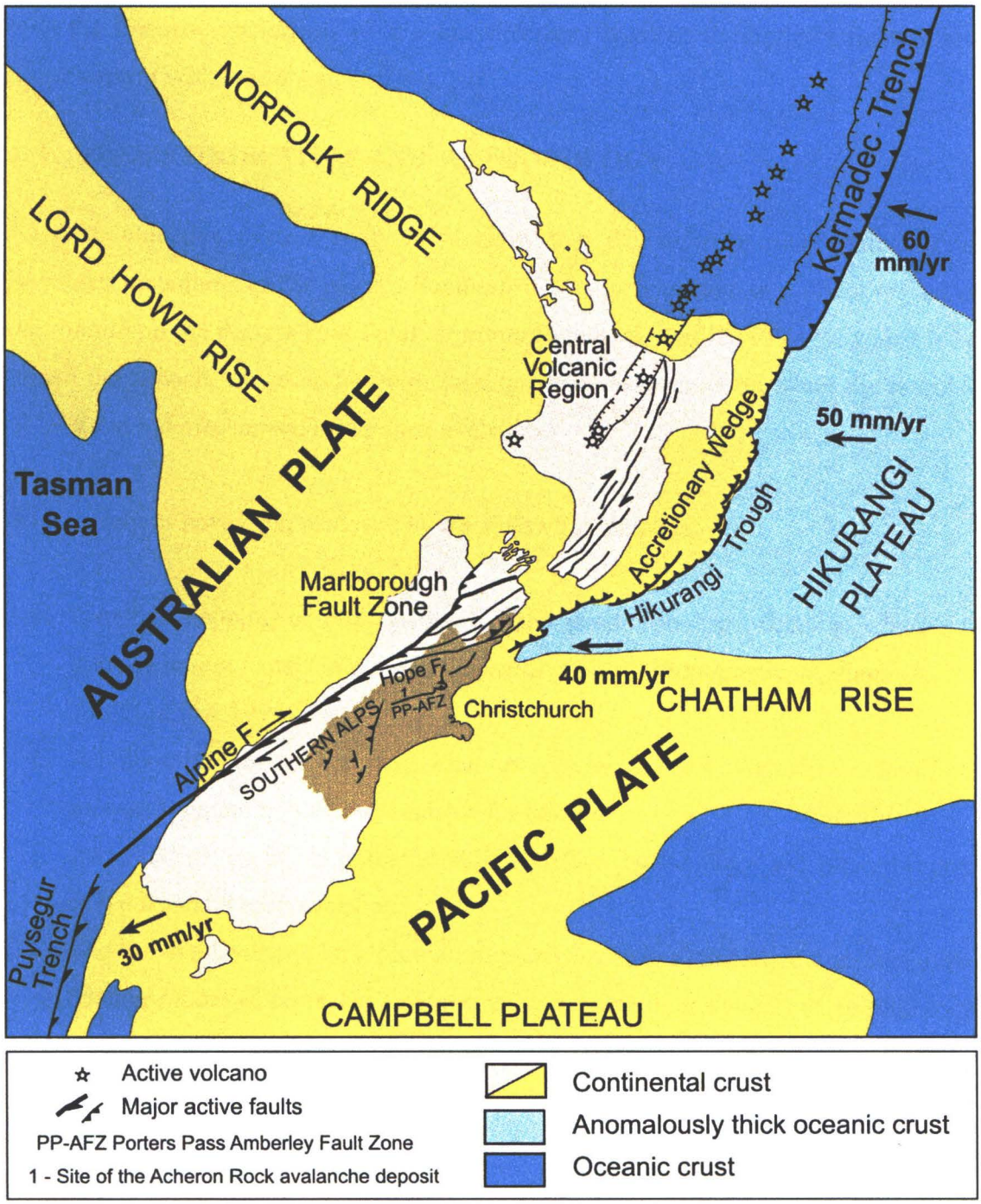

Figure 1.4: Map of the main structural features of the New Zealand micro-continent associated with the obliquely convergent Australia-Pacific plate boundary zone. The Canterbury region is indicated by the brown shading. The approximate site of the Acheron rock avalanche is indicated by the number 1 (Figure used with permission from Pettinga, 1998).

potentially the Porters Pass Fault in the South Island, there is need for identification and the planning of responses to minimize the impact of this hazard. At present very little is known about the frequency or effects rock avalanches may have on public infrastructure and the private sector (Whitehouse and Griffith, 1983).

1.2.1. THESIS OBJECTIVES AND METHODOLOGY

The main objective of this study is to show that the Acheron rock avalanche in the greywacke mountains of the eastern Southern Alps was triggered as a direct response to a fault rupture on the Porters Pass Fault; a prominent segment of the PP-AFZ which is buried beneath the deposit. A secondary emphasis has been to examine in detail the morphology and long run out mechanism of the rock avalanche.

These objectives have been achieved by the following methods:

1. Detailed mapping of both geological and geomorphologic features using a GPS-derived contour map in conjunction with 1:50 000 topographical maps (K35 Ed1. 1989 Ltd Rev 1998).
2. A literature review of the rock avalanche process including classification, morphology and typical mechanisms for failure.
3. An investigation of the potential failure surface, morphology and run out properties of the Acheron rock avalanche.
4. The use of a Dynamic long runout program (DAN) to determine the applicability of a friction model to represent fragmentation induced high velocity long runout of the rock avalanche deposit as proposed by Davies and McSaveney (2002).
5. Radiocarbon dating of a buried tree and other vegetation at several exposures of the Acheron rock avalanche and the underlying terrace contact to ascertain the age of rock avalanche emplacement.
6. The excavation of a trench across the Porters Pass Fault adjacent to the Acheron deposit aimed at locating evidence of a fault rupture corresponding with the deposit emplacement age.
7. The interpretation of the trench and terrace stratigraphy and radiocarbon ages to establish any link between the Porters Pass Fault and emplacement of the rock avalanche deposit.

1.3. REGIONAL TECTONICS

1.3.1. PLATE TECTONICS AND PROMINENT FAULT DOMAINS

The New Zealand micro-continent overlaps the oblique convergent margin of the east moving Australian and west moving Pacific plates (Fig. 1.4) (Pettinga et al. 2001). In the South Island of New Zealand, deformation of the plate boundary is represented by a complex transfer zone involving two principal systems, the Alpine Fault and the MFZ. These zones form the link between the obliquely converging and opposite dipping plates absorbing the convergence induced strain (Pettinga et al. 2001). Both systems display complex combinations of dextral strike-slip and reverse-thrust behaviour (Pettinga et al. 2001).

Recent investigations of the probabilistic seismic hazard in Canterbury and Westland established nine structural domains with which to assess the potential seismic hazard (Pettinga. et al. 2001). The criterion for development of a domain was based on relationships between tectonic setting, style, geometry and rate of deformation as described in Pettinga et al. (2001). For this study only three domains will be reviewed; the Alpine Fault, the MFZ and the PP-AFZ (Fig. 1.5).

1.3.1.2. ALPINE FAULT

The most prominent feature, the Alpine Fault is a southeast dipping oblique shear extending over 420 km across the western margin of the Southern Alps. Recent studies show it accommodates 70 – 75 % of the convergent plate motion in a narrow band of high strain deformation and is estimated to have a horizontal slip of 27 ± 5 mm/year and an average single event horizontal displacement of 4-8m (Norris et al, 1990; Berryman et al. 1992; Norris and Cooper 1997; 2001; Walcott 1998; Norris and Cooper 2001; in Pettinga et al. 2001). This fault can potentially produce very large earthquakes at upper crustal levels representing a major ground shaking source for the triggering of rock avalanches in the central Southern Alps.

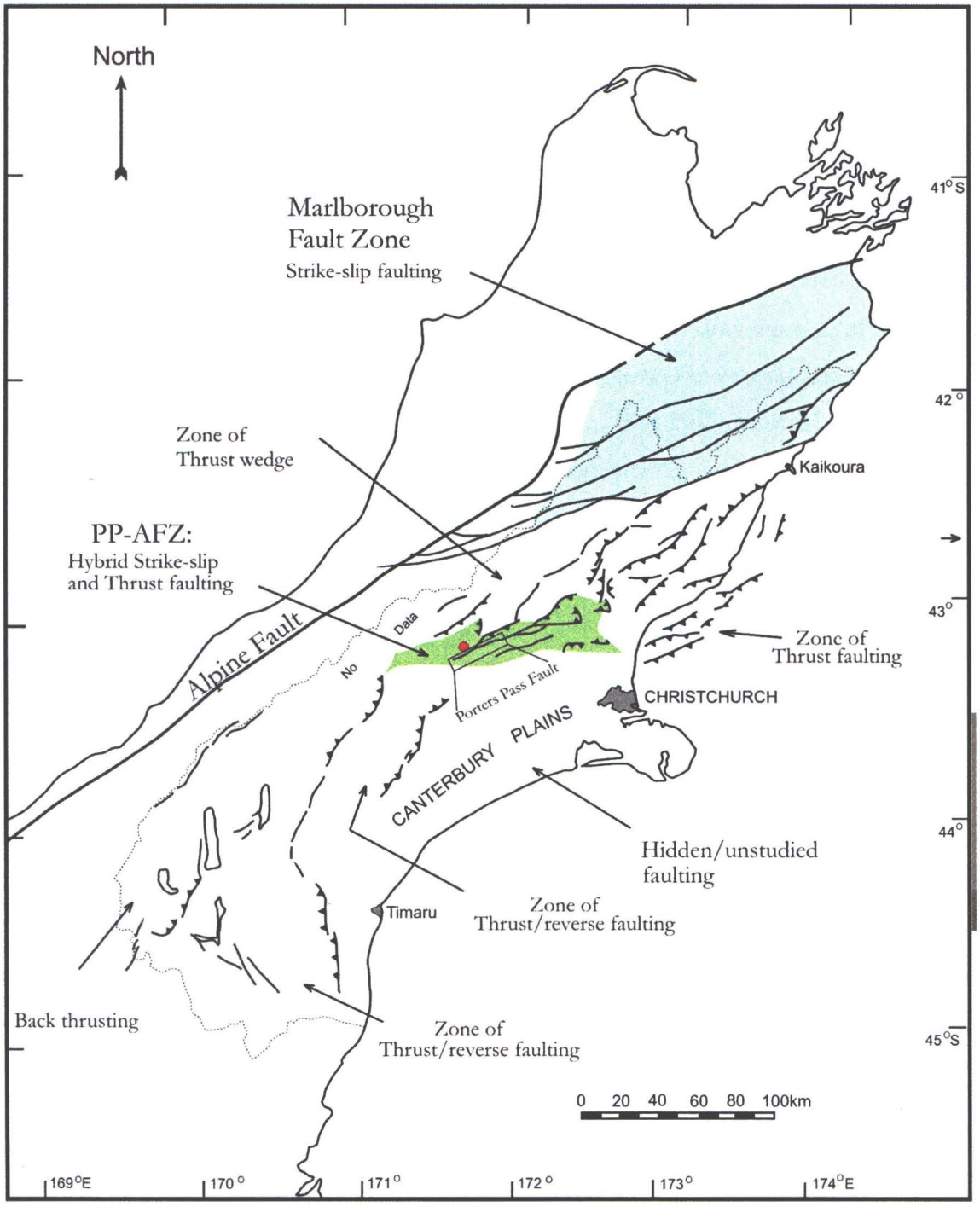

Figure 1.5: Summary map showing the structural setting of the Canterbury region. The Marlborough Fault Zone (MFZ) is shown as the torquoise zone north of Kaikoura. The Porters Pass-Amberley Fault Zone (PP-AFZ) is shown in green. The Red Hill valley can be identified by the red circle. (Figure adapted from Pettinga et al. 2001).

1.3.1.3. MARLBOROUGH FAULT ZONE

The Marlborough Fault Zone (see Fig. 1.5) (MFZ) is a series of northeast trending oblique strike-slip faults described as the most actively deforming structures in the Canterbury region (Eusden et al. 2000). This system includes the Hope, Clarence, Awatere, and Wairau faults (Pettinga et al. 2001). The zone absorbs a large component of plate motion as a complex pattern of strain partitioning associated with northeast trending (above mentioned) faults transferring the plate motion to the Alpine Fault (Pettinga et al. 2001). The slip rates across the Marlborough Fault Zone vary north and south but range between 30-54 mm/year which is substantial compared to the accepted rate of plate convergence of 40mm/year (DeMets et al. 1990 in Pettinga et al. 2001). This represents the second fastest onland slip with the Alpine Fault being the fastest (Berryman et al. 1992; Pettinga et al. 1998; in Eusden et al. 2000). At present the loci of strike-slip displacement is interpreted to be migrating southward with the highest slip rate presently on the Hope Fault ranging between 10-35mm/year (see Fig.1.4 Pettinga et al. 2001).

1.3.1.4. PORTERS PASS–AMBERLEY FAULT ZONE (PP-AFZ)

To accommodate the continent to continent transfer of strain, the MFZ is considered to be migrating southward forming a fault zone described as a juvenile diffuse belt of dextral oblique shear referred to as the Porters Pass–Amberley Fault Zone (PP-AFZ) (see Fig. 1.5) (Cowan, 1992; Cowan et al. 1996; Pettinga et al. 2001; Campbell, 2003). This is considered to represent the early development of the youngest of the MFZ transfers in response to the latest phase of plate boundary widening in the Late Pleistocene (Pettinga et al. 2001; Campbell, 2003). The PP-AFZ extends over 100 km between the Rakaia River at Lake Coleridge to north of Waipara and Amberley (Cowan et al. 1996). This follows an east north-east trend at a high angle to the regional NW-SE pattern of Mesozoic deformation (Gregg, 1964 in Cowan et al. 1996). The PP-AFZ consists of 11 individual elements, of which a minimum of 5 are considered Holocene active; Porters Pass Fault, the Mt Grey Fault, Coopers Creek Fault, Mt Thomas Fault, Lees valley Faults (Table 3 in Pettinga et al. 2001)

A slip rate ranging from 0.5–5.0 mm/year is reported for the fault zone, which displays good evidence for two large (M>7) earthquake ruptures in the last ~2500 year (Pettinga et al. 2001). This infers a recurrence interval for large earthquakes of approximately 1300-2000 years (Pettinga et al. 2001). A western strand of the PP-AFZ, the Porters Pass Fault, is a Holocene active discontinuous fault trace extending over 40 km between the Rakaia and the Waimakariri Rivers (Howard, 2001). Well-developed scarps appear intermittently along the fault ranging from 100m up to 1200m in length (Howard, 2001). Fault behaviour is right-lateral strike-slip, with a component of normal displacement in topographically high areas, with 33m of lateral displacement recorded along the fault trace over four to six earthquake events (Howard, 2001).

1.4. REGIONAL GEOLOGY

1.4.1. REGIONAL GEOLOGY

Two main rock types are present in Red Hill valley, however the basement greywacke sandstone and argillites of the Torlesse Supergroup are the dominant material. Made up of layers of quartzo-feldspathic sandstone and dark sandy mudstones, these beds can vary in thickness from thinly bedded (20-60cm) to large massive indurate sandstones and mudstone beds >10 metres thick. The greywacke is derived from the Permian-Triassic Rakaia Subterrane accretionary assemblage exposed to deformation from a series of collision and mountain building processes in the Jurassic and Cretaceous periods and again during the Cenozoic. Both the mudstone and the sandstone units have concentrations of pervasive fracturing and fault dissection. The latter of which displays crush-zones and gouge material (Campbell, 2003). Folding is also prevalent but the extensive colluvial cover prevents structural continuations to be traced accurately.

A small slice of marine sediments associated with the Cenozoic marine transgressions in the Castle Hill Basin is located in the west of the field area abutted against the Porters Pass Fault. These Porter Group rocks comprise limestone and tuffs from the late Oligocene Thomas Formation, marl from the Amuri Formation, and white quartz sands from the early to mid Oligocene Coleridge Formation. On the edges of the sequence greensand from the older Eyre Group was also identified.

1.5. GLACIAL GEOMORPHOLOGY

1.5.1. LATE QUATERNARY GLACIAL HISTORY.

The Rakaia glacier is considered to have had four periods of advance since 150 000 years B.P. The two oldest documented events are the Woodlands Advance (150 000 years B.P.) and the Tui Creek advance (56 000-70 000 years B.P.). More recently the Bayfield I-III advances of between 22,800 years B.P. and 19,750 years B.P. and the Acheron I-III advance occurring 17 000-14 000 years B.P. have impacted around the Coleridge area (Howard, 2001; Soons and Burrows, 1978). Good correlation exists with the northern outwash surfaces of the Blackwater advances in the Craigieburn Basin to the northeast. The youngest glacial sequence in the Rakaia valley is the Acheron advance (17 000-14 000 years B.P.) which is most visible immediately around the Lake Coleridge area and is the only glacial surface offset by the Porters Pass Fault (Howard, 2001).

The only remnants of glacial advance bordering the study area are that of the Bayfield I II and III (Soons and Burrows, 1978). The Lake Lyndon valley appears to have been ice free during the Bayfield advances, with the main ice-marginal features being moraines in the southwest of the valley and a succession of outwash surfaces sloping northward overlaid by recent alluvial fan deposits (Soons and Burrows, 1979).

1.6. CHARACTERISTICS OF STUDY AREA

1.6.1. STUDY AREA LOCATION

The Acheron rock avalanche is located 82 km west of Christchurch within the eastern ranges of the Southern Alps positioned 1 km west of a sub-alpine lake called Lake Lyndon. Red Hill valley is a small open valley trending northwest to southeast covering an areal extent of approximately 12 km^2. To the west, the study site is bounded by Red Hill, to the north by the Coleridge Pass and Mount Lyndon dominates to the northeast (see Fig. 1.2). The Porters Pass Fault which crosses the valley has been studied by Coyle (1988), and Cowan (1992, et al. 1996) who focused on a wider zone of deformation east of Porters Pass whilst Howard (2001) conducted a study of the western area between the Kowai and the Rakaia River. The location and structure of the fault remains poorly understood within the Red Hill valley.

1.6.2. PHYSIOGRAPHY

The study area is at the end of the southern extremities of the Craigieburn and Torlesse Ranges. The highest peak is Red Hill (1641m) located on the western boundary flanking the rock avalanche source basin. The distinctive rounded ridge lines and summits reflect a term of periglacial cryoplanation in the area. Two faults cross the site the Porters Pass Fault and the Red Hill Fault. The Red Hill Fault is a poorly constrained fault based on linear geomorphic features and displays no visible scarp expression. The Porters Pass Fault has generally well defined rupture scarps either side of Red Hill valley but has little or no surface expression in the valley itself. Smaller crush and shear zones cross the valley intermittently in a northeast-southwest direction.

1.6.3. HYDOLOGICAL CONDITIONS

The main drainage systems are the Red Hill stream, the Acheron River, the Rakaia River and Lake Lyndon. Drainage from the study area flows south along the Bluff River and Tributary One, tributaries of the Red Hill stream into the Acheron River which joins the Rakaia River north of the gorge. Several small wetland lakes exist immediately south of Lake Lyndon within a flat lying lake deposit sequence. Lake Lyndon is the most prominent hydrological feature in the area and is crossed by the Porters Pass Fault in its southern section. The present lake is thought to have been dammed behind encroaching alluvial fans to the south, but was once part of a system which drained into the Acheron river valley (Soons and Burrows, 1978; Gage, 1959)

1.6.4. CLIMATE

The climate of the study area is dominated by the barrier effects posed by the Southern Alps, and the predominantly warm mid–latitude westerly wind flow across the central South Island (Hayward, 1967; Bowden, 1983; Howard, 2001). Winter temperatures can range from –10 °C to +12 °C and above 1500m the land is often snow bound from May to November (Molloy, 1963; Howard, 2001). Summers in contrast are hot and dry, although still subject to snow at any time (Molloy, 1963).

Temperature fluctuations during winter cause active erosive freeze-thaw processes such as frost shattering, frost lifting and solifluction (Whitehouse, 1986: Howard, 2001). This is

considered the major contributor to physical weathering of the greywacke rock mass in the study area. Precipitation comes primarily from the southwest while the northwester dominates as the prevailing wind and consequently is the major agent for erosion and transportation of finer material (Molloy, 1963). Additionally, precipitation thins towards the eastern Southern Alps compared to more western mountain terrain due to the rain shadow effect associated with the orographic weather system.

1.6.5. SOILS

Soils in Red Hill valley are derived from the weathering of basement Torlesse group rock, and amounts of alluvium, loess, glacial till and periglacial solifluction (Molloy, 1963, Howard, 2001). The elevated sections of the study area above 1500m are dominated by bare rock or scree. The soils are predominantly steep-land yellow brown earths and podzols (Molloy, 1963, Howard, 2001). The low land terraces typically have yellow brown soil 30 to 60cm thick, overlying a sequence of oxidized clayey silts above fluvial gravels. The soil generally has poorly developed structure, a low nutrient content, and is subject to constant removal and deposition particularly by the prevailing westerly winds (Molloy, 1963).

1.6.6. VEGETATION

The vegetation of the study site is characterized by two distinct zones each corresponding to climate variations associated with differing elevations (Molloy, 1963). The first is referred to as the sub-alpine zone (600m–1000m) and is dominated by a heath called Dracophyllum acerosum and the short tussock grasses called Festuca novaezalandiae (Molloy 1963). Small relic clusters of beech forest *Northofagus solandri var. cliffortiodes* also survive above about 900m and are expected to be relatively unchanged since the deposition of the Acheron rock avalanche approximately predating 500 ± 69 years B.P. as based on the (NZ547) (Burrows, 1975). Matagouri stands are confined to exposed scree surfaces, shallow slope instabilities and the rock avalanche deposit. Also present are spear grass and some wetland plant species in the river bed.

An alpine zone extends above 1500m and consists of predominantly snow tussock grasslands, mobile scree and bare rock. The snow tussock species called Chinochloa rigida

is typically found in the leeward slopes in discontinuous patches, while the scree supported species are often highly dispersed and difficult to see (Molloy, 1963).

1.7. THESIS ORGANISTATION

Chapter One introduces the reader to the study area and describes the relevance of the research. The methodology is presented and a commentary on regional geology, descriptions of the Porters Pass-Amberley Fault Zone and the Alpine Fault is given.

Chapter Two brings the geology and geomorphology of the rock Avalanche deposit to the reader with a description of rock types and lithology present. Particular focus will be directed to the source scar and local faults within the area and their effect on the formation of the rock avalanche. A stability analysis will be run to locate potential failures planes along which the source rock mass failed.

Chapter Three introduces rock avalanches and discusses the classification and typical morphological characteristics of rock avalanches. A brief discussion of triggering mechanisms is given and a review of theories attempting to describe the mechanism for long run out is presented.

Chapter Four describes in detail the Acheron rock avalanche deposit with focuses on the dimensions of volume and area and morphological features associated with the run out. The locations of samples from the base of the rock avalanche for radiocarbon dating are described and new ages are presented. A run out simulation model (DAN) representing fragmentation induced high velocity long-runout is discussed and applied to the Acheron rock avalanche using the method outlined by Davies and McSaveney (2002).

Chapter Five details the paleoseismic investigation of the Porters Pass Fault in the Red Hill valley. The findings from trenching of the fault are presented and discussion is given on the consequences of these results.

Chapter Six discusses the implications of the new ages for the Acheron rock avalanche and its relationship to the Porters Pass Fault. Comparable rupture ages for the Alpine Fault are described and considered.

Chapter Seven summarises the main findings and proposes new ages for the Acheron rock avalanche deposition and a rupture along the small western segment of the Porters Pass Fault post-dating 700 years B.P.

CHAPTER TWO

GEOLOGY AND GEOMORPHOLOGY OF THE RED HILL VALLEY

2.1. INTRODUCTION AND OVERVIEW

This chapter identifies the geology and geomorphological features of the study area in order to describe the setting, and assess what influences these had on the formation of the rock avalanche. Particular attention was given to the location of faults crossing the field area and the structure of the source scar. An investigation of the structure pattern within the source scar was undertaken to identify the primary failure surface and the extent of the rock mass which failed within the basin. This was done on the premise that concentrations and persistence of the defects present within the rock mass would reflect the structural conditions that existed, prior to failure.

Investigations were carried out on foot using an adapted topographic map (20m contour intervals) and low level (1:8 200) and high level (1:55 000) aerial photography on which relevant detail was recorded. The field area extended from Lake Lyndon to 1 km southwest of the Red Lakes. Orientations of bedding identified in outcrop throughout the field area were measured to record the local rock structure however this study did not focus on detailed structural interpretations. The geological and geomorphic information is presented on an independent A2 map and a site-specific sketch plan of the trench area in Chapter Five.

The Torlesse Super-group greywacke dominates the geology of the Red Hill valley. Exposure of the basement is limited to areas of slope instability, typically in steep watercourses and elevated outcrop (Fig. 2.1). Extensively vegetated solifluction and colluvial material forms the principal surface cover to an unknown depth. Cretaceous-Tertiary cover rocks exist as a small isolated outlier, abutted against the eastern side of the Porters Pass Fault trace 1200m west of the Acheron deposit (Fig. 2.2).

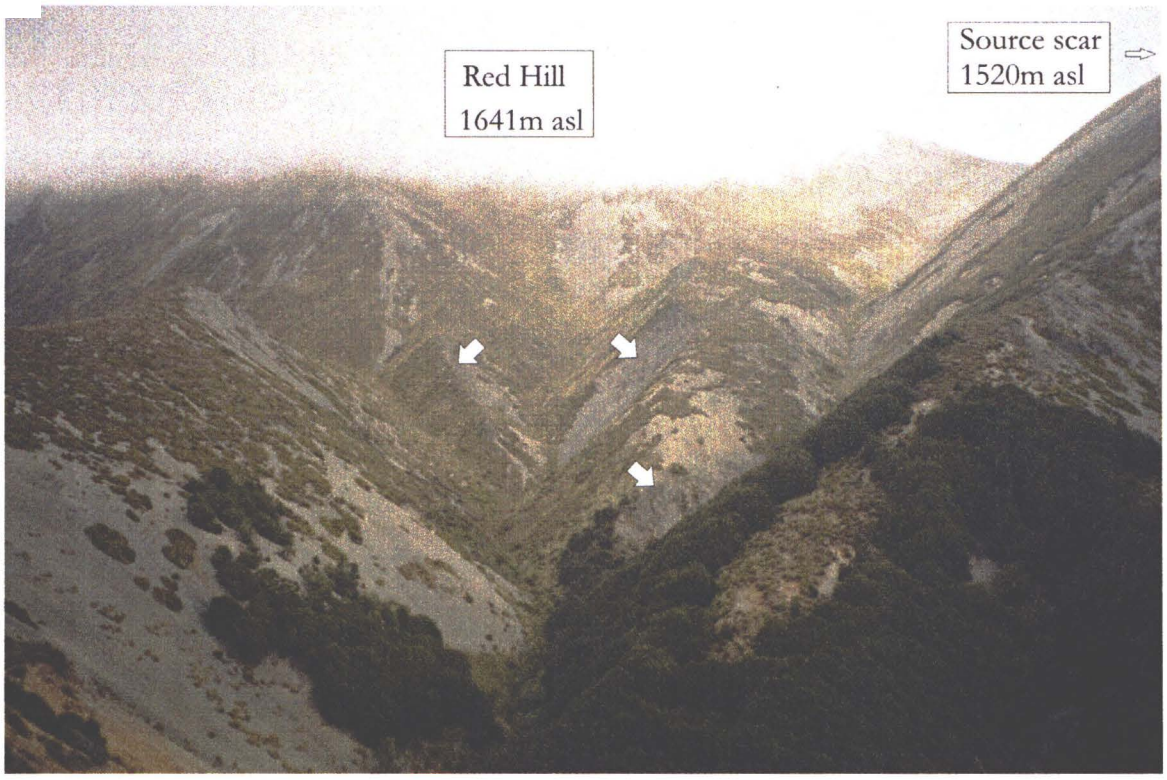

Figure 2.1: Typical areas of basement exposure in slips along steep elevated watercourses (white arrows). View of the head waters of Tributary One looking northwest toward Red Hill.

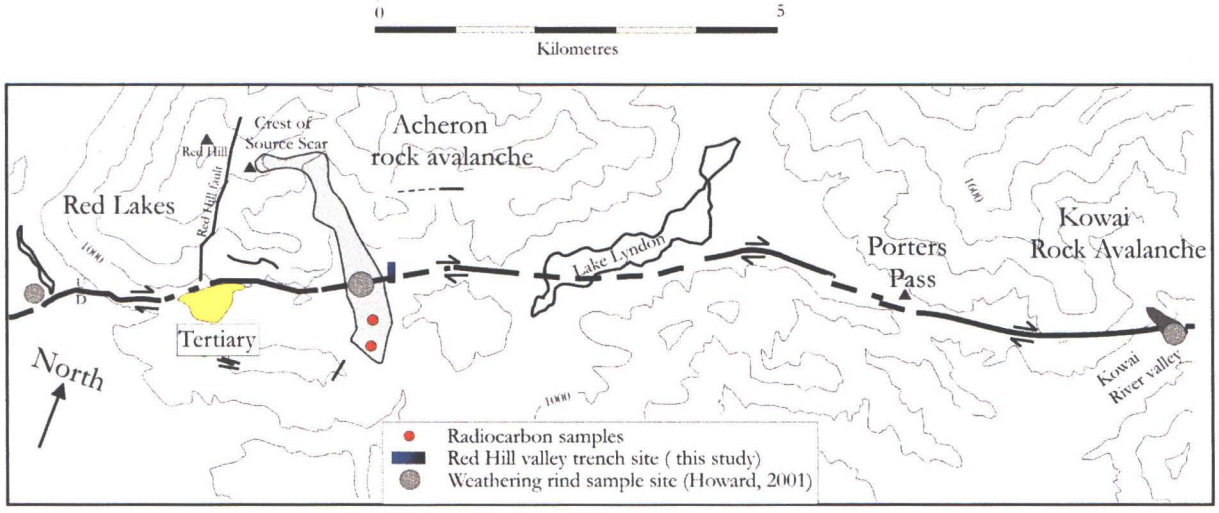

Figure 2.2: 1000m interval contour map showing the Porters Pass Fault between the Kowai River and Red Lakes. The Porters Pass Fault is shown by the heavy black line and minor faults are depicted by the thin black line. Weathering-rind sample sites from Howard, (2001) are shown by the grey circles. The radiocarbon sites and position of the Red Hill valley trench (this study) are shown by the orange circles and the filled box consecutively. A small outlier of Tertiary sediments abutted against the Porters Pass Fault is highlighted by the yellow fill. (Map adapted from Nicol et al. 2001; Howard, 2001).

2.2. REGIONAL BASEMENT GEOLOGY OF THE CENTRAL SOUTHERN ALPS

The geology of the South Island, New Zealand, is broadly divided into two provinces (Fig. 2.3). The older is the Precambrian–Devonian Western Province made up of remnant crust from the Gondwanaland continent intruded by Late Mesozoic granitoids (Bradshaw, 1989). The younger is the Mesozoic Eastern Province derived from Carboniferous to Cretaceous volcanic and forearc sediments and the Torlesse sediments associated with an accretionary wedge complex of a convergent plate margin (Bradshaw, 1989). Rocks of the Torlesse Supergroup make up the bulk of the Eastern Province and consequently the central Southern Alps (Fig. 2.3) (Whitehouse and Bradshaw, 1988).

Torlesse Supergroup greywacke is thought to have evolved from deepwater fan deposits at the base of continental shelf slopes (Bradshaw et al. 1980; Bishop et al. 1985). Gravity-induced slides of sands in submarine valleys formed turbidity currents transporting the sediment mass over the ocean floor fans, resulting in sequential layers of incoming sand and deepwater marine mud. A now deceased spreading centre conveyed the sediments of the future Torlesse Supergroup toward a collision with the Gondwanaland continent. The sandstone-mudstone sequences were scraped off from the top of the dense oceanic crust as it was subducted forming an accretionary prism complex leading to the future basement mass of the New Zealand continent.

The Torlesse Supergroup is divided into three major sub-terranes; The Permian-Triassic Rakaia sub-terrane, the late Jurassic-early Cretaceous Pahua sub-terrane and separating the two is the less extensive Eskhead sub-terrane which includes the complex Eskhead Melange (Whitehouse and Bradshaw, 1988; Howard, 2001). The basement rocks of the study area lie within the Rakaia sub-terrane.

The Rakaia sub-terrane was intensely deformed during the early Jurassic to early Cretaceous periods by two episodes of compression resulting in mountain building lasting approximately 150 million years. In literature, this is referred to as the Rangitata Orogeny causing folding and faulting of the Rakaia sub-terrane and exposing it to mild metamorphism forming metamorphic minerals including prehnite-pumpellyite, and vein minerals such as laumonite and calcite (Coyle, 1988). Collision ceased in the early-mid Cretaceous with changes in the

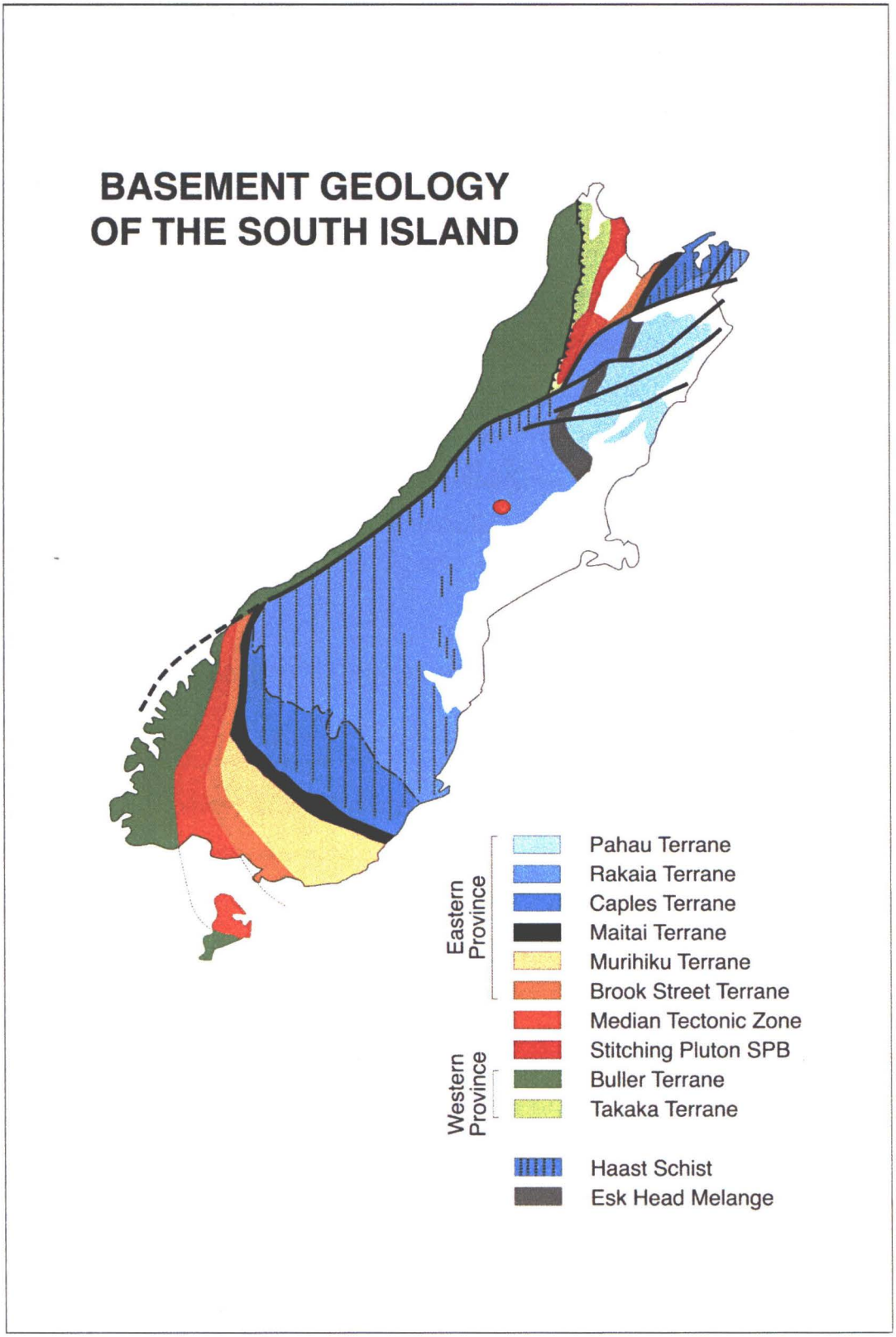

Figure 2.3: Basement geology of the South Island showing the Terrane boundary classification scheme of Bradshaw (1989) adapted from Anekant Wandras. The red circle pinpoints the position of the study area.

regional mantle convection system within the earth. This is thought to have caused a reverse of plate movement resulting in the onset of Cretaceous age extension separating the New Zealand landmass from the Gondwanaland continent.

2.2.1 GENERAL LITHOLOGICAL DESCRIPTION OF TORLESSE SUPERGROUP

The rock of Torlesse Supergroup is described as typically light grey to dark grey, well indurated, massive sandstone and argillite mudstones-siltstones. These are classified generally as feldsarenite and lithic feldsarenite, mudstone and conglomerate (Bradshaw, 1989; Coyle, 1988; Howard, 2001). Sedimentary structures can be identified within beds of mudstone, and were used to identify younging direction. Typical structure include grading, cross and climbing ripples, flame structures, parallel laminations, scour marks and sole marks (Whitehouse and Bradshaw, 1988).

2.2.2. GENERAL BASEMENT STRUCTURE OF THE RED HILL VALLEY

Strike lines from bedding were generally in a 100°-110°, or northeast to southwest direction. Small sections of exposure often displayed meso and micro folding but were often too weathered to allow accurate recording of orientation. Folding often appeared in association with local faulting but further investigation is required to confirm the relationship.

2.2.3. TERMINOLOGY

The procedure for describing Torlesse Supergroup units follows the method used by Coyle (1988) based on the system of Bradshaw (1972) using lithological description to define the Torlesse into four classes called lithotypes:

I Very thick - bedded sandstone

II Thin - bedded siltstone/mudstone

III Very thick - bedded mudstone

IV Volcanogenic association

2.2.3.1. VERY THICK SANDSTONE (I)

Intensely fractured by defects, these units are thickly bedded to massive with thicknesses ranging from <1m up to >10m. This is the dominant lithotype identified within the field area ranging between 60 and 70% of outcropping rock. Composition is of typical Torlesse Supergroup sediments predominantly quartz and feldspar with some minerals including chlorite, biotite and epidote (Coyle, 1988). Some units were identified in this study to contain matrix-supported clasts including sections of volcanogenic material. Sedimentary structure was rarely seen in the massive sandstone therefore was difficult to assign a younging direction. Most sandstone units were crossed by large calcite veins and pervasively fractured. Joint spacing ranged from close (0.25m - 1.0m) to moderate (1.0m - 2.0m). Defect persistence appeared high (5 - 10m) with a number of defects exceeding this, but some less persistent defects were identified. The average block size was generally large (0.1 – 1.0 m^3) to very large (> 1.0 m^3).

2.2.3.2. THIN-BEDDED SILTSTONE / MUDSTONE (II)

The second most prominent lithotype in the study area were the thinly bedded siltstone and mudstone with alternating sandstone sequences. These layers ranged in thickness from 5 - 60cm, and were the primary source of structural information including strike and dip of bedding and identification of sedimentary structures used for identifying the younging direction.

2.2.3.3. MASSIVE MUDSTONE (III)

Two major outcrops of massive mudstone were located in the study area. The first bounds the northern edge of the main head scarp of the rock avalanche source area, while the second is found in the lower section of the bedrock exposure within the v-notch landslide scar. Close inspection of these units showed a thin (5 - 20mm) moderately friable (able to be broken by the hand) sequence with undulating layering. Both units were between 30 - 50m thick, and showed uniform lithology. A concentration of fragmented dark mudstone in the lower rock avalanche deposit implies a massive mudstone source.

2.2.3.4. VOLCANOGENIC (IV)

Several extensive sections of reddy-orange coloured greywacke rock were found up the Tributary One valley on a degrading slope on the true right. The contact between the typical grey Torlesse rocks and the red rocks was difficult to identify but could be broadly defined by surface spalling rock and scree deposits that dominate the slope cover. The lithology ranges between massive sandstone to thinly bedded mudstone sequences all uniformly coloured reddy orange.

2.3. CRETACEOUS-TERTIARY COVER ROCKS IN THE RED HILL VALLEY

The Cretaceous-Tertiary outliers are remnants of a succession of cover rocks deposited ubiquitously in New Zealand (Fig. 2.4). These units form a thin transgressive-dominated sequence of Cretaceous to Pliocene limestone and quartzose sandstone, unconformably overlying basement rock of the Torlesse Supergroup (Young, 1997).

The cover rocks mark the western extent of the Cretaceous-Tertiary Canterbury basin that once extended east as far as the Chatham Rise, north to the Hope Fault and to the Southern Alps (Coyle, 1988). Uplift of these units occurred during the deposition of the Late Mata series and again during the Arnold series while a sustained period of major uplift rejuvenated in the Pliocene (Coyle, 1988).

Tertiary outliers in the region are typically confined as fault bounded pockets scattered across the eastern Southern Alps of North Canterbury. The extensive Castle Hill Basin in the northwest is the largest cover rock deposit in the local vicinity terminating near the study area along the Porters stream. Small Cretaceous-Tertiary pockets also exist in the west branch of the Kowai River bounded by the Benmore Fault, and along the Harper River demarked by the Harper Fault.

The Cretaceous-Tertiary marine sediments were located in the southwest of the study area at the termination of a 1.2 km long fault scarp mapped by Howard (2001) abutted against the south eastern up thrown side of the Porters Pass Fault (Fig. 2.5). Predominantly from the

Oligocene age Porter Group, they comprise coarse limestone and tuffs from the late Oligocene Thomas Formation, Marl from the Amuri Formation, and white quartz sands from the early to mid Oligocene Coleridge Formation. Greensand from the older Eyre formation was also identified in the lateral fringes of the sequence.

Outcrop was viewed immediately adjacent to the Porters Pass Fault and in four shallow slope failures falling into a steep thickly vegetated watercourse draining from a shoulder descending off the eastern face of Red Hill (Fig. 2.5). The unit appears to be an isolated narrow block only 200-400 m wide bounded by the Porters Pass Fault to the north.

Fig. 2.4: Stratigraphic Column for the Craigieburn Rangefront inferred to represent the basement rocks of the study area. The Tertiary sequences represent the outlier adjacent to the Porters Pass Fault southwest of the Acheron rock avalanche deposit.(from Young, 1997 p12).

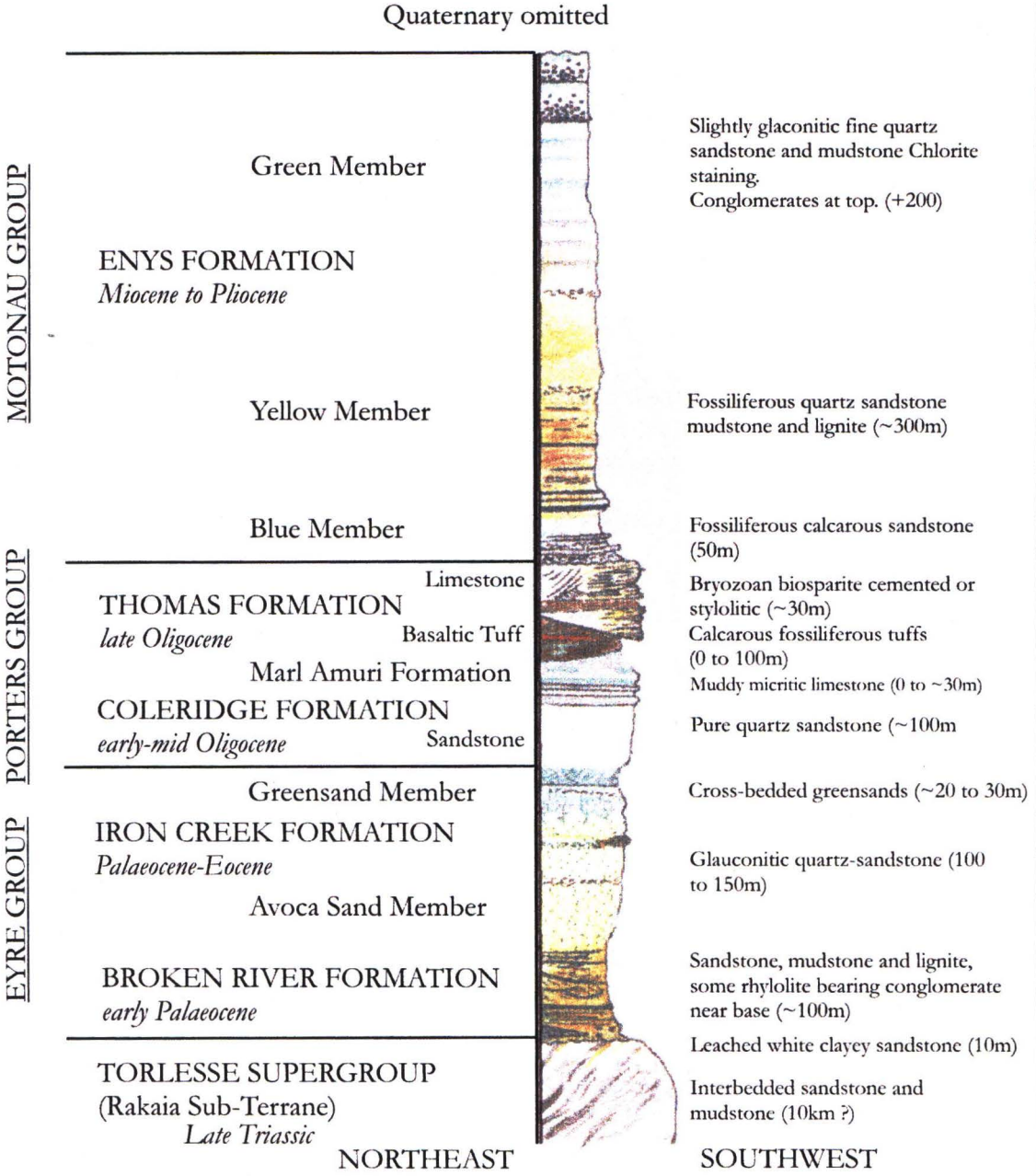

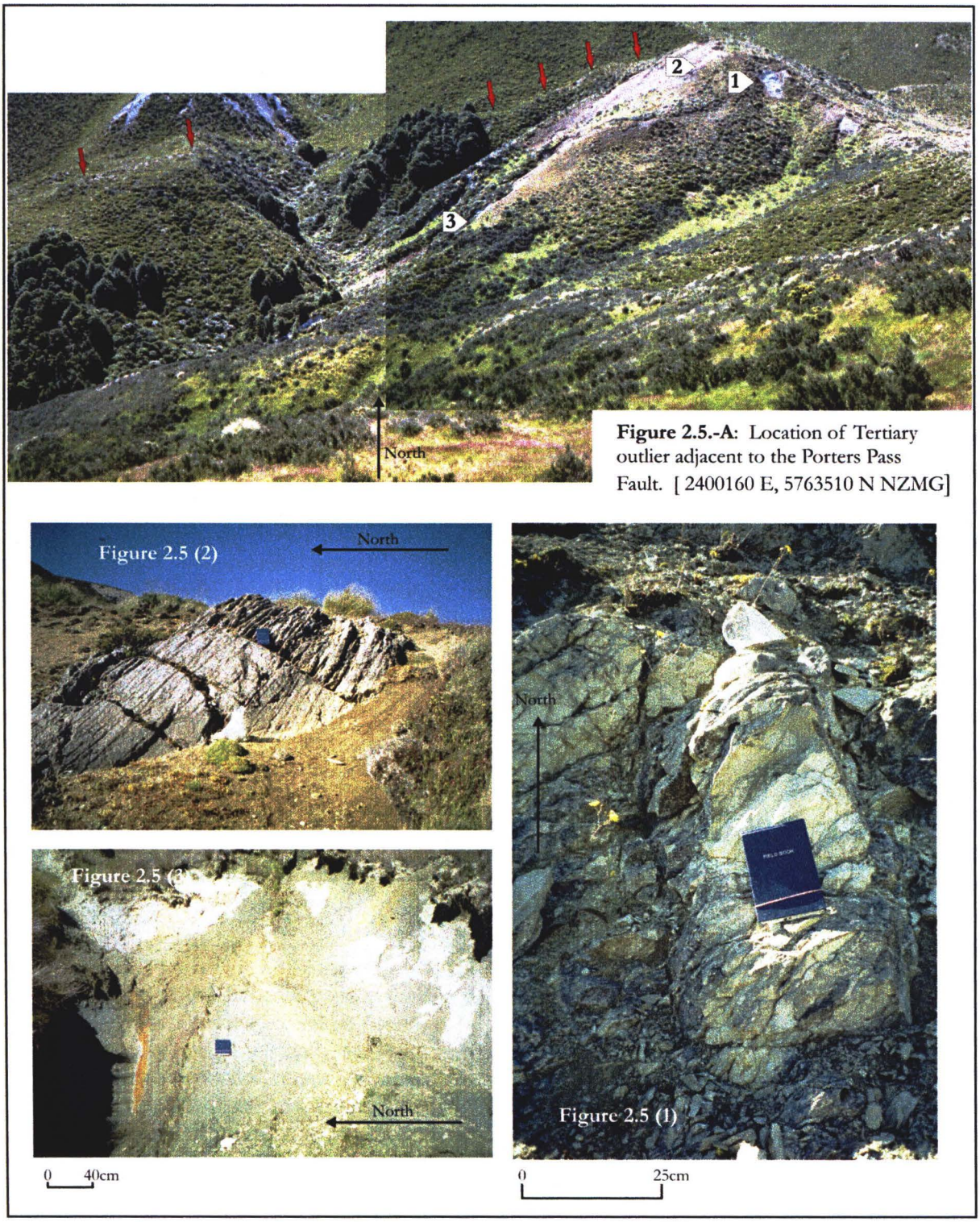

Figure 2.5.-A: Location of Tertiary outlier adjacent to the Porters Pass Fault. [2400160 E, 5763510 N NZMG]

Figure 2.5: Photograph of the Tertiary outlier on the western margin of the field area. Fig. 2.5 (1) mudstone and (2) limestone both dip north toward the trace of the Porters Pass Fault as outlined by the red arrows in Fig. 2.5 A. Fig. 2.5 (3) the greensand unit displayed no identifiable bedding causing difficulties in obtaining an orientation.

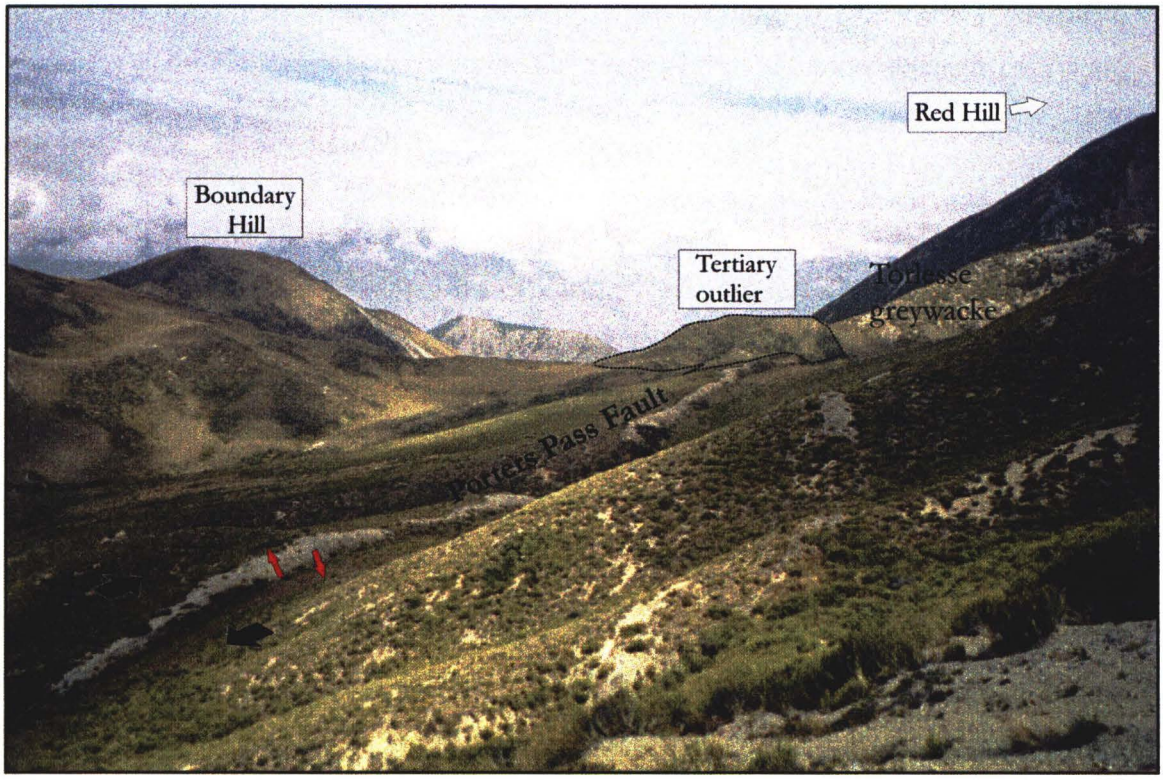

Figure 2.6: Photograph of the prominent 1200m scarp along the Porters Pass Fault extending from a saddle west of the Acheron rock avalanche before terminating in the west at the Tertiary outlier of Porters group marine sediments (outlined by the dashed line). The black arrows represent the direction of motion of the right-lateral horizontal displacement while the red arrows demonstrate the accumulative vertical normal displacement of 3-4m. The photograph was taken from the topographic saddle (western margin of Red Hill valley) above the Acheron rock avalanche deposit looking toward the southwest. Such dramatic scarps suddenly vanish in the Red Hill valley but remerge in the northeast immediately above Lake Lyndon.

The units are tilted towards the northwest and all appeared relatively friable, except for the styolitic limestone unit, which were well indurated. The maximum extent of the unit is not well constrained due to extensive scrub cover around the watercourse. The main diagnostic factor for determining their origin was the sequence of lithology, which closely resembled the stratigraphy of the Porter group as described by Gage (1970) and more recently by Young (1997) in the Castle Hill basin (Fig. 2.4).

At the top of the units, the limestone has a strike and dip of 034°/50° NW (Fig. 2.5.) This unit ranged from well-indurated styolitic limestone, to moderately well-indurated coarse fossiliferous rock containing shell fragments in a moderately coarse sandy matrix. Immediately east and beneath the limestone is a white siltstone or mudstone layered in thin (between 5 and 15cm) beds interpreted as being Coleridge Marl. This unit strikes along an orientation of 040° and dips slightly steeper than the limestone at 72° in a northwest direction.

Below the marl, located in a series of shallow earth flow scars, coarse dark green glauconitic sand beds cut by oxidised bands were identified and measured to gain an approximate orientation of 074° dipping 70° to the northwest. A well-indurated calcareous layer 30cm in thickness was also located on the far western riverbank closest to the fault trace, and was sub-vertical.

2.3.1. POSSIBLE RELATIONSHIP BETWEEN TERTIARY AND LOCAL FAULTING

The implications for the existence of the Tertiary outlier may be linked with the behaviour of the local faults (Fig. 2.8). It is unlikely that this isolated unit was formed from activity on the Porters Pass Fault, and is more probable that they are remnant of a larger deposit that once overlaid the area. Uplift and erosion has removed most of the rocks, a process occurring over much of the eastern Southern Alps. The proximately of the Craigieburn and Torlesse Fault systems in the Porters stream immediately to the north with similar lithologies, suggests a possible relationship through which further investigation of the site may uncover. The Red Hill Fault is a series of linear surfaces descending south between the source basin and Red Hill, and is inferred to be a potential continuation of the Craigieburn-Torlesse thrust systems, which predate the juvenile Porters Pass Fault segment (Fig. 2.7 Fig. 2.8 Howard, 2001).

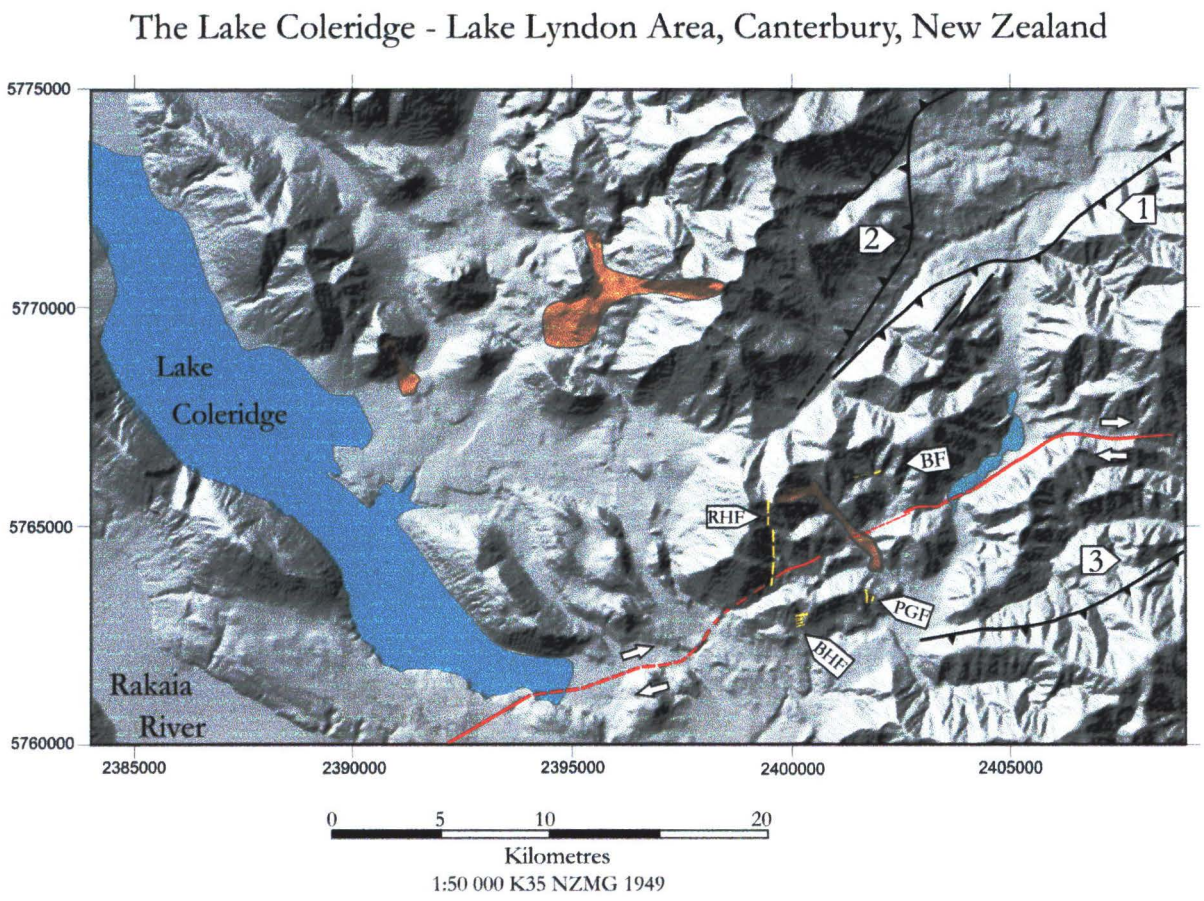

Figure 2.7: Surface elevation map (DEM) of the Lake Coleridge-Lake Lyndon area. Major faults are shown in Black: 1- the Torlesse Fault Zone, 2-Craigieburn Fault Zone, 3 is the Benmore Fault. The Porters Pass Fault is shown as a discontinuous red trace and can be seen traversing beneath the Acheron rock avalanche deposit (seen in orange). The yellow lines represent faults located in the Red Hill valley - Red Hill Fault (RHF), the Boundary Hill Faults (BHF), the Bluff Fault (BF) and Prickly Gully Fault (PGF). The two orange fills to the north represent the near-by Craigieburn and Ryton rock avalanches.

It can be inferred that there seems to be a preference for cover rock outliers to be bounded by thrust system rather than strike-slip systems such as the Porters Pass Fault. The Red Hill Fault may also intersect the Porters Pass Fault heralding a major segment boundary along the Porters Pass Fault line.

2.4. FAULT STRUCTURES WITHIN THE ACHERON STUDY SITE

Five faults were identified within the Red Hill valley however only one, the Porter Pass Fault, has been shown to be active during the Holocene (Table 2.1; Fig. 2.7 Howard, 2001). Little is known about the properties of the remaining faults; however, they are considered to predate activity along the Porters Pass Fault, and may be subject to reactivation as preferred zones of weakness for Holocene deformation. The foremost of these older structures is the Red Hill Fault, which descends south defined by a series of stepped geomorphic surfaces obliquely perpendicular to the Porters Pass Fault as seen in Figure 2.8. The remainder are exposed in minor slips within steep gullies. The Porters Pass Fault is considered to represent a likely source of seismicity, which could trigger the rock mass failure forming the Acheron rock avalanche

2.4.1. SUMMARY OF THE PORTERS PASS FAULT

The Porters Pass Fault can be traced as a series of discontinuous fault scarps for a length of 40km between the Rakaia and the Waimakariri Rivers. Examination of the fault during this study is based on three previous studies conducted by Coyle (1988), Cowan (1992, 1996) and Howard (2001). The initial work by Coyle focused on the Kowai River catchments to the east of the study area looking for and evaluating zones of shearing while Howard (2001) undertook a detailed corridor study along the 40km surface expression looking for evidence of Holocene rupture events. Howard (2001) put specific emphasis on the western section of the fault line extending from the Rakaia River in the west to Porters Pass some 5km east of Lake Lyndon (Fig. 2.7). Much of his work used low and high level aerial photography, and field-mapping techniques to map the trace based on offset geomorphic landforms.

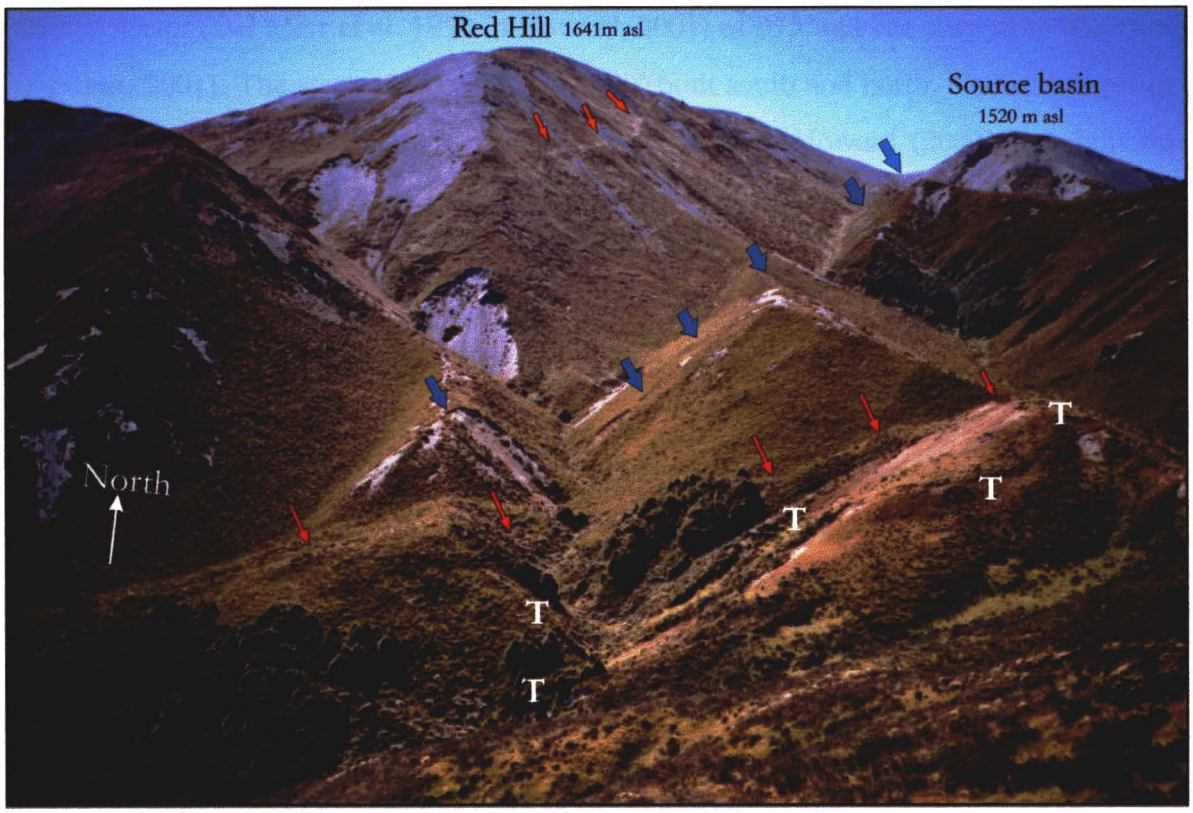

Figure 2.8: Photograph of Red Hill from Boundary Hill (looking north) showing the location of the Tertiary outlier (white T) and both the inferred Red Hill Fault (blue arrows) and Porters Pass Fault. (red arrows). A prominent ridge rent is outlined by orange arrows. The two main peaks are Red Hill in the centre of the picture and the crest of the rock avalanche source scar on the right. The inferred Red Hill Fault travels through the saddle between the two peaks descending along distinctive linear surfaces identifiable in the photo. The Tertiary rocks can be seen in exposures in the mid to lower forested areas. The Holocene active Porters Pass Fault traverses laterally immediately to the north of the Tertiary outlier. The converging paths of the two faults suggests an intersection may occur. [Sheet k35 Ed 1 1989 Ltd Rev 1998 2400160 E, 5763510 N NZMG]

Distinctive scarps occur fluctuating in length between 0.1 and 3km along the length of the Porters Pass Fault (Fig. 2.7 Howard 2001). These scarps can reach heights up to 3m and can vary greatly between buried or eroded, and well preserved linear structures (see Fig. 2.6) (Howard, 2001). The general direction of strike is 077°, which resembles the relative plate-motion vector (Del Mets et al. 1994 in Howard, 2001) of 075° but can vary from 058° to 098° (Howard, 2001). The steep scarps dip 70° to 80° both south and north. These changes in dip direction together with variation of faulting style enabled Howard (2001) to subdivide the fault into six sections to conduct a more detailed description of fault geometries. A brief description on the behaviour of the fault within these sections is given.

2.4.1.1. RED LAKES SECTION

The Porters Pass Fault strikes out from the base of Red Hill towards the Rakaia River for approximately 1200m before disappearing into the west towards Lake Coleridge (Howard, 2001). A set of five terraces which step up 18m above the nearby Red Lakes are offset both horizontally and vertically by the Porters Pass Fault (Howard, 2001). The average strike of 050° is noted by Howard as a deviation from the relative plate–motion vector of 077° and a dip angle steep to near vertical (Howard, 2002).

2.4.1.2. RED LAKES TO LAKE LYNDON (Site of the Acheron Rock Avalanche)

A change in strike to 075° occurs as the fault encounters elevated terrain associated with Red Hill. North facing up-slope dipping scarps of 2-3m in height extending over 1200m can be seen clearly in Figure 2.6. Similar dip direction and strike was recorded on a smaller length of scarp immediately west of Lake Lyndon some 5 km to the northeast. Within the Red Hill valley itself, little evidence of the fault exists as the Acheron rock avalanche deposit overlies the fault's pre-rock avalanche surface expression. Howard suggests that the fault formed a geometric jog to the southeast by 700m accounting for the strike offsets of the two adjacent scarps.

2.4.1.3. LAKE LYNDON TO PORTERS PASS

Unlike the previous sections, two changes in strike of 055° and 085° were recorded by Howard (2001). The fault crosses a hillside facing towards the northwest which is opposite to

that recorded both toward the east and west of this sub-section. The fault trace appears to curve around the sloping topography which Howard (2001) interpreted to represent a change in fault plane dip to the southeast, opposite to that previously observed.

2.4.2. SUMMARY OF THE PORTERS PASS FAULT WITHIN THE RED HILL VALLEY

Howard used strike alignment offsets from scarps found either side of the Red Hill to infer a change in fault geometry forming a jog or a step of some 700m to the southeast or down valley direction. During this study a small remnant scarp on the true right bank of the Bluff River was identified. The remnant scarp is considered to represent the fault structure post dating the burial of the valley by the rock avalanche. It is interpreted that a small overlapping step of faulting at the northeastern margin of the rock avalanche may result in a more direct strike across the valley towards the saddle at the northeastern termination of the 1200m scarp. This is supported by the proximity of a ridge rent or relaxation feature on the Hill 1249m (a.s.l see Map 1). It is possible that the rigidity of the fault induced by topography as previously proposed, (which resulted in a 700m step), has been overestimated. In reality the fault may behave in a more complex fashion. Further discussion of the Porters Pass Fault within the Red Hill valley will be presented in Chapter 5.

2.4.3. THE RED HILL FAULT

The Red Hill Fault is described as an east-dipping normal fault, trending northeast-southwest and intersecting the Porters Pass Fault obliquely-normal in a right angled junction (Fig. 2.8) (Howard, 2001). The recognition of the Red Hill Fault was based on aerial photo interpretations and field observations. No identifiable fault offset or trace scarps have been described in literature, however very distinctive geomorphic surfaces do delineate the strike of the fault, suggesting the fault has had a major impact on the local topography. During this study, recorded changes of dip direction of approximately 180° are interpreted to represent the deformation of the basement by the Red Hill Fault. The information was gathered from outcrops on the flanks of Red Hill west of the proposed Red Hill Fault dipping towards the south-southwest and numerous outcrop east of the inferred fault that follow the local structural trends dipping towards the north.

Table 2.1: Faults identified in the Red Hill valley field area

FAULTS	ACTIVITY	ORIENTATION		VISIBLE DEFORMATION	LOCATION OF EXPOSURES	FEATURES
		Strike	Dip			
~Holocene						
Porters Pass Fault (Lake Lyndon-Red Lakes)	ACTIVE	065°- 079°	70° - 90°	2-4m scarps	2402385E, 5765265N 2399940E, 5764020N	ca 40 km trace right-lateral strike-slip deformation
Pre-Holocene faults -						
Boundary Hill Gully	NON-ACTIVE	090°	80-90°	shear along argillite crushed argillite	2400225E, 5762975N	swarm of eight near-vertical faults in deformed argillite bands extending over several hundred metres
Prickly Gully	" "	040°	80°-90°	shear along argillite clayey-gouge deformed argillite	2401780E, 5763315N	deformed argillite beds- probable structural cause of slope failure in Red Hill valley on true right right valley side above the distal limit of the Acheron rock avalanche
Bluff River Fault	" "	060° approx	~	clayey-gouge	2402005E, 5766270N	hidden in talus slope
Red Hill Fault	" "	000°	~	linear geomorphic surfaces, no visible deformation	2399420E, 5765550N 2399580E, 5763910N	Possible interaction with the PPf immediately north of Boundary Hill

Howard (2001) also suggested that a possible kinematic association may exist with the western terminations of both the Cheeseman and the Torlesse Fault zones in the adjacent Porters River valley below the Coleridge Pass to the north. Both the Cheeseman and Torlesse Fault systems are thrusting basement Torlesse Supergroup rock over Cretaceous-Tertiary cover rocks. The Cretaceous-Tertiary rocks at those sites are similar to the cover rock sequences found adjacent to the Red Hill Fault. The Red Hill Fault is shown to trend between the crest of the source scar and Red Hill to the west (Fig. 2.7).

2.4.4. ADDITIONAL FAULTING WITHIN THE RED HILL VALLEY

Several smaller pervasive faults were identified crossing the southern side of a ridge between the Lyndon-road and Boundary Hill and near the headwaters of the Bluff River (see Fig. 2.7; Table 2.1). The former faults are found in gullies draining southward into the Acheron River trending at right angles to the strike of the ridgeline. They are exposed by shallow slope failures induced by concentrations of subsurface water permeating along the shear zones. The general strike of the faults range between 060° and 100° - 110°, sub-parallel and oblique to the Porters Pass Fault and dip consistently between 88° and sub-vertical; it is thought that there is some ambient relationship with the Porters Pass Fault structure. Faults are typically found within the less indurated argillite bands and broadly mirror their strikes. These faults are not considered Quaternary faults, rather remnants from an earlier period of deformation probably reactivated as preferential areas of weakness by more recent fault activity associated with the Porters Pass Fault.

2.5. GEOMORPHOLOGY OF THE RED HILL VALLEY

The deposition of the rock avalanche had a punctuated impact on the geomorphology of the Red Hill valley. Prior to the rock avalanche deposition, the geomorphology is inferred to be generated by the effects of periods of glaciations spanning the Bayfield I, II and III advances between >22 200 and 19 200 years B.P. (Soons, 1963). While the Rakaia glacier was not considered to have inhabited the Red Hill valley, influence from smaller sympathic glaciers may have created outwash sediment forming the terrace surfaces seen today.

Figure 2.9: View of the exposed contact between the Acheron rock avalanche deposit and the underlying terrace surface (site 3) described in Burrows (1975). The site of the buried tree etc excavated for radiocarbon dating (site 4) is located along the continuation of the contact at the bottom centre of the photograph. (Person lower centre right for scale).refer Fig. 2.10

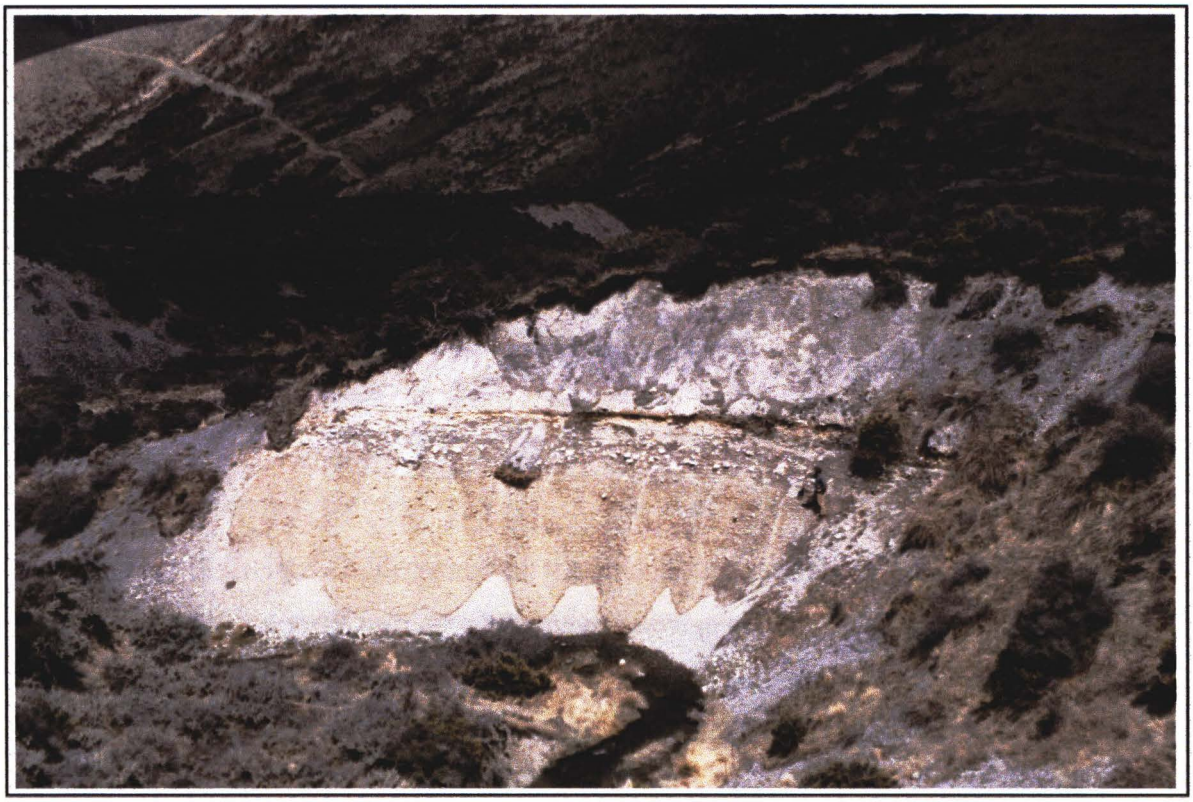

2.5.1. TERRACES

A distinctive feature of the field area is the 12 terrace surfaces found throughout the valley (see Map 1). Sections of the terraces are partially covered by the rock avalanche allowing excellent determinations of deposit thickness and correlation of the pre-avalanche surfaces with that of the overlying deposit. This situation also gave good credibility to buried tree samples found on the contact between the terrace and the rock avalanche for radiocarbon dating. The emplacement of the rock avalanche further up the valley has meant examples of terraces are concentrated along the lower Red Hill stream and the Bluff River; however, buried terraces are inferred to be present further up valley.

2.5.1.1. TERRACE STRATIGRAPHY

The stratigraphy of the lower unit is dominated by flat-lying gravels in a silty-sand matrix displaying clast sizes of between 5 and 20cm (Fig. 2.9; Fig. 2.10). The thickness of the gravels is unknown but is considered to exceed ~10m reflecting a long stable period of aggradation and valley fill. Clast source is most likely from the local upper catchments but transportation times would have been lengthy resulting in moderately uniform clast sizes and sub-rounded to sub-angular appearance. Colouration is a reddy-brown which distinguishes the unit from the overlying gravels. The most likely interpretation is that the gravel unit represents glacio-fluvial gravels from small glaciers relating to the Bayfield advances of the Rakaia Glacier older than 18,000 years B.P.

Interrupting the relative quiescence of the underlying gravels is a metre of coarse boulder material, which is poorly sorted and displays a coarse bedding structure; boulders up to 60cm in diameter penetrate the underlying unit creating a slightly irregular contact. Fresh grey colouration of the sediments implies a much younger length of exposure and deposition. The sudden change in sediment size records a particular change in the system within the valley. This may represent a short-lived event such as a flood or a landslide where the sediment source was close by and had spent a short time within the fluvial system.

Figure 2.10: The Quaternary stratigraphy of the Red Hill valley and Acheron rock avalanche deposit (compare to Fig. 2.9)

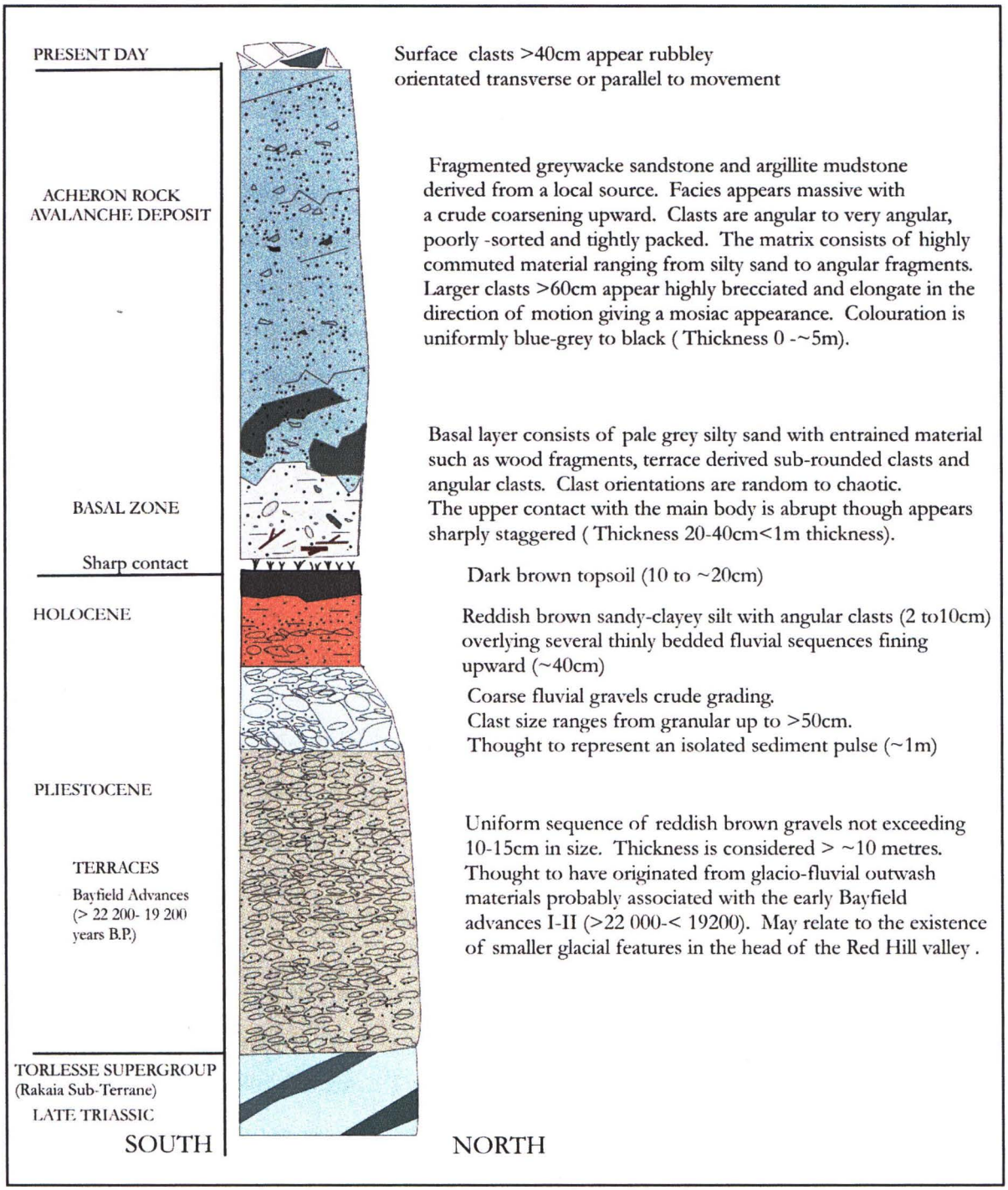

Overlying this unit exist fine gravels which display a sudden decrease in clast size between 5 and 15cm within the basal 50cm, and an increase in sandy matrix fining upward with well-bedded fluvial structure. This unit is ubiquitously associated with reddy brown silty clays in the top 20cm culminating in a 30 to 40cm silty clay soil horizon on the surface. The advent of soil represents a return to a stable system with no influx of fresh sediment. This may reflect channel migration of the river or down cutting of the bed level.

2.5.2. FLUVIAL SYSTEMS

The Red Hill valley has been shaped by the process of aggregation and more recently degradation over many thousands of years. With the deposition of the Acheron rock avalanche a massive change in all the fluvial systems occurred changing to a more dynamic regime. The nature of the waterway is expected to show a good record of tectonic uplift with the formation of wide sediment filled valleys followed by a long period of base-level drop causing incision and the well developed terraces seen today. Where the cycle is at present is not known but base-level is still considered to be dropping be it at a much reduced rate. Catchments are typically steep basins and prone to rapidly forming high episodic flows induced by intense rainfall.

2.5.3. INSTABILITY

Five large landslides were identified in the Red Hill valley listed in Table 2.2, and have impacted prominently on the valley geomorphology. The three largest landslides with volumes > 0.5×10^6 m^3 are briefly discussed.

2.5.3.1. THE V-NOTCH WEDGE FAILURE

The distinctive v-shape of the source area implies a wedge failure along distinct intersecting discontinuities. The deposit extends almost 1 km burying a substantial section of the upper Acheron rock avalanche deposit. The deposited material consists of uniform clasts sizes ranging from 20 to 40cm of greywacke from the Torlesse Supergroup. The age of the event is not known but is thought to have occurred within the last 500 years B.P. The shape and style of deposition is typical of episodic fan deposits released from narrow structurally controlled

Table 2.2: Landslides present in the Red Hill valley

LANDSLIDE (Lithology)	TYPE	SOURCE	LOCATION	DIRECTION OF FAILURE	VOLUME	RUNOUT LENGTH (Top of source scar to distal limit)	AGE
Acheron deposit (greywacke basement)	rock avalanche	east of Red Hill	2399650E, 5765620N	NE	6-9 x 10^6 m^3	3450 m	> 564 ± 56 years B.P. (NZ 547 Burrows, 1975) Probable age < 1200 years B.P. (this study)
Mt Lyndon-Bluff River rock avalanche (greywacke basement)	rock avalanche	south ridge of Mt Lyndon	2402540E, 5766140N	S	0.5-1 x 10^6 m^3	1800m	probably post-dates Acheron rock avalanche ~ 600 years B.P.
V-notch failure (greywacke basement)	wedge failure	below hill 1494	2400890E, 5766120N	S	0.5-1 x 10^6 m^3	1000m	post-dates Acheron rock avalanche. < 200 years B.P.
Landslide distal limit (greywacke basement)	probable wedge failure	above distal limit of the Acheron rock avalanche	2401635E, 5763650N	E	0.5 x 10^6 m^3	250m	post-date the Acheron rock avalanche
Terrace landslide (greywacke basement)	~	from Hill 1244m	2401630E, 5765720N	S	0.5-1 x 10^6 m^3	500m	predates the Acheron rock avalanche

gullies, rather than a more extensive rock mass collapse. However its real extent is not known and may include debris thought to be related to the Acheron rock avalanche plastered on the opposite valley wall.

2.5.3.2. BLUFF RIVER ROCK AVALANCHE

This deposit was found overlying the right margin of the arrow head shaped terrace set in the northeastern corner of the study area, hidden from view from aerial photograph by the extensive beech forest cover (refer Map 1). On this margin a series of levees were identified parallel to the watercourse draining from a northeast striking valley descending off the southwest face of Mt Lyndon. The levees vary in thickness but are typically several meters thick (maximum of 4m) and cross both levels of the arrowhead terrace set defined by the tree line. The deposit was also found on the opposite side of the Bluff River at the apex of a bend on top of a steep terrace defined by a levee depression descending in a southerly direction. Hummocky surfaces were also visible on the true left side of the river opposite the run-up deposit. It can be assume that at one time the river was temporary dammed and may have caused extensive erosion and flooding downstream. The beech forest on the debris suggests that this event occurred prior to 300 years B.P., and may reflect a seismic episode affecting the area.

2.5.3.3. THE ACHERON ROCK AVALANCHE DEPOSIT

The Acheron rock avalanche extends 3.5 km from the top of the source scar to the distal limit with a deposit volume of approximately 8-10 $x10^6$ m^3 (this study). The rock avalanche is the dominant feature within the study area covering almost the entire length of the valley. The hummocky surface and abrupt well-defined lateral margins and lobate morphology clearly define the area of the landslide. Trim lines and debris impacting against the valley sides delineate the run out path of the avalanche down the valley. A detailed investigation of the rock avalanche run out will be discussed in Chapter Four.

2.6. THE ACHERON ROCK AVLANCHE SOURCE BASIN

The largest tract of continuous outcrop in the Red Hill valley is located within the source scar of the rock avalanche. The bedrock structure of the outcrop was investigated to identify the likely defect surfaces along which the failure of the rock mass occurred.

The rock avalanche source scar is clearly identifiable in aerial photography (Fig. 2.11 bottom), and was confirmed during field reconnaissance. The scar is a small east facing cirque-shaped basin 500m east of the Red Hill (Fig. 2.11 top). The basin faces obliquely perpendicular to the main valley axis which trends southeast-northwest. Basin aspect is exposed to the traverse of the sun and both the north-westerly and easterly weather systems.

The surface geomorphology on the true left side is typical of terrain at an elevation of 1,100 m. a.s.l in the eastern Southern Alps with rounded ridgelines covered by patches of tussocks and scree with sporadic outcrops of Torlesse basement rocks. A small watercourse drains the slope below a saddle marking the margin of the basin (Fig. 2.11). In contrast, the true right side is an elevated narrow ridgeline perched above a slope of ~50° angled back into the basin in a northeast direction. The outcrops are highly fractured and blocky giving the appearance of an interlocking mass held together by gravity (refer Fig. 2.11). Extensive scree deposits dominate the mid to lower level of the basin while a series of elevated outcrops define the ridgeline. A steep descent south into the neighbouring valley is in contrast to the much smaller descent back into the basin of the source area to the northeast.

Rocks from the Torlesse Supergroup are the only rock type identified which displayed three lithotypes; massive sandstone (I) (70%), sequences of thin-bedded mudstones (II) (25%), and one section of massive mudstone (III) (5%). On the northern side of the lower basin are two dislocated blocks interpreted as wrench features formed during the release of the rock mass. These are considered to mark the maximum extent of the original insitu rock mass (See Fig. 2.11). Above the scar crest linear depressions were observed trending northwest-southeast interpreted as tension cracks probably relating to creep deformation prior to failure or post-failure relaxation effects (see Fig. 2.11 and Fig. 2.13).

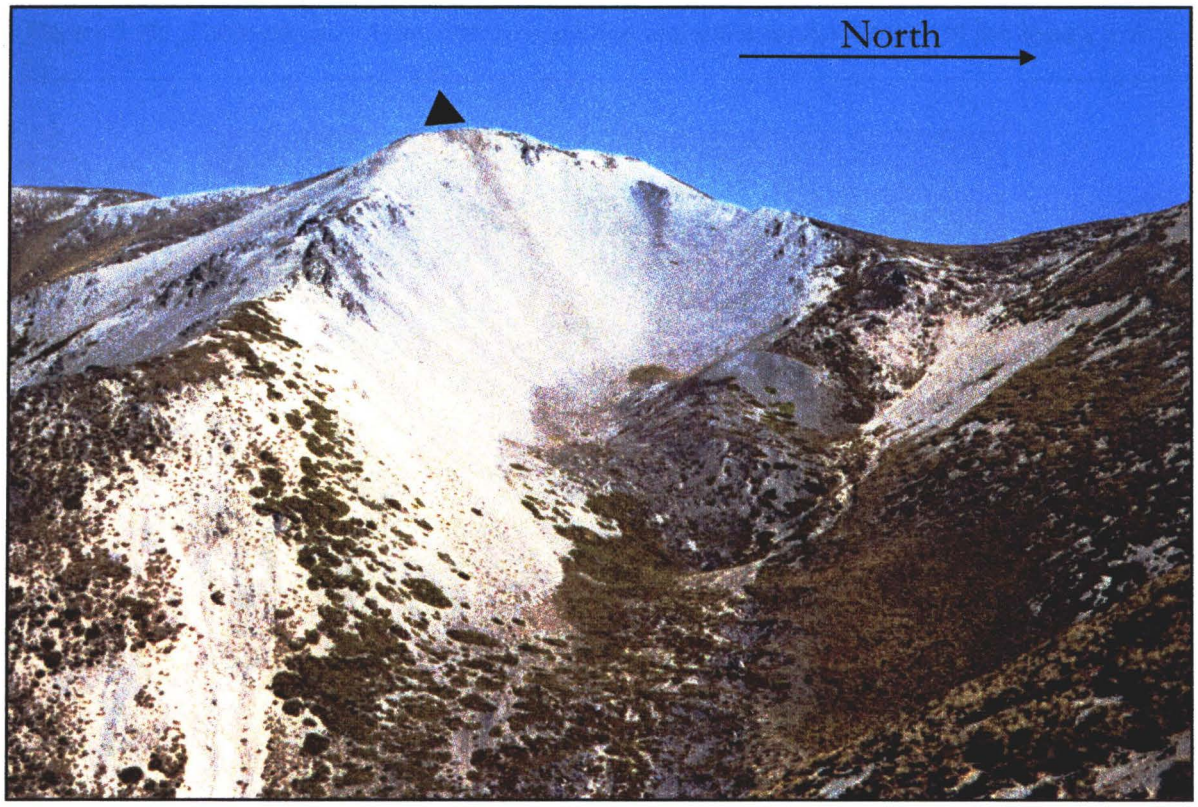

Figure 2.11: Aerial and west facing photographs of the Acheron rock avalanche source scar

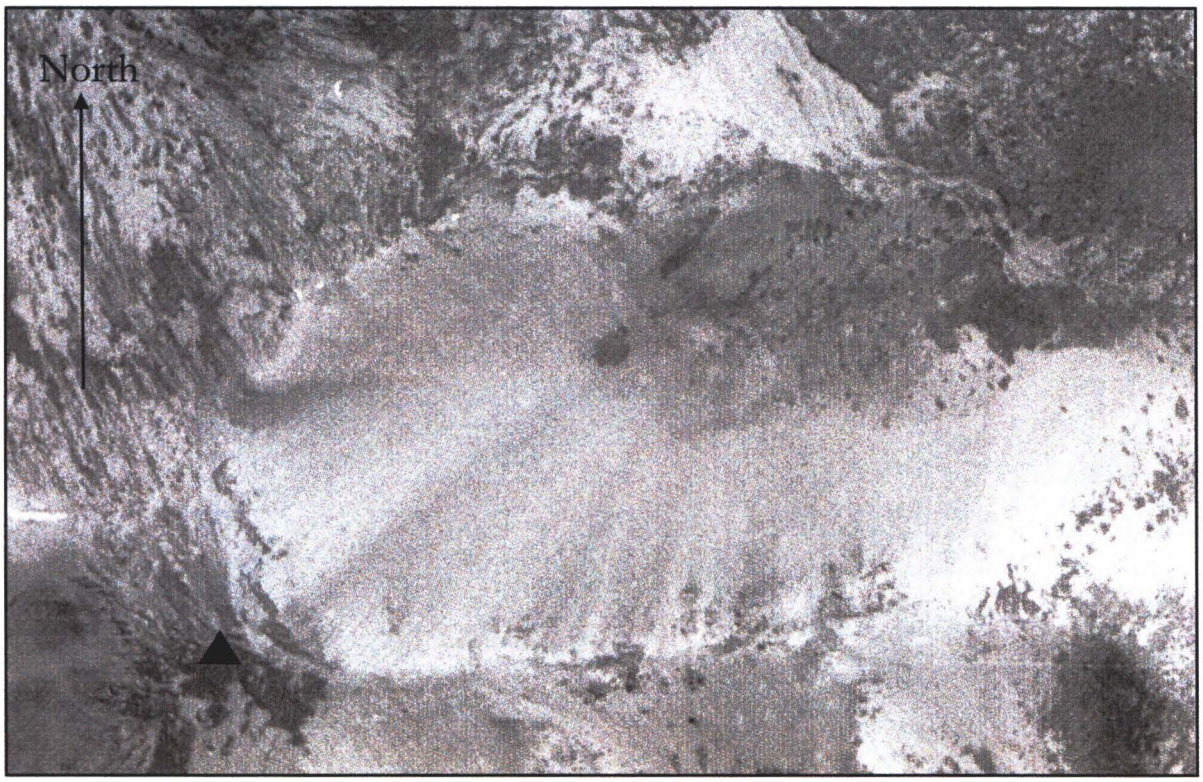

Figure 2.12: Photo-mosaic of the outcrop condition along the south ridgeline of the source scar

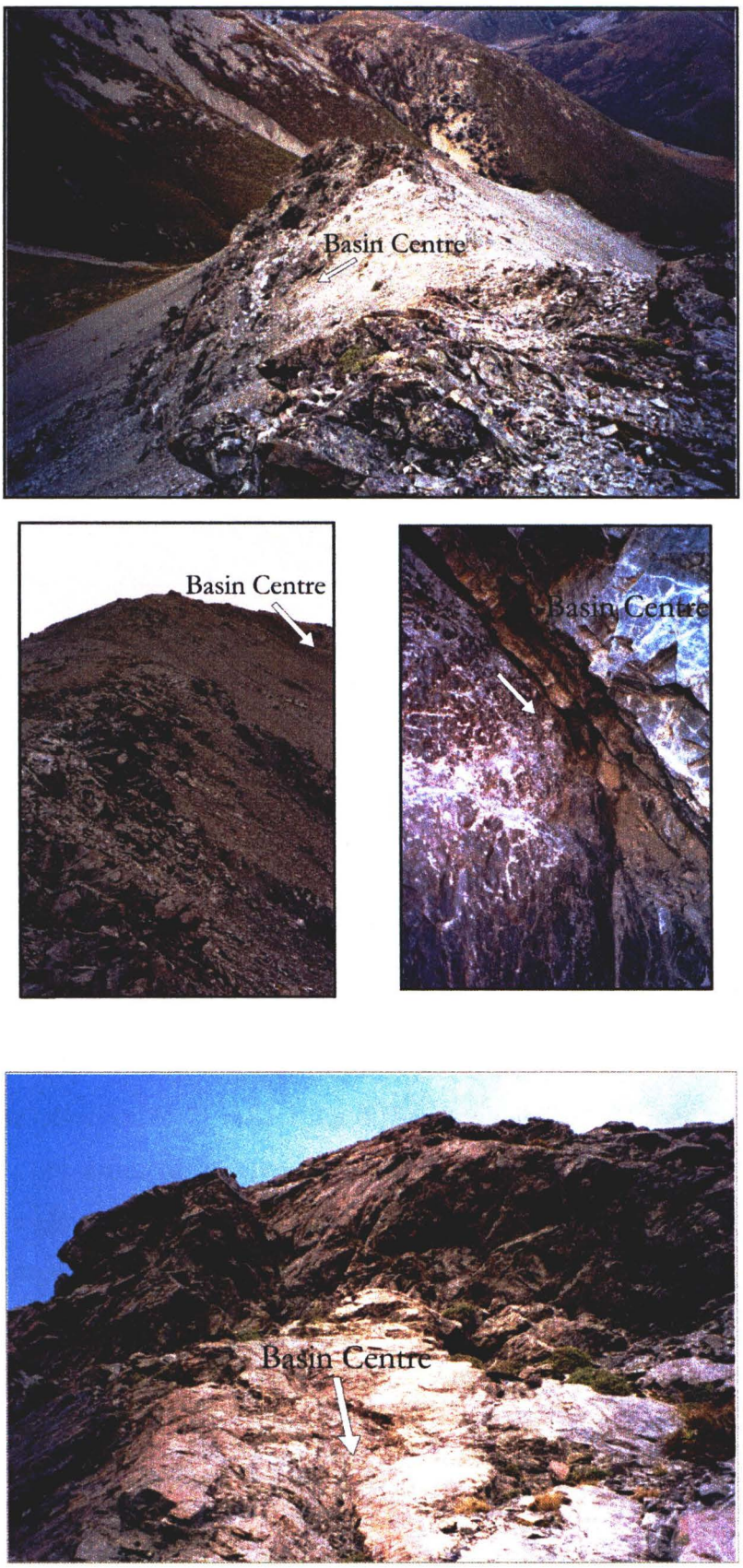

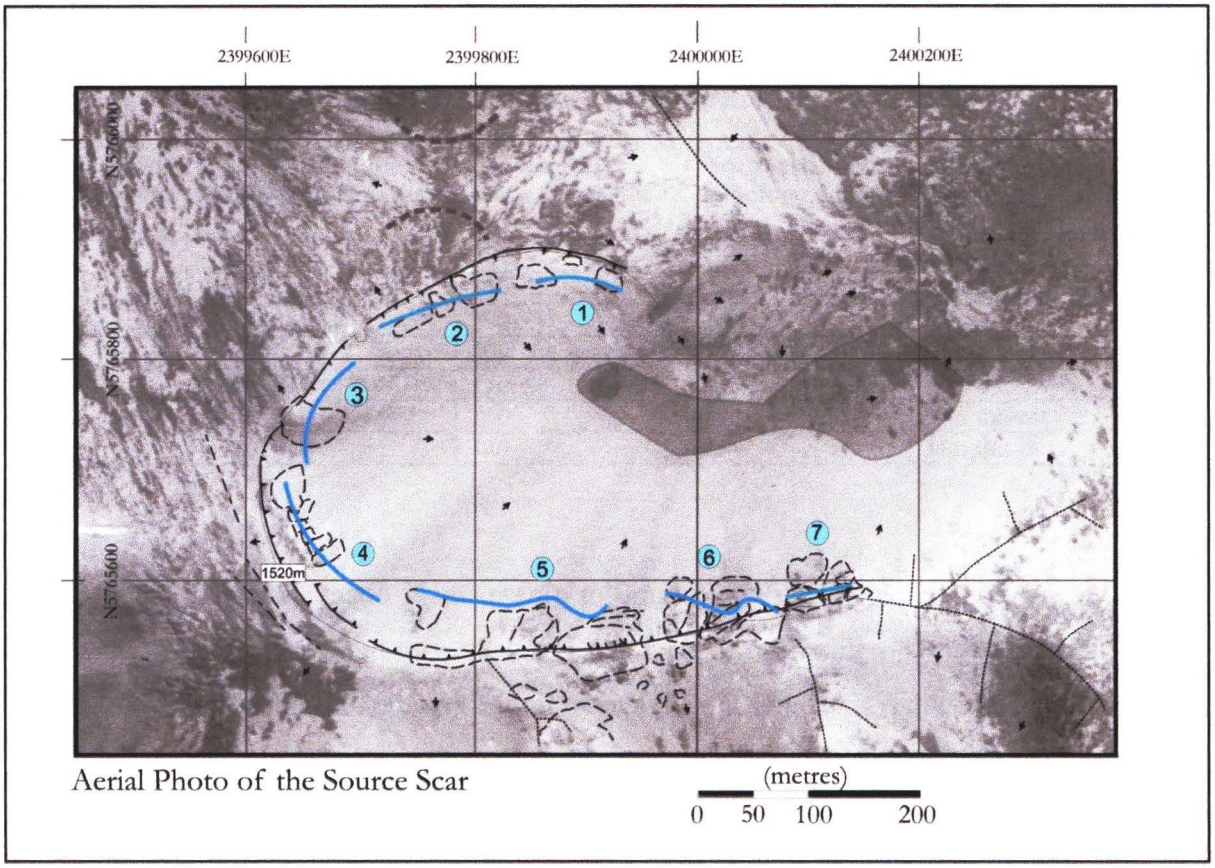

Figure 2.13: Aerial photograph of the Source Scar. The partitioning of the outcrop (outlined by the dashed lines) is identified by the numbered blue circles. In both text and tables the splitting up of the outcrop is described as either Traverse 1-7, Slope 1-7 or Section 1-7 however these all signify the same divisions as defined by the number. Tension cracks visible at the scar crest can be identified by the dash-dot lines trending NW-SE while the thin dotted lines represent ridge line topography. The black arrows show the direction of slope and the dark fill identifies the source basin floor.

The division of the outcrops (1-7) reflect the different directions of slope angle within the basin and broadly, the different lithotypes. Outcrop lithology was observed and bedding orientation, slope angle and the main joint patterns orientations were recorded. The amount of defect information able to be collected was dictated by safety. As outlined above outcrop was predominantly closely fractured massive sandstone, bounded on the down-slope side by units of thinly bedded mudstone-sandstone sequences and one section of massive mudstone north of the scar crest. Bedding was typically steep (>60°) dipping in a north direction into the basin centre and could be observed trending in an oblique line across the source scar.

Table 2.3: Table of partitioned outcrop sections within the source scar

Outcrop / Traverse	Slope orientation Dip/ Dip Direction	Slope height above basin floor (m)	No. of collected bedding / defects	Lithotypes Mss (I), thn-ms (II) and Mms (III)
1	40 / 168	50	7	Thn-ms
2	45 / 104	150	7	Mss,thn-ms
3	45 / 064	300	16	Mms
4	45 / 040	400	12	Mss thn-ms
5	50 / 037	210	11	Mss thn-ms
6	50 / 018	150	14	Mss thn-ms
7	50 / 012	130	7	Mss thn-ms

Steep unstable terrain made it unsuitable to employ scan line methods. Instead, data was collected in a sub-horizontal traverse across the base of each outcrop with particular attention given to bedding contacts and major joint planes (Fig. 2.12). This reduced the amount of data collected and the detail of representative concentrations of minor defects. Nevertheless, the objective was to identify general planes of failure, which is considered acceptable (see Appendix A.1 for defect data set and kinematic equal area stereo-plots).

74 defect and bedding orientations were collected and plotted on equal area net using the DIPS program. The contour-pole plot for all the data is displayed in Figure 2.14 which shows the distribution of poles. The largest concentration of 39 poles was around 180° representing bedding dipping steeply to the north toward the centre of the source basin for the most extensive outcrop sections 4-7. Sets were applied to five pole concentrations considered to best represent the pole distribution.

The Terzaghi weighting pole plot is also shown, however due to the terrain conditions during data collection the normal weighting was used. (Planes, pole plots and kinematic analyses can be viewed in Appendix A.1-5)

Figure 2.14: Contour and Pole plot of Defects of the Source Scar

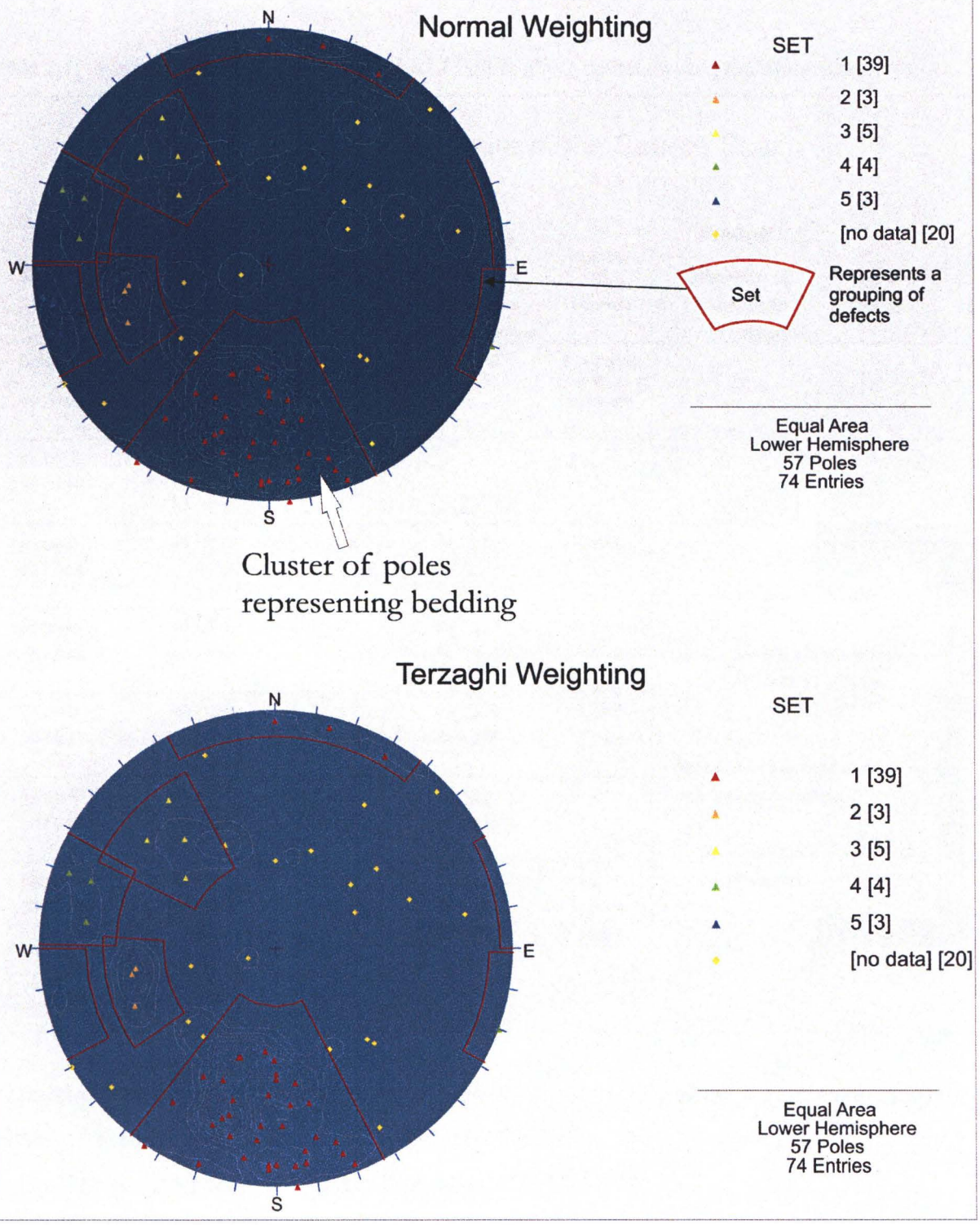

A summary of the results of the kinematic stability analysis can be seen in Table 2.4. The analysis used an equal area stereo-projection applying a friction angle of 35° to calculate instability potential for each of the 7 sections using the entire data set for each analysis. The results are based on the assumption that recorded defects were persistent within the pre-failure rock mass therefore would be reflected in the pole plot.

Table 2.4: Summary table of potential modes of failure along defects within the source scar.

Modes of Failure in the Source Scar

	Slope Traverse	Planar Orientation of Failure Plane *Dip / Dip direction*	Number of Planes	Toppling Orientation of Failure Plane *Dip / Dip direction*	Number of Planes	Wedge Orientation of Failure Plane *Dip / Dip direction*	Number of Planes
1	Slope 1	~		86 / 340	1 bedding	~	
	40 / 168	~	0	~	8 potential	~	0
		~		~		~	
2	Slope 2	~		~		~	
	45 / 104	~	0	~	0	~	0
		~		~		~	
3	Slope 3	40 / 050	1 joint	84 / 226	1 joint		**45 / 075**
	45 / 064	~		~		51 / 077	1 joint
		~		~		77 / 106	1 joint
4	Slope 4	40 / 045	2 joint	82 / 210	1 joint		
	45 / 040	[average]		84 / 226	1 joint	Sliding initiates on line of intersection	
		~		~		*Trend*	*Plunge*
5	Slope 5	40 / 020	2 joint	82 / 210	1 joint	026°	38°
	50 / 037	40 / 045	2 joint	84 / 226	1 joint		
		[average]		~		Wedge failure may occur between	
6	Slope 6	40 / 007	5 joint	82 / 210	1 joint	the following orientations:	
	50 / 018	[average]	1 bedding	85 / 180	1 joint		
		~		85 / 194	1 joint	*Dip directions:*	012° - 075°
7	Slope 7	42 / 003	3 joint	82 / 210	1 joint	*Slope angles:*	55° - 90°
	50 / 012	[average]	1 bedding	85 / 194	1 joint		
		~		85 / 180	1 joint		**50 / 012**

Friction Angle - 35° Ø

Potential planar failure was shown to exist between slopes 3 to 7 along a moderately dipping surface of between 40°/ 050° to 40°/ 003° into the basin centre. Toppling failure potential could occur along all sections except slope 2 (45° / 104°) (Table 2.4).

Slope 1 (40° / 168°) on the northern ridge line had the potential for failure along a plane 86°/ 340° which was analogous to bedding. If the friction angle was reduced below 35° to 30° then a tight cluster of eight poles would also be included in the potential zone for topple failure (see Appendix A.4). Slopes 3-7 all displayed toppling potential, with a number of poles in the potential zone of instability increasing progressively east along the south ridge. Typical defect orientations include 82°-85° / 180°-226°. Wedge failure could occur between sections 3-section 7 if the slope angles at the time of failure was between 55°-90°. Failure would occur along a line of intersection of 026°(Trend) / 38° (Plunge) in that order which is within the preferred oblique orientation for failure of 000°-090° as defined by the source scar profile.

2.6.1. INTERPRETATION

The bedrock structure trends obliquely southwest-northeast across the present day basin axis with a southerly younging direction. The main outcrop is located along the southern, east trending ridgeline, the central crown and north of the massive mudstone unit (sections 3-7 see Fig. 2.11, Fig. 2.12). It is reasonable to assume that the rock mass failed in a direction between 000° and 090° perpendicular to the strike of the bedding. The dominant failure plane is thought to be the steeply dipping thin argillite layers (10 to 40cm in thickness). Intersection of bedding with the opposite south dipping toppling planes and the shallow dipping planar orientations could provide a potential failure assemblage if the inherent shear strength was exceeded and the defects were persistent. The development of this system may occur naturally over time as a result of gravity loading within the rock mass, thus causing fracture growth particularly if the rock mass was over-steepened from post glacial processes. Fracture growth could also be accelerated by regular small magnitude earthquake events (M <6) resulting in fatiguing of the defect cohesion and increasing dilation, which reduces the shear strength of asperities (Erismann and Abele, 2001). If the shear strength of the dominant planes was sufficiently weakened overtime then strong motion from a larger earthquake could give the impetus to shear bonds and trigger the rock mass to fail along the pre-existing defect pattern. It is noted that a potential problem associated with this analysis is the gauging of the effect of relaxation fracturing of the scar immediately after the collapse. This could cause the defects measured during this study to be post-failure structure effects rather than the pre-failure conditions within the rock mass.

2.7. SUMMARY

The dominant outcrop within the Red Hill valley is greywacke sandstone-mudstone sequences. A small outlier of Tertiary marine sediments thought to be derived from the Oligocene age Porter group was found on the south-western termination of a prominent 1.2 km scarp of the Porters Pass Fault.

Only one Holocene active fault, the Porters Pass Fault, crosses the field area. Previous studies suggested that the offset of prominent scarps at the margins of the valley were absorbed by a 700m southeast jog of the fault line with the Red Hill valley. During this study geomorphic evidence suggests that the fault may cross the valley more obliquely possibly in response to a series of overlapping bends.

Five prominent landslides were identified within the valley with three deposits; the V-Notch, Bluff River Rock avalanche and the Acheron rock avalanche all exceeding 0.5 x 10^6 m^3 in volume. This indicates that the Red Hill valley is prone to large-scale rock slope instability.

The terrace stratigraphy represents glacio-fluvial gravels derived most probably during the Bayfield Advances predating 19,000 years B.P. It is probable that minor glaciers existed within the valley forming a sediment train resulting in valley aggradation. The remaining stratigraphy represents changes in the depositional system from short-term fluvial to minor fluvial sequences terminating in topsoil. The Acheron rock avalanche deposition has overlain these terrace surfaces (see Map1).

A defect analysis suggests that the outcrop within the source showed potential for both topple and planar failures assuming that the present defects are analogues to the conditions that existed prior to failure of the rock mass. It is likely that direct failure occurred along the weaker argillite and sandstone bedding contacts in combination with persistent steep south dipping and shallow north angled defects.

CHAPTER THREE

THE MECHANISMS AND MORPHOLOGY OF ROCK AVALANCHES

3.1 INTRODUCTION AND NOMENCLATURE

Chapter three introduces the landslide classification term of rock avalanche and gives a commentary on its characteristics including causative factors. Previously published research on the mechanism driving the phenomenon is then reviewed. Definitions from Fell, et al. (2001) will be used in this study as follows.

- Source is the space between the failure surface and the original rock mass.
- The route across the topographic surface taken by the debris below the source area is called the path.
- Run out refers to the distance between the toe of the source and the toe of the deposit.
- The term Travel Distance or Fahrböschung is the linear distance between the uppermost tip of the failure surface and the furthermost point of the debris (L).
- The Travel Distance Angle (Ø) is obtained using the equation $\tan^{-1}$ (F= H/L).
- Excessive Travel Distance (Le) is based on the equation outlined in Hsu (1975), Le = L-H / (tan 32°) where 32° is the angle of repose of broken rock.

3.2 DEFINITION OF THE TERM ROCK AVALANCHE

In 1881 Albert Heim observed the aftermath of the Elm rock avalanche. This event destroyed half the town of Elm and obliterated the hamlet of Untertal with a loss of life of 115 inhabitants (Hsu 1978; Voight, 1978). Using eyewitness accounts and observing the morphology of the debris, Heim was able to conclude that the rock flowed as a semi-coherent mass at considerable speeds, rather than by the accepted process of rock sliding (Hsu in Voight, 1978). In Hsu's biographical introduction about Heim he highlights Heim's conclusion from his famous 1881 report on the event which stated, "*rock falls did not slide,*

they crashed, and their debris flowed", a statement which Heim transformed into words forming the German term of Sturzstrom (rock fall-stream) to describe this phenomenon of rapid long run out (Buss and Heim, 1881 in Hsu, 1978; Voight, 1978).

The comparative English language term of "rock avalanche" was first used by McConnell and Brock (1904) during the investigation of the Frank slide in Alberta, Canada, which claimed 130 lives and has since become a common term describing the process (Evans, et al. 1989). However it is often replaced by the description of "rockfall-debris avalanche" from the widely applied classification scheme of Varnes (1978), creating ambiguities in assigning descriptions of the landslide properties (refer Table. 3.1; Fell, et al. 2001). This is exacerbated by the two differing approaches of the North American (Varnes, 1978; Cruden and Varnes, 1996) and the English (Hutchinson, 1988) schemes creating a problem for a universal working definition.

TABLE 3.1: Summary table of Cruden and Varnes (1996) landslide classification scheme

TYPE OF MOVEMENT	TYPE OF MATERIAL	ENGINEERING SOILS	
		PREDOMINANTLY	PREDOMINANTLY
	BEDROCK	COARSE	FINE
Fall	Rock fall	Debris fall	Earth fall
Topple	Rock topple	Debris topple	Earth topple
Slides - rotational	Rock slump	Debris slump	Earth slump
- translational	Rock block slide	Debris block slide	Earth block slide
	Rock slide	Debris slide	Earth slide
Lateral spreads	Rock spread	Debris spread	Earth spread
Flow	Rock flow (deep creep)	Debris flow	Earth flow (soil creep)
Complex	Combination of two or more principal types of movements		

The landslide classification schemes of Varnes (1978; 1996; see Table 3.1) and Hutchinson (1965; 1988; see Table 3.2) are the most widely accepted in the English-speaking world with both applying terms already established in the field, however both are slightly varied in their definitions and terminology (Hungr et al. 2001).

In literature, Varnes (1978) landslide classification scheme is the most prevalent and classifies a rock avalanches as a complex style of mass movement called *rock fall / rock slide-debris avalanche*. Varnes recognised that the rock avalanching process differs from the initial

failure process by applying a classification of complex and the application of two descriptor terms. However, this fails to adequately imply diagnostic factors such as the large volume of bedrock that fails or the range of styles of the initial failure movements (refer Table. 3.1).

TABLE 3.2: Abbreviated classification scheme suggested by Hutchinson (1988)

Table 2. Abbreviated classification of landslides suggested by Hutchinson, 1988 in Dikau 1996

A.	Rebound	
B.	Creep	
C.	Sagging of mountain slopes	
D.	Landslides	
	1	Confined failures
	2	Rotational failures
	3	Compound failures
	4	Translational failures
E.	Debris movements of flow-like form	
	1	Mudslides
	2	Flow slides
	3	Debris flows
	4	**Rock avalanches / Sturzstrom**
F.	Topples	
G.	Falls	
H.	Complex slope movements	

Comparatively, Hutchinson, categorised rock avalanching as "*debris movements of a flow like form*" and labelled the process with the German term describing rock avalanche of Sturzstrom (rock fall-stream)(Heim 1932, Hsu, 1978, Hutchinson, 1988 p 18; Hungr, et al. 2001). The use of Sturzstrom is considered synonymous with the definition of rock avalanche (Hungr et al. 2001). Hutchinson states that the Sturzstrom process can form by either the rock falling, sliding or toppling (1988), yet a direct linkage between all three forms of mass movement to Sturzstrom does not exist within the classification scheme limiting the clarity of the meaning (refer Table 3.2, Hungr, 2001).

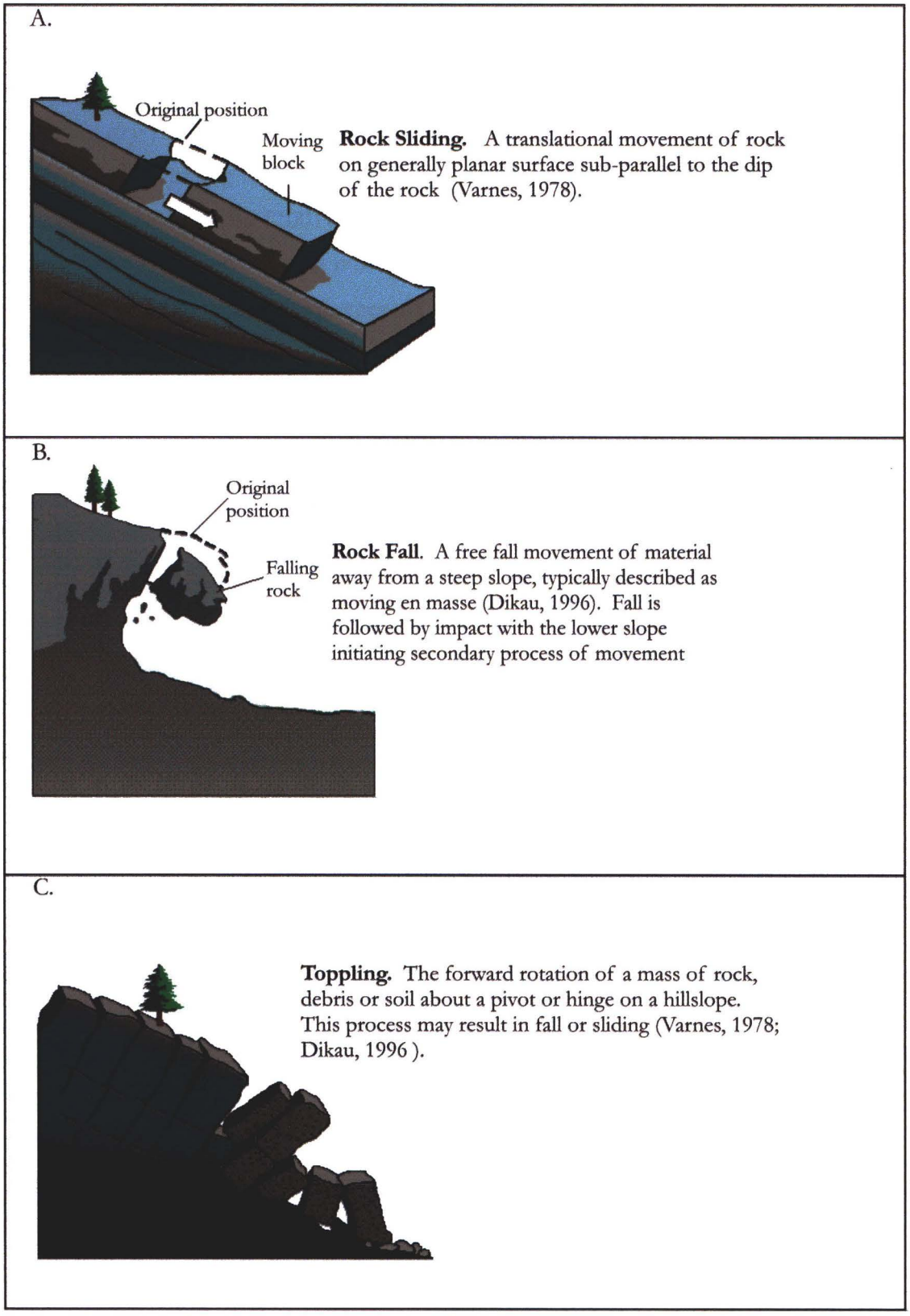

Figure 3.1 A-C: Model definitions of rock sliding, rock fall and toppling mechanisms of bedrock rock failure leading to rock avalanches

In literature reviewed during this study the two following definitions are most representative. Angeli et al. (1996) defines a rock avalanche based on the work of Hsu (1975), as "...a *large bulk of mostly dry rock debris deriving from the collapse of a slope or cliff and moving at high velocity and for a long distance, even on gentle slopes*" (Hsu, 1975; Angeli, 1996). This was advanced by Hungr et al. (2001) who proposed further modifications to clarify flow type landslides which they identify as the most hazardous landslide type, however lacked adequate detail in both the classification schemes of Cruden and Varnes, (1996) and Hutchinson, (1988). They proposed the formalisation that a rock avalanche is not derived from reactivated debris but instead forms following large-scale bedrock failure by either rock sliding or rock fall which are typical slope failure mechanisms (see Fig. 3.1.A-B for slope failure mechanisms) "*A rock avalanche is an extremely rapid, massive, flow-like motion of fragmented rock from a large rock slide or rock fall*" (see Table 3.3 Hungr et al., 2001).

The importance of clarification relates to the correct description of what a rock avalanche actually is (Dikau et al. 1996). A rock avalanche is not derived from previously deposited debris being remobilized as is inferred by Varnes "*rock fall / rock slide-debris avalanche*" (Cruden and Varnes, 1996), rather from a large relatively intact rock mass of no less than 1 x 10^6 m^3 (Whitehouse and Griffiths, 1983). Failure generally occurs along pre-existing defects, a process referred to by Davies and McSaveney (2002) as collapse. The immediate post-collapse transformation within the semi-coherent rock mass resulting in fragmentation, extremely high velocities and long runout distance if unimpeded by obstacles is what is referred to as a rock avalanche.

Interestingly, both Angeli et al. (1996) and Hungr et al. (2001) exclude the effect of toppling and creep process, such as Sackung or mountain sag leading to large failure which is a documented cause of rock avalanches in Japan and Italy (Fig. 3.1.C., Chiraga, 1998; Nicoletti, 1991). This mechanism commonly occurs in granitic and gneissic rocks and less frequently in metasedimentary rocks (greywacke) such as those of the Acheron deposit (Hutchinson, 1988; Nicoletti, 1991). A reason for the absence may relate to topple being supplanted by rock falling or rock sliding of the rock mass (Dikau, 1996). However, it is a process which Prebble (2001) identified as having a profound influence on mountain range collapse in the Southern Alps. For this study the definition proposed by Hungr et al. (2001), including the use of the term "rock avalanche" rather than Sturzstrom will be applied (refer Table 3.3).

TABLE 3.3: Suggested amendments to the classification of flow type mass movements (Hungr et al. 2001)

CLASSIFICATION OF LANDSLIDES OF THE FLOW TYPE				
MATERIAL	WATER CONTENT	SPECIAL CONDITION	VELOCITY	NAME
Silt, Sand, Gravel, Debris (talus)	Dry, moist or saturated	No excess pore-pressure, limited volume	Various	Non-liquefied sand (silt, gravel, debris) flow
Silt, Sand, Debris, Weak rock	Saturated at rupture surface content	Liquefiable material, Constant water content	Ex. Rapid	Sand (silt, debris, rock) Flow slide
Sensitive clay	at or above liquid liquid limit	Liquefaction *in situ* , Constant water content	Ex. Rapid	Clay flow slide
Peat	Saturated	excess pore-pressure	Slow to very rapid	Peat flow
Clay or Earth	Near plastic limit	Slow movements, plug flow (sliding)	< Rapid	Earth flow
Debris	Saturated	established channel, increased water content	Ex. Rapid	Debris Flow
Mud	At or above liquid limit	Fine grained debris flow	> Very Rapid	Mud flow
Debris	Free water present	flood	Ex. Rapid	Debris flood
Debris	Partly or fully saturated	No established channel, Relatively shallow, steep source	Ex. Rapid	Debris avalanche
Fragmented Rock	**Various, mainly dry**	**intact rock at source, Large volumes**	**Ex. Rapid**	**Rock avalanche**

Another descriptive factor appropriate for rock avalanches and not considered in earlier classification schemes is the introduction of a human response term to a velocity parameter called Probable Destructive Significance (Cruden and Varnes, 1996; in Fell et al. 2001). This concept has a similarity to the Modified Mercalli Intensity scale applied to seismic hazard assessments. While it is recognised that the velocity classes give poor division of landslide type, Hungr et al. (2001) suggested that velocity is the most important measure of hazard intensity to people. The modified Table 3.4 illustrates the vulnerability of people to the advent of a rock avalanche (class 7 extremely rapid) which rates the ability for human response to the advent of a rock avalanche as nil (Fell et al. 2001).

TABLE 3.4. Terms describing the velocity of a landslide and probable human response (Cruden and Varnes, 1996 in Fell et al. 2001)

Velocity Class	Description	Velocity) (mm / sec)	Typical Velocity	Human Response
7	Extremely Rapid	$5x10^{3}$	5m / sec	Nil
6	Very Rapid	$5x10^{1}$	3m / sec	Nil
5	Rapid	5×10^{-1}	1.8 m / hr	Evacuation
4	Moderate	5×10^{-3}	13m / month	Evacuation
3	Slow	5×10^{-5}	1.6 m / year	Maintenance
2	Very Slow	5×10^{-7}	16 mm / year	Maintenance
1	Extremely Slow			

Based on the description proposed by Hungr et al. (2001) the preferred definition of a rock avalanche for this study is as follows "*A rock avalanche is an extremely rapid, massive, mobile, flow-like motion of fragmented rock derived directly from a large bedrock failure from either rock slide / rock fall or a combination of either and toppling*" (Hungr et al. 2001).

3.3. DIAGNOSTIC CHARACTERISTICS OF ROCK AVALANCHES

Rock avalanches are found in collision zones of tectonically active mountainous regions such as the Andean mountains of South America, Russia's Caucasian mountains, the Southern Alps of New Zealand, the European Alps, and the Himalayas, the mountains of Japan, the Sierra Nevada and Rockies of North America and Alaska (Voight, 1978; Hungr et al. 2001, P.235). Originating from an elevated bedrock source above a valley floor they form following the detachment of a large relatively intact bedrock section exceeding 1 x 10^6 m^3 by either topple, slide, or fall movement (Hsu, 1975).

The rock avalanche process exhibits characteristics which distinguish it from other forms of landslide and types of flow. The mass volume is large and dry, and displays high mobility and extremely rapid velocity (Varnes and Cruden, 1996; Hungr et al. 2001). These properties enable the debris to travel over longer distances than that of normal rock fall or rock slide deposits typically defined as the 32° or the angle of repose for a broken rock (Heim, 1932 in Hsu, 1975; Melosh, 1987; Angeli et al. 1996). Velocities can exceed 20m / second enabling the mass to overrun topographic and man-made obstacles in the run out path, and reach heights of super elevation where deflected or impeded by valley sides. The run out time lasts only several minutes, and initiation can occur without warning which represents a significant hazard if people or communities are in the path (Hungr et al. 2001). The distance travelled, if not impeded, is typically several kilometres in length and can cover an area exceeding 100 000 m^2. Volumes of debris generally exceed that of the original source mass due to entrainment of surface material on the run out path, and dilation of the rock mass during collapse and fragmentation (Angeli et al. 1996). Scale factors of 4/3 and 20% are considered in literature to represent dilation and entrainment of the debris though how this was calculated was not apparent to this author (Nicoletti, 1991; Evans et al. 2001; Erismann and Abele, 2001). Slope angle does not appear to influence run out as long run out can occur on low angle surfaces which may reflect the driving mechanisms (Nicoletti and Sorriso-Valvo, 1991).

The deposit surface morphology typically displays lateral and transverse ridges, which Eisbacher (1984) interprets to represent sliding in the final stages of motion, and steep margins attesting to the sudden termination of the motion. Internally the rock avalanche is highly fragmented, displaying a basic inverse grading with a surface veneer of angular blocks

overlying progressively pulverised clasts and coarse silty sand material at the base (Mitchell et al. 2001).

The motion of run out is described as a semi-coherent flowing mass resulting in the preservation of internal vertical stratigraphic ordering, called the jig-saw effect which was described by Heim (Eisbacher and Clague, 1984; Hungr et al. 2001). This is often compared to a viscous liquid in scale models however recent work conducted by Davies and McSaveney (2002) on the effects of fragmentation-induced lateral earth pressures within a moving rock avalanche have suggested that an analogy with heavy vapour under positive pressure is more appropriate.

Typically lithology is regarded to be limited to granitic and gneissic rocks, massive sandstones and conglomerates (Whitehouse and Griffith, 1983; Eisbacher and Clague, 1984; Angeli et al. 1996; Hermanns et al. 1999). Hungr et al. (2001) suggests that rock avalanches can occur in most types of rock including pyroclastics if the scale of rock mass detachment is large enough. The main requirement is the presence of prominent defect patterns or closed fracture pattern which allows a large rock mass to be released as a relatively coherent block (McSaveney 1978; Eisbacher and Clague, 1984; Hungr et al. 2001).

3.4. STATISTICAL RELATIONSHIPS

Certain numerical relationships have been shown to exist between volume and distance travelled from source, with larger events $\geq 5 \times 10^6$ m^3 displaying greater mobility. This relationship is referred to in the literature as the size effect (Davies, 1982; Erismann and Abele, 2001; Hungr et. al. 2001). One of the most famous parameters in this relationship is the Fahrböschung or travel angle which is measured from the uppermost tip of the source scar to the furthest point of the distal deposit (see Fig. 3.2). Heim, who developed the term, noted that the travel angle, if slide motion were solely controlled by frictional forces, would equal the mean friction angle called the equivalent coefficient of friction. This angle has been shown to decrease with increasing size of the event, and is represented using a log–log plot in Fig 3.3 (Scheidegger, 1973; Evans et al. 1989; Fell et al. 2001).

Figure 3.2: Longitudinal cross-section of a rock avalanche deposit showing features described in text and used in the calculation of dimensions, mobility and velocity (adapted from Hewitt, 2002. Fig. 9, p 355).

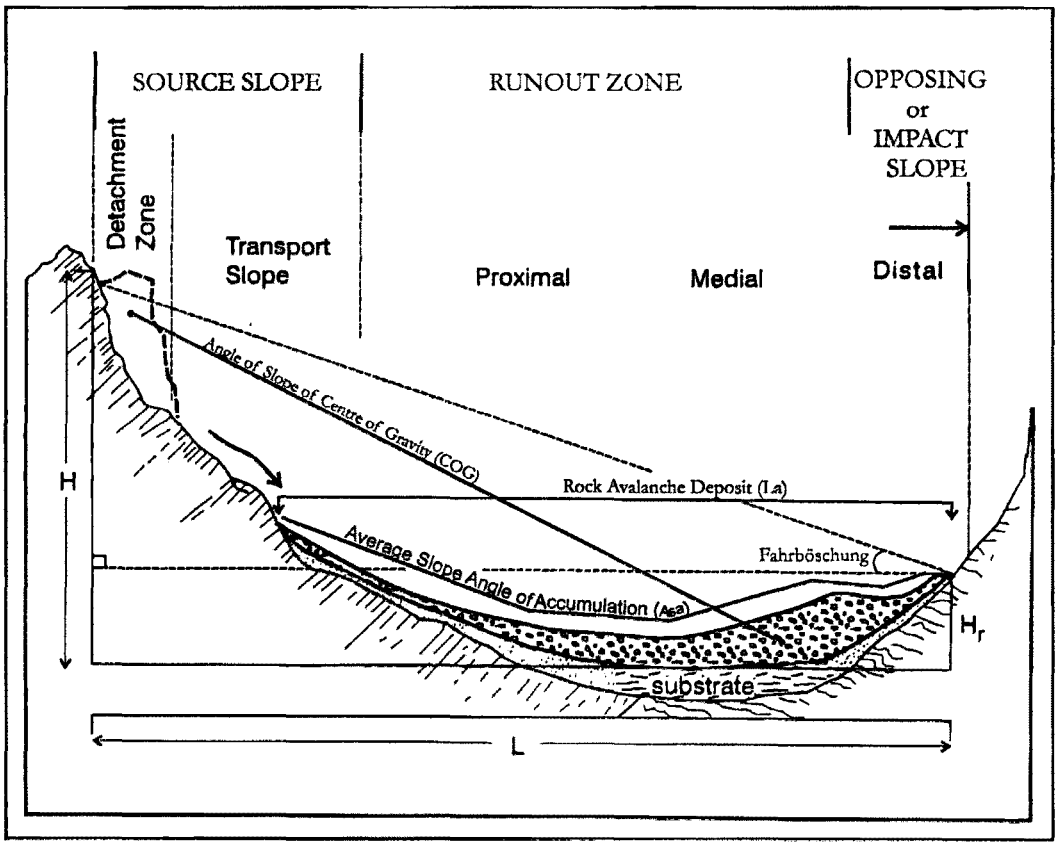

- H is the vertical distance between highest point of detachment and lowest reach of debris.
- Hr is the runup height,
- L is the maximum horizontal travel distance,
- La is the horizontal length of the debris accumulation zone,
- Asa is the average slope angle of the accumulation zone,
- COG slope angle of the line linking the centre of gravity of the rock mass and the centre of gravity of the debris,

- *Fahrböschung* is the slope angle from the highest point of the source scar to the furthest distal extent traveled by the debris,

The tangent of the *Fahrböschung* results in the coefficient of friction in the equation of excessive runout (Le) in Hsu (1975)and F in Fig. 3.3 and 3.4

Figure 3.3: Relationship between F (tan θ) and V (volume) for rock avalanches in the Canadian Cordillera compared with the Acheron rock avalanche.

The Scheidegger relation is plotted to assess comparability

Adapted from Evans and Hungr, (1989 p 444)

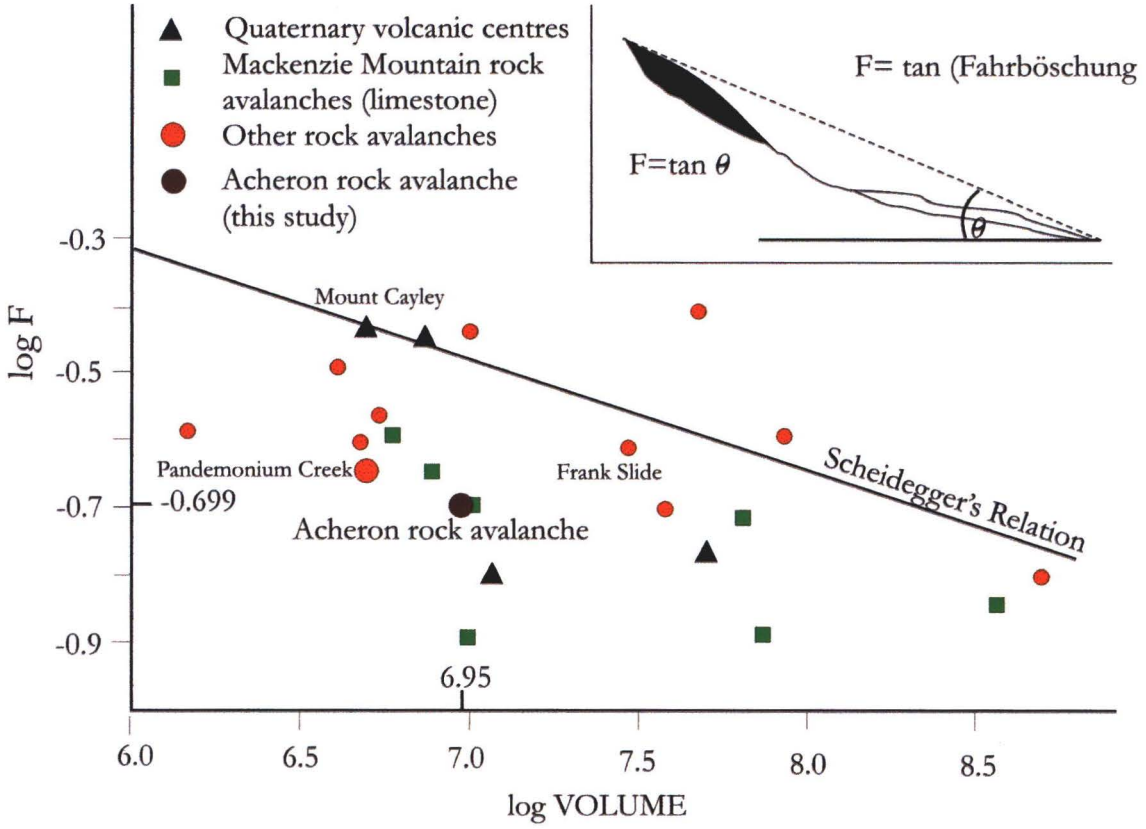

Figure 3.4: Graph of volume plotted against F(tangent of the travel angle). This demonstrates that as the volume of the landslide material increases, the tangent of the *Fahrböschung* (F) or travel angle decreases regardless of landslide type, size or mechanism driving the run out.

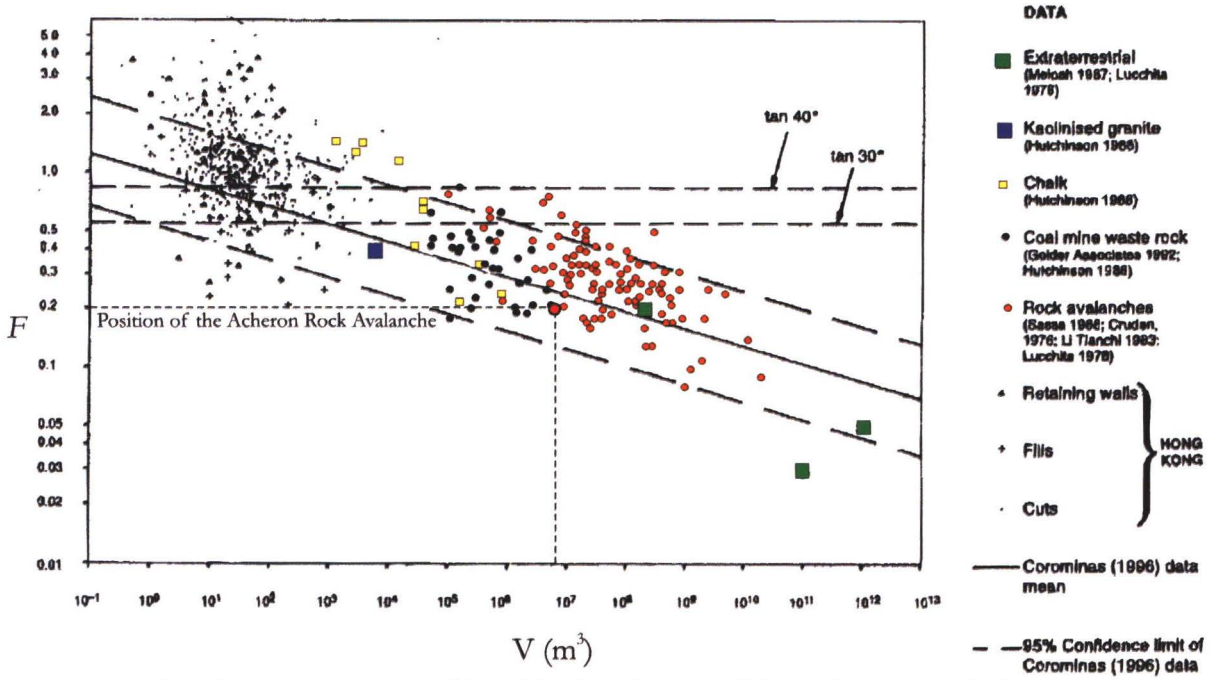

F = tan (travel angle) = tanϕ_a for landslides which break-up on sliding (Finlay et al 1999)

Hsu (1975), however, questioned the use of the equivalent coefficient of friction as a mobility indicator. He argued that the dynamic friction angle of broken rock of 32° should remain. Hsu (1975) developed the term "excessive travel distance" which could be shown to increase with increasing volume (Fell et al. 2001). Simply, the length of the horizontal line outside the 32° angle for typical fall of dry broken rock is the excessive travel distance or Le (Hsu, 1975; Fell et al. 2001). The Fahrböschung is still applied in literature because it gives simple determinations, even if debris is missing or volume estimates are inaccurate (Erismann and Abele, 2001).

Corominas (1996) attempted to clarify disagreements on the application of indices to represent landslide mobility or the ability to travel at high velocities over long distances beyond the fall slope of the rock mass. Using plots and regression equations for 204 landslides of different classes, Corominas found that regardless of the landslide size or the driving mechanism of run out, all landslides experienced a reduction in the angle of reach or the Fahrböschung (increase of run out relative to fall height) as the volume increases (see Fig. 3.4). This suggests the process is not solely unique to rock avalanches, and is represented by all classes of landslide (Fell et al. 2001). Corominas (1996) was able to confirmed Heim's application of the Fahrböschung or travel angle as a measure of the relative mobility of the rock avalanche, and verified its sensitivity to volume. Interestingly he suggests that fall height was found not to be a relevant factor. This was supported by Davies (1982), who observed from model experiments conducted by Hsu (1975) that fall height did not affect motion or extent, and suggested that fall heights actually exasperated scatter which typically accompanies rock avalanche behaviour plots. Davies (1982) instead favoured a relationship between deposit lengths against deposit volume, but this was designed for a deposit exceeding 10^7 m^3 and therefore is not applicable to this study.

Rock fall experiments conducted in Japan by Okura et al. (2000), using granite blocks falling on a granite path, demonstrated that a correlation did exist between rock fall volume and the run out distance. The long run out resulted from the increased opportunity for block to block impact, forcing the blocks at the front of the mass to extend further (Okura et al. 2000). Comparatively, run out of the centre of gravity (C.O.G.) of the mass reduced with increased volume. The reduction was assumed to be caused by increased impacts associated with the enlarged volumes. This occurred particularly rearward from the front of the mass, causing faster dispersion of the internal kinetic energy resulting in the C.O.G. being closer to the

fall slope (Okura et al. 2000). Acceleration of the front blocks and deceleration of the rear blocks due to collision also maintained the sequential order of the pre-failure mass (Okura et al. 2000). These results seem analogous to the conclusions of Davies et al. (1999) concerning fragmenting granular avalanches where proliferation of dispersive stress caused amplified spreading and runout, but increased deposition thickness in the proximal areas.

Davies and McSaveney (1999) importantly pointed out that it is unlikely that material from the top of the source rock mass would reach the distal limit of the debris, so within the debris body exists materials of different travel lengths and coefficients of friction. The result of this is that the coefficients of friction would not correlate easily to the differing static, dynamic basal or internal friction within the mass (Davies and McSaveney, 1999). Davies and McSaveney (1999) chose to normalise fall height, length and volume ratios and interpreted a size effect occurring at volumes less than $10^5 m^3$ and at greater than $10^7 m^3$. They interpreted this as a transition between the two volumes which was the result of rock fragmentation driving the mass. This suggested that the onset of fragmenting-induced long runout occurred at $\geq 1x10^6 m^3$.

For the purpose of this study the excessive travel distance equation of Hsu (1975) will be used. This equation gave the maximum runout distance in a runout prediction study conducted in Italy and features prominently in present day rock avalanche research (Nicoletti, 1991, Govi et al. 2002).

3.5. INFLUENCE OF PATH ON LONG RUNOUT

Large scatter in all numerical comparisons of volume and distance was considered to be partially the effect of the individual runout path (Davies, 1982; Corominas, 1996; Fell et al. 2001). The debris surface morphology, the distal rims and basal material show the interactions of the topography with the moving mass (Cruden, 1985 in Hewitt, 2002 p355). Nicoletti and Sorriso-Valvo (1991) attempted to categorise site specific morphological controls on rock avalanche motion by looking at deposit shape to identify any predictable patterns. Investigating 40 rock avalanche deposits, they were able to classify rock avalanche deposits into three types as shown in Fig 3.5. (from Nicoletti and Sorriso-Valvo, 1991).

Figure 3.5: Diagrams illustrate the three shape configurations that a rock avalanche can form as a result of geomorphic control of the run out path as defined by Nicoletti and Sorriso-Valvo, (1991).

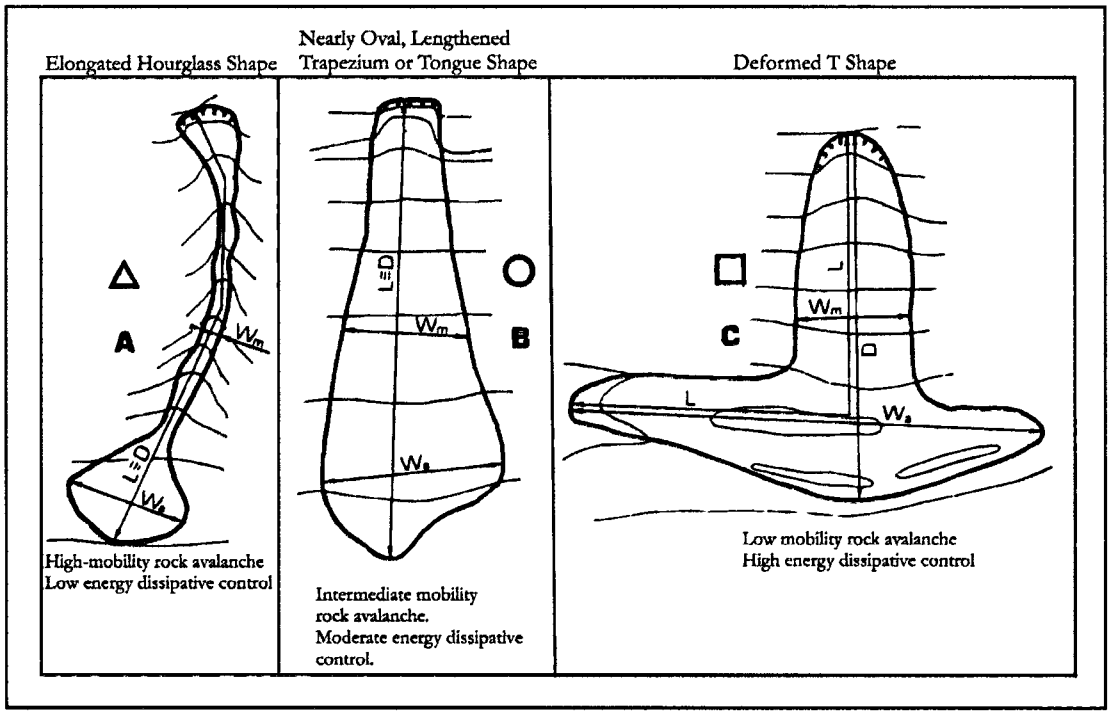

Figure 3.5 A. B. C: The three configurations that a rock avalanche can form as a result of geomorphic control of the runout path(From Nicoletti and Sorriso-Valvo, 1991).

L is the length of overall runout measured from the top most point of the head scarp to the farthest end of the deposit.

D is the length of the rock avalanche measured horizontally.
This will equal L in A and B situations but will be different in cases of C.

H is the elevation difference between the end points of line L.

W_m is the width of rock avalanche measured horizontally at D/2.

W_a is the horizontal component of the maximum width of the deposit zone.

Wm / Wa, Wm / L Wm /D, Wa / L, and Wa / D are indices that describe the rock avalanche shape (refer to Nicoletti and Sorriso-Valvo, 1991).

The first is an elongated hour glass shape model, typified by an amphitheatre fashioned source scar, narrow valleys which channel the debris mass and a widening valley in the distal area. This type, referred to as *A*, represents high mobility with low energy dispersion resulting from few obstacles in the runout path such as opposing slopes or valley bends. Type two or B is tongue-shaped, appearing long and straight due to an unobstructed spreading of the mass from little or no lateral confinement (Nicoletti and Sorriso-Valvo, 1991). This is described as moderate energy dispersion and mobility. The third class, C, represents a direct impact of the mass against an opposite slope resulting in high-energy dissipation or low mobility potential (Nicoletti and Sorriso-Valvo, 1991). Often this type results in a splitting of the debris, causing surging both up and down valley from the impact as shown in Fig. 3.6 I, II. (Nicoletti and Sorriso-Valvo, 1991). The shape is referred to as T shaped and is often associated with fallback ridges referred to by Hewitt as *Brandung* as shown in Fig 3.8 4 and 5 (Heim 1931 in Hewit, 2002). Nicoletti and Sorriso-Valvo (1991) showed that a reduction of mobility occurred from type A to type C as a result of the geomorphic surface.

The dimensions of the three deposit classifications (A-C) were placed into a series of ratios of horizontal deposit length (L), maximum width of the deposit (Wa), and width at half deposit length (Wm) and compared to rock avalanches of similar morphology to type A-C. Nicoletti and Sorriso-Valvo (1991) were able to show that broad but distinct differences occurred in each type due to geomorphology of the run out path influencing low to high energy dissipation Table 3.5).

Hewitt (2002) conducted a study of 50 rock avalanches in northern Pakistan and identified that the models for rock avalanche shape proposed by Nicoletti and Sorriso-Valvo (1991) did not take into account situations of complex geomorphology and rock avalanche shape resulting in incompatible variations of the type C T shape. Hewitt (2002) developed three further classes to represent his observations sufficiently. The first class (swash - Whitehouse and Griffith, 1983) referred to the climbing up and stalling of debris against an opposing slope as shown in Fig. 3.7 A. and Fig. 3.8. The more orthogonal the debris movement to the slope, the more defined the feature. The resulting deposited distal ridge referred to as a brandung or swash mark displays a steep front, dipping into the slope and is dependent on steepness of the slope and angle of impact as shown in Fig. 3.7 A-C and 3.8. 3-4 (Hewitt, 2002).

Figure 3.6: Variations of valley junction influence on rock avalanche deposition; an addition to the T-shape (C) defined in Fig. 3.5 (Adapted from Hewitt, 2002 c.f. Nicoletti and Sorriso-Valvo, 1991).

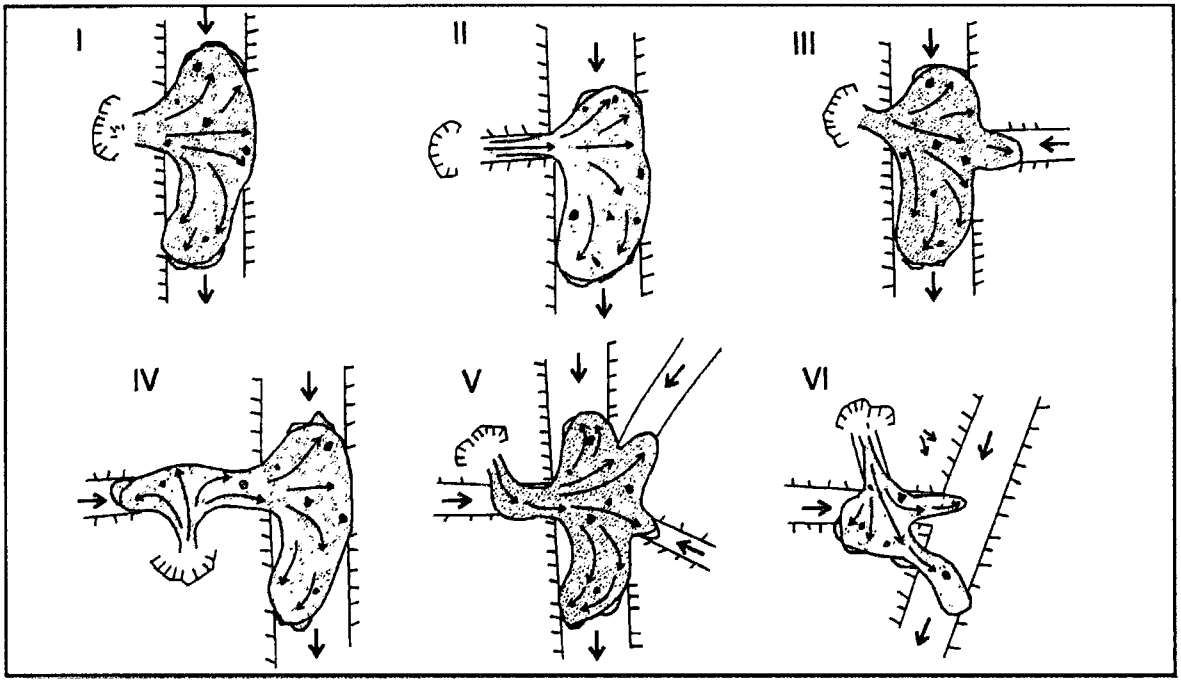

Main Valley T Shape

I. Main valley source and cross -valley deposit with up-valley and down-valley lobes.

II. Tributary valley source, main valley T-deposit.

Triple Lobe Types

III. Main valley source with up-valley and down-valley lobes, plus lobe entering and plugging tributary valley

IV. Tributary valley source and up-valley lobe plus main valley T shape.

Multiple Valley Junction and / or Lobe Type

V. Tributary valley source, deposit at junction of three other valleys. Multiple lobes with overtopping of interfluve.

VI. Tributary valley source with up-valley and down valley lobes and main valley lobes from overtopping

Table 3.5: Characteristic paramenters of the three types of geomorphic control from Nicoletti and Sorrio-Valvo, 1991

Geomorphic control	Vd (10^6 m^3	Le/ L (M± σ	H/L (M ± σ)	Wm/Wa (M ± σ)[a]	Wm/ D (M ± σ)	Wa/D (M ± σ)	D/L	Ice on path	Bends <<90°	Stopping	Fall-back Ridges
low-energy dissipative	<100	0.64± 0.10	0.22 ± 0.06	0.49 ± 0.32	0.11 ± 0.10	0.22 ± 0.14	1	often	often (sometimes)	mostly spontaneous	seldom
Moderate-energy dissipative	Any	0.66 ± 0.11	0.21 ± 0.07	0.76 ± 0.30	0.26 ± 0.13	0.38 ± 0.31	1	usually not	Often (seldom)	mostly spontaneous	seldom
High-energy dissipative	Any	0.56 ± 0.16	0.28 ± 0.10	0.36 ± 0.15	0.36 ± 0.17	1.06 ± 0.43	0.5-0.9	usually not	Often (always)	Forced	Often
Acheron rock avalanche deposit	approx 7.5 (this study)	0.695	0.2	0.25	0.025	0.1	1	unlikely	80° one	spontaneous	2 several

refer Chapter Four, Fig. 4.3 for application of above parameters to the Acheron rock avalanche deposit

The more oblique or gentle the slope, the greater spreading of the deposit that occurs and the less defined the brandung (Fig. 3.7 B, C. Hewitt, 2002). Hewitt's (2002) second class is the deflection of debris moving oblique to the impacted slope. This forms phenomena referred to as caroming or deflective rise and fall laterally along slopes as shown in Fig. 3.7 C. (Hewitt, 2002). In simpler terms, caroming is the near-parallel movement across a slope leaving a trim line above the height of the main mass. This represents interference of the moving mass causing a bobsled type analogy or lurching across the valley and glancing along the valley walls (Hewitt, 2002).

The third class is the splitting of the debris by an obstacle or an opposing slope. The shape of this effect, and that of the previous classes, can alter with variations of arrival time of debris and position within the vertical profile of the moving mass (Hewitt, 2002). Hewitt, (2002) also observed that discrete debris-debris interactions can occur such as later arriving masses forming pressure ridges and mounds against frontward debris slowed or stalled by topography. These observations imply that rock avalanche morphology should be recorded in detail to develop more comprehensive models.

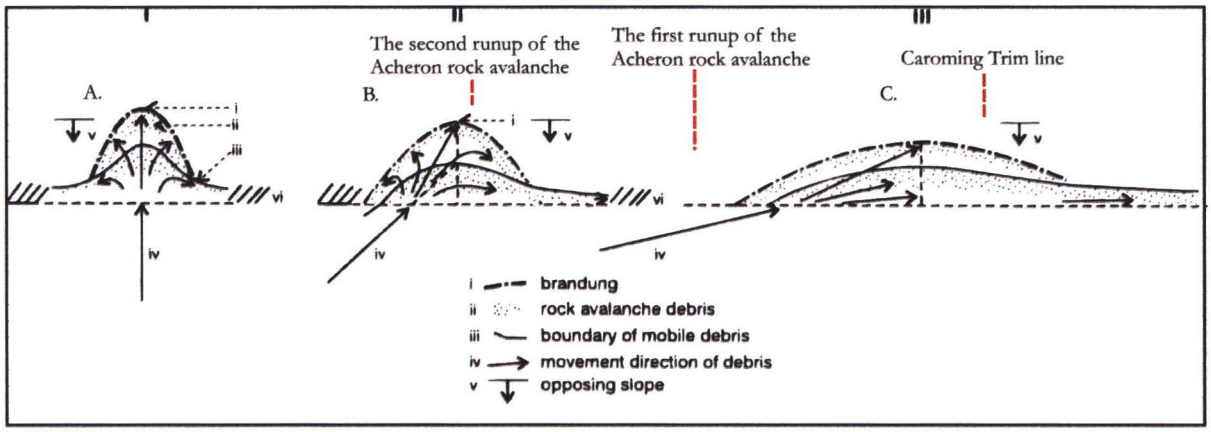

Figure 3.7 A-C: A simplified geometric relationship between rock avalanche movement and opposing valley walls as they influence the shape (form) and degree of development of brandung (fall-back ridges) and deflection of debris moving across a slope (in Hewitt, 2002). The dashed red lines represent the form of the Acheron rock avalanche for the first and second run ups and the prominent caroming or trim line described in Chapter Four (see Map 1).

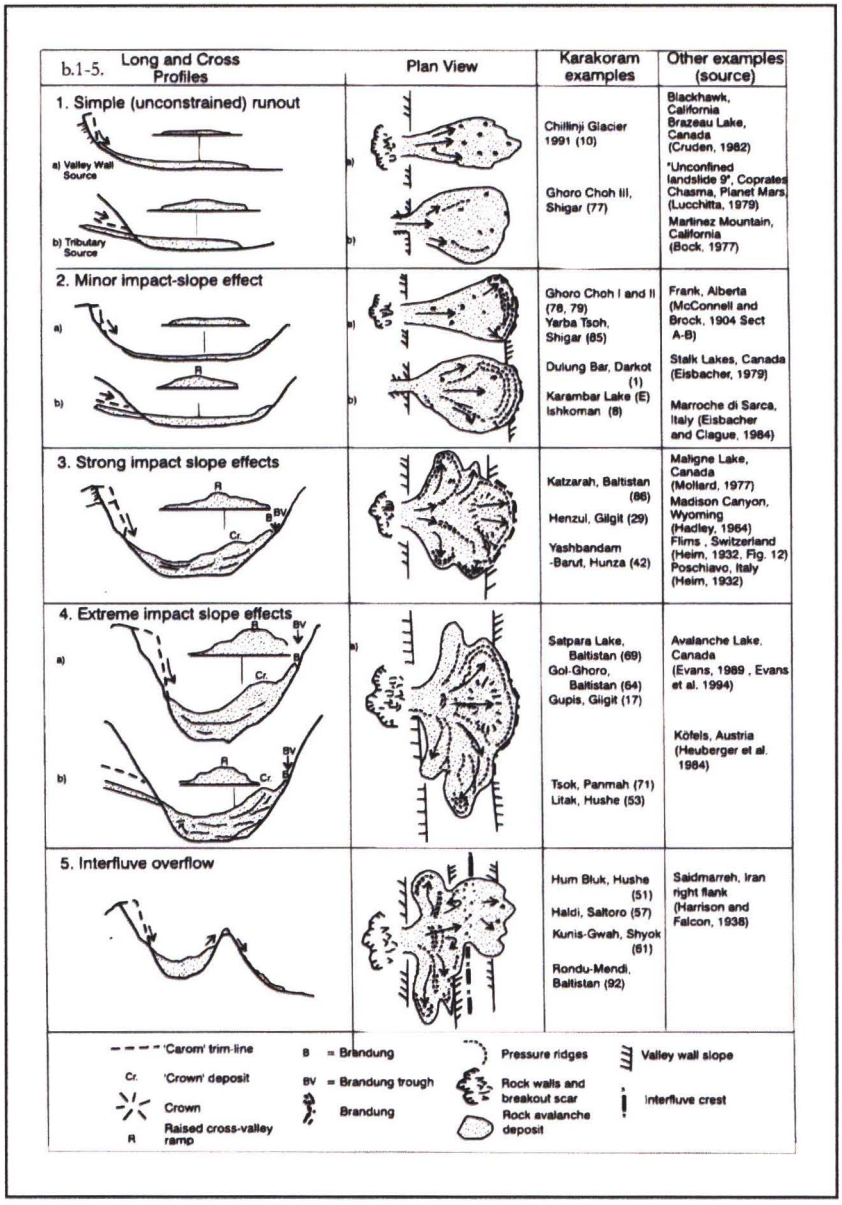

Figure 3.8 1-5: Schematic cross-sections and plan-forms of cross-valley rock avalanche deposits. Attention is directed to the geometric relationships of the debris emplacement to opposing slopes particularly the formation of brandung or fall-back ridges (c.f. Hewitt, 2002).

3.6. CONTROLS ON FAILURE

Large rock mass failures forming rock avalanches occur in steep bedrock slopes which contain several prominent fracture systems dissecting the otherwise competent rock formations (Eisbacher and Clague, 1984; Angeli, 1996). Eisbacher and Clague, 1984) identified three styles of slopes prone to producing rock avalanches (see Table 3.6).

- Scarp slopes in sedimentary rock,
- Dip slopes in sedimentary rocks,
- Fracture controlled slope in gneiss and granite.

TABLE 3.6: Summary of the main slope styles prone to forming rock avalanches. (Taken from Eisbacher & Clague (1984, 48-49 p.)

Slope type	Lithological Type	Failure Type
Scarp Slopes	Limestone, Dolomite successions Conglomerate	Forward toppling, backward rotation and sliding, or by complex internal collapse. Proceeded by the development of arcuate crown cracks.
Dip Slopes	Thick-bedded carbonates Conglomerate Sandstones	Failure controlled by bedding planes. Highly susceptible if characterised by smooth bedding planes or intercalated shale type horizons outcropping above the valley floor. Slope angles range from 10° -30°. Slopes exceeding 50° generally involve buckling and topple failure with propagation of shear planes burgeoning along the base of the failure. Failure is explosive overcoming friction angles (Ø) of 28°-32°.
Fracture Controlled Slopes	Gneiss Granite Schist Meta sedimentary rocks	Failure along composite fracture zones that intersect the internal planar fabric of the rock mass at high-angles, day lighting at the base of the rock mass. Failure is preceded by long development period where crown cracks and fractures develop into multiple potential rupture surfaces.

The geometry of the failure plane is determined by prominent discontinuities, such as bedding planes, exfoliation joints, cleavage, fractures and faults within the mass, that dip in toward the valley as seen in Fig. 3.9 (Hermanns et al. 1999). Progressive growth of the discontinuities creates the conditions necessary for large-scale failure (Eisbacher & Clague, 1984) Detachment then involves a rapid release of the rock mass, by sliding or falling (Eisbacher and Clague, 1984).

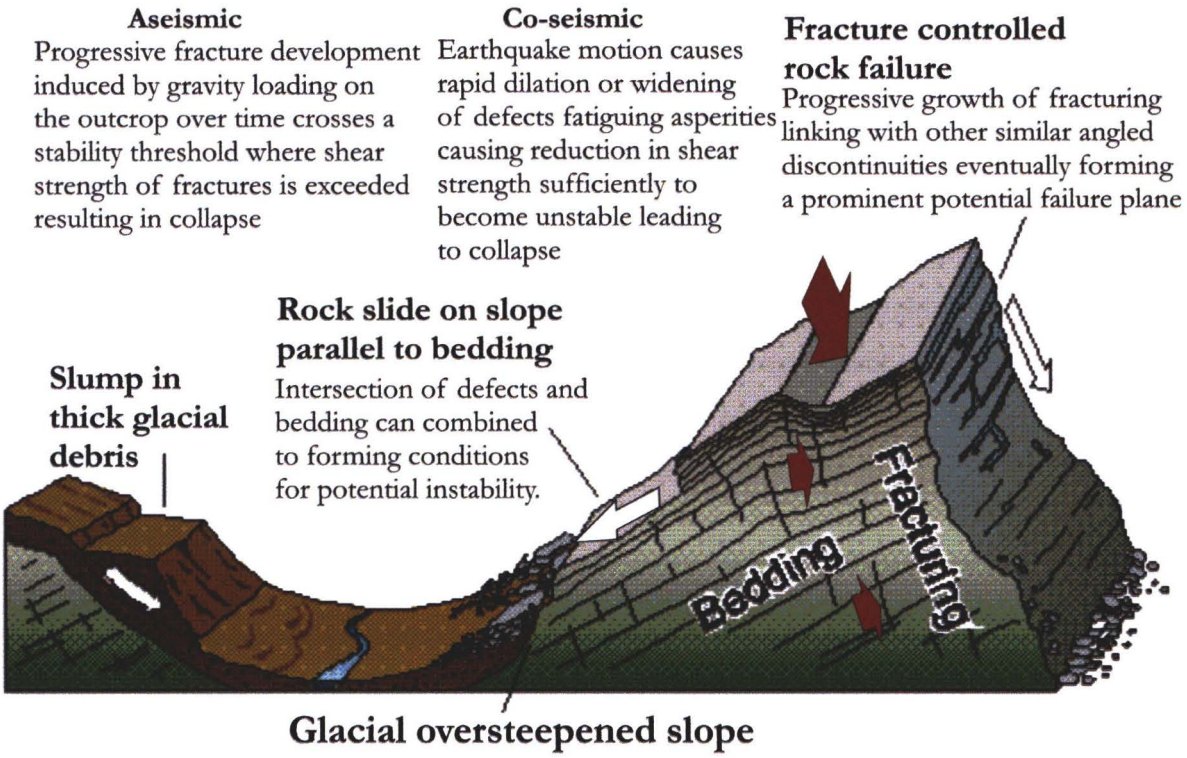

Figure 3.9: Model demonstrating the interaction of bedding and fractures producing the conditions for a large rock mass collapse forming rock avalanches. In the case of the Acheron rock avalanche, the role of bedding and fracturing as seen in this diagram would be reversed. The fracturing would define the shallow planar slide surface, while thinly bedded bands of Argillite offer sub-vertical detachment surfaces sloping into the basin centre (refer Chapter Two; diagram sourced from British Columbia, Canada, Ministry of Energy and Mines www.gov.bc.ca.)

3.7. TRIGGERING MECHANISMS

Rock avalanches can be triggered by earthquakes, storm events, rock weathering, removal of toe support, and human interference. Worldwide there is a tendency to assign the triggering of a rock avalanche to a seismic source rather than that of rainfall (Voight, 1978). This may relate to the preponderance of steep elevated slopes and mountain building processes to tectonic collision zones as outlined in the text earlier, regardless of the presence of earthquake activity. In New Zealand six historic rock avalanches have occurred but only two events were recorded as triggered by earthquakes.

One of the main requirements to form a rock avalanche is the rapid failure of the rock mass which is a factor compatible with an earthquake rupture (Hungr et al. 2001). Erismann and Abele, (2001) state that earthquakes are one of the most important force-generating

mechanisms, and go on to describe it as a single stroke release mechanism (Erismann and Abele, 2001). Eisbacher and Clague (1984) also observed that rapid detachment of intact blocks forming rock avalanches are typically caused by seismic shaking within the epicentral area of Mw $\geq$6 magnitudes (Eisbacher & Clague, 1984). The effect seismic shaking has within a rock mass is the widening of fractures and defects, resulting in a reduction of cohesion or shear strength of the planes asperities and surface roughness. This can occur over long periods of time from successive earthquakes progressively reducing shear strength and increasing the susceptibility of the loosened rock to fail (Voight, 1978 p13). Erismann and Abele (2001) describe this as a fatigue mechanism typically in areas of frequent smaller earthquakes.

Paleoseismic studies often use clusters of rock avalanches as geomorphic paleoseismic indicators (Cowan et al. 1996; Jibson, 1996). Eisbacher and Clague (1989) state that the biggest rock avalanches can be found close to the surfaces of seismic rupture (Hadley, 1964; Solonenko, 1977; Keefer and Tannaci, 1981 in Eisbacher & Clague, 1984). Studies of rock avalanches in North Eastern Argentina identified clustering of 55 deposits along mountain fronts bounded by active faults. The rock avalanches in this case were considered to represent neotectonic activity in the region (Hermanns and Strecker, 1999).

Another condition causing instability is the over-steepening of valley sides following glacial retreat, particularly in the Southern Alps of the central South Island. The removal of the ice results in relaxation within the rock mass and a redistribution of strain and stress causing crack development, dilation of joints over a period of time and potentially instability (Erismann and Abele, 2001). Whitehouse and Griffith's (1983) compilation of New Zealand rock avalanches, however, postdate the likely period of instability following the recession of the ice after the last phase of glaciation approximately 10 000 years B.P. Over-steepening is therefore suggested by Whitehouse and Griffith, (1983) to be a precondition rather than a trigger. McSaveney (2002) in a recent investigation of non-seismically triggered rock avalanches (in the Mt Cook national park) recognized that climate change over historical time may initiate some rock avalanches in isolated cases. Two examples occurred off Mt Fletcher in the Mt Cook national park in 1992. In these occasions progressive melt of glacial ice, which McSaveney attributed to a century of climatic warming, unloaded the toe of the steep slope resulting in two rock avalanches within one year.

The 1991 Mt Cook event failed along a prominent fault plane when retrogressive failures released the supporting buttress (McSaveney, 2002). Internally the condition of the source scar was shown to be extremely disaggregated and closely jointed, referred to in McSaveney, (2002) as incoherent. This may have been a controlling factor in the failure, allowing a minor instability to trigger a large-scale collapse (McSaveney, 2002). McSaveney (2002) noted that it would be reasonable to assume that the closely jointed material found at Mt Cook along the Main Divide Fault could exist throughout the area. This condition may also have implications for other similar fault systems along the central Southern Alps.

Ambient fluctuations of the diurnal temperatures from above to below freezing along the Southern Alps causes periglacial activity such as ice wedging and talus production, and implies that associated de-stressing on steep slopes causing joint dilation and creep may play a role in the disaggregated condition of the rock mass and on its ability to fail. McSaveney (2002) disagrees, observing that the carapace of ice and snow on the summits of the mountains in the Southern Alps acts as a shelter to the effects of erosion. This is supported by Erismann and Abele (2001), who observed that freezing, is a fatiguing process rather than a single stroke release mechanism. McSaveney (2002) suggests that the only effective method for large-scale erosion to meet the regional tectonic uplift is via the shedding of large sections of mountain slope. The failure is achieved by the bulging of the rock mass along fractures and dilating defects causing instability which could be set off by a comparatively minor slope failure (McSaveney, 2002).

Similarly Kilburn (1998) suggests that collapse can occur as deep-seated brittle failure as shown in Fig. 3.9. He describes instability occurring when gravity loading and fracture growth overwhelm the shear strength within the rock body with collapse occurring where the asperities and chemical bonds are weakened or too few. This can occur from chemical weathering and by water pressure along the areas of weakness. Kilburn describes a scenario of crack propagation starting as a population of new cracks growing exponentially with size until a major plane is formed as in Fig. 3.9 (1998). Once the major plane is developed a sudden decrease in shear resistance may push the equilibrium to an imbalance, creating a large slope failure (Kilburn, 1998). Kilburn (1998) acknowledges that the time frame on these events is unknown but may be distinguished by identification of pre-failure accelerated dilation of defects. While Kilburn suggests there is a role for water within a rock mass is large, Melosh (1987) noted that few if any recorded events were initiated by heavy rain.

3.8. THEORIES FOR LONG RUNOUT BEHAVIOUR

3.8.1. BACKGROUND

Two schools of study emerged in the 20th century attempting to explain the long-runout process. The first was the grain collision theory of Heim (1932), and the second was the theory of air lubrication or air cushioning.

The main proponent of this school of thought was Shreve (1968) who undertook a detailed study of the Blackhawk slide in the Lucerne Valley in southern California. He proposed that the debris slid rather than flowed on a thin layer of trapped compressed air in a hovercraft style, causing excessive run out distances on the underlying low angle alluvial surface (Shreve, 1968; Melosh, 1987). Goguel (1978 in Melosh 1987) went further, suggesting that basal friction caused heating resulting in steam which formed the necessary lubrication. Kent (1966 in Hsu, 1975) also postulated this theory that a bed of solids becomes fluidised when kept in suspension by a rising current of air. All these theories have been disregarded by the implausible physics relating to high permeabilities of the rock avalanche debris and the discovery of rock avalanches on the Moon and Mars. These extraterrestrial examples plot alongside terrestrial examples in run out length versus volume graphs, suggesting a process outside of earth's atmosphere (see Fig 3.4, Melosh, 1987; Davies, 1982).

The alternative branch of thought studied the flow mechanisms of granular material, an idea proposed by Heim (1932 in Hsu, 1975) and based on the work on the investigation of grain flow conducted by Bagnold (1954; 1966a; 1966b).

3.8.2. GRANULAR FLOW

Albert Heim was the first to recognise the sequential order in a sturzstrom deposit and subsequently the idea of confined grain collision (Voight, 1978). "*...the mass broke into thousands of pieces...the uppermost debris would catch up and impact with the front propelling the front debris faster.*" This would create the situation where the rear units could not overtake the front, thus retaining the sequential ordering of units yet maintain the transfer of kinetic energy throughout the mass in the form of thousands of fragments confined together unable to follow individual paths (Heim, 1932; Hsu, 1975). This confined collision of

individual grains was further confirmed from Heim's observations. "*...the internal motion of debris consisted of a myriad of high energy collisions among individual grains resulting in the maintenance of the original kinetic energy*" (Heim, 1932 in Davies, 1982). Hsu also highlighted the similarity of this description with Bagnold study of cohesionless grain flow (Hsu, 1975).

Bagnold conducted a series of grain flow experiments between 1950 and 1966. These experiments considered that when densely congested grains were dispersed in a flowing medium they acted as a fluid. The dispersive force generated from the effective weight of the grain mass and the resultant collision movement of these concentrated grains is called grain flow (Bagnold, 1954; 1956 in Hsu, 1975). Bagnold argued and proved in experiments that a static grain mass can not flow without dispersion or the ability to spread. The movement preference was upward against the downward body force or overburden weight. Bagnold was able to show the existence of a dispersive stress normal to the direction of motion of flowing grains with the dispersive stress originating from collisions of grains in high concentration (Bagnold, 1954 in Hsu, 1975).

Davies et al. (1999) described the divisions in approach to the grain collision concept as those who proposed a reduction of basal friction, and those who hypothesised reduced internal friction.

3.8.3. BASAL FRICTION REDUCTION

This concept considered that the increased shear occurring at the base of the moving rock mass causes higher dilation of granular material at the base. This was considered to result in a reduction of grain concentration and the dynamic friction. The consequence of this was an increase or prolonging period that the mass could be in motion (Davies et al. 1999). Two theories applying the basal friction concept were mechanical fluidisation and self-undrained loading (Campbell, 1989).

3.8.4. MECHANICAL FLUIDISATION

This concept is used in commercial industry to motivate motion in granular material such as pouring salt. It was first proposed for rock avalanche run out by McSaveney (1978) at the Sherman rock avalanche in Alaska to explain the areal extent thickness of the deposit. McSaveney considered the source of the initiation of mechanical fluidisation may have been seismic, causing the debris to become dilated and slide while concurrently thinning and spreading (McSaveney 1978 in Davies, 1982). The principle behind mechanical fluidisation as described in Davies (1982) is a high-energy input into a mass of granular material causing high impulsive contact between individual grains, resulting in them becoming statistically separated and dilated. The internal shear stress resistance is reduced which is a condition shown by Bagnold (1954 in Davies, 1982) that allows the mass to flow under gravity when dilated. The source of the energy input is considered by Davies (1982) to be the differences in velocity between the stationary underlying material and the base of the high speed debris mass at a minimum velocity of 7 m / second, a process which Bagnold showed with the dilation of a grain mass when exposed to unidirectional shear (in Davies, 1982). However, Davies (1982) considered mechanical fluidisation to insufficiently reduce basal friction, and therefore not to explain long run out rock avalanches.

The self –undrained loading concept (Sassa 1988, Abele, 1997, in Davies et al. 1999) suggests that the reduced friction stems from the saturated or near saturated underlying alluvium which displays very little shear strength. This becomes effectively deformed with the overriding rock avalanche mass and acts as a lubricating layer (Davies et al. 1999). The self-undrained loading theory requires an underlying alluvium deposit, and the physical incorporation of the alluvium mantle into the base of the rock avalanche. This incorporation of deposited fluvial material can be seen within exposed sections of the Acheron rock avalanche, however in exposures of the basal contact, the rock avalanche deposit overlies undeformed Beech forest leaf litter suggesting this process fails to explain the run out process in its entirety.

3.8.5. BASAL MELTING

The main proponent of this hypothesis was Erismann (1979 in Davies, 1982) where by motion was produced by the presence of a thin layer of molten rock at the base of the flow caused by friction and high pressure. This reaction releases carbon dioxide gas which reduces

the apparent friction (Okura, 2000). The model was relatively successful as it could be replicated with the use of thermodynamic analysis and was recorded at an example in the field. Basal melting could also be applied to extra-terrestrial examples. However, this was not identified at the Acheron rock avalanche deposit, where the overlying debris showed little disturbance of underlying forest litter, and was not shown to melt snow underlying the Sherman rock avalanche in Alaska (McSaveney, 1978 in Davies, 1982).

3.8.6. MECHANISMS OF REDUCING INTERNAL FRICTION

In this concept, reduced internal friction results in an increase in spreading of the translating rock avalanche mass without increasing the translation of the centre of the mass (Davies, 1982) This results in more similarity to examples in the field, however does not fully explain long run out (Davies et al, 1999). Prominent in the reduced internal friction hypothesis is the theory proposed by Melosh (1987), where dry granular material is acoustically fluidised creating the conditions for long run out distances to occur. The concept of acoustic fluidisation involves a large volume rock avalanche producing abundant amounts of acoustic energy during initial failure. This acoustic energy results in a reduction of the direct stress between grains allowing slip to occur at low shear stresses (Davies et al. 1999). If the rate of vibration or acoustic energy exceeds any dissipated into the rock mass then the surplus can facilitate motion (Melosh, 1987).

3.8.7. DYNAMIC FRAGMENTATION

As surmised by Davies et al (1999) none of the existing solutions appear to realistically or fully explain the long run out process in its entirety as it occurs in nature. A new concept based on recent work of Davies and McSaveney (2002) introduced a process called Dynamic Fragmentation. This was based on the pulverised internal state of the deposits seen in exposures in the field. Over the previous seven years this hypothesis has been developed on the principles of mechanical fluidisation, granular flow and rock fragmentation (McSaveney 1978; Davies 1982; Davies and McSaveney, 1999; Davies et al. 1999; Davies and McSaveney, 2002).

Davies and McSaveney (2002) conceptualise that a confined explosive disintegration of rock occurs at a smaller scale than that of insitu jointing or structural discontinuities. A process very similar in mechanism to the explosive properties of rock burst within highly stressed rock or an explosive failure of an unconfined compression test (Davies and McSaveney, 2002). This kinetic energy creates a positive isotropic interactive pressure on the clasts within the internal body. The result is to cause dilation of the rock mass in continuous explosions on surrounding clasts, causing exceptional spreading thus driving the long run out and pulverising the internal mass (Davies and McSaveney, 2002). This concept has the advantage of being able to express energy through the entirety of the run out, often a limiting factor in previous theories (Melosh, 1987; Sassa 1988; Abele, 1997; in Davies and McSaveney, 2002). The principle of dynamic fragmentation stems from the static–dynamic fragmentation (Davies and McSaveney, 2002). The former is the nucleation of flaws at low strain rates. When growth of a flaw fails to relieve the applied elastic strain rapidly enough it forces more flaws to nucleate and dynamic fragmentation occurs (Davies and McSaveney, 2002). The boundary between static–dynamic fragmentations is a function of the size of the fracturing mass, and decreases in size exponentially as the volume of the mass increases (Melosh et al. 1992 in Davies and McSaveney, 2002). Much of the evidence stems from the scallop shaped conchoidal surfaces and impact scars on rock samples from deposits (Davies and McSaveney, 2002).

Davies and McSaveney outlined their hypothesis of fragmentation in a sequence applied to Falling Mountain rock avalanche which occurred in 1929 in the Arthur's Pass National Park.

"*...as the rock mass fails, granular flow occurs rapidly replaced by fragmentation with a shallow surface mantle of granular flow. The fragmenting rock mass displays the rheology of a heavy vapour under positive pressure rather than that of a liquid in Bagnoldian models. The isotropic dispersive stress dilates the mass invoking increased spreading with normal internal and basal kinetic friction co-efficient occurring. The inter-granular stress falls below that required for fragmentation causing a resumption of granular flow and the settling of the dilated mass until motion ceases*"(Davies and McSaveney, 2002 p 15).

3.9. SUMMARY

- Variations in the definition of rock avalanche caused by differences in approach of the widely applied North American landslide classification scheme of Varnes (1978) and the United Kingdom classification of Hutchinson (1988) have created ambiguities and short comings in describing rock avalanches. Hungr (et al. 2001) proposed a revised definition to retain the entrenched terminology while making their application less ambiguous. In particular the addition of large rock fall/rock slide absent in previous definitions (Hsu 1975; Varnes, 1978; Hutchinson, 1988; Cruden and Varnes, 1996; Angeli et al. 1996; Hungr et al. 2001).

- The definition applied in this study was that outlined by Hungr et al. (2001) "*...a rock avalanche is an extremely rapid, massive, mobile, flow-like motion of fragmented rock derived directly from a large bedrock failure from either rock slide / rock fall or a combination of either and toppling*".

- The application of velocity by Cruden and Varnes (1996) fails to accurately distinguish landslide type, however with the addition of a human response parameter it demonstrates that human response to a rock avalanche is nil.

- Rock avalanches are found predominantly in tectonically active collision zones throughout the world. They exhibit certain characteristics which distinguish them from other forms of mass movement. They form following the sudden collapse of a large bedrock mass from an elevated source. They display high mobility, extremely rapid velocities, and can travel several kilometres over relatively small slope gradients. Internally the rock is pulverised with a crude inverse grading resulting a capping of large blocks on the surface. The debris during run out appears massive and semi-coherent. Rock avalanches can form in any rock type so long as it can fail on a large enough scale.

- A numerical relationship between volume and travel angle or Fahrböschung has been shown to exist. Scheidegger (1973) plotted the volume to travel angle using a log scale to minimise scatter showed a decrease in travel angle with increasing volume.

Hsu (1975) suggested that the use of the travel angle is incorrect and proposed an equation called excessive travel distance based on the angle of repose of broken rock. Both are in use today. Corominas (1996) identified that any type of landslide experiences a reduction of travel angle with an increase of volume suggesting that it is not unique to rock avalanches. He confirmed the application of the travel angle as a measure of mobility which was sensitive to volume and stated that fall height was not a relevant factor.

- Runout simulations in Japan demonstrated that runout length was directly related to volume. This was caused by block to block impacts causing increased dispersion of kinetic energy rearward of the debris front while resulted in a retreat of the centre of gravity of the mass, preservation of stratigraphy and an increase in distance reached by the frontal blocks. This is confirmed by Davies in granular avalanches (1999). Davies and McSaveney (1999) suggest that assumptions of coefficient of friction are incorrect due to the different travel distances of grains within the mass. They normalised height and length to volume ratios and found a size effect occurred at $< 10^5$ m^3 and at 10^7 m^3 which they interpreted to represent the onset of fragmentation induced long run out initiating between the two values.

- Scatter in statistical analysis is in part due to the influence of the topography in the runout path. Nicolletti and Sorris-Valvo (1991) resolved 3 types of rock avalanche shape to the relative mobility as low, moderate and high dissipation potential.

- Hewitt (2002) identified limitations in the type classification models and included definitions such as caroming or sideways movement of debris across a slope, the term brandung or debris runup and the influence of the angle of impact on their formation. Hewitt's observations indicate that rock avalanche morphology should be recorded in detail to develop more comprehensive models.

- Eisbacher and Clague identified 3 type of slope as prone to large collapses forming rock avalanching, scarp slopes, dip slope and fracture controlled slopes.

1. Scarp slope is common to limestone and conglomerates and fails by forward toppling, backward rotation or complex internal collapse. Crown cracking is often present preceding the event.

2. Dip slope occurs in carbonates conglomerates and sandstones. Failure is controlled by the bedding planes along angles of 10°-30°. Steeper slopes involve buckling and topple failure.

3. Fracture controlled slopes occur in granites, gneiss, schist and some meta-sedimentary rocks. Failure occurs along growing fracture zones that intersect the planar fabric of the rock mass. Failure is often preceded by crown cracks.

- Rock avalanches can be triggered by earthquakes, ice plugged drainage and tectonic uplift. Typically they are associated with earthquakes due to concentrations of deposits in proximity to tectonically active zones and seismic activity. Seismic motion acts as a prominent single stroke release mechanism of the rock mass while smaller magnitude events act as a fatigue stress on the discontinuities shear strength.

- Glacial over-steepening of valley sides is not considered a trigger mechanism however two events in 1992 at Mt Fletcher where thought to be related to a retreating glacier and loss of toe support. McSaveney identified closely concentrated jointing and incoherent state of the rock mass at Mt Cook and Mt Fletcher and suggested this may exist along the fault zones of the Southern Alps. He observed that rock avalanches are the only form of erosion large enough to match uplift and suggests that the internal structure is so disaggregated that a comparatively minor slope movement could cause mountain side to collapse. Similarly Kilburn postulates that the ongoing growth of defects within a mass can result in increasing potential instability resulting in subsequent failure. This may manifest as de-stressing and gravity loading over time.

- Previous explanations for long run of rock avalanches have focused on reducing basal friction or internal friction however neither has been successful in explaining the phenomenon as it occurs in nature (Davies and McSaveney, 2003).

- The dynamic fragmentation hypothesis proposed by Davies and McSaveney, (2002) is based on observations of pulverised material observed within the deposits. This hypothesis suggests that an explosive form of fragmentation called dynamic fragmentation is occurring as explosive failures of rock material confined within the fragmenting mass. The confinement of the high kinetic energy released from the innumerable continuous explosions causes dilation of the rock mass resulting in exceptional spreading and longer run out.

CHAPTER FOUR

DESCRIPTION AND MORPHOMETRIC ANALYSIS OF THE ACHERON ROCK AVALANCHE

4.1. INTRODUCTION

This Chapter will look in detail at the dimensions and morphology of the deposit and investigate the age evidence for its deposition. The run out will be modelled using the DAN program to test the fragmentation theory proposed by Davies and McSaveney (2002).

The Acheron rock avalanche, one of 42 greywacke derived rock avalanche deposits located within the central Southern Alps displays typical characteristics of a rock avalanche; pulverised internal material, long run out and interactions with the valley geomorphology, such as debris run ups of the valley sides. The source of the rock avalanche is a scar near the head of the Red Hill valley which shows the structural characteristics which have contributed to the collapse of the rock mass forming the rock avalanche. The area below the source scar called the run out has been divided into four zones focusing on diagnostic quantitative features, particularly debris run out interactions with valley geomorphology, velocities and dimensions of length and volume summarised in Fig. 4.3.

The age of the Acheron rock avalanche was considered to be between 570 – 400 years B.P. based on radiocarbon dating, weathering-rind ages and lichenometry (Burrows, 1975; Whitehouse and Griffith, 1983; Bull and Brandon, 1998; Howard, 2001). Paleoseismic investigations of the PP-AFZ suggested that this date may represent a period of earthquake activity along the fault zone based on a population of six landslides including the Acheron deposit occurring within 1 km of active faulting (Cowan et al. 1996). More recently, Howard (2001) undertook trench investigations along the Porters Pass Fault which underlies the deposit. He argued strongly that there was no stratigraphic evidence in the excavated trenches to suggest that rupture along the trace occurred post 800 years B.P. Instead Howard (2001) proposed that the youngest rupture event occurred between 1700 and 800 years B.P. most probably at 1000 ± 100 years B.P. During this study the rock avalanche was redated to verify the age of the emplacement.

The long run out simulation (DAN) will model the Acheron deposit by back analysing the rock avalanche run out to replicate the velocity and run out distance found during field investigations. Lateral earth pressure coefficients representing the effect of fragmentation within the rock avalanche mass will be applied to a friction model within the DAN simulation to test the hypothesis of Davies and McSaveney (2002) of dynamic fragmentation induced long run out.

4.2. ROCK AVALANCHES IN THE CENTRAL SOUTHERN ALPS

4.2.1. DISTRIBUTION AND PREVIOUS WORK

The record of rock avalanche activity in New Zealand is based on the work by Burrows (1975) Whitehouse (1983) Whitehouse and Griffith (1983), and McSaveney (1992b, 1993, and 2002). Whitehouse and Griffith (1983) identified 46 rock avalanche deposits using 1:40 000 to 1:60 000 aerial photos over a 10,000 km^2 area of the central Southern Alps (see Fig. 4.1). From the compilation, 42 deposits were composed of greywacke sandstones and mudstones and exceeded an arbitrary volume of 1 x 10^6 m^3 (Fig 4.1, Appendix B Table 1).

The difficulty with this type of compilation is the effect active geomorphic processes found in the Southern Alps have on the longevity of deposits, a problem that Cowan et al. (1996) identified when discussing the potential of rock avalanches as paleoseismic indicators. The record of Whitehouse and Griffith (1983) reflects only the remaining deposits that were recognisable in the geomorphically active alpine valleys and large river catchments of the Southern Alps. Similarly, McSaveney (2002) noted that Whitehouse and Griffith, (1983) had not included any deposits that fell on glaciers, which are areas of steep terrain and potential sites of rock avalanching. McSaveney (2002) went on to suggest that any evidence of rock avalanches would be destroyed by a glacier within a period of 100 years. Whitehouse and Griffith, (1983) accounted for probable deposit population loss by assuming a complete record exists that for the past 1700 years and calculated that rock avalanches occur statistically only one every 94 years (Whitehouse and Griffith, 1983). This was interpreted to represent episodes of large earthquake events and a few intense storms (Whitehouse and Griffith, 1983). In the last hundred years in the Southern Alps, more than six rock avalanche events occurred of which less than half were earthquake triggered (McSaveney, 2002).

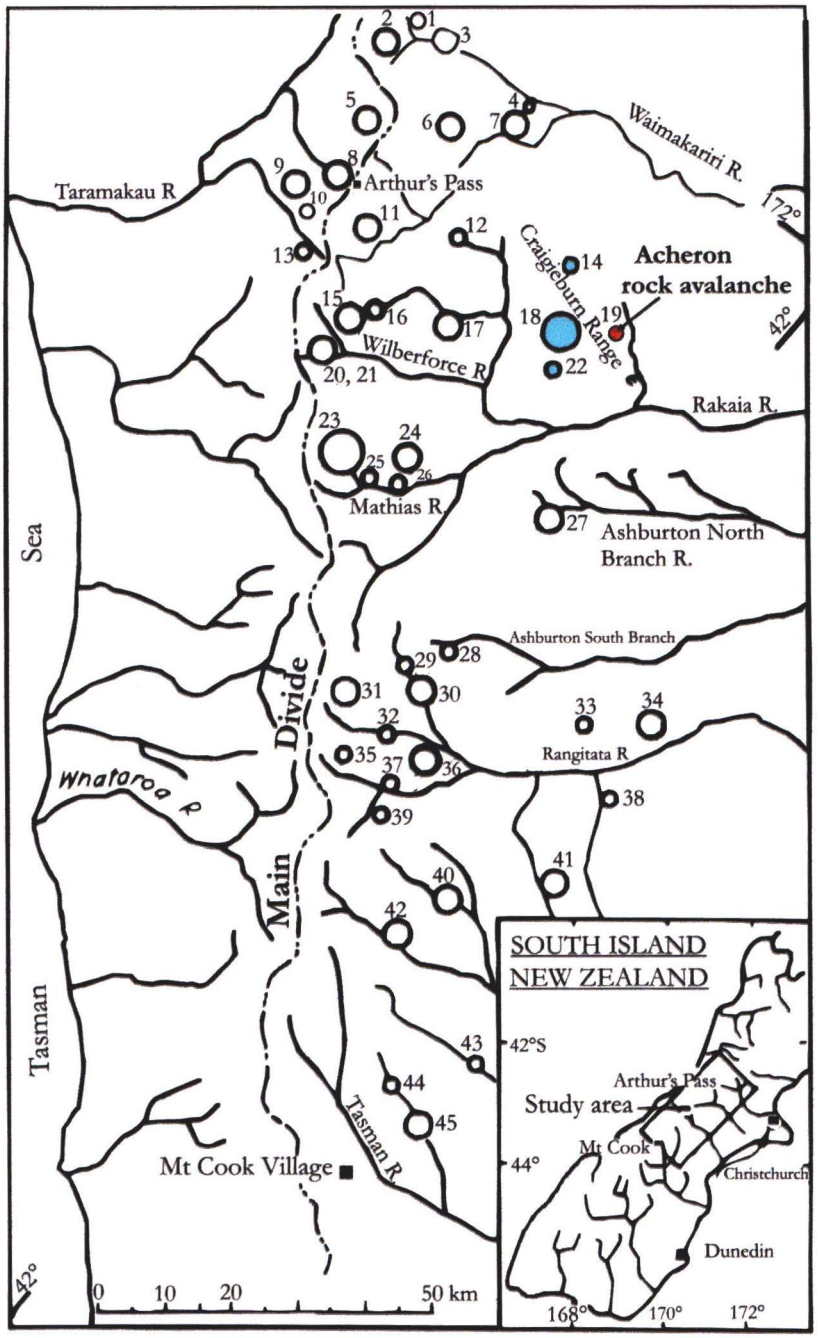

Figure 4.1: Distribution of greywacke rock avalanche deposits in the Central Southern Alps (from Whitehouse and Griffith, 1983)

The circle size indicates the magnitude of the deposit volume. o Small circle = 1 - 10 10^6 m^3
O Medium circles = 100 x 10^6 m^3
◯ Large circles = >100 x 10^6 m^3

The numbers beside the magnitude circles correlate with a Table 1 from Whitehouse and Griffith (1983) displaying volumes and age estimates of each of the deposits (refer Appendix B.1 Table 1) The single red filled circle represents the Acheron rock avalanche deposit and the blue filled circles identify rock avalanche deposits found nearby within the Craigieburn Range - Porters Pass area

McSaveney's (2002) studies of the three rock avalanches in the Mt Cook region that occurred in the last eleven years give a good insight into the frequency of these events. The rate of their recurrence indicates that the potential rock avalanche activity in the Southern Alps could be more frequent than presently expected. McSaveney (2002) observed that many rock avalanches occur on high mountain slopes where gravitational collapse is the only effective erosion process able to keep up with glacial and fluvial valley incision. He surmised that this represents a balance between regional uplift and erosion. A reassessment of landslide frequency based on the historical events suggests an expected frequency of large mountain collapse of $>10^6$ m^3 is 1 per 20–30 years; similar to that applied to the European Alps (McSaveney, 2002).

4.2.2. HAZARD POTENTIAL

Whitehouse and Griffith (1983) describe the hazard potential posed by rock avalanches as "remote", but recognised that in special cases rock avalanches may represent a significant problem. An emerging factor in the recognition of the hazard is the identification of a slope susceptible to large failures and run out paths that encourage high mobility. McSaveney (2002) commented on the abundant closely spaced defects found at the Mt Cook and Mt Fletcher rock avalanche source scars, and suggested these may be present throughout the Southern Alps. Prebble's (2001) observation of the important influence of deep-seated topple failures in the Southern Alps, especially in conjunction with folding and weak thin argillite layers, suggests there is a potential for underestimating the hazard.

Large rock mass failures forming rock avalanches are described as occurring suddenly without warning (Eisbacher and Clague, 1984). This is rejected by Kilburn (1998), who suggests slow deformation and fracture development may be occurring but not recognised. He also states this is supported by a lack of data available on pre-collapse accelerations of defect growth (Kilburn, 1998). In the Southern Alps, the development of fractures defining large potential instability in areas of remote transport corridors may be overlooked or hidden by talus materials.

The extremely rapid velocity of rock avalanche (>5m/second) renders human response, including the ability to evacuate, as nil (refer Chapter Three Table 3.4, Fell et al. 2001). The

only response to the hazard is avoidance however this is complicated when the threat is unrecognised. If crack development is identified in conjunction with potentially hazardous run out, remote GPS warning systems can be installed to monitor accelerated dilation of cracks. This is the only realistic method for warning and does not forewarn events triggered by sudden seismic activity. A detailed investigation of mountain valley sides and crests to locate sites of rock relaxation should be undertaken on all alpine transport corridors, settlements and even areas of recreational activity.

4.3. THE ACHERON ROCK AVALANCHE DEPOSIT

4.3.1. BACKGROUND

The Acheron rock avalanche deposit is located 82 km west of Christchurch and immediately south west of Lake Lyndon on the margin of Castle Hill Basin. The deposit is one of several large catastrophic failures of elevated bedrock found in the eastern central Southern Alps (refer Fig. 4.1, Appendix B Table 1, from Whitehouse and Griffith, 1983). The rock avalanche is of significance due to its long run out (3.5 km) and location at the eastern margin of the Southern Alps within 15 km of the settlement of Springfield and 5 km from State Highway 73. The distal limit of the rock avalanche terminates 700 metres from the popular Lyndon road and buries a Holocene active section of the PP-AFZ called the Porters Pass Fault suggesting the triggering mechanism may have been derived from this source (Fig. 4.2).

4.3.2. MAPPED EXTENT OF THE ACHERON ROCK AVALANCHE

Data and observations were gathered during the 2002-2003 field seasons utilizing 1: 8 000 and 1: 8 200 aerial photos. The lack of surface detail on the lower half of the deposit on both 260-K35 1: 50 000 topographical maps and geological maps created the need to develop a contour map to accurately display the surface morphology and deposit dimensions. This was achieved using a GPS survey (see Map 1). Previous peripheral investigations of the rock avalanche by Burrows, (1975), Whitehouse and Griffith, (1983), Bull and Brandon (1998) and Howard, (2001) were also utilised. Figure 4.3 displays the dimension information of the rock avalanche. Figure 4.3 A. shows the Digital Elevation Map (DEM) depicting the divisions of the deposit by colour each representing segments of the source basin and run out to be discussed in the later sections.

Figure 4.2: 3-D Surface map of the Red Hill Valley depicting the path of Acheron rock avalanche run out (in red). The darker red shows the run out path while the lighter red illustrates the source scar, location of debris run ups used for velocity calculations, trim lines and the known extent of debris. The Porters Pass Fault is shown as a black line trending east to west. An inferred trace across the rock avalanche deposit is depicted with the dashed line. The Red Hill Fault trending below Red Hill is identified by the larger dashed line. The position of the outcrop of Tertiary rocks is pinpointed by (T) adjacent to the Porters Pass Fault in the west of the field area.

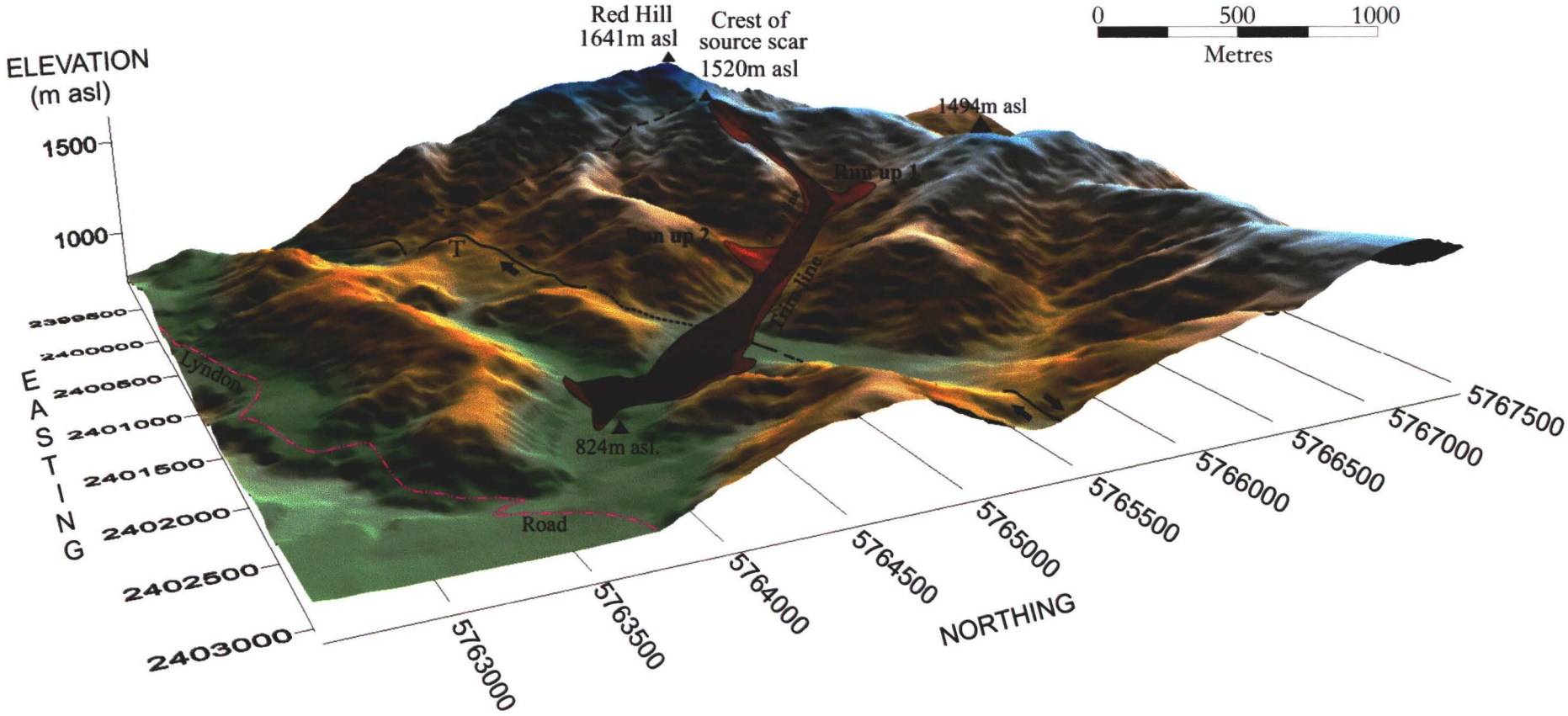

FIGURE 4.3: A-J.Statistical data for the Acheron Rock Avalanche (Adapted from Govi et al, 2002; Hewitt, 2002; McSaveney, 2002)

Acheron Rock Avalanche Deposit

Location: Red Hill Valley, off the Lyndon road, Canterbury, New Zealand.
Grid Reference (NZ map grid) 1:50 000 K35
2401575 E, 57648445 N
Rock Type: Torlesse greywacke
sandstone / mudstone
Source Scar Aspect: NNE
Elevation - Maximum: 1520 m (asl)
Minimum: 824 m (asl)

B. Area

Source Scar Plan Area (Sr)	112 000m^2 (GPS)
Deposit Plan Area (Sd)	720 000m^2 (GPS)
Total Area Plan	832 000m^2

C. Volume Estimates

Observed Thickness

3 m [river exposure - lower deposit] 2401725E, 5764420N [NZMG]

Deposit Zones -Estimated Thickness	*Estimated Thickness*	*Area*	*Volume*
Upper Runout area (>15m)	15m	295 138m^2	4427070m^3
Impact Hill	25m	63 766m^2	1594150m^3
Mid Deposit	7.5m	245 536m^2	2455360m^3
Lower Deposit	3m	167 107m^2	501321m^3
Total estimated volume now (rounded to nearest 10^5)			**8 900 000m^3**
Dilation ratio (Evans et al. 2001) 4/3	20%	minus	**1 500 000m^3**
Total Estimated Volume of mobilised rock		*Vd*	**7 500 000m^3**

D. Run Out Statistics

(Distances measured from GPS Pathfinder plot)

Fall height (H) - top of scar to distal limit	700m		
Runout (L)	3450m		
Horizontal distance (D) §	3000m		
Farboschung (tangent (H/L)	11.4° (0.20)		
Excessive Travel Distance (Le) (**Le=L-H/tan32°**) (Hsu, 1975)	2400m		
Mobility Index (H/L)*	0.2		
Mobility Index (Le/L)*	0.633		
Length of Accumulation (La) *	2950m		
Slope Angle of Accumulation (Line of best fit)*	11.2°	ave 10.5	
Planimetric width D/2 (Wm)*	175 / 2 = 87.5	(refer Fig 3.5	and Table. 3.5)
Maximum Planimetric Width (Wa)*	350m	"	"
Wm / Wa**	0.25	"	"
Wm / L**	0.025	"	"
Wm / D**	0.025	"	"
Wa / L**	0.1	"	"
Wa / D**	0.1	"	"

E. DAN Simulation Model

Internal Friction Angle (Ø)	27°
Earth Pressure Coefficients	5.5, 5.2, 9.9
Maximum Velocity at (X) =1123.70m	164 km /hr
Duration of event	55 seconds
Travel Angle	18.05°
Fahrboschung	11.34°
Ratio	0.33
Depositional Area	880 000m^2
Volume	9 500 000m^3

F.

Mean Slope of Source Scar	38°
Orientation of Runout: Initial Run Out	083°
New Direction	151°
Gentle Bends < 70° Change in Direction	68°

G. Debris Runup Superelevations

Height of Decent Slope (h_1)	1150m asl
Run up 1 (h2) v = (2gh)0.5	80m
	39.6 m /sec
Run up 2 (h_2) v = $(2g\,h)^{0.5}$	80m = h (NZMG) 39m
Maximum Speed $(2gh)^{0.5}$	39.6 m /sec
Mean velocity	142.56 km/ hr at

H. Estimated Age of Deposition (yrs B.P.)

Burrows, (1975) (Conventional Age)	500 ± 69 yrs BP
Bull and Brandon, (1998) lichen (< 84.3mm)	460 ± 10 yrs BP
Howard, (2001) W.R (0.83mm)	490 ± 50 yrs BP
This study (Conventional Age)	1152 ± 51 yrs BP

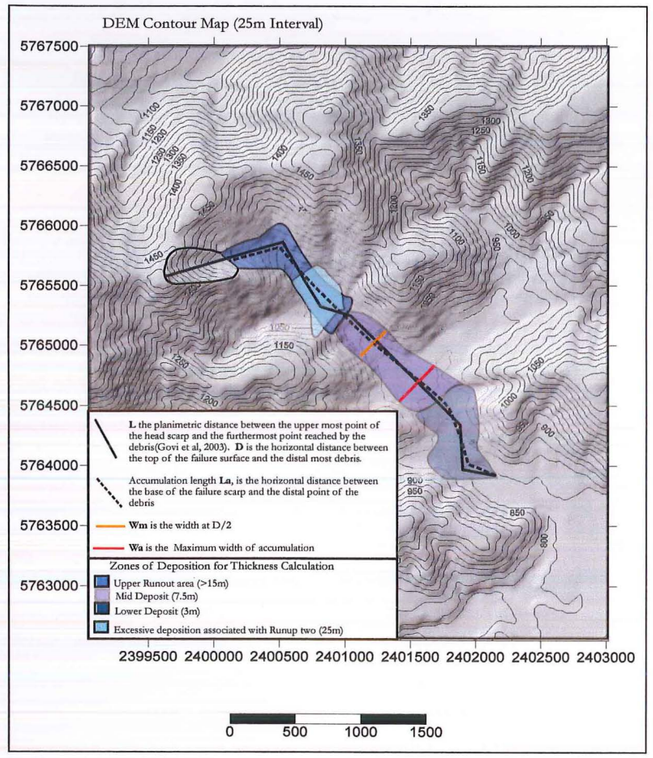

A. Map of the Acheron rock avalanche and morphometric measurements

I. (From Abele, 1974 in Govi, 2002)

		This Study	*DAN Model*
Average thickness of accumulation (*f*)	Vd / Sd =	10.4m	12.5
Relative thickness of accumulation (*f*)	[(Vd/Sd)/√Sd]	0.0123	0.0147
Spreading (Sd/Sr) (*ff*)	6.43		
Relative Hollow (*fff*)	0.13	0.3	

J.

Failure Planes	**Planar** Dip/dip direction	**Toppling** Dip/dip direction
Northern Ridge Section 1	~	86° / 340°
Central Section 2	40° / 050° - 40° / 045°	84° / 226° - 82° / 210°
Southern Ridge Section 3	40° / 020° - 40° / 050°	82° / 210° - 85° / 180°
	40° / 003° - 40° / 007°	

Notes:
§ (as in Fig. 1 A & B Nicoletti and Sorriso-Valvo, 1991)
* (morphometric data decribed in Nicoletti-Sorriso-Valvo, 1991 in this study Fig. 3.5
** (Indices that describe the shape of the rock avalanche in Nicoletti and Sorriso-Valvo, 1991)
f (allows comparison of rock avalavanches of different magnitude from Abele, (1974) as in Govi et al., 2002)
ff (Abele, (1974) as in Govi et al., 2002)
fff (Ratio between maximum hollow in the detachmnet zone and its widith, measured at the same elevation (Abele, 1974) as in Govi et al., 2002)
(†) as decribed in Whitehouse and Griffith (1983)

See Fig. 4.3.A.

- The clear zone corresponds to the rock avalanche source scar
- The upper run out segment is represented by dark blue
- The transparent pale blue represents excessive sedimentation associated with run up two
- The purple describes the mid zone where the spreading of the debris occurred
- The grey indicates the distal zone

4.3.3. DIMENSIONS AND STATISTICS OF THE ACHERON ROCK AVALANCHE

Morphological and statistical data including references to the different equations for velocity, area and volume, and excessive travel distance are included in Fig. 4.3 A-J. The format for describing morphology follows the approach outlined in Govi et al. (2002).

To estimate a rock mass volume the source scar was initially measured using a GPS survey of the outline at 112 000m^2. Difficulties existed finding the correct deposit volume. Methods using cross-sections of the scar at 100m intervals calculated 14 x 10^6 m^3 while volumes using the area defined by the GPS of 112 000m^2 multiplied by the mean of the estimated rock mass thickness of 113m equated to 12.5 x 10^6 m^3. Other estimates were taken from the deposit volume discussed below and corrected for dilation and incorporation of 20% or 1.5 x 10^6 m^3 (McSaveney, 1978; Evans et al, 2001) equating to 7.5 x 10^6 m^3 which appears more realistic. Until a more reliable method can be applied the corrected deposit volume of 7.5 x 10^6 m^3 will be used to describe the mobilised rock volume.

The volume calculated for the Acheron rock avalanche deposit from this study was 8.9 x 10^6 m^3, which is an increase of nearly 40 % from that indicated by Whitehouse and Griffith (1983) in Table 1 in Appendix B of 6 x 10^6 m^3. The planimetric deposition area was calculated at 720 000 m^2 using a GPS survey around its margin which suggests it is accurate as a minimum two dimensional value. The area is larger than the 610 000m^2 inferred in previous studies (Whitehouse and Griffith, 1983).

The average thickness of the accumulation zone is 10.4m seen in Fig. 4.3.I. This was derived from dividing the deposit area of 7.2 x 10^5 m^2 into the estimated volume 7.5 x 10^6 m^3 and is consistent with 10m ± 2m of Whitehouse and Griffiths (1983). The maximum run out (L) of the Acheron rock avalanche is considered to be 3500m, which is close to the average for the size of volume and fall height (H - 700m) (as in Nicoletti and Sorriso-Valvo, 1991 Fig 2). The dimensions shown in Fig. 4.3.D resulted in a *Farböschung* of 0.18-0.20 which represents moderate to high mobility (Chapter Three Table 3.5). The excessive travel distance (Le) of Hsu (1975) was calculated at 2400m as seen in Fig. 4.3.D. The length of debris accumulation was measured to 2950m. The average slope angle of the present-day surface is between 8.3°-11.2°. The mobility index Le/L compared to fall height (H) also showed moderate mobility. The Wm / Wa ratio plots in the low mobility range however Wm / D is between moderate to high mobility (Chapter Three Table 3.5 refer also to Nicoletti and Sorriso-Valvo, 1991 Fig 2).

According to the parameters outlined in Nicoletti and Sorriso-Valvo (1991), as displayed in Chapter Three Fig. 3.5., the valley types A-B are representative of the Acheron rock avalanche, which displays high to moderate mobility and low to moderate energy dispersion. The first 1500m of run out are confined by a broad 150 metre wide valley channelling the debris, encouraging mobility while the valley widening over the remaining run out distance probably encouraged deceleration and stalling. Hewitt (2002) describes a rock avalanches as *"a highly kinetic mass that lacks cohesion and tensile strength therefore moulds to the valley shape. When the confinement is removed the mass and the highest velocity will be projected directly out of the valley in a hose effect"*. It is this effect which enables smaller deposits such as the Acheron rock avalanche to achieve greater run out relative to their fall and volume (Nicoletti and Sorris-Valvo, 1991 in Hewitt, 2002).

4.3.4. COMPOSITION AND INTERNAL STRUCTURE

Exposure of the rock avalanche base is limited to three areas of active fluvial incision and bank erosion. Much of the 700m long path cut by the river has become inundated by the slumping of rock avalanche debris into the river bed as the river migrates across its river plain. The interior of the lower Acheron rock avalanche consists of "highly fragmented very poorly sorted, angular gravels, sandy gravels, and silty-sandy gravels displaying crude coarsening upward" (Mitchell, et al. 2001 p.1).

Figure 4.4. A. Close up photograph of the site three exposure showing the different layers of the terrace and the structure of the overlying rock avalanche deposit. **B.** Sketch plan of the site three river cut exposure describing the internal structure of the rock avalanche overlying the terrace surface.

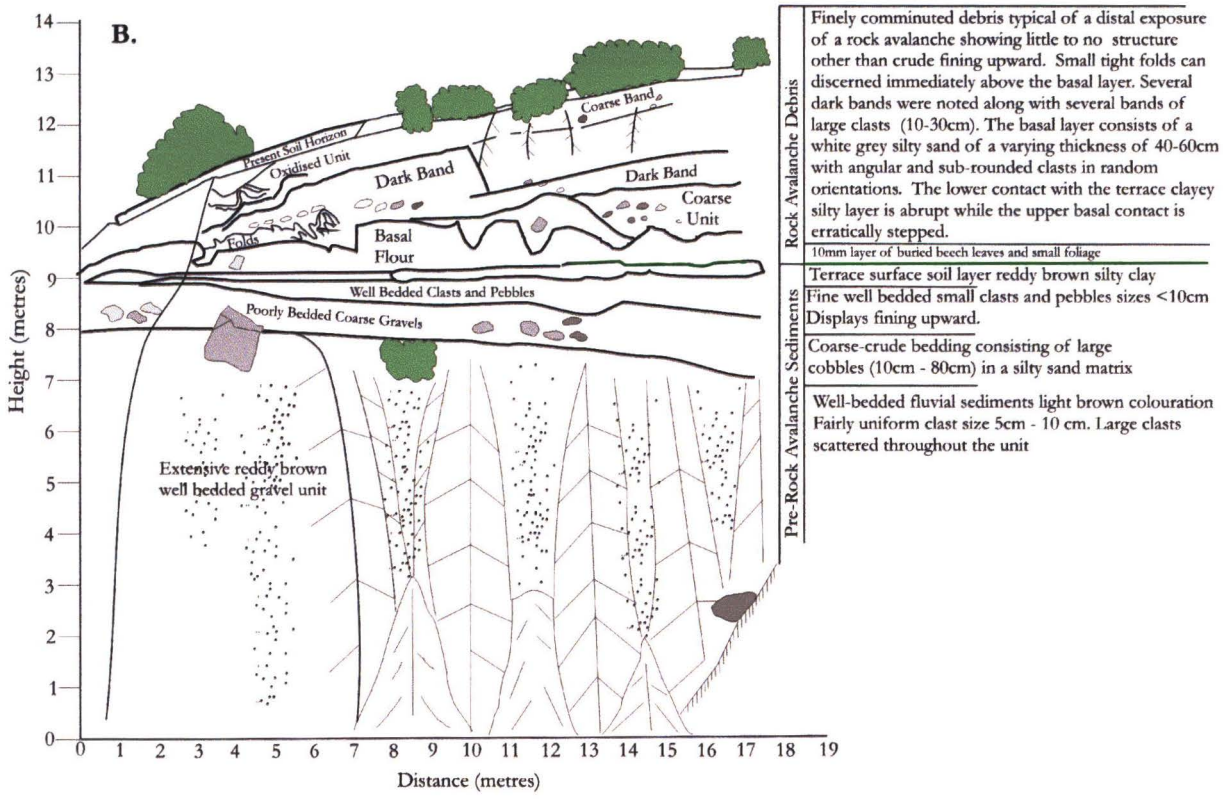

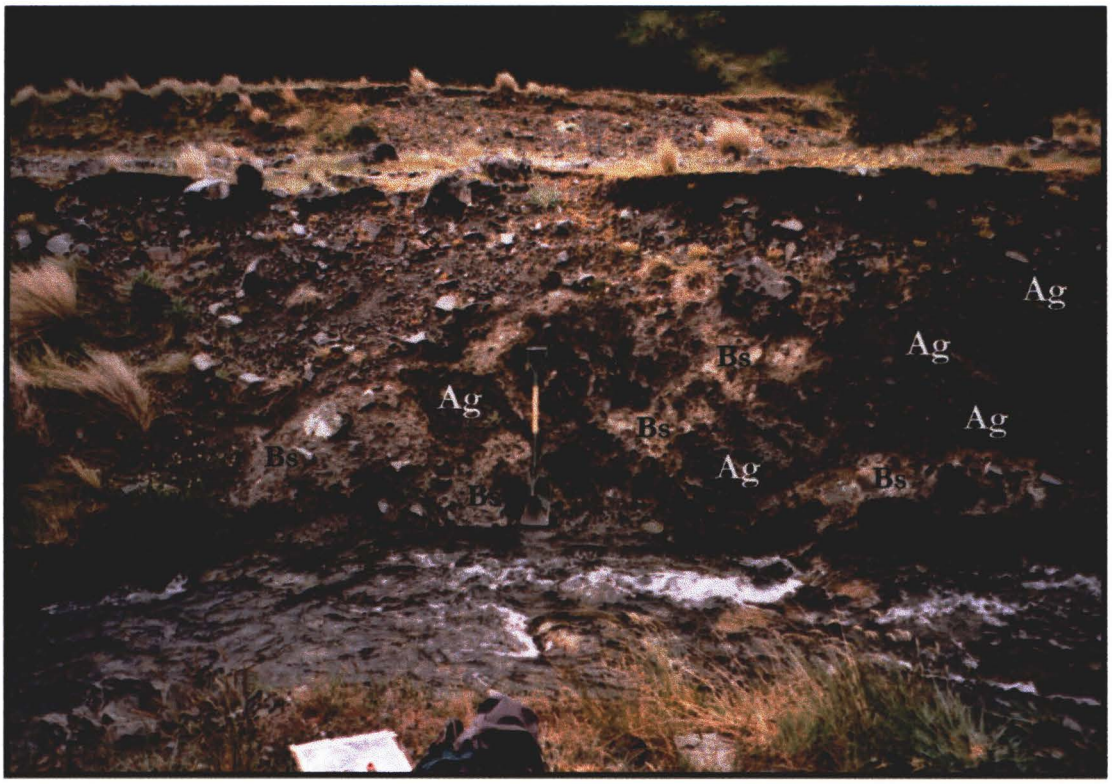

Figure 4.5: View of a distal exposure of the rock avalanche basal zone in the southern bank of the Red Hill Stream below the confluence with the Bluff River. The dark lenses represent highly-fragmented argillite and sandstone boulders (Ag) deforming with the white grey silty sand of the basal layer (Bs). The undulating appearance may reflect deceleration of the rock avalanche front causing a turbulent motion at the base. The green handled spade is approximately one metre in length.

The main exposure at site three (Fig. 4.4), shows a white–grey to light brown silty sand basal layer with a stepped upper profile containing wood fragments, rounded fluvial clasts and coarse angular fragments in random positions. Above this layer is highly fragmented greywacke and argillite material. Within this unit fold-like compression features can be observed on the lower left sloping in a southerly down-valley direction. At the base, plant foliage and terrace soils are relatively intact suggesting that emplacement at this point had slowed and was less destructive in comparison to further up valley; inclusion of wood and foreign clasts in the basal zone imply some excavation of the underlying surface by the rock avalanche. Exposures in the river bank near the distal limit show distorted clusters of elongated dark highly fragmented argillite and greywacke boulders (Fig. 4.5). This appears to be erratically incorporated into the basal silty sand layers giving the appearance of turbulent deformation. When saturated, the fragmented argillite material appears similar to clayey gouge found in a shear zones in Prickly Gully 500m to the southwest.

4.3.5. DEPOSIT THICKNESS

The site three river cut exposure shows a thickness of 3-4 metres. This matches the settled thicknesses of lobes overlying adjacent terrace surfaces near the distal extent of the deposit. The height differences between the proposed fault scarp (northeastern margin adjacent to the Bluff River) and the rock avalanche give a reasonable estimate of 7-10m thickness for the mid zone. This is also supported by differences in height between other surfaces near by using GPS. The reduction of thickness is considered to be a result of thinning associated with spreading, however isolated thickening may have also preferentially increased sections of the mid zone. Above the mid section an abrupt increase in slope angle from 7° to 17° occurs. This may represent normal changes in elevation near the head of the valley or reflect excessive proximal deposition associated with the rock avalanche. The excessive deposition caused by run up two is 25 m above the surface level and extends across the width of the valley as seen Fig. 4.3 A. Evidence in literature suggests that large portions of the rock mass accumulate proximal to the fall slope (Strom, 1996; Davies and McSaveney, 1999; Okura, 2000). This creates uncertainties about the depth of the valley floor between the fall slope (el. 1300m) and run up two (el. 1000m). It is considered by this author that an inferred thickness of >15m is acceptable assuming a minimum of 50% increase in deposition in the upper zone compared to the mid and lower zones.

4.4. THE SOURCE SCAR

4.4.1. MAPPED GEOLOGY

The source scar is found in a small tributary basin facing east-northeast near the headwaters of the Red Hill valley (refer Fig. 4.3.A. Fig. 4.6). The shape is distinctively cirque-like, with a raised lip at the opening before a steep descent down into the valley floor (refer Fig. 4.6 and Fig. 4.7 B). Ongoing talus production and minor instability created problems interpreting the pre-failure rock mass dimensions and the style of failure. The source rock is derived from Torlesse greywacke sandstone and argillite mudstone at a maximum elevation of 1520m (asl) as described in Chapter Two. The original failed rock mass is likely to have extended to a maximum height of between 100-300m above present basin floor (el. 1300m) at the foot of the source scar. This was estimated based on the height of the remnant source scar and the shape profile of adjacent topography. The plane area of the basin is 112 000m^2 with an estimated volume of between 7.5 x 10^6 m^3 as listed in Fig. 4.3.B and discussed in section 4.3.3.

Exposed bedding surfaces at the base of elevated outcrop dip steeply northward at an angle of 60°-85° into the basin centre (refer Fig. 4.6). The outcrop is crossed by multiple bands of thinly bedded argillite and sandstone sequences (40-60cm thick) bounded against massive sandstone and a massive mudstone unit located north of the scar crest. Eisbacher and Clague (1984) identify that argillite layers are typical points of weakness. It is probable therefore that the failure could have occurred along or in conjunction with these bands as implied in Chapter Two.

4.4.2 DEFECT ANALAYSIS

The pole-plot of bedding and defects showed a concentration of poles in the southwestern region of the stereonet reflecting the bedding dipping in a north-northeast direction and some defects parallel to bedding (refer Chapter Two Fig. 2.14). Comparatively the stability analysis identified shallow planar dipping defects descending into the basin centre and opposite dipping toppling planes as potential failure mechanisms in the basin (Chapter Two Table 2.4). All defects were assumed to be persistent representing the structure present prior to failure.

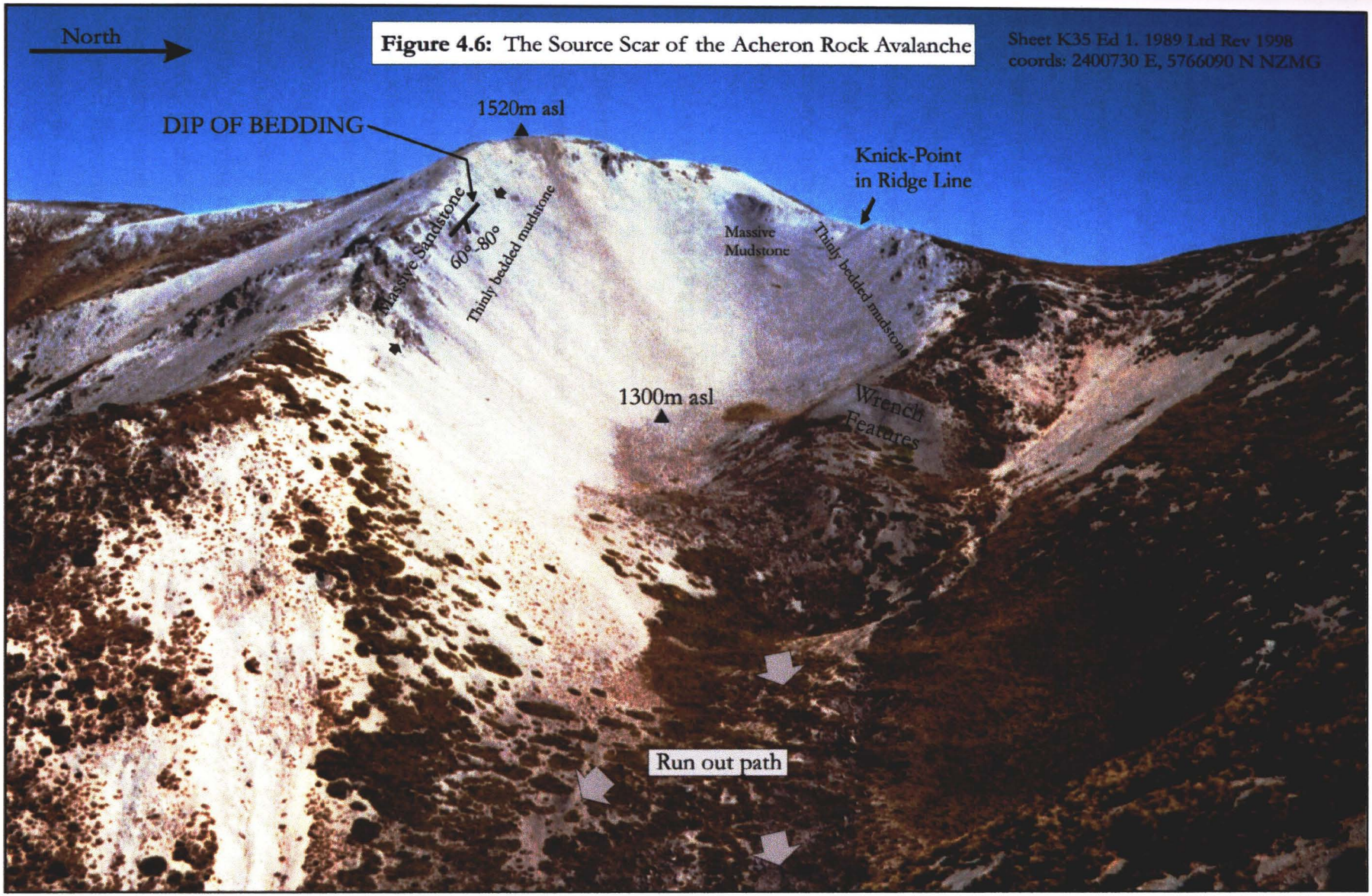

Figure 4.6: The Source Scar of the Acheron Rock Avalanche

On the western and southern sections of the basin, planar failure surfaces dip at an angle of 40°, ranging in dip direction from 003° to 050° while toppling planes dip 82°-85° in a direction of 180°-226° away from the basin centre. The average present-day slope dip direction for the section is 34°, making this a potential candidate for instability. The opposite northern outcrop is dominated by steeply dipping defects of 86° with dip direction of 340°. This region was shown to be prone to potential topple failure in a southerly direction. Wedge failure was also identified along a line of intersection 026° plunging 38° obliquely across the basin between the southeastern outcrop and the massive mudstone unit between the slope dip direction of 018° to 064°. The structural information, and the shape of the scar, suggests the source mass was an elongated body of rock striking in a northwest to southeast direction, and extending obliquely across to a nick point in the ridge north of the massive mudstone unit as seen in Fig. 4.6. This matches the direction of the tension cracks at the crown of the apex of the source basin (refer Chapter Two, Fig. 2.13). The failure model may resemble a deep-seated failure in rock described in Fig. 3.9 (Chapter Three) where progressive growth of fractures over time results in potential instability along a combination of defects and bedding planes.

4.4.3 FAILURE INTERPRETATION

The large-scale rock mass failure is inferred to have occurred in a succession of large separate slope failures of over-steepened bedrock resulting from the loss of buttress support following the initial failure of a section of outcrop. This is considered analogous to the key block concept described by Goodman and Shi (1985). The key block theory proposes that the loss of a critical block which maintains the stability within a rock mass, would cause supported blocks to fail resulting in a more extensive collapse (Goodman and Shi, 1985). In the Red Hill valley the central crown of the basin is more elevated than the adjacent outcrop, suggesting this is the primary source of failure and initial source of instability (see Fig. 4.6). Large depressions several metres in depth trend parallel to the headscarp and sub-parallel to bedding, implying that creep deformation occurred as the rock mass neared failure or failed. The creep process is well-documented in historical rock avalanches in Japan (Chiraga, 1998). The outcrop seen in the present day is highly fractured, but whether this is related to relaxation fracturing after the rock mass collapse is uncertain. The northern outcrop is considered to have failed consequentially.

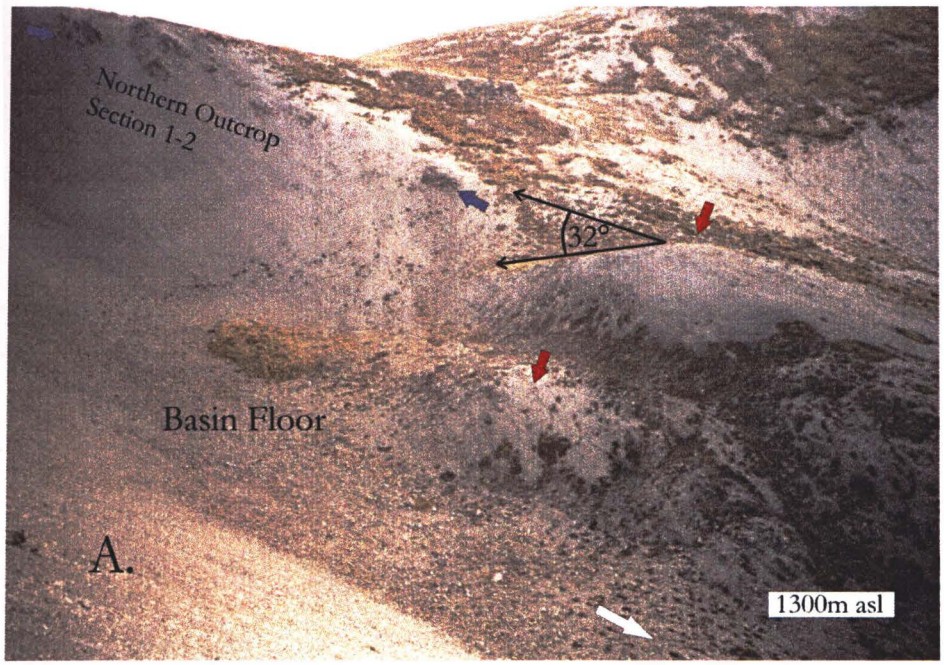

Figure 4.7: Sequence of three photographs of the source scar base from the southern ridge line looking north-northwest. **A:** The red arrows delineate the wrench features with an estimated angle of displacement. The blue arrows show the outcrop on the northern ridge line (sections 1-2) while the white arrows demonstrate the direction of debris motion. **B:** The black arrows show five lateral mounds perpendicular to the direction of motion. The sudden decline marks the lip of the source basin and the beginning of the fall slope / run out path.

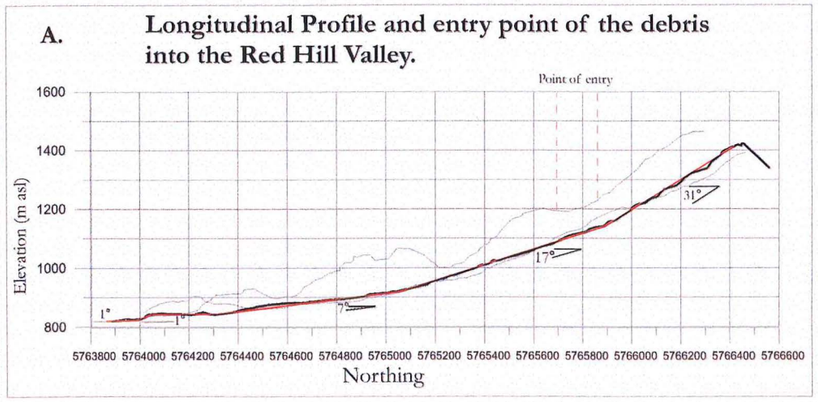

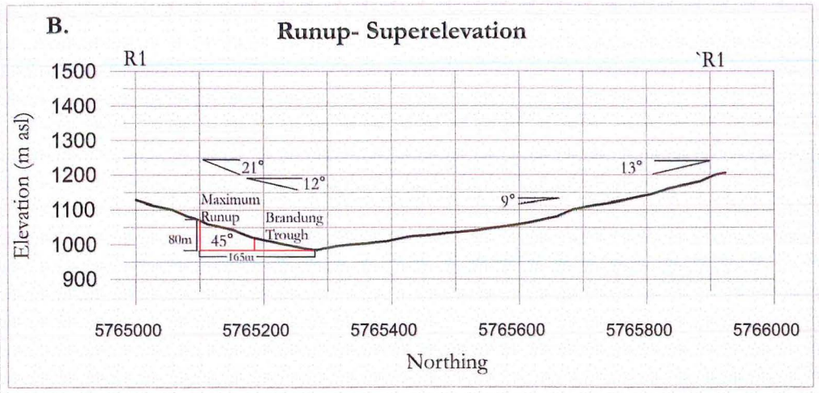

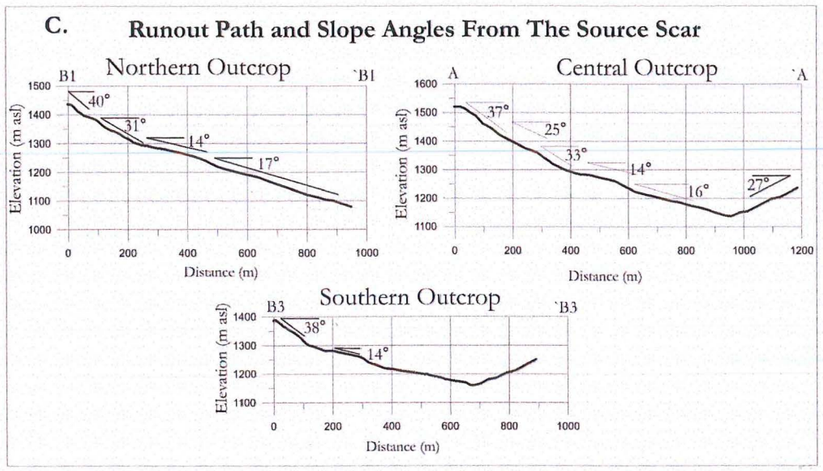

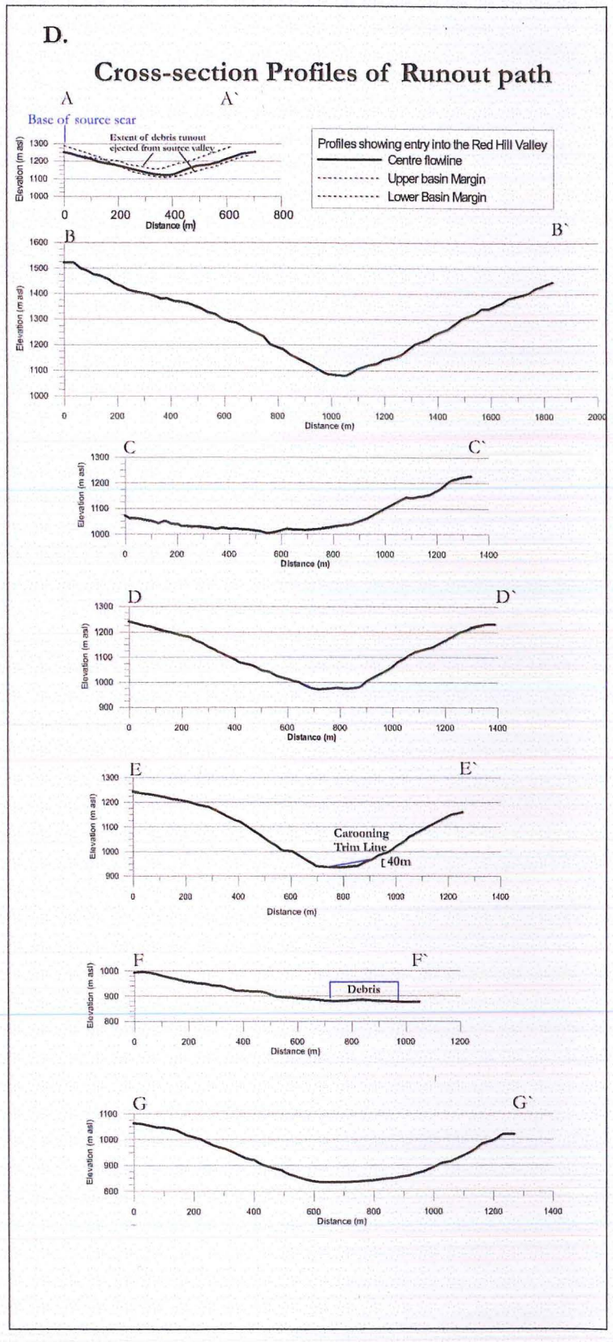

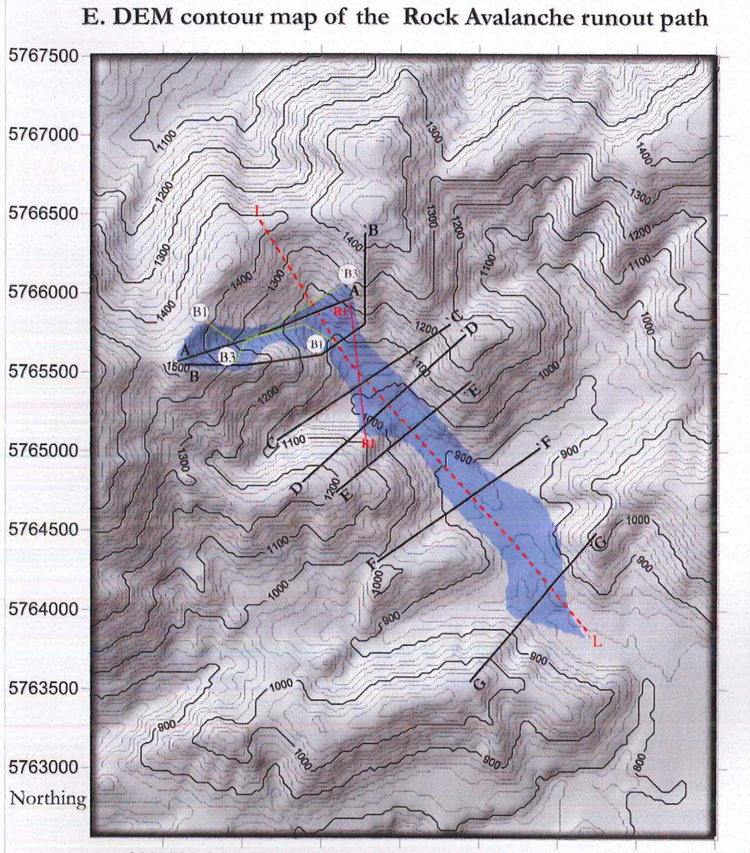

The white dashed line defines the outline of the source scar and debris of the Acheron Rock Avalanche. The black cross-sections can be viewed in the neighbouring figure and represent runout path profile. Blue lines represent slope profiles of the three aspects of the source scar. The Red Line shows the longitudinal slope of the Red Hill valley

Figure 4.8: Profiles of the Red Hill valley

- **A.** The longitudinal slope profile of the Red Hill valley and entry point of the rock avalanche debris into the valley.
- **B.** The slope angles of a run up of debris caused by a topographic obstacle used in velocity assessment.
- **C.** Slope profile of the three outcrop aspects in the source scar and run up one as the debris enters the Red Hill valley.
- **D.** Cross-section profiles of the run out path down Red Hill valley showing morphological features such as corooning and spreading.
- **E.** A grey scale and 25 m contour map showing the location of the Acheron rock avalanche deposit and profiles.

Immediately east of the northern outcrop, two sections of the original ridge line were displaced rotating approximately 30° probably as the northern slope failed. (Fig. 4.7 A). This may indicate failure direction and the areal extent of the original rock mass.

4.5. THE RUN OUT PATH

The runout of the rock avalanche is shown by the use of colour in Fig. 4.3 A. The longitudinal profile of the avalanche path can be seen in Fig. 4. 8 A. The cross-sections of the valley along intervals considered by the author to represent the valley shape can be viewed in Fig 4.8.D. The location of the profiles on a DEM can be seen in Fig. 4.8.E.

At the head of the Red Hill valley above the rock avalanche debris, the valley profile has a surface gradient of 30° ± 2° decreasing to 17° ± 2° below where the rock avalanche debris entered the valley. This change probably represents the deposition of debris during the initial run out. The slope surface then decreases abruptly to 7° ± 2° where the valley opens out into the cross-valley junction with the Bluff River and reduces further as the debris cross the lower terraces near the distal extent. The average surface slope angle of the accumulation zone (between the base of the source scar and the tip of the distal limit of the debris) was calculated as 10.5° while a line of best fit (using Grapher 4) gives a gradient of 11.2° in Fig. 4.8. The underlying surface of the run out path is considered to be narrow and steep in the proximal area defined by the dark blue in Fig. 4.3.A and wide sub-horizontal terrace surfaces and channels in the lower section seen as purple and grey in Fig. 4.3.A. The path analysis includes estimations of velocity from run up profiles based on the simple factor $(2gH)^{0.5}$ (where g is gravitational acceleration and H is the height of the run up of the debris) of which are displayed in Fig. 4.3 G and 4.8.C.

4.5.1. UPPER RUN OUT

The run out descended from an elevation of 1300m (asl) along a path orientation of 083° before entering the Red Hill valley in a progressively oblique angle of 110° based on the inferred centre line of the flow path in Fig. 4.8 E. It crossed the valley at an elevation of 1125m, striking the opposite valley wall. It is considered that some spreading and partitioning of the debris occurred up-valley, with a component of deflected run up reaching

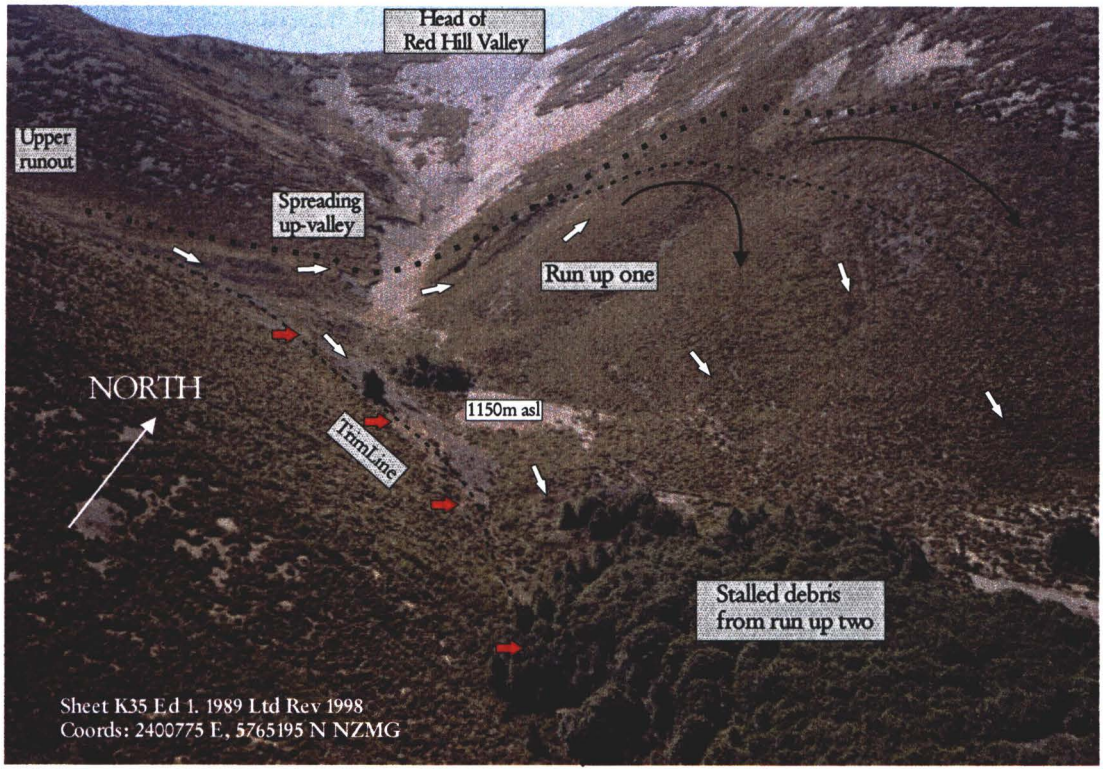

Figure 4.9.A: View looking north from above run up two across to run up one. The red arrows mark the true right margin defined by a trim line and solitary beech tree depicting the veering SW motion of the debris. The heavy dotted line illustrates the maximum possible reach of debris. The dashed line marks the probable extent of run out one. The white arrows show direction of flow.

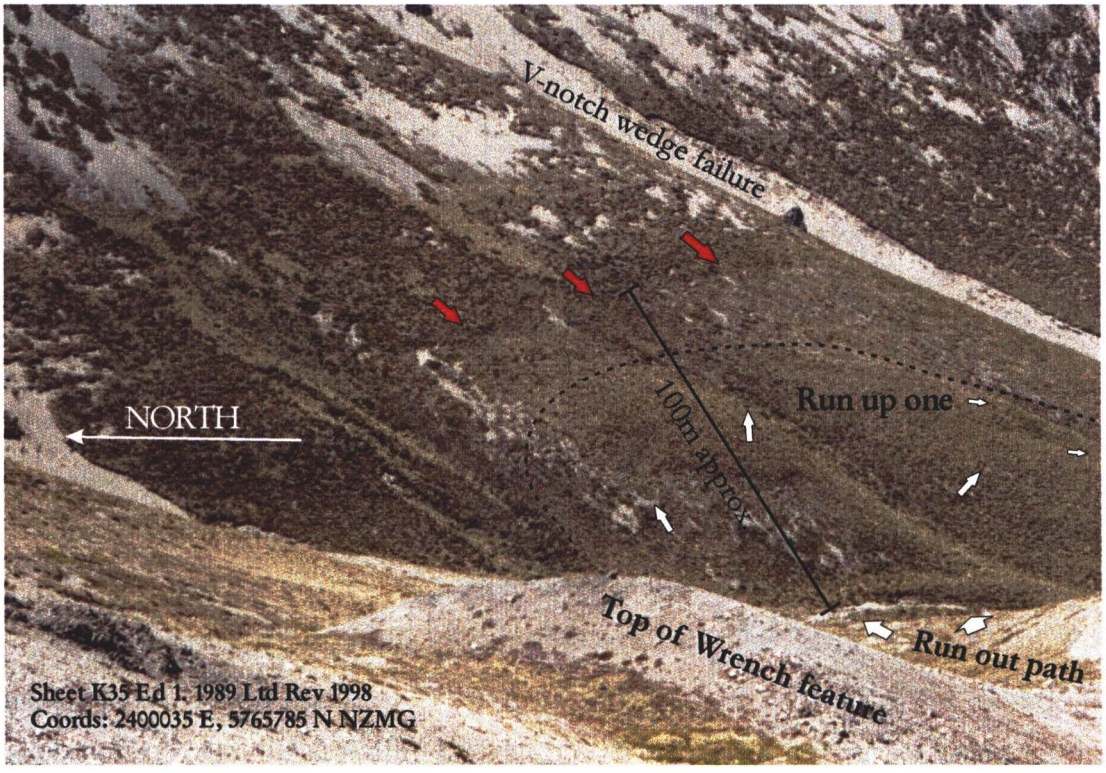

Figure 4.9.B: View east above outcrop 1 and wrench features. The red arrows mark a change in slope profile and vegetation which may represent the extent of run up one. The probable limit of the run up is outlined by the thin dashed line. The white arrow show the run out path..

an elevation of 1200m (asl) or 60-80m vertical height before descending south across the face. A large portion of the debris also veered south and followed the true right side of the valley, where a substantial caroming or trimline feature is visible. The only evidence for run up is a bulging of the lower slope and a subtle change in vegetation defined on the slope by a semi-circular shape (Fig. 4.9). For the purpose of estimates of velocity a maximum height of 80m was assigned to run up one (refer Fig. 4.3 for equation definitions). Descending from the slope (el. 1100m asl) the debris move south 40° to a direction 150° slightly oblique to the valley axis of 137°, forcing a substantial portion of the debris to impact directly with a north facing slope on the south bank of tributary one at an elevation of 1000m (asl) forming the second run up (Fig. 4.3.G, Fig. 4.10). This is considered to have reached a height of 60-80 metres forming a classic brandung or fall back ridge as seen in Fig. 3.8 resulting in deposition of debris across the breadth of the valley to an approximate thickness of 25m above the present day surface. This is depicted in Fig. 4.3 by the transparent light blue overlying the darker blue of the upper run out segment. This impact would have completely sealed off the tributary water way on the true right and partially blocked the Red Hill valley. On the true left river bank of tributary one, a cluster of 1m deep depressions interpreted to represent tree stump were observed on an east-dipping surface which may possibly have been a flood effect from the dam or a later debris flow. Post deposition establishment of beech trees clearly delineate the extent of the run up (Fig. 4.10). The debris are partially covered by a large wedge failure extending out from the true left valley side, and by recent fluvial and possibly debris flow activity.

4.5.2. MID ZONE

Following the impact associated with run-up two, the late arriving and remaining debris were deflected and partitioned over to the opposite north-eastern valley side, causing a superelevated glance or trim line across the slope (Fig. 4.10). This trim line extends 500 m in length on the true left side of the valley 35 m above the present valley floor as seen on Fig. 4.10. The trim line terminates at the mid zone where the valley gradient flattens to 7° (el. 900m) and the path widens from 150m to over 350m but can be followed further down-valley as a steep margin within the deposit. The flat terrain (called the mid zone) appears to have caused the debris to spread out laterally and begin to decelerate along an orientation of 138° (refer Fig. 4.10).

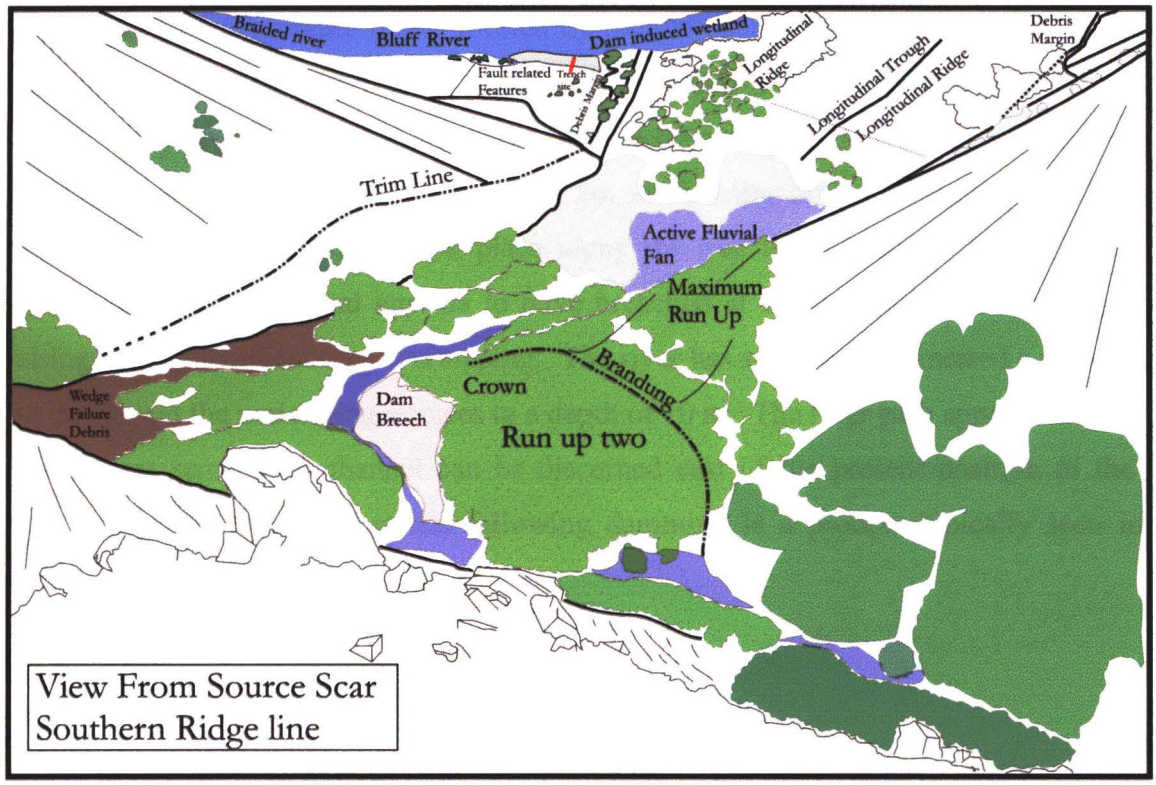

Figure 4.10. Photo and sketch of the interaction of the debris with the valley during run out. Particularly a caroming trim line, a runup from an impact with a topographical obstacle (Run up two used for velocity calculations) and the spreading of the debris with reduced topographic confinement. The surface morphology of the lower deposit can be seen in the upper right of the photo including a longitudinal depression thought to be related to an underlying buried terrace . The trench site and the effect of damming of the Bluff River are highlighted(refer Chapter Five) . Forested remains of the rock avalanche debris can be viewed as light-green fill and overlying debris from a later wedge failure are highlighted brown.

Distinctive flow ridges are visible within this zone, and are considered to be caused by areas of compression or pressure ridges formed by mobile debris running against stalled debris or underlying topographical obstacles impeding movement. The most prominent features in this section are a large longitudinal depression in the centre of the deposit, steep lateral margins and the presence of large clasts exceeding 2m in diameter on the forested true left surface. Damming of the Bluff River took place along the true left or northeastern margin of the deposit (el. 875m asl), and appears to have breached at a low point following aggradation raising the bed level causing overtopping. The river has subsequently incised a route through the debris and the underlying terraces to a depth of 10 m. The river path appears to be new, as a redundant semi-filled channel can be discerned east of the present position of the Bluff River. Incising of new channels following damming is a process typically seen in rock avalanche deposits (Hewitt, 2002).

4.5.3. DISTAL ZONE

Below the mid zone at el. 870m the debris on the northeastern margin again encountered the true left valley side. This caused a slight deflective rise across the slope and a change in travel direction to 177°, before descending onto the oldest terrace (T1) surface to decelerate and stop just beyond the present day terrace edge. This is clearly identifiable by the first lobe crossed by the access road on the true left (see Map 1). On the true right margin a lobe flowed along a T2 terrace surface crossing the Red Hill stream (el. 850m), and impacting at low velocity against a northeast facing hill forming a minor fall-back ridge. The Red Hill stream was dammed at this point, and formed a wet land extending 100m up valley. The breach is narrow and similar in morphology to that described in tributary one dammed during run-up two. The orientation of the lobe is 195°-200°, and is discernible by a triangular pocket of exposed T2 terrace surface (see Map 1). Beyond the dammed tributary a slight change of elevation occurs and marks the termination of motion. Terrace sets are well established showing T1-T3 surfaces all of which have been overridden by the debris descending onto the river bed. The maximum extent of the rock avalanche is considered to be a further 200m beyond the lobe margin based on the presence of plastered basal deposits similar to those observed at the site 3 exposure within an incised river bank (refer Fig. 4.5). This is described as grey-white silty sand matrix containing clasts of fluvial gravels similar to that observed in the walls of incised terraces and overlain by highly fragmented argillite. Subtle shape irregularities on the T2 and T3 terrace surfaces imply that the deposit may have extended

beyond this point. Whether this mobility is the result of the mass motion or the drop down the terrace sets to the Red Hill stream is uncertain. However the river bed rock avalanche exposures appear to be insitu and not redistributed by the river. Interestingly the river bed level has eroded through the debris but has not incised beyond that of the valley floor as defined before the rock avalanche event, which suggests a geomorphic equilibrium may exist.

4.5.4. EMPLACEMENT SEQUENCE DISCUSSION

4.5.4.1. UPPER RUN OUT ZONE

The debris descended from the source basin and immediately encountered the opposite west facing valley side referred to as run up one. The effect of run up one on energy dissipation of the rock avalanche is considered to be low because of the 2353m of the accumulation zone or runout path remaining beyond run up one. This supports the conclusion that the bulk of the mass was deflected across the slope rather than directly impacted against the opposite valley wall.

Run up two involved a direct impact of part of the debris front into the hillside resulting in a probable deflection and split of the moving mass. This caused high dissipation of the masses kinetic energy resulting in a 25m thick deposition of debris over approximately 65 000m^2 area. It is uncertain how this affected the remaining run out. However the stalled debris would have acted as a considerable obstacle to later arriving debris suggesting that a large portion was in motion at the same time and place and by-passed the impact of run up two travelling a further 1560m down-valley.

4.5.4.2. MID ZONE

The longitudinal depression along the centre of the mid deposit almost certainly represents a buried terrace extending up the valley rather than separate deposits. A similar effect can be seen in the redundant waterway east of the current path of the river through the deposit. An alternative idea is that spreading associated with sudden release from the confinement of the valley sides may have caused an increase in active dispersive pressure to the areas of low pressure, resulting in a depressed centre. This may also have contributed to the slowing down of the main mass and a thickening of the deposit between el. 900-875m.

4.5.4.3. DISTAL ZONE

The presence of lobes in the lower section of the deposit implies partition of the debris mass, which can be attributed to the obstacles in the run out path (Hewitt, 2002). This is based on two points identified in Hewitt (2002).

The first is the topographic interference along the run out path. From the first deflection of run up one, the timing of debris would have differed over its areal extent. The effect of run up two would have further separated the debris with the caroming on the true left side showing evidence of this. The second point is the stalling of the main mass; the stopping of the central mass in the mid zone would deflect later arriving material, causing it to split off creating lobes (Hewitt, 2002). Thickening in the mid zone of the deposit demonstrates mobility had slowed down and was being overrun by later faster debris supporting this observation.

The direction of the final lobe positions of 195°-200° on the true right, and 177° on the true left, deviates from the valley axial trend of 137° by between 30°-60°. This suggests that the rock avalanche emplacement may have occurred in stages where the bulk of the debris lost mobility beyond the position of the fence line crossing the deposit today (el. 865m see Map 1). The later more mobile flows concentrated on the true left were deflected by the renewed narrowing of the valley sides resulting in a 30°-60° change in direction. The fact that this occurred suggests that the debris was still extremely mobile at (el. 875m) 3000m of the run out.

4.6 THE AGE OF THE EVENT

4.6.1. PREVIOUS STUDIES

The first date for the Acheron rock avalanche deposition was a radiocarbon age (NZ547) derived from wood retrieved from a river cut exposure in a tributary of the Red Hill stream (site 3 in this study see Fig. 4.11, Burrows, 1975). Burrows (1975) described a buried forest horizon overlying yellow-brown soils located on reddish horizontally bedded gravels. Above this layer Burrows (1975) noted the unweathered poorly-sorted angular pebble and cobble gravels which were interpreted to represent the rock avalanche deposit. Burrows (1975) extracted wood samples from along the exposure presumably from the buried forest horizon which was radiocarbon dated at (NZ547) 500 ± 69 years B.P.

Later age studies of the Acheron rock avalanche deposit were aimed at assessing its potential as a paleoseismic indicator for Holocene rupture events along either the Alpine Fault or the Porters Pass-Amberley Fault Zone (Porters Pass Fault). This included lichenometry, and two greywacke rock weathering-rind ages (Whitehouse and Griffith, 1983; Bull and Brandon, 1998; Howard, 2001).

The lichen study conducted by Bull and Brandon (1996; 1998) examined regional rock fall events associated with ruptures on the Alpine Fault, and used a polymodal distribution of the measured maximum diameters of lichen to determine an emplacement age and subsequently episodic rupture events. At the Acheron deposit prolific populations of lichen diameters of 84mm or less were measured representing an age of 460 ± 10 yrs BP (using the normal Gaussian distribution) supporting the NZ547 age of 500 ± 69 yrs BP (Bull and Brandon, 1996, 1998; Howard, 2001). The two weathering rind ages identified slightly differing modal peak thicknesses. Whitehouse and Griffith (1983) calculated 0.66mm while Howard (2001) measured a modal peak of 0.83mm. The 0.83mm thickness from Howard's study placed the rock avalanche within the 1992 weathering rind calibration curve of McSaveney (1992) representing an age of 490 ± 55 years B.P. (Howard, 2001). Howard (2001) averaged the combined ages from the different dating techniques and calculated a mean age for the deposit of 464 ± 79 years B.P (545 – 385 years B.P).

To identify stratigraphic evidence of paleoseismic rupture, Howard (2001) conducted four trench investigations along the Porters Pass Fault (which underlies the Acheron rock avalanche deposit). Howard unable to find evidence for a rupture around 500 years B.P, instead proposed 1000 ± 100 years for the timing of the last fault movement (Howard, 2001). This age was derived from two radiocarbon dates (Wk 9241 cal 1604 ± 82, Wk 9236 cal 870 ± 76 years B.P.) from a trench excavated at Porters Pass, and one from a test pit (Wk 9234 cal 949 ± 22 years B.P.) three km to the west of Porters Pass (Howard, 2001). Howard appears to have averaged the three dates to obtain to an age estimate of 1000 ± 100 years B.P.

To confirm the age of the rock avalanche and find evidence of a relationship to Holocene paleoseismic activity along the Porters Pass Fault, the north-eastern margin of the site identified in Burrows (1975) was resampled and a new site located several hundred metres down stream was also sampled. All grid references for sample locations are Sheet: K35 Ed 1. 1989 Ltd Rev 1998 presented as Northing and Easting N.Z.M.G.

4.6.2. SAMPLE SITES

Incision of a channel through the lower Acheron rock avalanche deposit by a tributary of the Red Hill stream has exposed the contact between the rock avalanche and the underlying terrace surface at four sites containing buried wood shown in Fig. 4.11.

4.6.2.1. SITE ONE (Coords: 2401840E, 5764010N NZMG).

In the most distal section of the rock avalanche, the river has eroded and removed most of the rock avalanche deposit. However, remnants of the basal zone consisting of white-grey silty-sand with angular to sub-rounded clasts and wood fragments in a random position exposed in a riverbank as shown in Fig. 4.12. This site is away from the sample site identified by Burrows (1975) (site three-four) as seen in Fig. 4.11 and is within a mixing zone interpreted to be immediately above the contact with the pre-rock avalanche surface. A wood sample of was retrieved from this site.

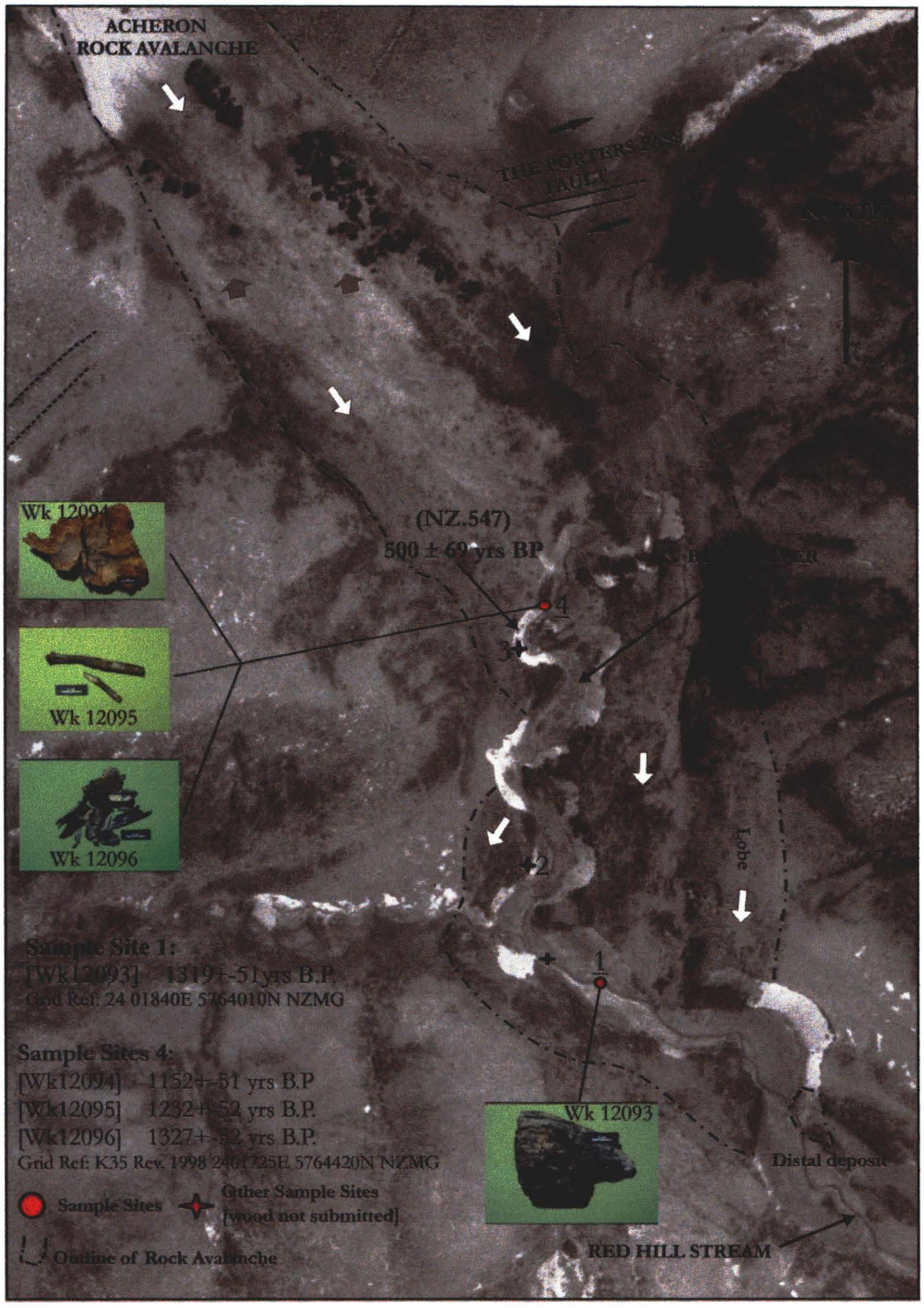

Figure 4.11: Aerial photograph of the lower Acheron rock avalanche deposit showing the location of buried wood (sites 1-4) The localities where wood samples selected for radiocarbon dating were collected can be identified by the red circles (site 1 and 4) while unsampled sites are pinpointed by a red star. The area inferred to be the sampling site for both weathering-rind and lichen studies extends north beyond site 4. The positions of both the NZ547 sample and the Porters Pass Fault as described in Chapter Five are also shown. The grey arrows show minor lineaments similar in orientation to the fault crossing the deposit discussed in Chapter Five.

4.6.2.1.1. SAMPLE DESCRIPTION (Wk 12093) (Refer Figure 4.14 A)

The wood fragment of *Northofagus solandri var. cliffortiodes* exceeds 20cm in length, displayed growth rings, heartwood and some remnant bark (see Fig. 4.15 A.). The extremities of the wood are rounded suggesting entry into the fluvial system or forest litter prior to the rock avalanche event or the product of damage incurred during burial by the Acheron rock avalanche deposition.

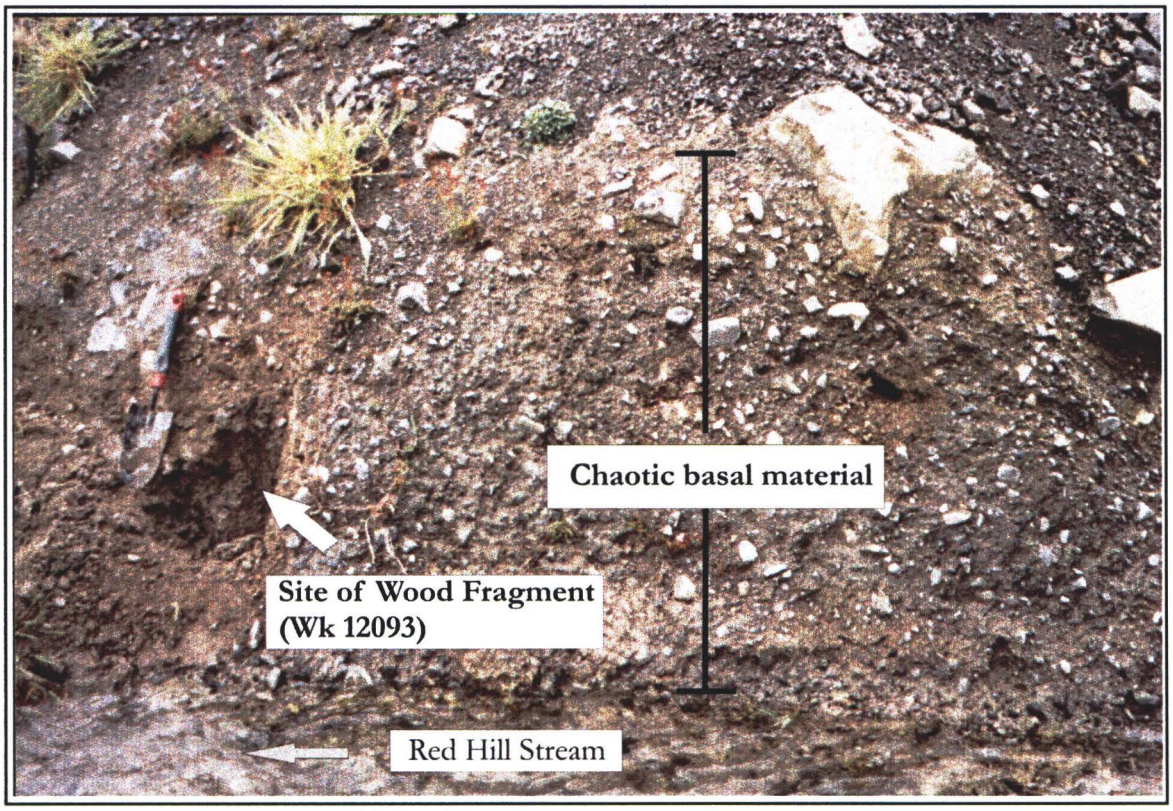

Figure 4.12: Location of sample Wk 12093 (wood fragment) in the southern stream bank near the rock avalanche distal limit below the confluence of the Bluff River and the Red Hill stream. The unit is made of basal rock avalanche material consisting of white grey silty sand containing wood material, angular fragments and inherited sub-rounded clasts in random orientations.

- Buried wood was also identified by not collected in Red Hill stream watercourse 10m upstream from Wk 12093 submerged at the contact between the terrace and rock avalanche shown in Figure 4.11 (Coords: 2401775E, 5764040N NZMG).

- SITE TWO (Coords: 2401735E, 5764190N NZMG)

  Wood was located above the contact between the terrace and an isolated lobe on the true right of the rock avalanche shown in Fig. 4.11. Wood appeared to be penetrated by modern vegetation and uncertainty exists to their reliability for dating therefore was not sampled.

- SITE THREE (Coords: 2401725E, 5764420N NZMG)

This site is the one identified in Burrows (1975) and is the largest section of exposed contact in the study area which includes site four at its eastern extremity as shown in Chapter Two Fig. 2.9. Wood fragments were found within the zone of mixing to a height of 40cm above the terrace surface-rock avalanche contact however due to the lack of large intact wood samples displaying growth rings no sample was extracted from this site.

4.6.2.2. SITE FOUR (Coords: 2401730E, 5764420N NZMG).

This locality had the most abundant and best source of buried plant material. Found at the southeastern limit of the site three exposure containing a buried tree, profuse leaf litter, and small sticks with bark cover. Erosion of the exposure has occurred by down cutting of the stream but also from water seepage along the rock avalanche and the terrace surface contact. This site faces towards the southeast (137°) away from the sun, reducing diurnal wetting and drying of the samples offering a good dating opportunity of the contact and upper surface of the terrace (see Fig.4.11). Certainty can be given to the burial of the samples by the Acheron rock avalanche, particularly by their orientation which appears flattened in a down valley direction.

The stratigraphy displays reddish brown sandy gravels overlain by yellow-brown silty clay interpreted to represent the terrace surface layer immediately below the soil horizon (Fig. 4.13). Above this extends 3-4m of blue grey angular coarse rock avalanche debris. The wood material was found directly in the contact and the top 5cm of the silty clay layer (Fig. 4.14). The material within the silty clay layer is thought to be the result of the tree sample being pushed into the top of the terrace by the weight of the overlying rock avalanche debris. Three wood samples were retrieved from this site for radiocarbon dating (Fig. 4. 15 B-C).

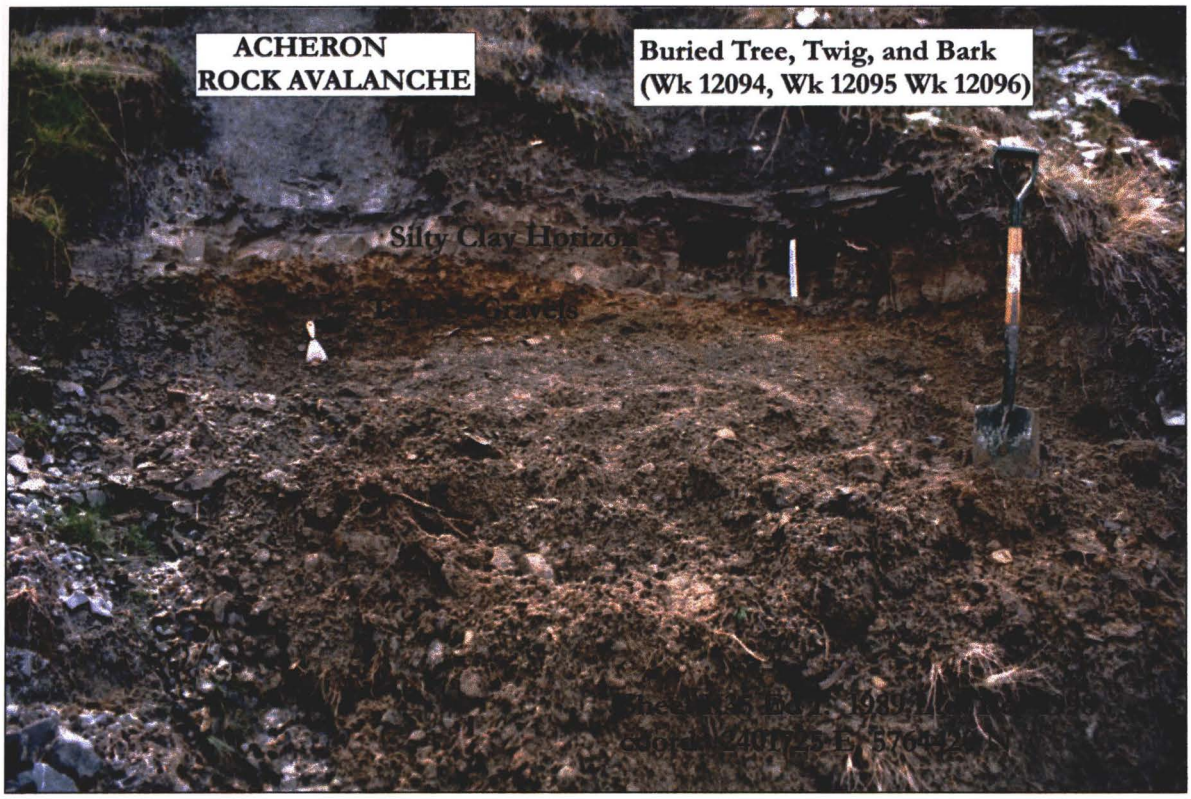

Figure 4.13: Photograph of the site four exposure showing the position of the buried tree, twig, and bark at the sharp contact between the rock avalanche deposit (blue-grey colouration) and the silty clay and reddy brown gravels of the underlying terrace surface (T2). This is consistent with the stratigraphy observed at site three (seen in Fig. 2.9 and Fig. 4.4). The green handled spade is approximately one metre in length.

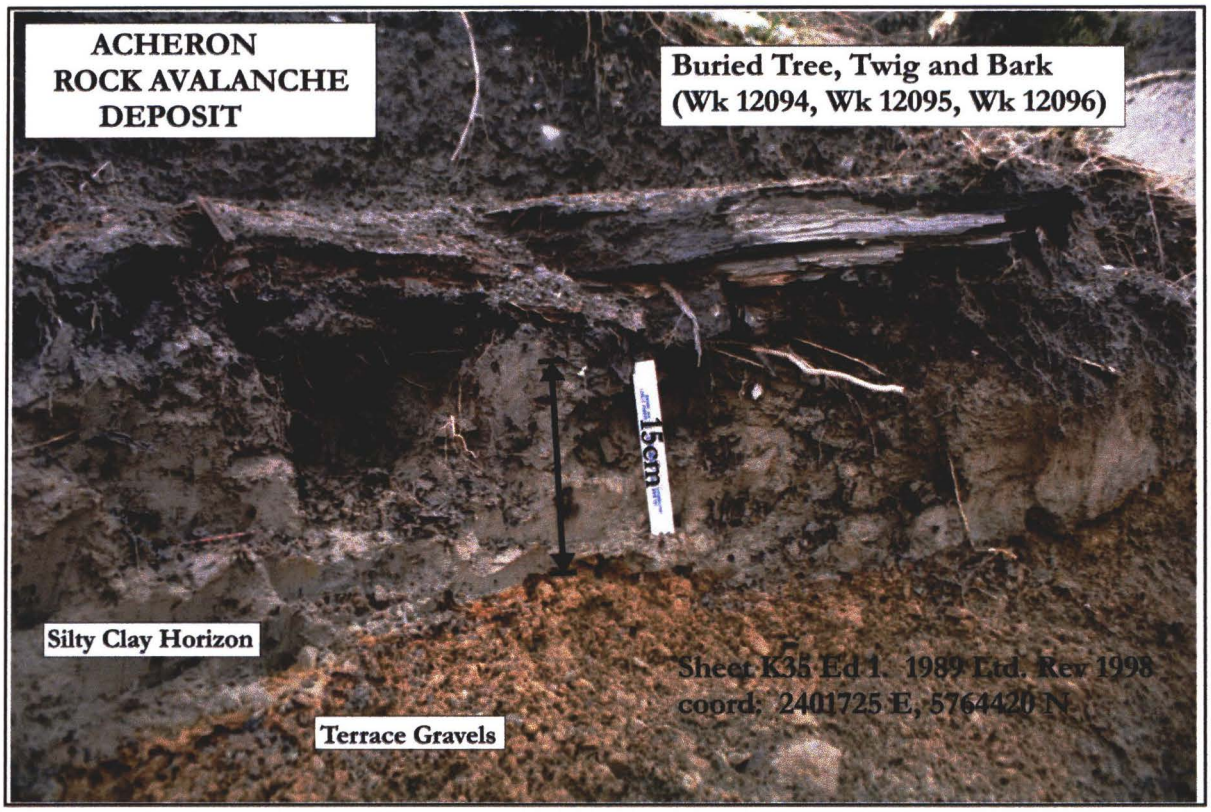

Figure 4.14: Close-up photograph of the site 4 exposure containing the buried wood, twig and bark in the contact between the rock avalanche and the terrace material.

4.6.2.2.1. SAMPLE DESCRIPTION (Fig. 4.12 B-D)

BURIED TREE (Radiocarbon sample Wk 12094) (refer Fig. 4.15 B)

The sample is a cut cross-section from the base of the trunk of a remnant tree identified as *Northofagus solandri var. cliffortiodes* excavated from the top of the terrace surface (see Fig. 4.14, Fig. 4.15 A., Prof. Butterfield pers comm. 2003). This sample is considered to have a growth age of 76-80 years based on the 76 ± 5 counted growth rings. The tree is lying in an easterly direction down valley displaying strong evidence for being flattened during the rock avalanche event.

BURIED STICK (Radiocarbon sample Wk 12095) (refer Fig. 4.15 C)

Around the buried tree in the upper silty clay layer of the terrace is abundant stick fragments with bark and some with distinct growth ring. One stick sample was collected displaying growth rings of 10 ± 5 years as seen in Fig. 4.15.C.

BURIED BARK FRAGMENTS (Radiocarbon sample Wk 12096) (refer Fig. 4.15 D)

Bark fragments interpreted to be from sticks and proximal to the buried tree were located around the buried tree sample within the silty clay of the upper terrace layer. The bark forms from growth cells in the cambium or sapwood and typically accumulates over the trees life (Prof. Butterfield pers comm. 2003). The barks relationship to the rock avalanche emplacement is based on its proximity to the excavated tree.

4.6.3. CONSIDERATIONS ASSOCIATED WITH SAMPLE CHOICE

The objective when dating an event in a known position is to find a piece of wood best reflecting or representing the time of burial with the smallest associated inbuilt age (McFadgen, 1982). This refers to the growth age or the living age of the tree, and the time between the death of the sample and the occurrence of the event called the storage age (McFadgen, 1982). A tree could lie prone on the forest floor or be preserved in a swamp for an unknown period of time before burial (McFadgen, 1982). McFadgen refers to this time lapse as the *Storage Age* and suggests that this must be added to the age of the *Tree Age* to gain the actual total inbuilt age (McFadgen 1982). Just as important is the stratigraphic position of the sample in relation to the event layer. McFadgen (1982) identified three stratigraphic positions that can occur relative to the horizon marking the event; described as above the event, within or contemporaneous to the event and below the event. This can affect the usefulness of the inbuilt age and results in dates referred to as maximum age, close to the event, minimum age or unknown age (McFadgen, 1982). The ideal sample should have a known small inbuilt age, retrieved from a contemporaneous position giving a close result. It is also important to understand the structure of a tree when choosing the most reliable sample.

The youngest component of a tree is the wood surface located between the outer bark layer and the sapwood (Prof. Butterfield pers comm. 2003). It is here that the growth region of a tree exists in a layer called the Cambium which is made up of a thin band of cells. These cells divide adding new bark to the outer of the Cambium and new sapwood to the inside. Comparably, smaller tree fragments such as twigs and small branches are also considered good samples for dating because their life span is short and often best represent the actual time of burial by having negligible inbuilt ages (McFadgen, 1982).

TABLE 4.1: Radiocarbon ages and their significance for the deposition of the Acheron rock avalanche. Ages presented as conventional ages of years B.P (Before 1950) unless otherwise stated. (Refer to Appendix C.2 for calibration diagrams)

Radiocarbon Age (Years BP) 1950	**Location Sheet: K35 Ed 1 1989 Ltd Rev 1998**	**Stratigraphic Description**	**Interpretation of Age Significance**
Wk 12093 1319 ± 51 yrs B.P.	Site One 2401840E, 5764010N NZMG.	Wood within basal silty-sand unit of lower rock avalanche deposit with angular to sub-rounded clasts.	Dates the distal extent of rock avalanche and is located within the basal rock avalanche deposit.
Wk 12094 1152 ± 51 yrs B.P.	Site Two 2401730E, 5764420N NZMG	Cut cross-section from trunk of buried beech tree at contact between in soil horizon and the rock avalanche.	Contemporaneous sample killed during the deposition therefore dates the occurrence of the event.
Wk 12095 1232 ± 52 yrs B.P.	Site Two 2401730E, 5764420N NZMG	A twig buried around tree at the contact between silty clay of terrace layer and the overlying rock avalanche deposit.	Retrieved from a contemporaneous position and has the smallest probable inbuilt age.
Wk 12096 1327 ± 52 yrs B.P.	Site Two 2401730E, 5764420N NZMG	Bark fragments buried around buried tree in the silty clay of the upper terrace layer.	Forms as an accumulation as the tree grows potentially reflecting the total age of the tree.

4.6.4. INTERPRETATION OF AGE RESULTS

Radiocarbon ages are presented as conventional ages (as given in the age reports by Waikato University radiocarbon dating laboratory refer Appendix C.2). Conventional ages can be calibrated against the international calibration curve for terrestrial samples, to produce the calibrated ages referred to in the diagrams in Appendix C.2. They are adjusted for New Zealand by applying the New Zealand correction of 27 ± 5 years. Results displayed in calibrated years BP can be viewed in Appendix C Table 3.

Wk 12093 Wood fragment from Site One 1319 ± 51 yrs BP.

Wk 12094 Cut cross-section from buried tree at Site Four 1152 ± 51 yrs BP.

Wk 12095 Buried Twig from Site Four 1232 ± 52 yrs BP.

Wk 12096 Buried Bark fragments retrieved from Site Four 1327 ± 52 yrs BP.

Figure 4.15 A-D: Samples submitted to Waikato Radiocarbon Dating Laboratory

SITE ONE

SAMPLE Wk12093

This sample was deemed fairly well preserved and intact (Fig. 4.12, Fig. 4.15 A). The outer edge of the wood was convolute, which is considered typical of the outer area of a tree (Prof. Butterfield pers comm. 2003). Drying cracks inside the sample, typically point into the heart which was recorded on the sample indicating a largely intact specimen. This sample had visible tree rings suggesting a negligible though potentially unknown inbuilt age. The location of the wood in the white grey silty sand of the basal material implies it was incorporated into the rock avalanche base from an unknown position further up valley. The age of 1319 ± 51 years B.P. is the second oldest date, suggesting an unknown inbuilt age.

SITE FOUR

SAMPLE Wk 12094

The buried tree's outer half had partially deteriorated but still enabled an accurate ring count to be conducted to 76 ± 5 rings (refer Fig. 4.15 B). The cross-section ring was cut from the basal trunk region which may reflect the entire life of the tree resulting in ages of the oldest part of the tree as well as the youngest. However the sampling process was from the outer ten rings (F. Petchley, pers comm. 2003). This sample is the most contemporaneous of all the samples dated suggesting that the inbuilt age was solely the growth age (refer Fig. 4.13). The resulting age 1152 ± 51 years B.P. would therefore reflect a maximum age of the tree. Conversely the comparatively young date suggests that contamination by younger carbon may be present, however the chemical pre-treatment during the testing makes this unlikely (Hogg, pers comm. 2003). The excellent relationship to the stratigraphy and the highly probable death during the deposition of the Acheron rock avalanche supports the use of this sample age.

SAMPLE Wk 12095

The twig sample has an age of 1232 ± 52 years B.P. which is the second youngest. The inbuilt age is expected to be negligible and was retrieved contemporaneously giving a close age for the event. The radiocarbon age would also reflect an average age of the entire specimen. In contrast the date of the twig is older than the buried tree sample (Wk 12094) which implies an inbuilt age. This may represent storage of the specimen on the forest floor before the actual event resulting in an age older than the rock avalanche.

SAMPLE Wk 12096

The age of 1327 ± 52 yrs BP for the bark fragments (Wk 12096) is the oldest of the four samples and is considered to reflect the growth age of a tree. Because bark accumulates over the life of the tree, dated bark material may be representing an age older than that of the younger wood immediately beneath, which may reflect why it has the oldest date. Equally it may be derived from another buried tree present within the exposure. It is considered that the bark is not the best sample to use to represent the emplacement of the rock avalanche but does signify a maximum age for its deposition.

4.6.5. DISCUSSION ON THE RESULTS

The combined four dates show a consistent overlapping range of ages as seen in Table 4.1. This demonstrates a probable timing for the emplacement of the Acheron rock avalanche as closely post-dating the age range. However, from these four radiocarbon dates what sample best represents the age of the Acheron rock avalanche and potentially a rupture on the Porters Pass Fault.

A statistical analysis using the standard errors was applied by Waikato University Radiocarbon Laboratory to compare the sample dates of Wk 12094 (buried tree) and Wk 12095 (twig). Using the *t*-test, a statistical test designed to investigate if the two dates are dissimilar or not, *t* was calculated for the two samples giving the number 1.09.

To be able to demonstrate that the results are statistically different, *t* must be greater than 3.84 (Hogg pers comm. 2002). This means that the two dates are statistically identical and the fact that one sample appears older and the other younger is therefore irrelevant (Appendix C 2).

Regardless of the statistical similarities the close contemporaneous position of the buried tree (Wk 12094) in conjunction with the youngest age of 1152 ± 51 years B.P is considered by the author to best represent the close age that the rock avalanche occurred and potentially a paleoseismic event along the Porters Pass Fault or Alpine Fault.

4.7. DAN RUN OUT SIMULATION

The appreciation of the destructive hazard posed by rock avalanches has led to advances in the numerical prediction of long run out. An advocate of this is Oldrich Hungr (Hungr, 1995, 1996, 2001). While the idea of predictive run out is not new, Hungr (1995, 1996, 2001) developed a model which could apply a variety of rheological mechanisms, and parameters such as topographical confinement, material properties, internal stiffness (Koerner 1976; Perla, et al. 1980; Hutchinson, 1986; Savage and Hutter, 1989; Hungr, 1995 and others). Previous modelling attempts focused on a single rheological model using a lumped mass Eulerian framework widely used in hydraulics (Fell et al, 2001). Comparatively, the DAN simulation utilises a numerical one-dimensional Lagrangian solution to the equations of motion enabling it to simulate dry granular flow using a curvilinear coordinate profile (McLellan and Kaiser, 1984; Hungr, 1995; Davies & McSaveney, 2002 see Fig 4.16).

The model is able to divide the mass up into a predetermined number of slices perpendicular to the basal surface (run out path) and calculates the forces on individual slices and its boundaries at each time interval (Davies and McSaveney, 2002). To run a simulation, the DAN model requires geometry of the run out surface including width, the geometry of the pre-failure source rock mass, properties of the rock mass, cross-section parameters and properties of the chosen rheological model (Davies and McSaveney, 2002).

The flexibility of the program allows a range of seven rheologies to be applied to different case-study situations ranging from debris flows to dam failures to best simulate run out (Hungr, 1995, 1996). Hungr, (1996) identified three rheological models representative of the process of rock avalanching-induced long run out, which performed well when tested in the field and laboratory (Hungr, 1995, 1996; Evans et al. 2001; Davies and McSaveney, 2002). These are the Voellmy turbulent flow model, the Bingham flow model and the Frictional model

Figure 4.16: The Lagrangian mesh in curvilinear coordinates.

C Boundary blocks are numbered 1, 2 etc
C Mass blocks are numbered 1a, 2a 3a

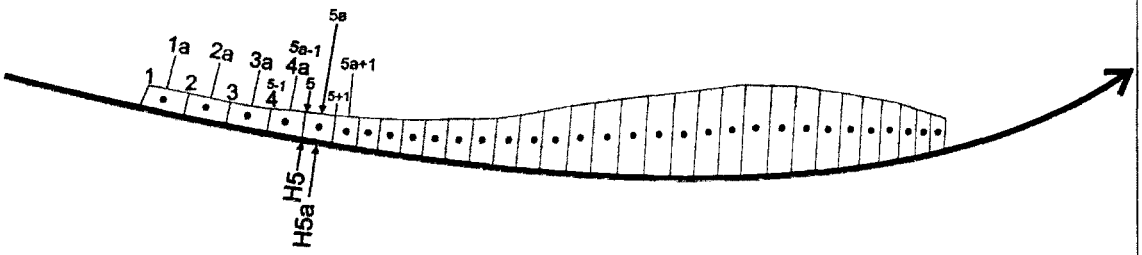

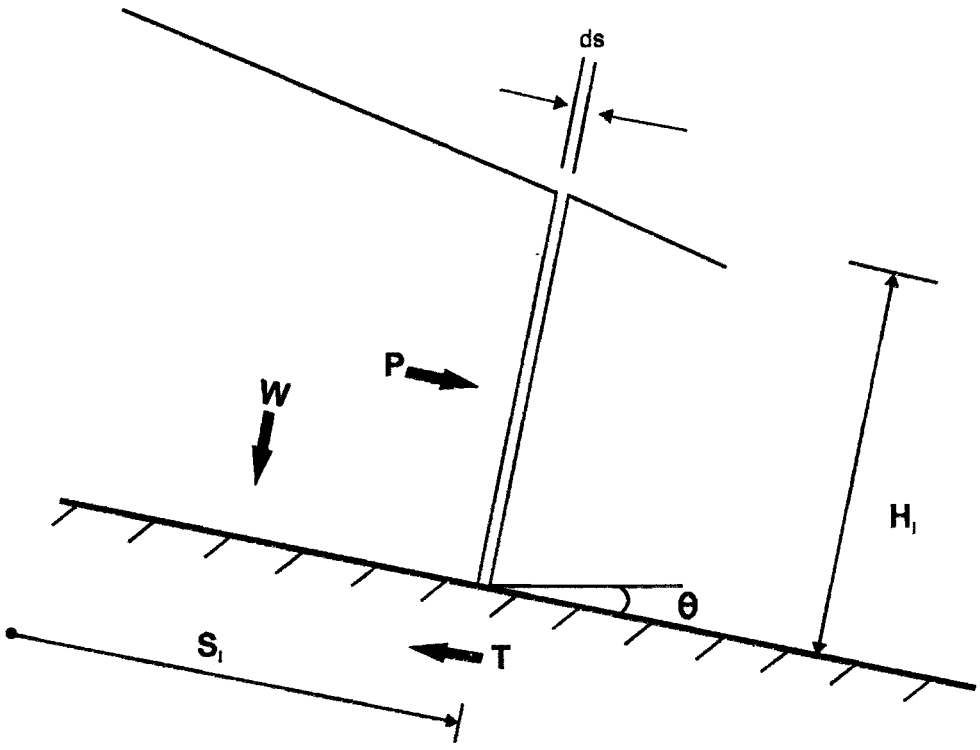

Mass-Referenced flow model: Forces acting on a boundary block
(Adapted from Hungr, 1995)

4.7.1. RHEOLOGICAL MODELS COMPATIBLE TO ROCK AVALANCHES

All three rheology models are based on the premise that the resisting force, *T*, which acts at the base of the moving mass, reacts to specific parameters such as individual rheology properties, the debris mass thickness, *H*, and mean velocity of the run out, *V* (Hungr, 1995). It is these differing function relationships which distinguish each model (Davies and McSaveney, 2002).

Comparative testing of the three rheologies by Hungr (1996) showed the Voellmy model to reasonably simulate the total run out in 70% of cases and produced the most consistent results in landslide properties including debris spreading, distribution and velocity. In comparison the Bingham model consistently overestimated length and velocity and overstated the amount of longitudinal spreading of the debris (Hungr and Evans, 1996). Similarly, this occurred in the Frictional model, which resulted in slightly unrealistic velocities but not as much as the Bingham model (Hungr and Evans, 1996). The Frictional model was shown to reasonably simulate the Mt Cayley rock avalanche run out case-study with the exception of slightly high velocities (Evans et al. 2001). For the purpose of this study only the Friction model will be investigated due to its application to the theory of fragmentation which will be described below. Descriptions of the Bingham and Voellmy models can be found in Hungr (1995), Hungr and Evans (1996), Evans et al. (2001) and Fell et al. (2001).

4.7.2. THE FRICTIONAL MODEL

The fundamental assumption of the Friction model is that the resisting force (T) is a function only of the effective normal stress acting on the base of the flow, and is therefore independent of velocity (Hungr and Evans, 1996). The resultant stress is dependent on flow depth, H, pore-pressure and unit weight of material (γ) (Hungr, 1995; Evans et al. 2001) and is considered to form a narrow zone of high shear stress within the finest material near the base of the mass (Hungr, 1995).

The expression is:

[1] $$T = A\gamma H(\cos\theta + a_c / g)(1 - r_u)\tan\phi$$

T is the resisting force acting at the base of a flow mass,

θ is the run out path slope angle,

$a_c = v^2/R_v$ is centrifugal acceleration which is dependent on the vertical curvature radius of the path R.

r_u is the pore pressure coefficient $_{considered}$ to be zeros for dry granular flow representing rock avalanching.

Φ is the dynamic friction angle

The main parameter within the model is the bulk friction angle, which is related to the effective dynamic friction angle through the use of the pore pressure ratio (Hungr and Evans, 1996).

4.7.3. FRAGMENTATION APPLICATION OF THE DAN SIMULATION MODEL USING THE FRICTIONAL MODEL

Based on the theory of fragmentation presented by (Davies et al. 1999) outlined in Chapter Three, Davies and McSaveney (2002) sought to replicate the effect fragmentation had on rock avalanche run out which lacked quantitative testing to support their hypothesis. This was achieved using the DAN run out simulation and a Friction rheological model (Hungr, 1995; Davies and McSaveney, 2002). In the laboratory, Davies and McSaveney (2002) tested dry sand models with normal earth pressure coefficients, and then increased the earth pressure coefficients representing dispersive stresses resulting from fragmentation. The consequence of which caused a maximum increase in run out distance of more than 450 % (Davies and McSaveney, 2002).

4.7.3.1. RANKINE EARTH PRESSURE COEFFICIENTS

The following description of Rankine earth pressure coefficients is based on that described in Davies and McSaveney (2002). The term earth pressure refers to the maximum lateral pressure able to exist at a given depth in a granular material as a result of overburden stress

(Davies and McSaveney, 2002). If the material becomes active then the material is able to expand laterally reducing the pressure suddenly. This is called k_a. If compression occurs laterally then the maximum lateral earth pressure suddenly increases. This is referred to as k_p or passive. Both active and passive pressure coefficients relate to the internal friction angle (Ø) of the material.

Davies and McSaveney (2002) identified that during fragmentation, the maximum lateral stress within the mass exceeds the ambient overburden stress, a condition which could be represented by increasing the earth pressure coefficient. It is the presence of the excess stress which causes the relative long travel distance of the debris in both the DAN model and the fragmentation theory. The DAN model applies the earth pressure along the thickness of the slice or block to derive the force on each individual slice (Davies and McSaveney, 2002). Similarly Davies et al. (1999) theorised that fragmentation pressures are also a function of depth making the Friction model a compatible comparison for this application (Davies and McSaveney, 2002). The choice of coefficient of internal friction of $Ø = 27°$ was based on the current angle-of-repose of scree in the scar at Falling Mountain (Davies and McSaveney, 2002).

The 1929 seismically triggered Falling Mountain rock avalanche deposit in the western Southern Alps was utilized by Davies and McSaveney (2002) as a field example to test the fragmentation hypothesis. The DAN model was shown to satisfactory replicate the internal stress resulting from fragmentation, increasing the dispersive stress in an inverse relationship by increasing the earth pressure coefficients in association with zero pore pressure. This appeared most successful when following a central flowline down the run out path subsequently avoiding features such as debris run up against topographic obstacles. Davies and McSaveney (2002) acknowledged that using a Friction model to represent a fragmenting rock avalanche may be over-simplified however this does demonstrate the effect fragmentation has on rock avalanche run out.

The method outlined by Davies and McSaveney (2002) in the Falling Mountain example has been applied to the Acheron rock avalanche to test the applicability of the model to rock avalanche deposits in the Southern Alps.

4.8. THE ACHERON ROCK AVALANCHE DEPOSIT SIMULATION USING THE DAN PROGRAM WITH THE FRICTION MODEL

4.8.1. SITE CHARACTERISTICS

The Acheron rock avalanche is located in the eastern Southern Alps of inland Canterbury, 80km west of Christchurch. It has an approximate deposit volume of 9×10^6 m^3 with a run out path width ranging between 151m to 400m. The length of the deposit from the crest of the source scar to the distal most debris is 3500m occurring over a fall height of 700m resulting in a fall height to run out length ratio of 0.2.

Both volume and deposit widths are an order of magnitude smaller than that observed at Falling Mountain; however Davies and McSaveney (2002) showed that the DAN model represented motion in both fragmenting and non-fragmenting granular avalanches regardless of scale. Similar to Falling Mountain the debris material consists of Torlesse Supergroup greywacke from a source scar normal to the longitudinal valley profile.

The source area is a cirque-shaped basin filled by debris from the event, and later periglacial erosion has formed extensive scree deposits. Immediately below the basin is a smooth undulating surface descending normal to the main valley profile. The upper run out section is partially buried by an extensive talus fan from a wedge failure on the true left of the valley (Fig. 4.17). Opposite the fan, three extensive mounds of debris located against a hill (1249 m) which the rock avalanche impacted called Run up two, halting some material while deflecting the remainder (Fig. 4.17). Within the upper run out zone only sporadic exposures of debris were observed which are overlain by recent alluvium and fluvial activity, and consequently are difficult to infer a thickness or extent. A trim line on the true left extends from the talus fan down valley reaching a height of 35m above the deposit.

The lower half of the deposit displays steep lateral ridges defining the debris margins and partially overlies at set of terraces which gave good control on deposit thickness and width. The furthermost debris consists of remnant basal material plastered against a T2 terrace surface. While the material properties are similar between the Falling Mountain and Acheron deposits, the topography differs. The Acheron rock avalanche is found in less

Figure 4.17: Aerial photograph of the Acheron rock avalanche deposit illustrating the source scar and run out path (stippled line). Debries identified within the valley are depicted in orange. The single profiles line A-A' identifies the longitudinal flow-line applied to the DAN long run out simulation.

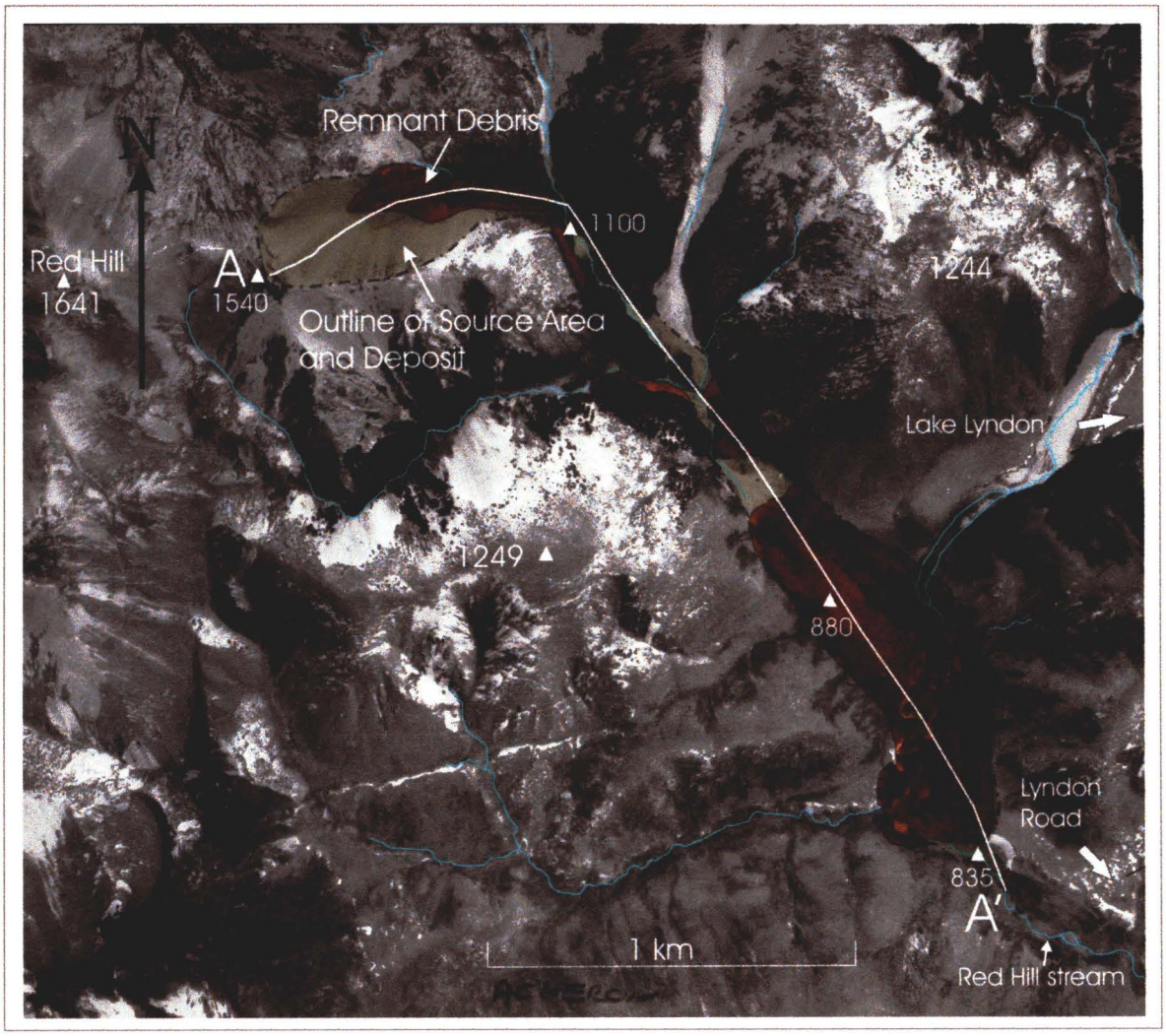

elevated sub-alpine terrain (source scar crest 1520m asl) with rounded periglacial ridges and with shorter periods of snow inundation. This is in contrast to the steep angular elevated ridgelines of Falling Mountain (1901m asl) to the west centred near the main divide of the Southern Alps.

The age of emplacement of the Acheron deposit is considered in this study to closely post-date (Wk 12094) 1152 ± 51 years B.P. The cause of failure is unknown but is considered seismic however this means only assumptions about the pre-failure rock mass volumes and style of failure can be made.

4.8.2. RUN OUT GEOMETRY

The coordinates for the run out path were taken from the 1:50 000 topographic DEM using Surfer 8 and presented as a cross-section using the Grapher 4 program (refer Fig. 4.18A, Table. 4.1). Allowances for the pre-surface were based on two assumptions. The first was that deposited material thinned towards the distal margin, and the second was based on laboratory evidence showing a large proportion of the mass remained near the foot of the fall slope (Davies & McSaveney, 2002). Thickness of the lower half of the deposit was adequately obtained from several river cut exposures incising the deposit as seen Fig 4.4. The source rock mass volume was computed by trial and error relating to adequacy of run out distance, slope angles of outcrop in the upper source scar, and adjacent slope profiles.

The extent of the run up of debris exiting the source area was difficult to assess, and the valley sides impacted by run up one and two were not able to be modelled in conjunction with the remainder of the deposit using the one dimensional run out path geometry of the DAN model. The flowline therefore followed the centre line of the run out path by-passing both features and terminating at the very distal point of the deposit (Fig. 4.17). This assumption removes important physical dimensions from the analysis, but it is still considered to accurately represent the run out.

4.8.3. TESTING THE FRICTION MODEL SIMULATION

Initially the parameters outlined in Davies and McSaveney (2002) were applied to test the acceptability of the Friction Model to the Acheron setting. To simulate both non-

fragmenting and fragmenting motion three earth pressure coefficients were selected from Table 2, presented in Davies and McSaveney (2002 p. 792).

Non-fragmenting earth pressure coefficient of	ko = 0.5, ka = 0.2, and kp = 4.9.
Fragmenting earth pressure coefficients of	ko = 5.5, ka = 5.2, and kp = 9.9
Fragmenting earth pressure coefficient of	ko = 6.5, ka = 6.2, and kp = 10.9

(*As applied at Falling Mountain flowline A'- B'*)

The next objective was to standardise the testing procedure by finding settings which were suitable to this case study, and to investigate their effect on the run out distance. The results are summarised in Table 4.2. Subsequent variations of settings were found to alter run out distance by several hundred metres which is considered to be tolerable.

To check the acceptability of the internal friction angle (Ø =27°) a series of simulations were run using a range of internal friction angles (Ø) between 24° to 35° for each of the fragmenting coefficients and even numbers 16° up to 34° for non-fragmenting earth pressure coefficients (refer Appendix D Table 2). As expected, a linear trend showing an increase in run out distance with decreasing friction angle was observed. Applying a Ø = 27° friction angle, with pressure coefficient ko = 5.5 the rock avalanche reached a distance of 3477m while ko = 6.5 only reached 3290m but over a shorter time period. The non-fragmenting earth pressure reached only 1450m (Fig. 4.18). When a friction angle of 26° was applied both the fragmenting coefficients were within or exceeded 55m of the distal limit. The required friction angle for the non-fragmenting run out of 3500m was 16°, which is considered unrealistic for greywacke material.

Applying the Rankine earth pressure coefficient of k_o = 5.5, k_a = 5.2, k_p = 9.9 representative of rock avalanche induced fragmentation caused an increase in the run out distance of 140% from 1450m to the 3475m, a difference of over 2000m (Fig. 4.18). This shows that with the addition of a fragmentation parameter, the Friction model can successfully replicate the effect of dispersive stress in a fragmenting rock avalanche, thus supporting the findings of Davies and McSaveney (2002).

The choice of 27°-26° as applied at Falling Mountain for internal friction angle (Ø) appears reasonable for the Acheron rock avalanche. A friction angle $\geq$ 28° caused the mass to

FIGURE 4.18: DAN run-out simulation using the friction model with earth pressure coefficients for a non-fragmenting (Red) and fragmenting (Blue) induced run-out

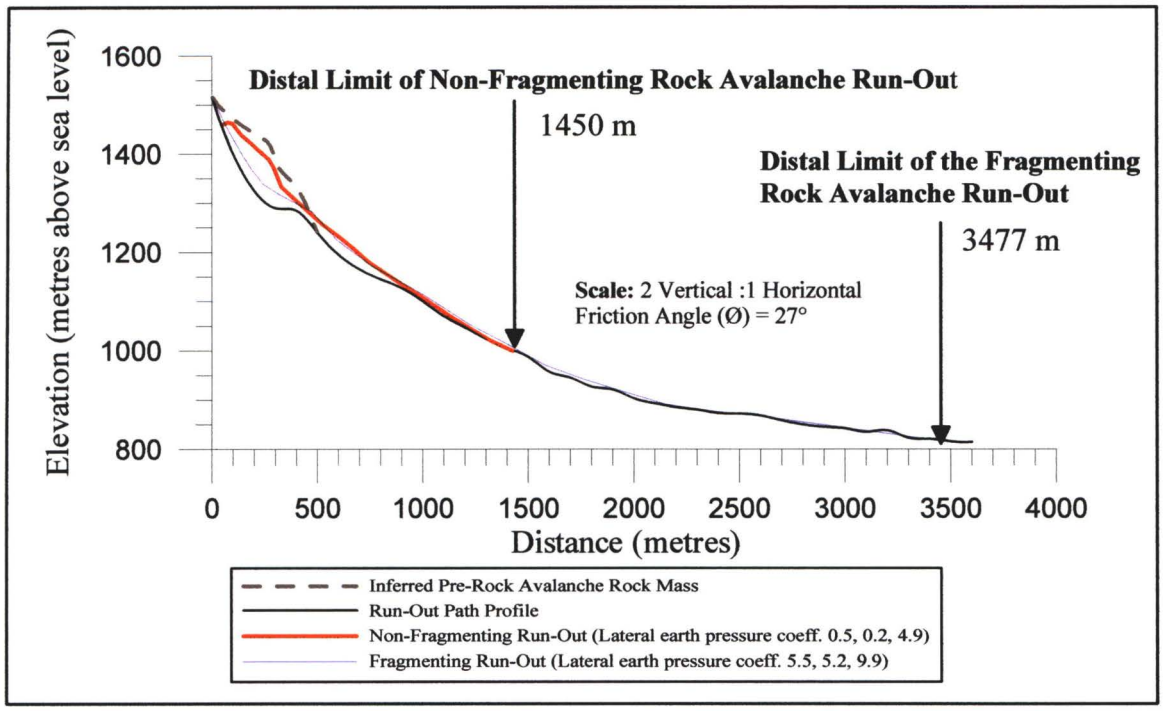

TABLE 4.2: The effect of Friction Angle (Ø) on fragmenting and non-fragmenting rock avalanche run-out

Earth Pressure Coefficients			Friction Angle	Run-Out Distance	Travel Angle	Fahrböschung	Run-Out Mechanism
ko	ka	kp	Ø	(metres)	(0°)	f(0°)	
A.	Simulated distances reached by the debris when applying a Friction Angle of 27°						
0.5	0.2	4.9	27°	1451	24.18°	19.65°	Non-Fragmenting
5.5	5.2	9.9	27°	3475	18.05°	11.35°	Fragmenting
6.5	6.2	10.9	27°	3290	17.4°	11.85°	Fragmenting
B.	Friction Angle (Ø) required to reach the Acheron rock avalanche run out distal limit of 3450m						
0.5	0.2	4.9	16°	3657	14.91°	10.77°	Non-Fragmenting
5.5	5.2	9.9	27°	3475	18.05°	11.35°	Fragmenting
6.5	6.2	10.9	26°	3345	17.05°	11.72°	Fragmenting

regularly fall short of the target distance by 400m for the both the fragmenting earth pressure coefficient simulations. Friction angles (Ø) of $\leq 25°$ overextended the reach of the mass by 150m and greater (Refer Appendix D Table 2).

An independent run out simulation was run with the ideal settings and parameters, using an earth pressure coefficient of ko = 5.5 with a friction angle of 27° to check reproducibility. This simulation achieved a run out distance of 3480m with a travel angle of 18.05°. This resulted in a *Fahrböschung* of 11.34° (0.2) with a maximum velocity of 165 km / hr covering an area of 878 000m^2 (refer Fig. 4.19, Fig. 4.20 A-C).

4.8.4. COMPARISON OF RESULTS WITH FIELD ESTIMATES

Attempts at modelling the volume of the Acheron rock avalanche source rock mass using Surfer 8 and cross-sections of the source scar gave values ranging from 12.5 x 10^{6}m^3 up to 14 x 10^6 m^3. Previous estimates by Whitehouse (1983) of 6 x 10^6 m^3 appear conservative. The DAN model volume estimate of 9.5 x 10^6 m^3 is comparable to that of the infield estimates of 8.9 x 10^6 m^3 which was derived from the deposit area. The depositional area calculated from the DAN simulation was 880,000m^2 from a volume of 9.5 x 10^6 m^3 with no allowance for dilation or the addition of material from the run out path into the mass. Comparatively the Acheron rock avalanche deposit area was estimated using a GPS outline of the deposit which gave a reliable planimetric area of 720 000m^2. This is considered to undervalue the actual three-dimensional area of the hummocky deposit so is considered conservative. It was from this, a deposit volume was calculated resulting in 8.9 x 10^{-6} m^3. By subtracting a dilation factor of 20% (Evans et al. 2001) a source rock mass volume estimate was made of 7.5 x 10^6 m^3. Interestingly the initial pre-failure area applied to the Dan model enlarged by 87.2 % during deposition and comparatively the field estimates of the original rock mass to deposition area enlarged 84.4 %. This adds reliability to the area and volume calculations between the two methods. The thickness distribution calculated by the DAN model over the first 500m of run out below the source scar ranged from 30m to 16 metres (refer Fig. 4.19, Fig. 4.20. C); this coincides with the site immediately below run up one offering an opportunity to estimate the debris volume at this point. The centre of gravity of the debris is at an elevation of 1384 m (asl) and a distance of 877m along the run out path with a thickness of 34 metres (see Fig. 4.19).

Figure 4.19 A: A Longitudinal profile of the Acheron rock avalanche run out path and inferred pre-rock avalanche topography

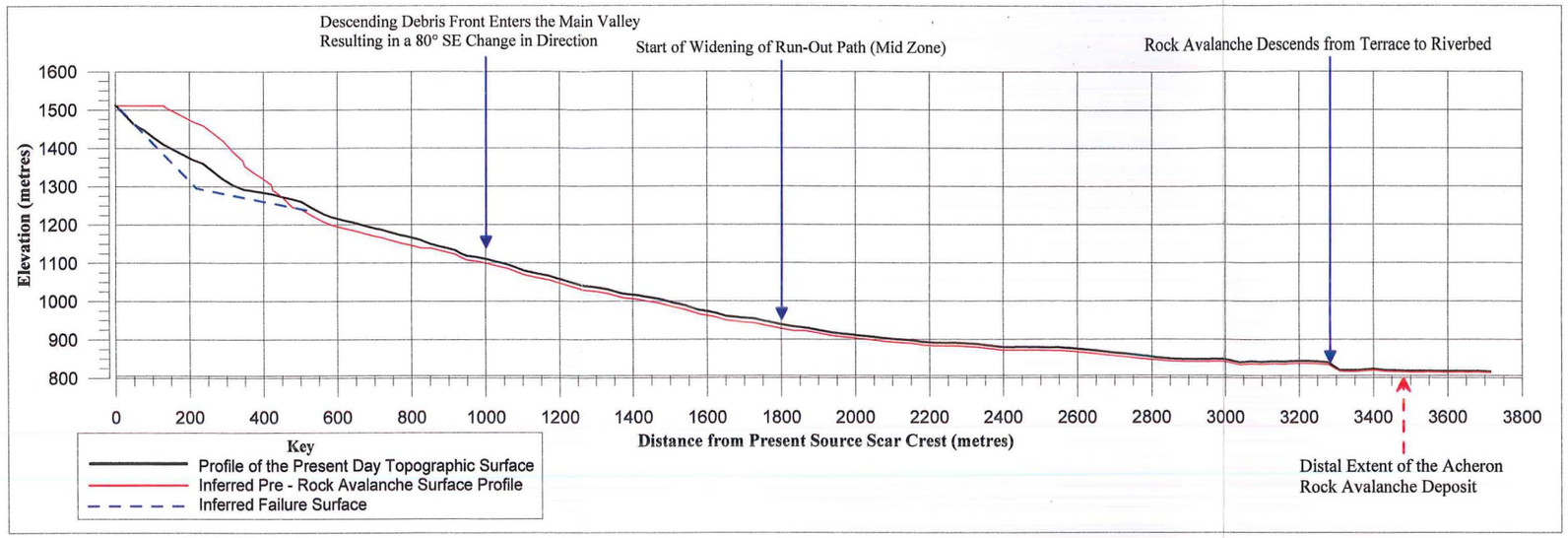

Figure 4.19 B: DAN run out simulation profile and statistical results for the Acheron rock avalanche applying the optimum parameters

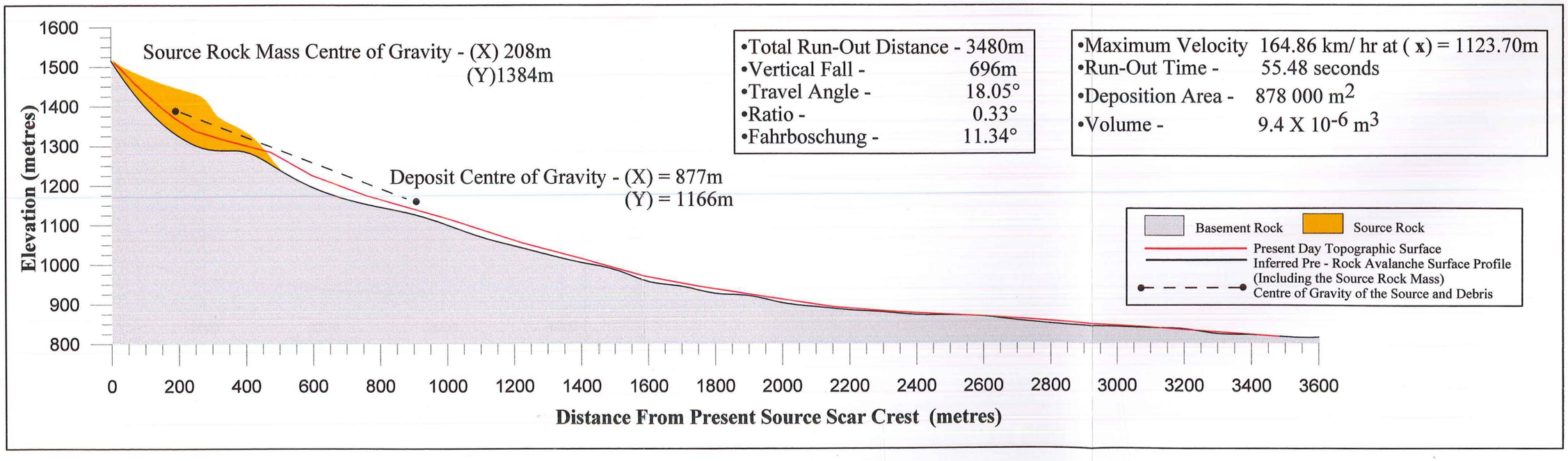

FIGURE 4.20 A-C: Graphed results of DAN Run Out simulation; **A.)** Profiles of run out path compared to path width. **B.)** Run Out velocity over distance travelled. **C.)** Deposit thickness relative to the run out distance.

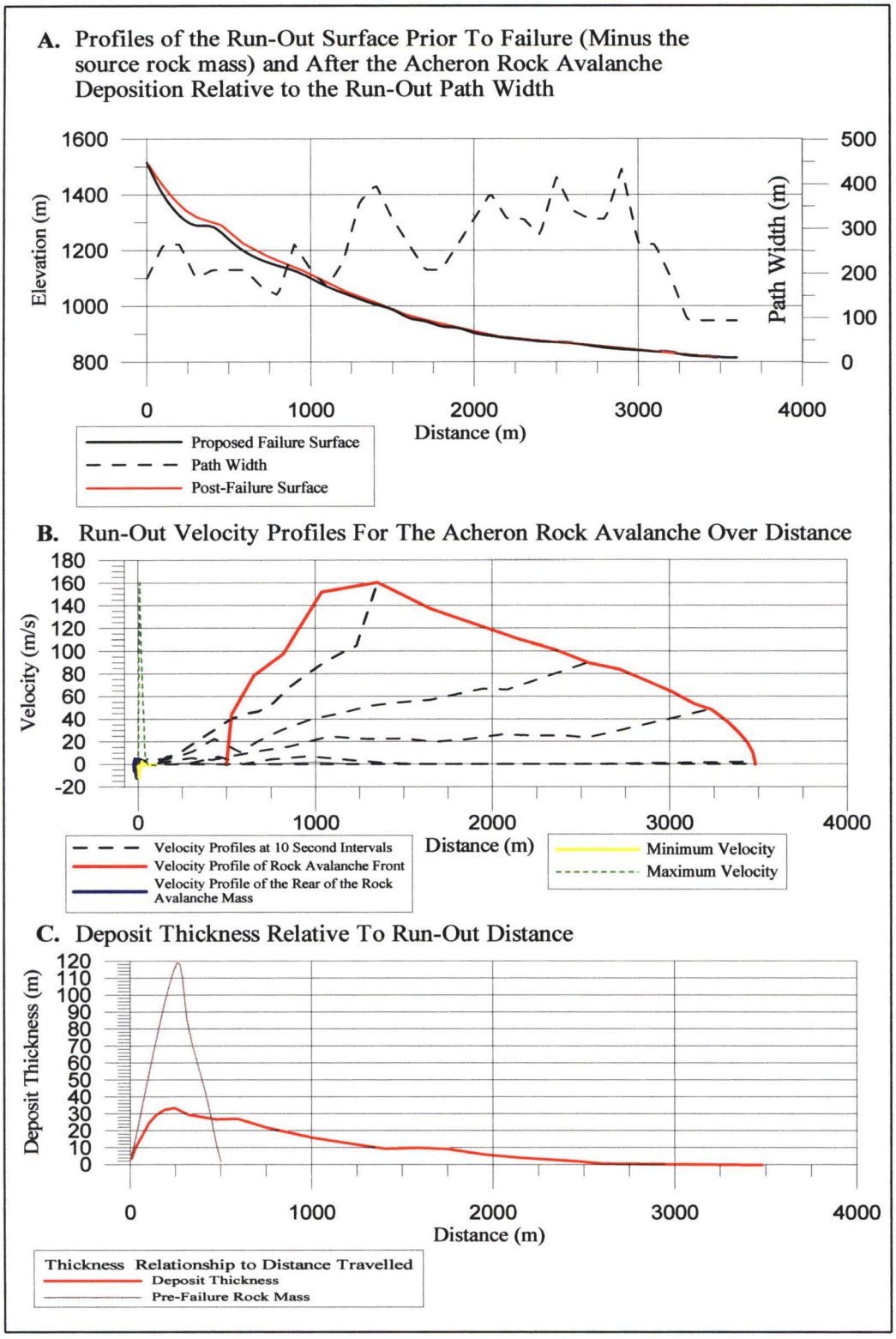

This suggests the approximately half of the deposition during run out occurred immediately below the source scar (Fig. 4.19, Fig. 4.20 C).

The maximum velocity of 165 km / hr for the debris front as modelled by the DAN simulation is slightly larger than that calculated for the Acheron-based field estimates of 140 km / hr which were based on the simple equation $(2gH)^{0.5}$ (where g is gravitational acceleration and H is the height of run up of the debris as described in an earlier section) but appears reasonable considering the accuracy of the field-based equation (see Fig.4.20 B). The DAN model found that maximum velocity peaked at a run out distance of 1123m placing the deposit front between run up one and two (Fig. 4.19 and Fig. 20 B). As the run ups were both excluded from the simulation and little evidence of run up one was observed in the field it can be assumed that a velocity of 140-160 km / hr would have caused the debris to partially impact onto the opposite-facing slope of run one reaching a vertical height of 60–80m. Run up two represents a run up height of between 60-80 metres and a maximum velocity of 140 km / hr which matches the velocity of the DAN simulation at a similar distance of 145 km / hr.

Overall the DAN simulation showed a comprehensive compatibility to a field example when similar parameters of path and volume are estimated and applied to the model. The DAN simulation model appears to realistically duplicate run out of a large greywacke derived rock avalanche suggesting it could be a valuable and under utilised tool in hazard assessment in the Southern Alps of the South Island.

4.9. SUMMARY

The central Southern Alps rock avalanche compilation of Whitehouse and Griffith calculated 1 / 90 year recurrence frequency for rock avalanches exceeding 10^6 m^3 (1983) assuming a complete record of rock avalanche deposition for the last 1700 years B.P. McSaveney (2002) revised the frequency interval to 1 / 20-30 years by using historical rock avalanches and suggested that examples deposited in glaciated areas would have been removed from the record. The data collected by Whitehouse and Griffith (1983) needs to be expanded to develop more detailed rock avalanche models.

The Acheron Rock avalanche travelled 3500m over a vertical fall of 700m resulting in a *Farböschung* of 11.4° or 0.20. The deposit area is calculated at 720 000m^2 with an estimated volume of 8.9 x 10^6 m^3. An estimated volume for the initial failed rock mass was 7.5 x 10^6 based on the deposit volume corrected for a 20% change in volume associated with dilation and incorporation of debris along the run out path. The length of the accumulation zone from the lip of the source basin to the distal most point is 3000m with an average slope angle of 10.5°. A velocity of approximately 140 km / hr was estimated from run up two. The run out properties suggests high to moderate mobility, with partitioning of the mass occurring due to topographic obstacles in the run out path.

Previous dating of the rock avalanche has inferred an age of emplacement at approximately 570 - 400 years B.P. (Burrows, 1975; Whitehouse and Griffith, 1983; Bull and Brandon 1998; Howard, 2001). New dates from contemporaneous wood samples extracted from the contact between the terrace surface and the deposit show an age ranging from 1370 -1100 years B.P. The youngest and most reliable sample is a buried beech tree (Wk 12094) which has been dated at 1152 ± 51 years B.P. This is considered to represent the maximum and close age for the rock avalanche emplacement and may also represent a seismic event on the Porters Pass Fault at around 1000 ± 100 years B.P. as identified at Porters Pass by Howard (2001).

The DAN long run out simulation successfully replicated the velocity and distance of the Acheron rock avalanche by applying earth pressure coefficients of ko 5.5, ka 5.2, ka 9.9 representing fragmentation-induced long run out. The friction angle of 27° achieved a run out distance of 3480m with a travel angle of 18.05° and a *Fahrböschung* of 11.34° which matches that observed in the field for the Acheron deposit of 3500m with a *Fahrböschung* of 11.43°. The maximum velocity of 165 km / hr for the debris front as modelled by the DAN simulation is comparable to that calculated for the Acheron rock avalanche of 140 km / hr which were derived from run up heights of the debris. The DAN model volume of 9.5 x 10^6 m^3 is comparable to that of the infield estimates of 8.9 x 10^6 m^3. The deposition area calculated by DAN of 880,000m^2 is also similar to the planimetric area of 720 000m^2 derived for the rock avalanche. The DAN model has been shown to reliably model greywacke derived rock avalanches in the central Southern Alps and has potential applications for long run out simulation of sites of potential instability on elevated slopes in the central Southern Alps of the South Island.

CHAPTER FIVE

PALEOSEISMICITY OF THE RED HILL VALLEY SITE

5.1. BACKGROUND

As described in Chapter Four, a new radiocarbon age of 1152 ± 51 years B.P. has been determined for the deposition of the Acheron rock avalanche. This differs from ages of between 430–570 years B.P. presented from previous studies using radiocarbon, weathering-rind thickness and lichenometry age estimates (Burrows, 1975; Bull and Brandon, 1998; Howard, 2001). The new age does show similarity to the event one (1000 ± 100 years B.P) proposed by Howard for the most recent rupture along the Porters Pass Fault. To further examine the possible coseismic relationship between the new rock avalanche age and the trench dates for event one in Howard's (2001) Porters Pass excavation, a trench site was identified immediately adjacent to the northeastern margin of the Acheron rock avalanche deposit. The choice of the site was influenced by three considerations.

- Howard (2001) proposed the existence of topographically induced segment boundaries along the Porter Pass Fault, one of which, the Red Lakes, is proximal to the source scar of the rock avalanche. These segment boundaries are thought to be areas of concentrated seismic motion. The north dipping angle of the source scar failure planes would be orientated normal to the propagating waves from a rupture along the Porters Pass Fault, further amplifying the impact of the seismic energy by exposing fractures to maximum potential dilation in the direction of motion.

- Secondly only one landslide along the PP-AFZ (Glentui-Landslide Two 1210 ± 190 years B.P. based on weathering-rind ages in Cowan et al. 1996 Fig. 6.1) resembling the 1000 ± 100 yrs BP age estimate is known to exist. This implies that a rupture event did not occur along the breadth of the fault zone, and instead was confined to the west along the Porters Pass Fault probably between the Kowai River valley east of Porters Pass, terminating at the structural boundary proposed at Red Lakes west of the Acheron deposit. Based on this assumption representation of the rupture event could exist within the Red Hill valley, making it a viable site to trench.

- The third consideration was the general lack of information on the Porters Pass Fault between the Red Hill valley and the saddle west of Lake Lyndon. The trace of the Porters Pass Fault has been mapped as extending beneath the lower part of the rock avalanche suggesting a coseismic relationship is an obvious hypothesis to test.

5.2. SITE SELECTION

Very little surface expression of the Porters Pass Fault crossing the Red Hill valley exists, and certainly little evidence was identified prior to this study. This is mainly the result of the deposition of the rock avalanche along the length of the valley axis. Prior to this study, surface expression relating to the fault was confined to well-formed northwest dipping scarps found southwest and northeast of the field area, terminating at topographic saddles bounding the Red Hill valley (Fig. 5.1; Howard 2001). Earlier studies generally inferred the fault to strike laterally across the valley connecting the adjoining scarps at either of the valley margins. Howard (2001), who conducted the most recent investigation, suggested that near the northeastern intersection with the rock avalanche, the fault formed a segment boundary producing a 700m jog or step to the southeast (see Fig. 5.1).

Geomorphic mapping during this study identified an expression elevated above neighbouring geomorphic surfaces (see Fig. 5.2 A). The consistent matching strikes of 075° and dips of 75° for both bounding scarps at the valley margins did not initially resemble the strike of the proposed scarp site (046°). However on closer examination lineations crossing through the proposed scarp appeared to mirror peripheral scarp strikes.

The scarp expression is a 65m long elongate feature striking eastward towards Lake Lyndon and raised to a height of 2-3m above surrounding topography (Fig. 5.2 A). The slope on the southeast or Bluff River edge drops steeply at an angle of 50° for a length of 12m, while on the northern side it displays a gentle gradient with increasing steepness toward the northeast highlighted by an oblique lineation defining the scarp axis (Fig.5.4 and 5.2.B). The two subtle changes in scarp slope are thought to define the orientation of faulting through the structure (Fig. 5.2 C). Partially buried by the rock avalanche, the exposed width of the scarp varies from 33m at the rock avalanche margin to < 20m where it terminates at a narrow watercourse trending 080° (Fig. 5.2 A-C; Fig. 5.4).

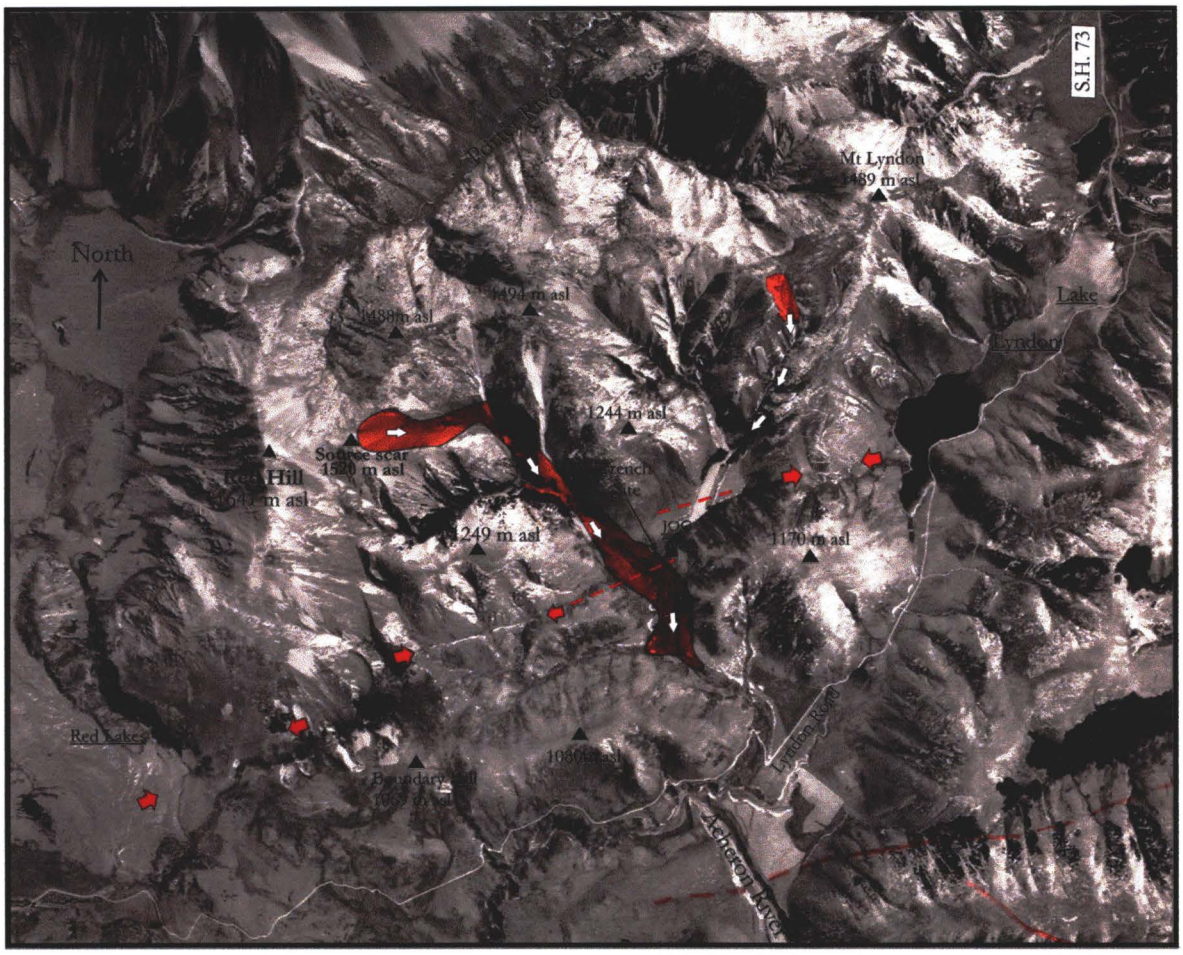

Figure 5.1: Enlarged aerial photograph showing the field area between Red Lakes in the west and Lake Lyndon to the northeast. The red arrows delineate the well defined fault scarps of the Porters Pass Fault present on either side of the Red Hill valley which Howard (2001) used to identify a misalignment interpreted to represent jogs of the fault trace (dashed red line). The site of the trenching (this study) is marked in the centre of the photograph. The Acheron rock avalanche is shown in red fill and the white arrows show the direction of movement down-valley. The inferred source of the Bluff River rock avalanche is visible immediately west of Lake Lyndon. (S/N 5688 A/8 (Lake Coleridge-Mt Hutt).

Figure 5.2.A: Landscape photographs of the proposed Porters Pass Fault scarp and trench site. The position from which photographs B & C were taken are shown by the Black letters B and C. Redundant drainage outlets into the Bluff River are shown by the white arrows at the base of the photo. The intersection of the terrace surface with the ponded sediment cover can be seen below the black C and above the middle white arrow. The small orange arrows show an observed offset of the rock avalanche margin. The blue arrows delineate a small scarp feature trending west into the rock avalanche deposit. The white arrows in the top of the photograph pinpoint the source scar.

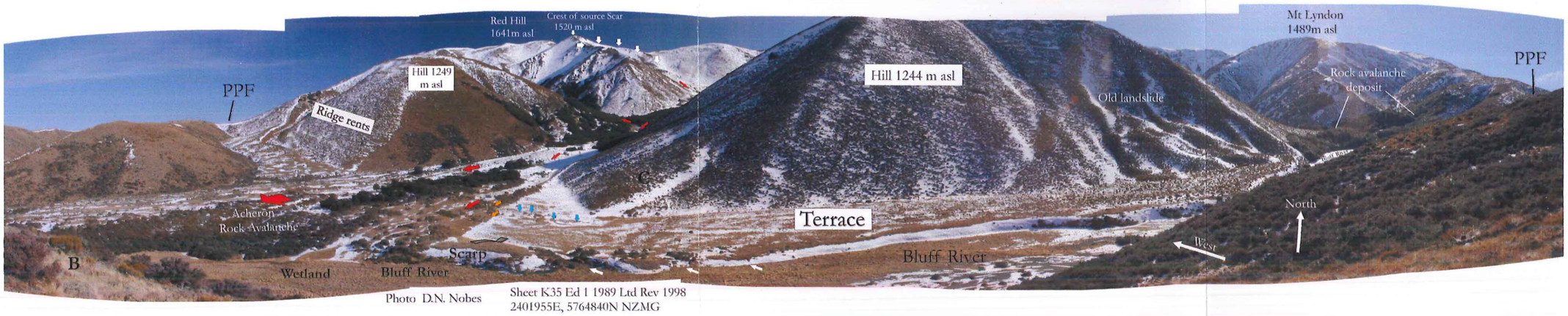

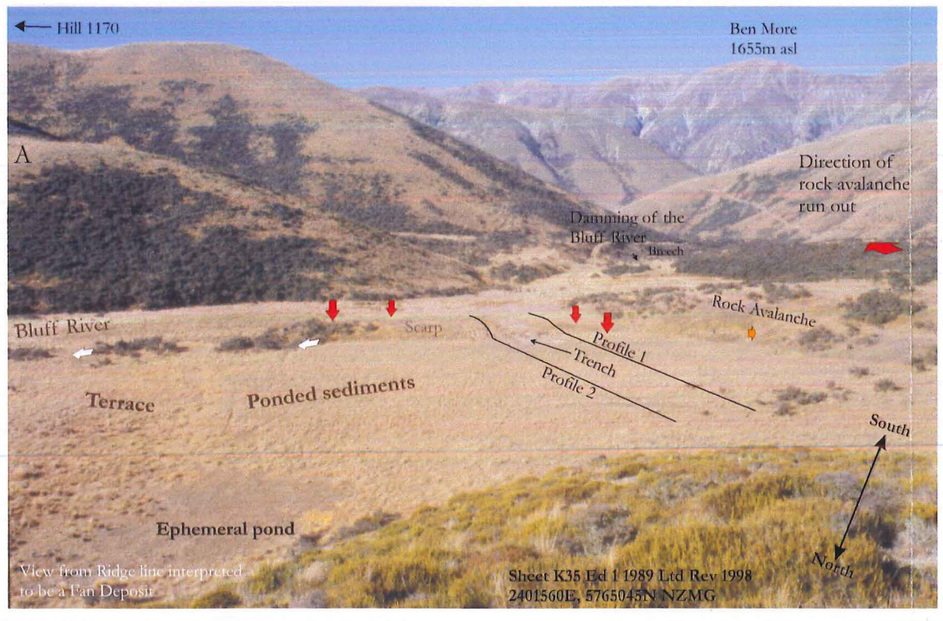

Figure 5.2 B: View south from the fan deposit toward the scarp protruding out from the margin of the Acheron rock avalanche deposit. The two 100m Ground Penetrating Radar profiles are shown by the black lines curving over the fault scarp. The scar from trenching can be seen descending the northern side of the scarp. The red arrows delineate the trend of the faults through the structure. The yellow arrow highlights the slump out of the side of the rock avalanche in line with the trend of the faults. The terrace surface on the left side terminates at the ephemeral pond and is overlain by sediment cover delineating the extent of ponding following damming of the Bluff River. The white arrows show the trend of redundant drainage outlets trending in sympathy with faulting.

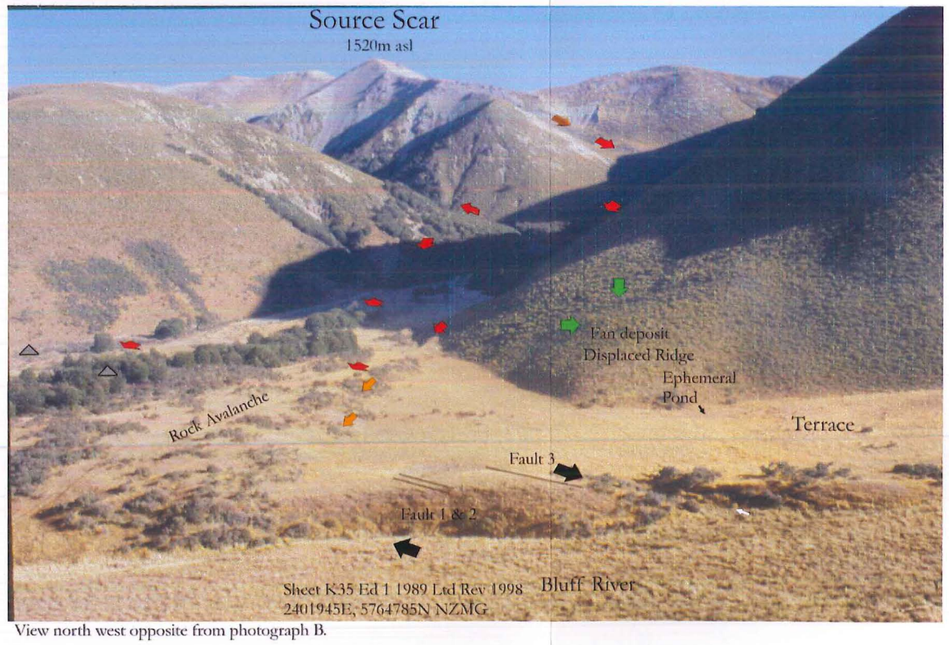

View north west opposite from photograph B.

Figure 5.2 C: Photograph of the south side of the scarp structure. The faults are delineated showing dextral offset of the scarp. The red arrows demonstrate the path take by the rock avalanche. The green arrows show the feature interpreted as a fan deposit observed in the GPR profiles and the trench stratigraphy. The expression considered to be related to the scarp structure is the right of the white arrow delineating the trend of the drainage outlet.

Beyond the watercourse is a second less defined expression bounded on its northeastern side by a similarly orientated linear depression (Fig. 5.2 A and B; Fig. 5.4). This secondary feature is considered to relate to the main proposed scarp. The present shape of the scarp has been modified by erosive actions of the adjacent braided river system, masking much of the actual fault effects and the true strike. However, a probable fault related distortion of the shape immediately west of the opening of the water course remains (Fig. 5.2 C). No outcrop exposure of the fault line was located within the immediate valley.

The main fault evidence within the Red Hill valley consists of secondary features such as lineaments termed ridge rents visible on the south-facing slope on the true left of the western tributary valley, as shown in Fig. 5.2 A; Fig. 5.3). Minor lineaments can also be discerned on aerial photographs (Fig. 5.3; Fig. 5.4) trending obliquely across the rock avalanche deposit and terminating against the eastern limb of Hill 1249 (Fig. 5.2). This is highlighted by a thickening and localised increase in elevation of the deposit bounded on either side by two post-deposition stands of beech trees extending westward from the main tree stands, which trend south in the direction of rock avalanche deposition (Fig. 5.3 and Fig. 5.4).

The presence of lineaments and the thickening observed on the Acheron deposit implies that the rock avalanche may possibly predate the most recent rupture on the Porters Pass Fault, but possibly post-date the development of the fault scarp. In the area northeast of the deposit, geomorphic features can be identified which trend sub-parallel to the lineaments crossing the deposit. These are listed on the sketch plan Fig. 5.4 and Fig. 5.2 A.-C. The above observations question the reliability of the deposit post-dating the last rupture along the Porters Pass Fault, although a far simpler hypothesis is that the last rupture produced the Acheron rock avalanche deposit.

To investigate the shallow subsurface area around the scarp a traverse of five auger holes was undertaken across the scarp and over a discrete flat-lying surface thought to contain cover sediments immediately to the north (Fig. 5.5). This identified varying thickness of clayey silt or loess overlying a coarse granular material (Fig. 5.5). In the flat-lying area the clayey silt occurred to a depth of 90cm but decreased in thickness to 40cm across the northern face of the scarp expression, then increased to 55cm several metres from its southern margin. Similar clayey silt material was also identified one metre above the floor of the riverbed on the Buff River or southern side of the scarp structure.

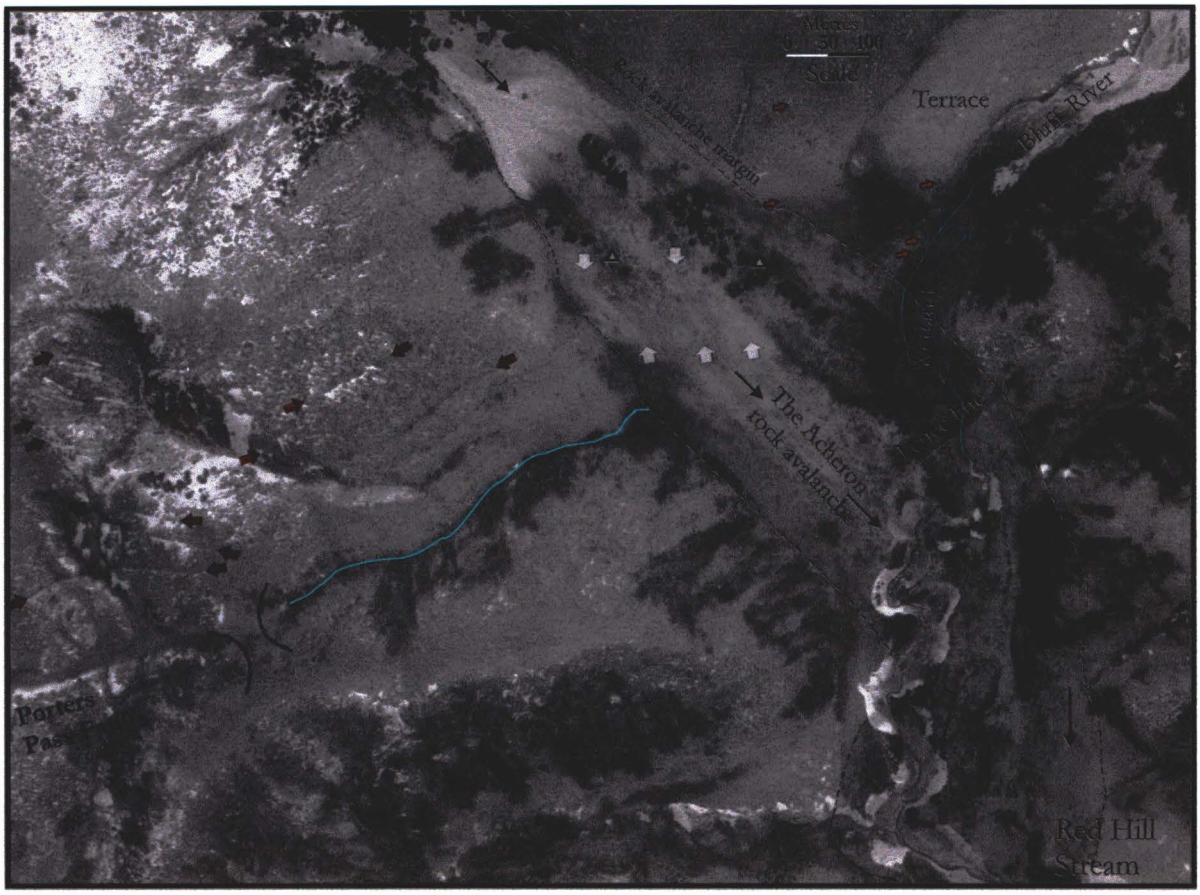

Figure 5.3: Aerial photograph showing the mid zone of the Acheron rock avalanche crossed by the Porters Pass Fault. The start of the prominent western peripheral scarp(1200m) of the Porters Pass Fault can be seen (as in Fig. 2.6) on the lower left corner west below the saddle. A zone of lineaments obliquely crossing the rock avalanche deposit are marked by the white arrows but are difficult to identify without stereo-pairs. Ridge rents and other fault related lineaments are shown by the red arrows. The orange arrows delineate the trends of geomorphic features such as redundant water channels that correspond to the orientation of the white arrows possibly delineating the position of faulting. The two triangles mark areas of coarse boulders, debris mass thickening and high elevation on the deposit and are thought to reflect the presence of a buried fault scarp below.

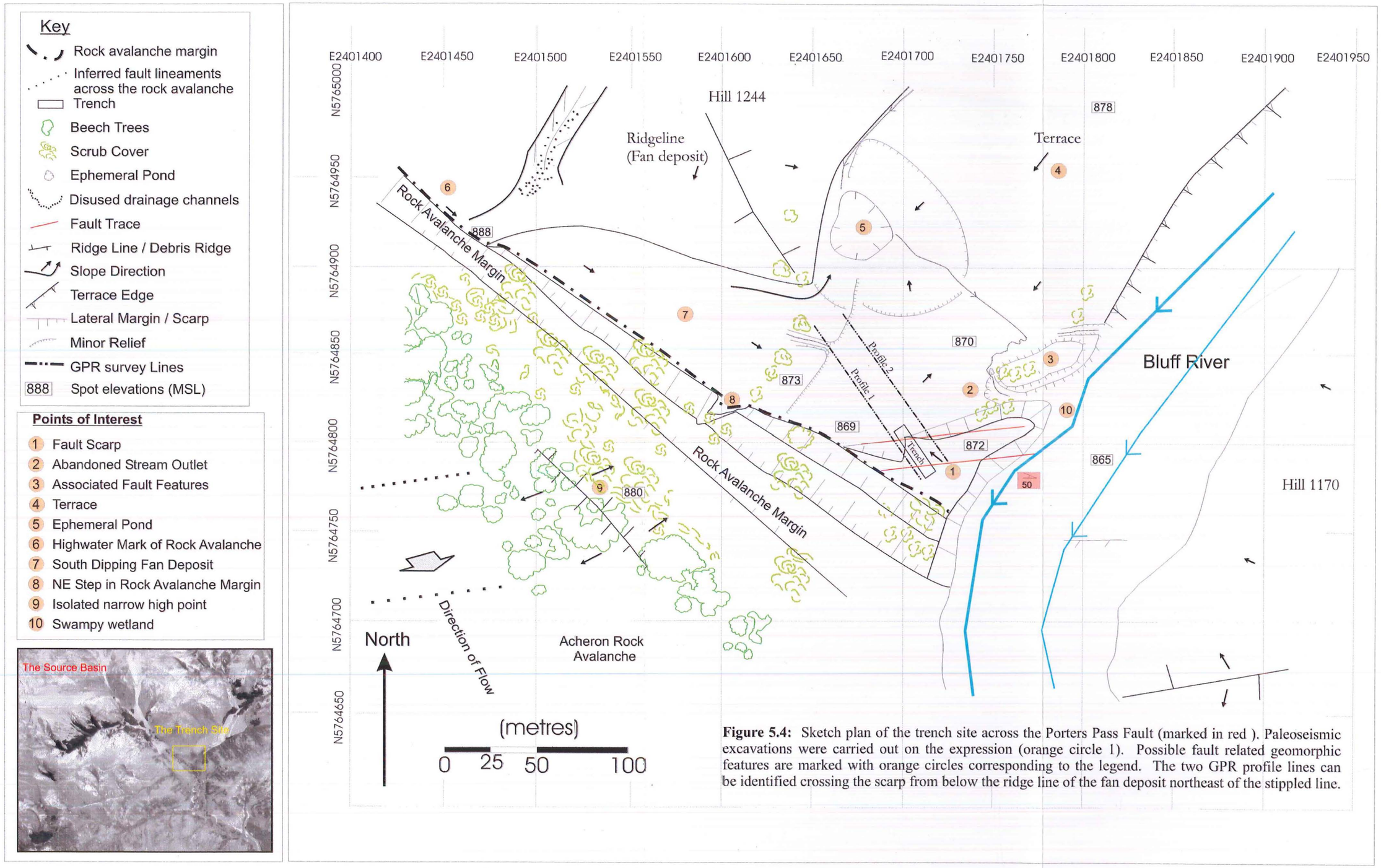

Figure 5.4: Sketch plan of the trench site across the Porters Pass Fault (marked in red). Paleoseismic excavations were carried out on the expression (orange circle 1). Possible fault related geomorphic features are marked with orange circles corresponding to the legend. The two GPR profile lines can be identified crossing the scarp from below the ridge line of the fan deposit northeast of the stippled line.

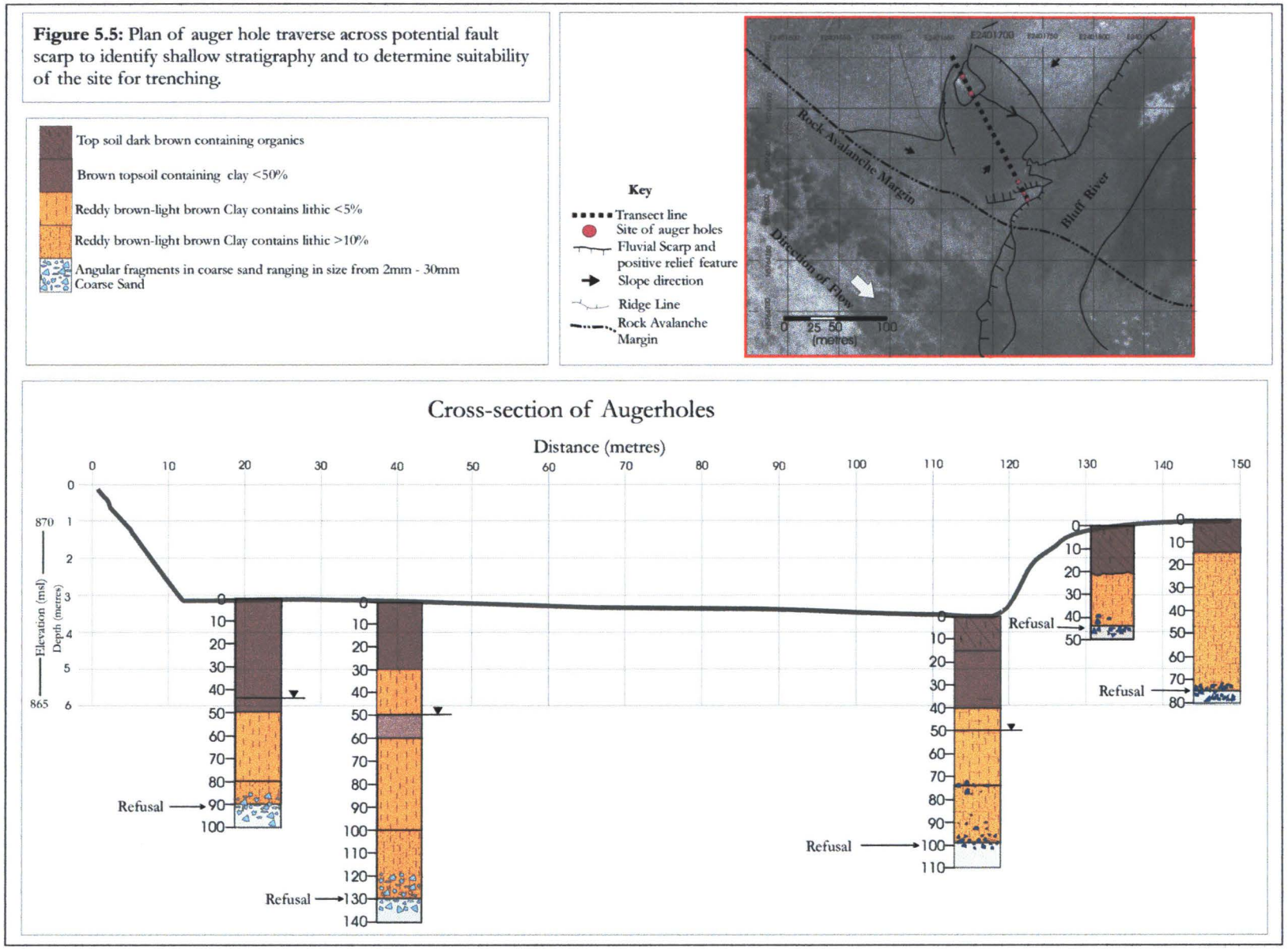

Figure 5.5: Plan of auger hole traverse across potential fault scarp to identify shallow stratigraphy and to determine suitability of the site for trenching.

This gave the appearance that the scarp was "wrapped" in the clayey silt suggesting that during its deposition, the structure was less elevated and or submerged.

The entire section of cover sediments is tightly bounded on four sides by the steep margin of the rock avalanche deposit, the proposed fault scrap, an extensive terrace surface and a large ridgeline (Fig. 5.2 A. and Fig. 5.4). These landforms are interpreted to have aided ponding and the separation of coarser material by isolating the site from the surrounding valley. A depression is located at the base of the ridgeline where the terrace and flat-lying surface intersect, approximately 100 m north of the trench site (Fig. 5.11 B). The source of the clayey silt is most probably over-bank deposits from flood events which contain few clasts or granular material, however it may also be derived from an aeolian origin. Importantly there appears to be a fault trace passing beneath the rock avalanche presenting a source for a coseismic trigger.

5.3. GROUND PENETRATING RADAR

To expand on the geomorphic evidence presented above a geophysical survey was conducted across the proposed fault scarp and the adjacent flat-lying area (Fig. 5.2 B Fig. 5.4). This consisted of a basic walk-over electromagnetic survey to locate anomalies, followed by a series of detailed traverses using Ground Penetrating Radar (GPR). The lack of scarp expression other than the proposed feature limited a detailed interpretation and model of the fault prior to the surveys, however the existence of the proposed scarp implied that faulting was near the surface at that locality. The application of GPR typically gives shallow subsurface information by identifying distinct boundaries between different lithologies represented as changes of reflection and intensity of the positive and negative pulses (refer Appendix E). The penetration depth expected for this site was between 10m to 20m, delineating the extent of the soft sediment content of the flat-lying area and the faulting within the scarp.

The GPR survey consisted of two profiles, ten metres apart traversing the scarp feature (refer Fig. 5.2 B; Fig. 5.4 for profile location). Fig. 5.6 and Fig. 5.7 shows the radar profiles topographically corrected, but with a vertical exaggeration of 5:1. Fig. 5.8 A and B shows the profiles at 1:1.

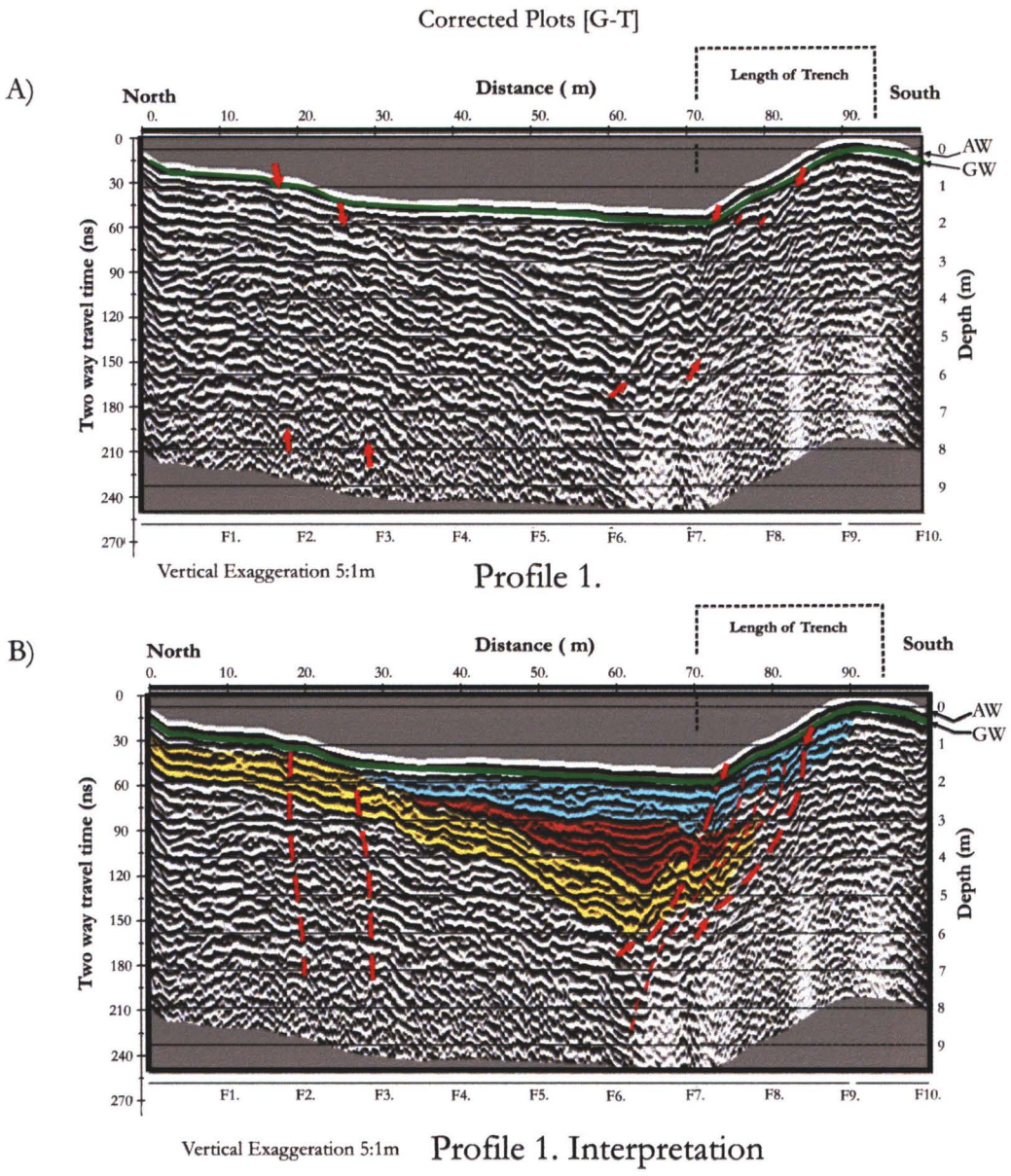

Figure 5.6: Profile 1 processed georadar data recorded from adjacent to the Acheron rock avalanche in Red Hill valley. Profiles appear after dewow filtering, rubberbanding, and topographic correction. The black and white lines represent positive and negative pulses AW - air-wave, GW- ground-wave. A). The profile before interpretation: the red arrows identify irregularities in the pulse signals. B). The dashed red lines are inferred to represent fault propagation. The three colour fills represent distinct boundaries considered to reflect changes in stratigraphy. These appear as fluvial channel fill (red) and low energy sedimentation (blue). Below this is a prominent south dipping unit which abutts abruptly against the north dipping raised section of the proposed scarp. Initial interpretation suggests that the two opposite dipping units are related but have been disturbed by strike slip and normal faulting.

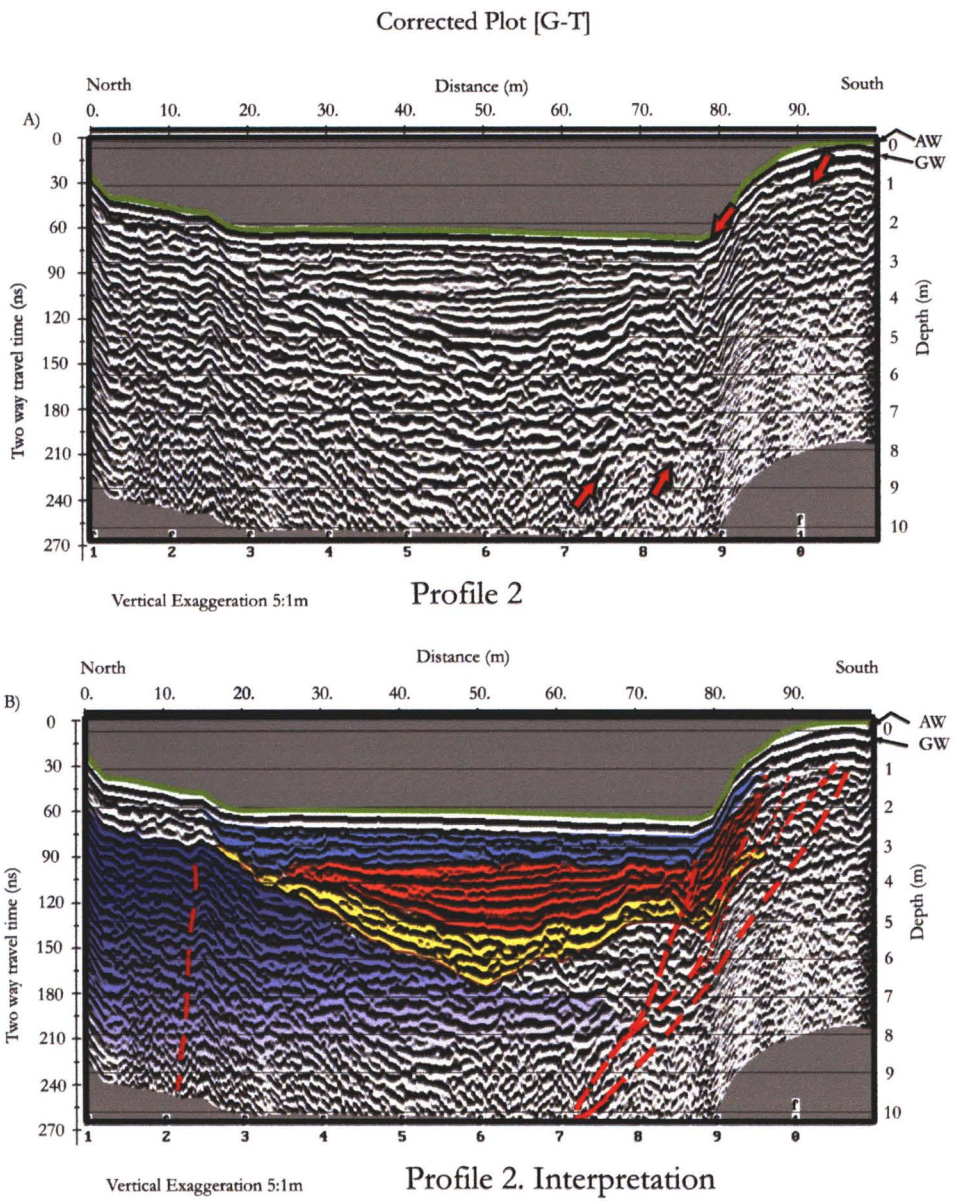

Figure 5.7: Profile 2 located 10m northeast of profile 1 (see Fig. 5.4). Processed georadar data recorded adjacent to the Acheron rock avalanche in Red Hill valley. Profiles appear after filtering with dewow, rubber-banding and topographic correction. The black and white lines represent positive and negative pulses, AW - air wave, GW - ground wave. A) is the corrected profile before interpretation. The red arrows identify zones of pulse signal disturbance. B) shows the inferred location of faults (dashed red lines) and boundaries interpreted to represent fluvial sediments (orange and yellow) and flat-lying ponded material (blue). The underlying south dipping purple unit is considered to represent a buried fan deposit or an extension of a southerly trending ridge line / fan deposit (see Fig. 5.2). This unit appears to have been disturbed probably by faulting causing it to appear to be dipping in opposite directions.

The variations of slope angle on the northern side (proposed dip direction of the scarp) defined the position of the survey lines for the two GPR profiles (see Fig. 5.2 B). Profile one traversed the western shallow angled slope adjacent to the rock avalanche deposit, while profile two extended over the steeper northeastern section near the redundant drainage outlet (Fig. 5.4).

Both profiles display similar packages of layered reflections converging against an abrupt series of north dipping discontinuities (Fig. 5.6 and Fig. 5.7). The northern extent of the top two units (light blue and orange) thin out on the dipping slope of the lower units (yellow and purple-clear) compared to that in the south where they appear to be dragged up and deformed. This indicates probable faulting activity occurring in the zone of signal disruption between profile distances 60-90m. It also implies that the faulting resulted in the warping of both units, therefore post-dating their deposition and establishing a potential age datum.

The top flat-lying layer (blue) is considered to correspond to the clayey silt layer of 1-1.5 m thick identified in the auger holes approximately, while the lower packages can be separated into two distinct units. The upper section (orange) appears to represent ponded channel deposits abutted against the scarp. This is based on the narrow channel form of the lower reflection layers of the unit, and the relatively flat-lying surface pinching out above the south dipping units at a distance of 30m along both profiles. The uniform angular clasts retrieved from the auger transect suggest a short term fluvial history if that interpretation is correct.

The lower layers (yellow and purple / clear) show distinctive south dipping reflections that abutt against the faults in the south and extend to the surface in the north of both profiles. This coincides with a raised relief feature between profile distances of 10 and 20m. This unit appears to represent a debris fan derived from an isolated ridge line (seen in Fig. 5.2. A. and Fig. 5.4) which may be a remnant fan deposit. Coinciding with the surface relief features (distance 10-20m) is a series of tight-folded reflections extending up through the lower layers most visible on profile two (Fig. 5.7). This is considered to represent another strand of faulting or a relaxation feature associated with main fault deformation on the south of the profiles. It is proposed that the purple / clear unit extends the length of the profiles beyond the zone of faulting and its present deformed state depicts warping and uplift of 2-4m. There also appears to be fault-like disturbances between distances 40m-60m, which dip south in the opposite direction to those delineating the fault scarp.

Figure 5.8: Profiles 1 and 2 stretched (H=V 1:1) showing the the true angle of the sediment packages and the inferred faults as they would appear in the field.

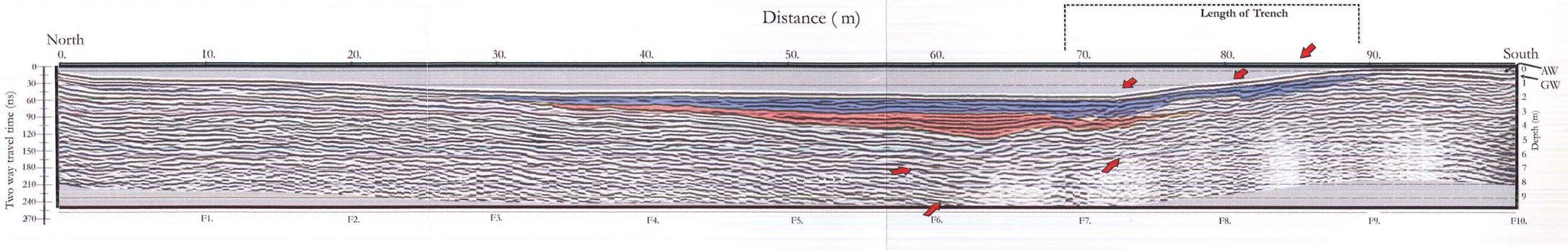

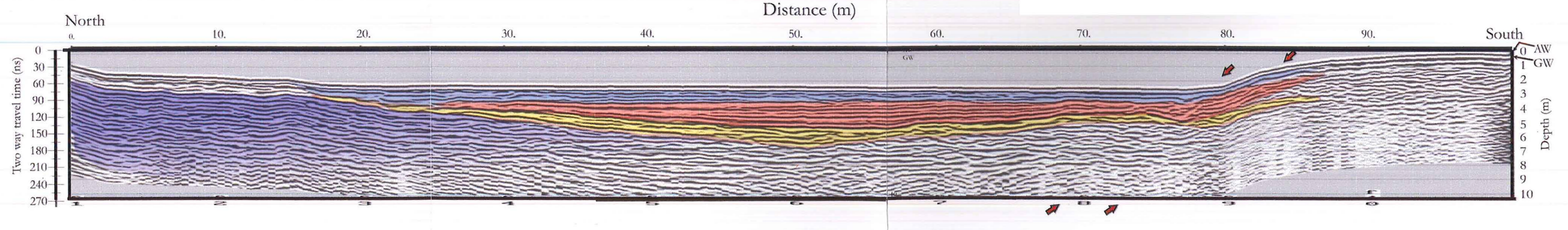

The results of the GPR survey show clusters of offset reflection pulses dipping north, which are interpreted to be multiple fault strands extending below the penetration depth of the GPR deforming discrete reflection packages interpreted as a sequence of soft sediments. The deposition of the soft sediments is thought to pre-date faulting. A large south dipping unit is considered to be a fan deposit also deformed by the faulting, causing a reversal of dip in the zone of deformation. No greywacke basement was identified. Profile one in Fig. 5.6 displays a flatter topographic gradient and appeared to exhibit discontinuities closer and more accessible to the ground surface. These results encouraged the use of this site as the most likely to divulge the location of the Porters Pass Fault in the Red Hill valley.

5.4. STRATIGRAPHIC TRENCH INVESTIGATION IN THE RED HILL VALLEY

5.4.1. BACKGROUND

The critical phase of a paleoseismic investigation is the gathering of stratigraphic evidence. This is achieved by excavating a trench across a fault line or zone. It is well documented in the literature that to maximise the success of a trench investigation of a fault, certain on-site conditions should be present (Fougere, 2002). The site of the excavation should intersect a zone of active faulting confined to a narrow zone of activity. Multiple strands of a fault zones may dissipate rupture energy, reducing the rupture evidence found in the trench (Fougere, 2002). This may cause ambiguous interpretations of earthquake history and reduce the certainty of any explanation (Fougere, 2002). The local site must also display a good potential to collect carbonaceous materials for radiocarbon dating, and be subject to little or no erosion of the paleo-surfaces (Fougere, 2002). Typically, these environs include swamps or small depressions (McCaplin, 1996). While the site selected for trenching in the Red Hill valley is found away from colluvial sources such as slopes, it appears to have been subject to discrete episodes of sedimentation which is expected to show the history of faulting.

The trench was excavated across the sloping northern surface of the scarp four metres northeast of profile one. This crosses the low angle surface displaying the oblique lineaments but immediately adjacent to the start of the abrupt steepening of the slope (Fig. 5.4). The trench angle was orientated approximately north–south perpendicular to the scarp expression, but slightly oblique to the lineaments due to uncertainty of the exact orientation of the faults.

Difficulties were encountered in the gaining permission to conduct trenching on the site which is a Crown administered Pastoral Lease. This involved a lengthy process including the drafting of a legal agreement between parties, concerning site rehabilitation and the type of work undertaken. Approval from the Department of Conservation was also a primary requirement.

5.4.2. TRENCH UNIT DESCRIPTIONS

A log of the northeast wall of the trench is presented in Figure 5.9. The trench extended for 21m and to a maximum depth of almost 3m. The units are described as comprising clay-bound fan deposits, interbedded with minor thinly bedded fluvial-like sequences (Unit 1). Above the fan deposit is reddy brown clayey silts thought to be derived from either ponding or an aeolian source (Unit 2). This is overlain by a thin soil horizon of dark brown topsoil consisting of silts and sandy clay (Unit 3). Typically topsoil is thin and slow to develop, probably reflecting periods of quiescence. The main displaced units are the fan deposits and the overlying clayey silt. No fault gouge was recorded.

UNIT 1

The coarse deposits (Unit 1) consisted of angular blocky clasts and fragments of greywacke gravels in a coarse sand and clay matrix. Difficulty existed in identifying discrete division due to the homogeneous nature of the unit, however the bands of large block clasts (20-30cm) are considered to represent the sub-boundaries within the units. A reduction of large block clasts occurred with depth, coinciding with a corresponding reduction of clay content and an increase in sand. Differences that defined each sub-unit were percentages of clay fraction, amount of bedding structure, and frequency of large clasts sizes (outlined in the trench log by differing shades of brown).

Within these units exists intervening beds of coarse sand and small angular clasts not exceeding 50mm in size (Unit 1C). These discrete layers did not exceed 30cm in thickness, and displayed fining-upward bedding structure implying localised short term fluvial activity. Near the trench floor in the southern 10 metres, clay content reduces with less frequent large clasts (Unit 1 A-B) while the upper metre contains a dominant sandy clay matrix with frequent large clasts 20-30 cm in size. During the first six metres (from the southern end

toward the northern end of the log) the clasts appear to lie horizontally showing slight imbrications parallel to the trench. This alters abruptly between 14m-16m to a distinctive north dipping orientation. The presence of water in the base of trench in the northern half reduced the detail, particularly immediately below the thickest section of the clayey silt in the northern end. However it was noted that Unit 1 flattens out.

UNIT 2

The reddy brown clay silt sections (Unit 2) are interpreted as overbank deposits. No coarse sediment layers or bedding structure was identified except thin oxidised laminae in the top clay layer between the upper palosol and the topsoil along the 19–20m sections (Fig. 5.9).

Two buried soil horizons were exposed in the northern end of the trench. They appear to incline back up slope, mirroring the angle of the underlying Unit 1, and converge together into the present soil horizon. This gives the appearance of a hinge point responding to a dropping footwall during a fault rupture. Both layers contained charcoal, but the upper horizon contained only fragments therefore charcoal was only retrieved from the lower horizon where it was more abundant (Wk 13112 653 ± 54 years B.P.). A smaller organic horizon extends out from the northern margin of the trench between the two palosols with a thickness of 1-2 cm, but disappears rapidly over a length of one metre. The lower soil was radiocarbon dated (Wk 13034) 661 ± 34 years B.P., showing a consistency of age with the charcoal (Wk 13112) 653 ± 54 years B.P. The upper soil was also radiocarbon dated using AMS (Wk 13033) 765 ± 42 years B.P., giving a date which exceeded the age of the lower palosol.

Material was sampled along a vertical profile adjacent to the northern margin of the trench to identify the content of the clayey silt material to determine an aeolian or fluvial source. The Atterberg limit test identified the material as plastic silt, suggesting a quantity of clay content within the samples (see Appendix F.2). A portion of the same samples were subjected to X-ray Diffraction (XRD) and grain size analysis (refer Appendix F 1-3).

The XRD showed only trace elements of Kaolinite and Muscovite. The dominant mineral was quartz, typically 60-75%, with smaller portions of albite (20-35%). Kaolinite was 5% throughout the entire unit, with traces of muscovite recorded in the material immediately above the gravel at the base of the trench and in the upper section near the surface. The prominent changes correspond to variations of the amount of quartz to albite. At the base

12cm above the underlying Unit 1 clast material, the quartz was reduced to its lowest limit of 60% while the albite peaked at 35%. The palosols had quartz 65% and albite 30%, while samples retrieved from immediately below the topsoil and below the upper palosol have 75% quartz with 20% albite (See Appendix F.3).

Grain size distribution analysis showed a greater than 50% of silt size material, with a clay fraction of 3-8% below the lower soil horizon (2A) increasing to 14% for the material between the two palosols (2A-2B). Below the lower palosol (2A) the sand content is minimal between 2-4%. The section between the two paleosols contained the largest amount of sand (more than 12%), while the upper section between the topsoil and the upper palosol had only 4% sand (see Appendix F.1).

Silt size material dominates the samples, with a small fraction of sands and less than 15% clay. It is considered that the clayey silt is derived from ponded sediments. The flat lying oxidised laminae in the top northern margin of the trench and the overall flat position of the silt sediments suggest they are derived from ponding, probably associated with damming of the Bluff River by the Acheron rock avalanche deposition. This is supported by the evidence in the GPR logs which depict the layer to thin out against the underlying south dipping fan material on the northern side of the profiles (see Fig. 5.8). The increase of sand content above the lower palosol is thought to relate to a second flood event post-dating the lower palosols formation.

5.4.3. FAULT AND STRUCTURES & CRITICAL RELATIONSHIPS

Within the trench, three faults were identified, with a possible fourth defining the main change in slope seen the in the trench outline (see Fig. 5.9). This is delineated by the prominent dipping of the coarse clasts in Unit 1. No strike-slip offsets were recorded from the faulting, as was expected in a trench orientated normal to the strike of the fault planes in a strike-slip fault system. All the faults offset both the coarse clasts of Unit 1 seen as grey-brown and the clayey silt shown as orange in Fig. 5.9, and dip north at angles between 60°-70°. The fault zone is thought to extend beyond the trench site or concentrate at depth below the base of the trench. This may reflect the high level of sedimentation at the site predating faulting.

Faulting can be observed over a width of 12 m measured at the base of the trench base. No obvious shearing of sediments could be identified within either unit, but changes in clast orientation and the vertical displacement of the overlying clayey silt defined the style and amount of fault movement. The squaring of the scarp where the faults exit the northeastern side of the structure supports the dextral movement seen elsewhere on the Porters Pass Fault (see Fig. 5.2 C). The faults all trend at 078° which match the lineaments obliquely crossing the scarp feature and the fault scarps on the valley margins.

Fault one and two located between 3-5 m metres from the southern end of the trench are separated by 50-60cm. The main displacement is down-dislocation of a wedge of sediment between the two faults highlighted by displacement of the overlying clayey silt and sub vertically oriented clasts. A small bulge in the surface profile between 0 and 2m (from the southern trench end) may represent the faulting. Possible offset of a thinly bedded fluvial sequence (Unit 1C) and coarse clast layer (Unit 1B) was recorded, but the offset layer could not be picked up beyond the faults which makes it difficult to confirm. Clayey silt material from the overlying layer (Unit 2) was observed to have been dragged down into fault two for more than 30cm. This extends to 1.5m on the unlogged southwest face. At the trench floor the faults were difficult to determine within the angular gravelly material of Unit 1A.

Two faults are inferred to have been located with the remaining northern section. The first is considered to be defined between 13-15m by the pinching out of the cover clayey silt and its reappearance two metres north. The sub-horizontal layer of coarse clasts appears to have been dragged down. It is thought that this may represent the major component of deformation and uplift of the scarp, with the remaining faults acting as relaxation features. However, no fault plane could be positively discerned within the gravely unit.

The third recorded fault is an abrupt 40cm vertical offset of Unit 1 and the clayey silt layer between 15 and 16m along the trench. Above the offset occurs the hinge point of the converging soil horizons. At the base of the soil is a slight offset, suggesting that faulting occurred through the feature. The footwall appears to be sagging in a normal fault style; creating space for further sedimentation.

The total probable displacement within the trench measured from the position of the lowest Unit 1 below the buried soils layers to the where the coarse material intersects with the topsoil is 2m (see Fig. 5.9). This is consistent with the observations of Howard, (2001) who calculated from ten sites an average of 1.7m for vertical displacement along the Porters Pass Fault. It also matches the characteristics of local scarps on adjoining valleys of 2-3m (Howard, 2001). The strike of 078° for the faults is very close to the 075° described for the fault section between Red Lakes to Lake Lyndon by Howard (2001). The strike of 078° and the normal component of displacement observed in the trench appear also to fit Howard's (2001) model for topographically-induced modification of faulting kinematics.

This is originates from the differing faulting styles observed by Howard, (2001) in the low glacial topography west of Lake Coleridge of oblique slip, with components of reverse; described as analogous to the relative plate motion, compared to the predominantly strike-slip and normal faulting observed in areas of steep terrain northeast of the Red Lakes. Howard (2001) suggested that this variation represents the effect of steep topography, such as that in found in the Red Hill valley, altering the properties of the fault causing variations of stress and strain away from the relative plate motion (Howard, 2001).

5.4.4. LOCALISED GROUND DEFORMATION

The scarp expression was obliquely cut by faulting, with the lower fault (Fault 3) defining the crest of the scarp and Fault 1 and 2 bounding the western margin of a distinct squaring of the scarp where all faults (1,2 & 3) obliquely begin to cross the river bed (see Fig. 5.2 C). A small slump in an east direction out of the rock avalanche margin also corresponds to the trend of the faults (see Fig. 5.2 B). Two redundant waterways identified on the sketch plan appear parallel to the faults trend (see Fig. 5.4). On the other side of the redundant watercourse, a raised expression seen in Fig.5.2 A, C; Fig. 5.4 is considered to define a wider zone of deformation and a possible insight into the type of faulting.

Seasonal spring drainage from the ephemeral pond drains parallel to terrace and trench site intersection and undergoes an abrupt dogleg westward (dextral), before reaching the redundant outlet into the Bluff River (Fig. 5.4).

The Red Hill valley Porters Pass Fault Trench

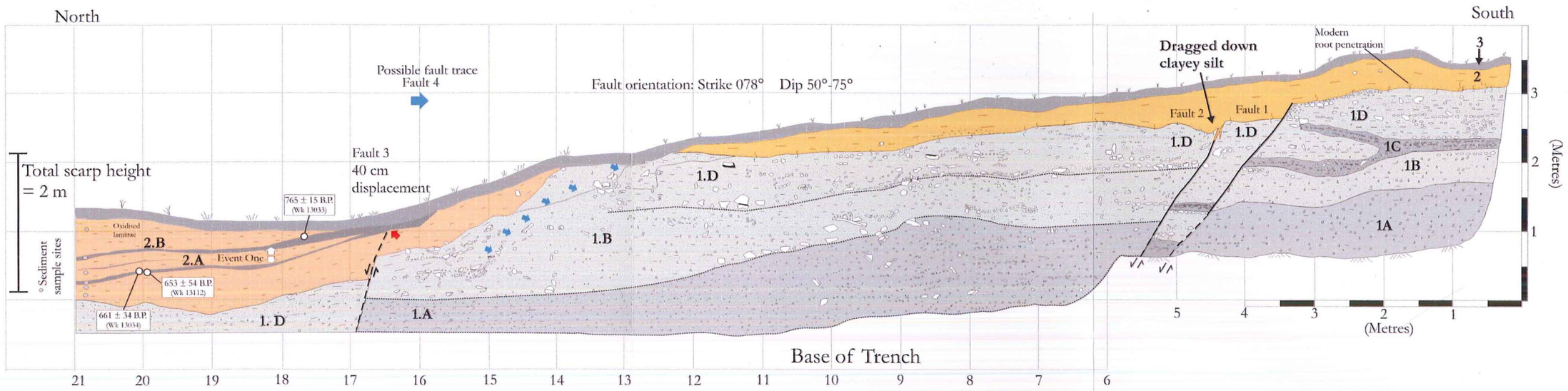

	Description	Interpretation	Event Horizon
3.	Soft dark brown topsoil with a thickness ranging between 10-20cm	Modern topsoil formed on the older units 2-3	
2.B / 2.A	Paleosols dark brown containing charcoal fragments	Soil (2.B) formed on unit 2 Soil (2.A) formed on unit 2	← Most recent inferred event
2.	Soft light brown to reddy brown clayer silt. Thickness ranges between 20-110cm	Overbank deposit may represent creation of space associated with footwall drop	
	Greywacke derived sediments		
1.D	Angular blocky clasts 20 -30cm, found in a coarse sandy clay matrix (> 50%) containing angular fragments of 20-30mm. Basic bedding sequences defined by the large blocky units.	Fluvial deposit or fan deposit sediments	
1.C	Smaller uniformly sized angular fragments (10-20mm) in a coarse sandy matrix appearing well sorted with bedding and fining upward. Bedding sequences between 10-15cm thick. Abrupt contact with the upper blocky clay bound unit. Clay fraction (< 50%)		
1.B	Angular fragments in a coarse sandy clay matrix. Clay fraction is reduced compared to the upper gravel unit with weathered granules 5-10mm and layers of block clasts 10-30cm.		
1. A	Angular fragments 10-20mm in coarse sandy matrix with reduced clay fraction (< 50%). Block fragments visible throughout. Sequences of bedded fragments showing the angle of the slope of the unit.		

Summary

- At least one rupture event occurred illustrated by the dragging down and offset of the overlying clayey silt (Orange) and inferred to displace the lowest paleosol (2.A) below the converging hinge point of the two paleosol horizons with the present-day soil horizon (red arrow).
- The event postdates the formation of the angular gravels (grey) and the formation of the lower paleosol. Two samples dated at 661 ± 34 yrs BP(Wk 13034) and 653 ± 54 yrs BP (Wk 13112) represent the older bracket.
- The date for the upper paleosol or youngest bracket of 765 ± 42 yrs BP is considered to be derived from a secondary source such as wind blown material.

Radiocarbon Dates (Conventional Age)

- (Wk 13033) 765 ± 42 yrs B.P - Paleosol 2.B. AMS Dating
- (Wk 13034) 661 ± 34 yrs B.P Paleosol 2.A.
- (Wk 13112) 653 ± 54 yrs B.P Charcoal within the Paleosol 2.A

Figure 5.9: Face log of the Red Hill valley trench excavated across the Porters Pass Fault adjacent to the northeastern margin of the Acheron rock avalanche

This is considered to have formed with the advent of the raised expression northeast of the fault scarp forcing the water to drain towards the channel outlet. The lineaments identified crossing the rock avalanche appear parallel to the 078° strike identified for the faults (see Fig. 5.3; Fig. 5.4). The jump in elevation for the section of the forested northeastern margin of the rock avalanche also appears to coincide with the western linear extension of the fault traces, suggesting post-deposition uplift or the existence of a prominent scarp predating the rock avalanche deposition (Fig. 5.4). The lack of continuation of the elevated material across the deposit may be explained by the existence of a buried terrace coinciding with a longitudinal depression trending north-south up the deposit.

5.5. INTERPRETATION OF TRENCH EVIDENCE

Two soil horizons have been identified in the north end of the trench within a total of 1.2m of clayey silt overlying coarse material (Unit 1). This represents three episodes of sedimentation. The clayey silt layer (Unit 2 in trench log) contained very little to no sand and fluvial structure and therefore most likely represents overbank deposits resulting from flood events or blockage of the adjacent Bluff River. This is supported by the lack of evidence for similar clayey silt stratigraphy below Unit 2 within the trench or the GPR profiles (Fig. 5.8.) The probable cause of the initial inundation can be attributed to the deposition of the Acheron rock avalanche which filled the Red Hill valley, completely cutting off the river several hundred metres south of the trench site. The radiocarbon ages for the lower buried soil horizon (2A) (Wk 13034 palosols) 661 ± 34 years B.P. and (Wk 13112 charcoal) 653 ± 54 years B.P. consequently also reconfirms the new radiocarbon age for the Acheron rock avalanche of (Wk 12094) 1152 ± 51 years B.P. Faulting is inferred to post-date the formation of the paleosol 2A based on the vertical displacements of both Unit 1 and the silts below the soil horizon convergence point (Fault three), which is also interpreted to be part of the 2A unit (Fig. 5.9). A slight discordance was observed at the base of the soils, suggesting vertical offset, however displacement of the material is not visible beyond the topsoil. This is not unusual for strike-slip faults which tend to die out before rupturing the ground surface (McCaplin, 1996). The movement of 40cm was most likely taken up by foot wall sag. The presence of dragged down silt material in Fault two supports the occurrence of faulting activity, but this is based on the assumption that the clayey silt on the top of the scarp is associated with the material below the 2A horizon. If the silts are from the same origin, then faulting is considered to have occurred post-dating the formation of the lower

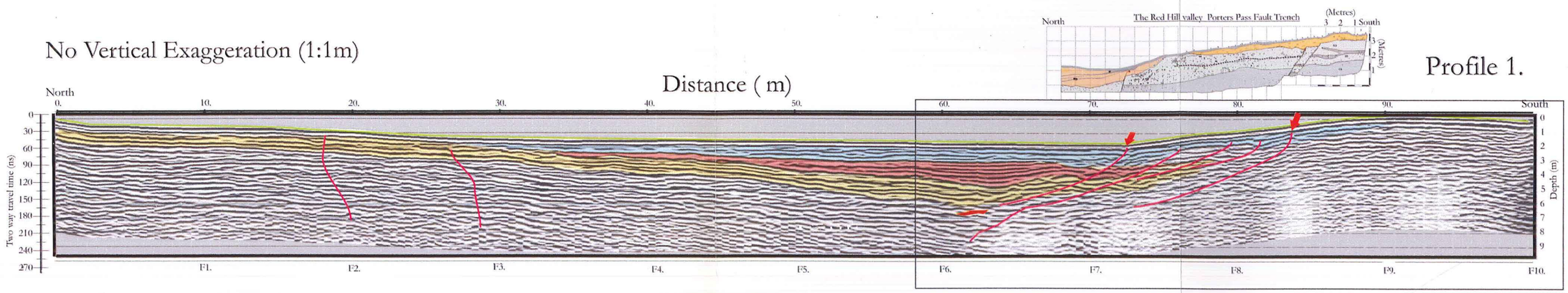

The Red Hill Valley Porters Pass Fault Trench

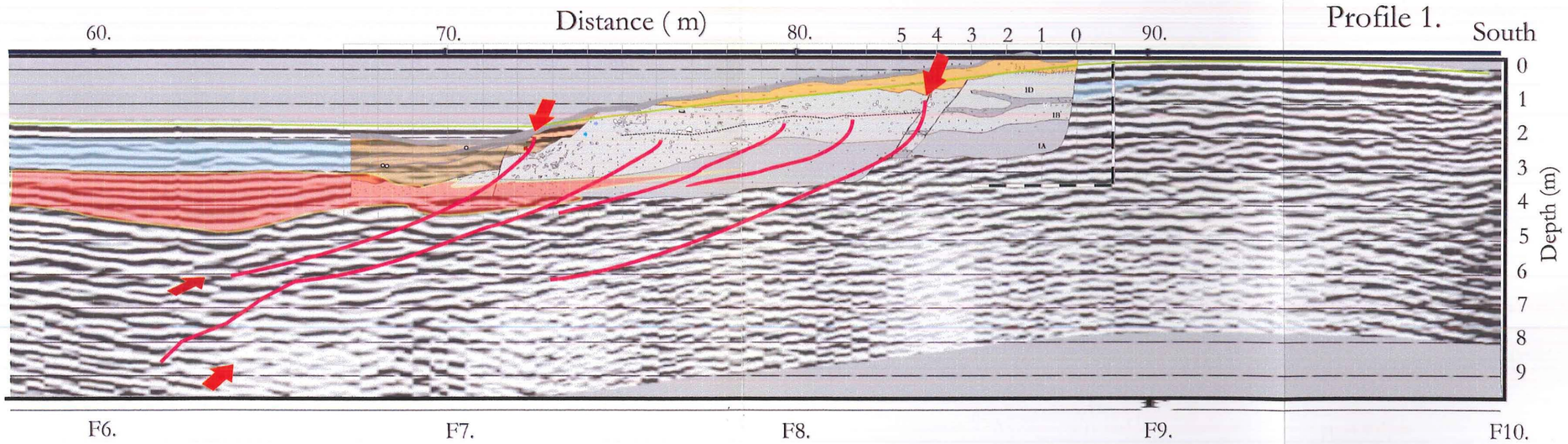

Figure 5.10: Comparison between G.P.R. Profile 1 and the Red Hill valley trench log. Faults 1 and 2 match with the Profile 1 as does Fault 3. The inferred faults between distance 74-83m may reflect the existence of unseen faulting within the coarse angular gravels of the fan deposit (Unit 1) or lithological differences such as variation of clay content or finer materials.

soil horizon (2A) giving a maximum age of (Wk 13034) 661 ± 34 years B.P.

The 2A horizon is overlain by 20cm of clayey silt, with a sand fraction of 12%, representative of another episode of ponding. Whether this is fault-induced or solely derived from flooding is uncertain as no fault evidence exists except the vertical offset of the 2A clayey silt and the termination of both paleosols at the same point. However, it is probable that 2B represents the younger bracket of the event. The radiocarbon age for the upper paleosol (2B) (Wk 13033) 765 ± 42 years B.P. appears older than the underlying palosol by over one hundred years. The variation may have been related to the dating of discrete particulates within the soil sample which can come from an older source by wind, surface water flow processes or gravity induced down-slope movement.

A second damming event was identified 1 km upstream of the Bluff River from the trench site. Rock avalanche debris form a substantial brandung or run up debris mound on a forested terrace surface on the western bank at a narrow bend on the river (see Fig. 5.1; Fig. 5.2 A). The rock avalanche is considered to be derived from the western flanks of Mt. Lyndon. This implies that the river was dammed at this point, which breeched and may have resulted in a high flow of water down-valley against the already aggraded riverbed level formed by Acheron deposit event. However there is no age control on this occurrence, therefore it could potentially explain the burial of either the lower 2A or the upper 2B horizons.

Differences in the ponded sediment thickness also exist. Only 20cm accumulated above the 2A event horizon compared to the underlying 20-50cm thickness while 40cm of sedimentation covers the 2B horizon which establishes the present-day surface. This may support a flooding interpretation where the thicker units representing more substantial flooding events such as damming of the river. It is also noted in that long term ponding would cause accumulations of preserved organics absent from the stratigraphy appearing as thin paleosols rather than peat (H. Rother, pers comm., 2003). It is observed that the two paleosols (2A, 2B) both thin out near the northern end of the trench, suggesting that the horizons were less developed away from the scarp and that ponded water may have existed between the burials of both soil horizons.

5.6. PALEO-AGE INTERPRETATION

A single rupture episode postdating 700 years B.P. is proposed for the Porters Pass Fault in the Red Hill valley west of Lake Lyndon, based on the identification of two buried soil horizons in a trench excavated across the fault line. The older (lower bracket) paleosol 2A is interpreted to be vertically offset by 40cm. The maximum vertical displacement identified during the trench excavation is approximately 2m, which is consistent with observations of vertical movement by Howard along the Porters Pass Fault (2001). The age of the lower paleosol (2A) (Wk 13034) of 661 ± 34 years B.P. and charcoal (Wk 13112) 653 ± 54 years B.P is similar to the 700-500 years B.P. age suggested for instability along the PP-AFZ (Cowan et al. 1996).

Cowan et al. (1996) recorded three landslide events along the eastern PP-AFZ that correspond to a faulting event post dating 700 years B.P; the Ashley landslide (490 ±70 years B.P.), the Glentui Slide One (600 ± 100 years B.P) and the Lees Valley deposit (580 ± 90 years B.P.), (ages being based on rock weathering rind thickness refer Fig. 6.1). The Glentui Slide One and the Lees valley ages are similar to the age of paleosol 2A. The Ashley landslide, however, appears 100 years younger than the age range presented for the 2A, but matches Bull and Brandon's (1996) lichenometry age of 460 ± 10 years B.P. and Howard's weathering rind age of 490 ± 55 years B.P. for the surface of the Acheron rock avalanche deposit adjacent to the Red Hill valley trench.

Lichen ages produced for the Kowai rock avalanche 8 km northeast were 580 ± 10 and 421 ± 10 years B.P. the younger of which coincides with a rapid decline of rind thickness populations post dating 474 ± 45 years B.P. as identified in Howard's study (Bull and Brandon, 1996; Howard, 2001).

The Red Lakes terraces west of the trench produced a weathering-rind age of 690 ± 50 years B.P. for the oldest (T1) surface. This terrace set was actively deformed by the faulting which Howard acknowledges could be the result of one or more surface rupturing events in the last ca 700 years (Howard, 2001). This age is within age range of the paleosol 2A and within 4 km of the Red Hill valley trench.

The study of the Porters Pass Fault conducted by Howard (2001) found no rupture evidence post-dating the upper peat layer of (Wk 9236) cal 870 ± 76 years B.P. which brackets event one in trench four at Porters Pass (2001). The lack of faulting evidence at Porters Pass suggests that deformation at Red Hill and the Red Lakes would have to occur west of Porters Pass implying the presence of segmentation of fault activity along the fault line. This does not explain the corresponding landslide evidence that exists to the east along the PP-AFZ. In contrast the vertical to horizontal movement ratios (from offsets along the fault trace) Howard (2001) calculated for the Porters Pass Fault appears to decrease rapidly between Lake Lyndon and Red Lakes. This may represent the burial of displaced features, or the reduction of motion west beyond Lake Lyndon resulting in little recorded fault deformation within the valley. The 2m vertical displacement is considered to be cumulative, suggesting a series of similar sized events have occurred at the Red Hill valley site.

The ages for the weathering-rind thicknesses and lichen size populations of 490 ± 55 years B.P. and 460 ± 10 years from Howard, (2001) and Bull and Brandon (1998) for the Acheron rock avalanche probably reflect a disturbance of the rock avalanche surface associated with the post 700 year B.P. rupture identified in the trench. This may have caused resetting of the surface debris rocks resulting in ages younger than the Acheron rock avalanche emplacement.

5.7. SUMMARY

During the present field investigation of the study area, a small northeast trending expression was identified as a potential scarp formed by the Porters Pass Fault. Minor lineaments identified obliquely crossing the rock avalanche surface also question whether the rock avalanche post-dated the last event on the fault. To investigate this, a ground survey using Ground Penetrating Radar (GPR) was undertaken. Two traverses of the terrace feature identified several continuous shallow boundaries of sediment dipping towards and abutting against the proposed scarp. Further analysis of the data showed offsets and disturbance of pulse reflections. This has been interpreted to be the result of propagating faults.

Trenching of the scarp identified three faults and a possible fourth striking 078°. Two buried soil horizons were identified within the clayey silts of Unit 2 in the northern end of the trench, with the lower soil unit (2A) offset vertically by 40cm with a total vertical offset of the scarp of 2m. The two ages for the lower buried soil (Wk 13034, paleosol) 661 ± 34 B.P. and (Wk

13112 charcoal) 653 ± 54 years B.P show a consistency of age and appear broadly consistent with the average surface ages of the Acheron rock avalanche of 464 ± 79 years B.P. and the period of instability identified by Cowan et al (1996) along the PP-AFZ between 700-500 years B.P. The upper soil (2B) age of (Wk 13033) 765 ± 42 years B.P. is more than one hundred years older than the lower soil horizon (2A), however this may relate to the origin of discrete particulates within the dated paleosol being deposited from an older source by processes such as gravity induced movement down slope.

The deposition of the Acheron rock avalanche is considered to have dammed the Bluff River, a tributary of the Red Hill stream, causing ponding and sedimentation. In total, three episodes of inundation of the area have occurred resulting in the accumulation of 1.2m of clayey silt, burying two established soil horizons. The first event coincides with the Acheron rock avalanche deposition forming paleosol 2A, the second is considered to represent a rupture along the Porters Pass Fault resulting in sag of the footwall focusing ponded water eventually forming soil horizon 2B. The third period of sedimentation may reflect a later event caused by another rock avalanche damming the Bluff River 1 km upstream, or an unrelated episode of flooding in the river.

It is proposed that faulting occurred along the Porters Pass Fault west of Porters Pass post-dating the maximum age of the Acheron Rock avalanche of 1152 ± 51 years B.P., and probably taking place around 650 ± 50 years B.P. causing the lineaments on the surface of the rock avalanche and presumably resetting the weathering-rinds and modal lichen size populations.

CHAPTER SIX

COSEISMICITY OF THE ACHERON ROCK AVALANCHE

6.1. INTRODUCTION

The key impetus to this study is to examine the potential co-seismic relationship between the Acheron rock avalanche and the Porters Pass Fault; a prominent strand of the Porters Pass-Amberley Fault Zone. Understanding the relationship is critical for evaluating the usefulness of rock avalanches as paleoseismic indicators in the central Southern Alps. McSaveney (2002) noted that only two out of six historical rock avalanches in the Southern Alps were seismically triggered and the previous chapters showed examples of rock avalanches; the 1991 Mt Cook avalanche and 1992 Mt Fletcher avalanches (McSaveney, 2002) which were not triggered by earthquakes.

Recently the Acheron rock avalanche has come under examination to determine its relationship to fault activity (Cowan et al. 1996; Howard, 2001). Peripheral studies dating the deposit surface have assumed a co-seismic origin based on a succession of similar ages principally supported by a single radiocarbon age of 500 ± 69 (NZ547) interpreted by Burrows (1975) to represent faulting along the Porters Pass Fault (Whitehouse, 1981; Whitehouse, 1983; Whitehouse and Griffith,1983; Bull and Brandon, 1996; Jibson, 1996; Orwin, 1998). Similarly, some of the same studies have questioned the reliability of any landslide as an unambiguous seismic signature (Cowan et al. 1996, Howard, 2001). However the latter observations were supported by the absence of an event horizon of an equivalent age (700-500 years BP) during trenching along the Porters Pass Fault by Howard (2001).

During the present study four new ages (interpreted to closely pre-date the deposit) from samples excavated from reliable stratigraphic positions at the base of the rock avalanche showed an overlapping spread of ages between 1380–1100 years B.P. The most contemporaneous sample (Wk 12094) cut from a buried tree was dated to a conventional age of 1152 ± 51 years B.P. which bares a remarkable resemblance to the 1000 ± 100 year B.P. date proposed by Howard (2001). As discussed in Chapter Five Howard's date arises from

buried peat layers bracketing the youngest identified rupture in a trench (trench four see Fig. 6.6) immediately east of Porters Pass and a buried peat layer in a test pit located 3 km further to the west (2001). The Acheron rock avalanche therefore offers a unique opportunity to test the relationship between landslides and localised fault rupture and interpretation inconsistencies associated with dating of geomorphic surfaces using lichenometry and weathering-rind thickness ages.

Dates from previous studies and radiocarbon ages will be presented as conventional ages in years before present (B.P refer Fig. 6.1). Calibrated ages 1σ-2σ are listed with conventional ages in Appendix C and if presented in the text will be preceded by the prefix cal.

6.2. REVIEW OF PALEOSEISMIC APPLICATION LANDSLIDES

The relevance of any prehistoric landslides as a paleoseismic marker is limited by the level of confidence that can be obtained in the triggering mechanism (Jibson, 1996). This is the fundamental problem for the application of paleo-landslide as any coseismic association can only ever be based on circumstantial evidence and historical events (Jibson, 1996; Cowan et al. 1996; Howard, 2001). Interpretations of the coseismic processes subsequently can vary from extremely strong to extremely tenuous and has been a source of much debate in literature concerning the relevance of prehistoric landslides as paleo-markers (Voight, 1978; Jibson, 1996; Cowan et al. 1996; Howard, 2001).

Often the presence of several landslides overlying or along active range front fault zones are assumed to represent a coseismic relationship such as in the Andean mountains of Argentina and the Acheron rock avalanche in the Red Hill valley (Burrows, 1975; Jibson, 1996, Hermanns and Strecker, 1999). However, many inherent complexities exist when assuming the coseismic link between earthquake and landslide. These are distorted by time and limited knowledge of the failure process.

Cowan et al. (1996) used the example of the 1929 Arthur's Pass (Ms 7.2) and Murchison (Ms 7.8) earthquakes and the 1968 Inangahua (M_S 7.4) earthquakes to show the problems in distinguishing individual earthquake events from multiple closely spaced seismic episodes over short time periods. All three rupture events occurred within a period of 39 years, but would likely appear to be a single event in the geologic record using dating techniques such as

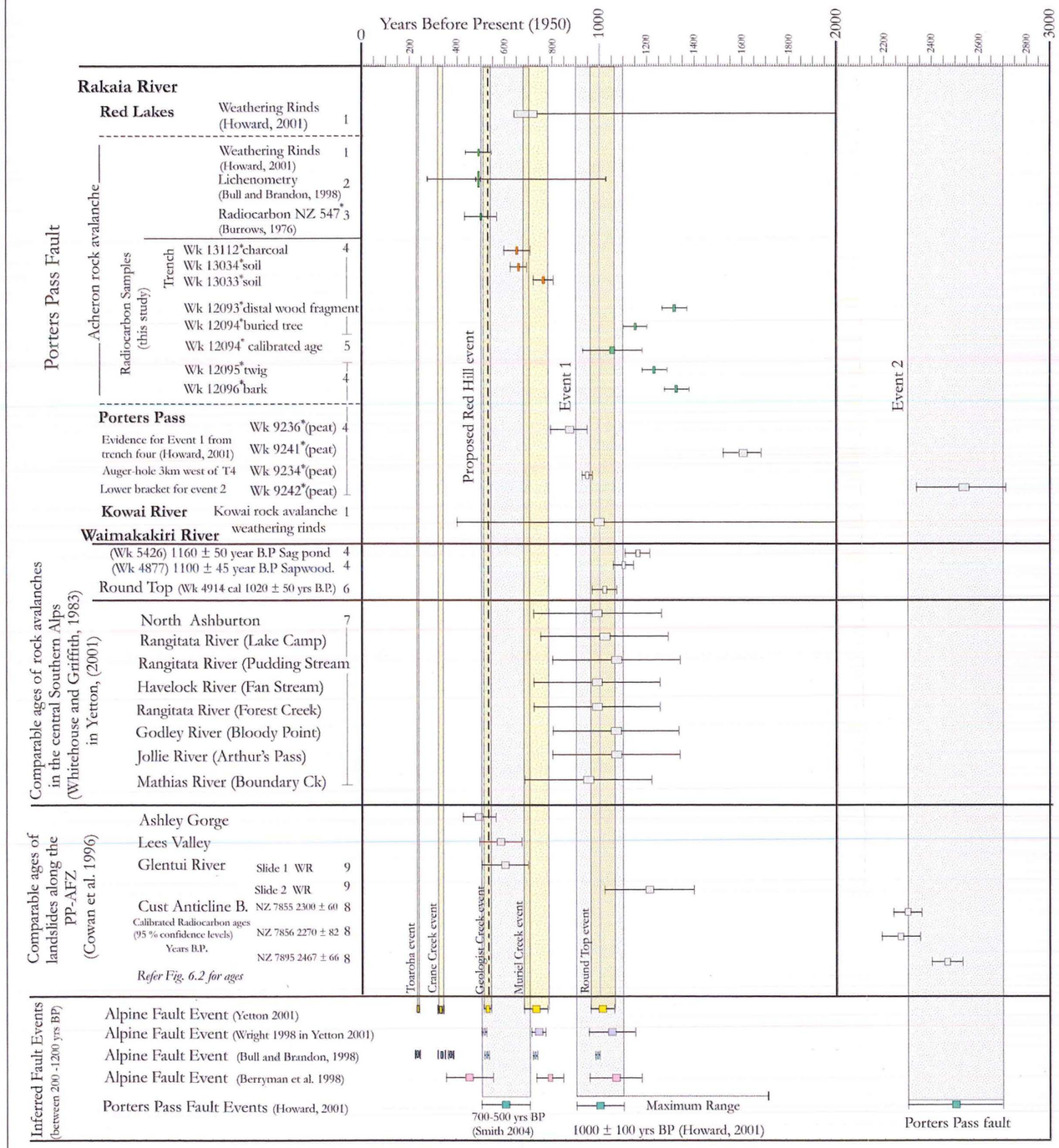

Figure 6.1: A correlation of landslide and rock avalanche ages along the PP-AFZ and the central Southern Alps in conjunction with dates excavated from trenching at Porters Pass (Howard, 2001) and Red Hill valley (this study) bracketed between 1200-200 years BP. These ages are compared to proposed earthquake events on both the Alpine Fault and Porters Pass Fault (Yetton, 2000; Howard, 2001).

The filled boxes illustrate the conventional age or modal peak age of the samples while the horizontal lines represent the error bars or population ranges. The five calibrated radiocarbon ages will display the prefix *cal.* Inferred earthquake events from the Porters Pass Fault are coloured grey (including a new earthquake age of between 700-500 yrs BP from this study) while events on the Alpine Fault are shown as yellow (based on the chronologies complied byYetton, 2000). Other studies of the Alpine Fault are displayed to show age comparisons for Alpine Fault earthquake events. (Wright et al. 1998 purple; Bull and Brandon, 1998-green; Berryman et al. 1998-red).

Ages are presented as yrs B.P. (Years Before Present -1950 AD.) All ages are recalculated from A.D. to B.P. assuming the present as 1950 A.D. Detailed discussion on age correlations in the central Southern Alps is later in this chapter.

SUMMARY IMPLICATIONS FROM THE AGE EVIDENCE

A strong age correlation exists between the Acheron, Round Top and eight other rock avalanches in the central Southern Alps with earthquake events between approximately 1200-900 years BP. This coincides with stratigraphic evidence identified within a trench at Porters Pass across the Porters Pass Fault (Howard, 2001) and rupture age correlations from Alpine Fault studies (Yetton, 2000; etc). Both the Acheron and Round Top rock avalanches are radiocarbon dated from reliable stratigraphic positions and represent the narrowest age range for coseismic failure (assuming that they were both triggered by the same event). Large errors (± 270 yrs) are associated with the 8 rock avalanches in the central Southern Alps reducing their application to rudimentary.

W.R.- Rock weathering-rind thickness * refer Appendix 3 Table 3.1 Radiocarbon Ages

1. Rind dates calibrated with a 0.2mm running average displayed ± one standard deviation as displayed in Howard,(2001).
2. Modal lichen ages and range of measured lichen populations for the Acheron rock avalanche (Bull and Brandon, 1996 in Howard, (2001)
3. Sample NZ 547 conventional radiocarbon age 500 ± 69 yrs B.P. (Burrows 1975)
4. Radiocarbon ages conventional
5. Calibrated radiocarbon age Wk 12094 Buried Tree 95.4% confidence level (this study)
6. Calibrated radiocarbon age from heartwood corrected by 95 ± 5 calendric years for the number of tree rings 95% confidence level from Wright (1998).
7. Rock avalanche weathering-rind ages are recalibrated to the McSaveney (1992) calibration curve from Table 8.4 in Yetton (2001) derived from Whitehouse and Griffith, Table 1(1983).
8. Calibrated radiocarbon ages (95% confidence levels) based on compilation by stuiver and Reimer (1986) of tree ring data with -30 radiocarbon years offset as recommended in Stuiver and Pearson (1986). Landslides ages along the Porters Pass - Amberley fault zone as displayed in Table 2, page 6029 Cowan (et al, 1996).
9. Rock weathering rind ages from Table 2 in Cowan et al (1996)

radiocarbon age estimates. This becomes problematic when assimilating comparable rock avalanche ages to an earthquake event as in this study. The use of weathering-rind dating and lichenometry does reduce this effect if they can be proved to be reliable dating tools.

Both Cowan et al. (1996) and Whitehouse & Griffith, (1983) also note that the longevity of a rock avalanche deposit in the Southern Alps of New Zealand is limited by highly active geomorphic processes, reducing the reliability of frequency and age distributions of landslides to earthquakes. Cowan et al. (1996) proposed that 2200-2450 years B.P. was the limit for reliable populations of rock avalanches deposits in the Southern Alps; a fact supported by Whitehouse and Griffith (1983) but disputed by the observations made by McSaveney (2002).

Chapter Three attempted to show that in New Zealand, large bedrock failures forming rock avalanches can be triggered by either aseismic or coseismic processes. Historically in the Southern Alps only a third of recorded rock avalanche events were seismically triggered (McSaveney, 2002). However the non-seismic examples (Mt Cook, Mt Fletcher) were confined to areas of historical glacial retreat and / or highly concentrated fracturing associated with the Main Divide Fault Zone. It could be implied that more competent rock masses (closely fractured rather than highly concentrated fracturing) remain stable and require a seismic trigger to accelerate fatiguing of defect bonds or initiate collapse. The historical examples may be therefore anomalous distorting the dominantly seismically induced rock avalanche process.

Comparatively apart from the obvious problems associated with paleo-landslides, Jibson, (1996) reaffirms the significance of clusters of landslides in a seismically active area as probably coseismic. Solonenko (1977) also agrees that the largest landslides frequently occur in the corresponding zone as the strongest earthquakes and even states that collapses in highly seismic areas tend to be repeated in the same region. Interestingly, he identifies that failures can occur after the seismic event, where the conditions for failure (fatiguing) were created by the main shock but took time to occur as seen after the 1960 Chilean earthquake (Solonenko, 1977). This would have implications for assigning an earthquake event to a landslide deposition age particularly over extended time periods. Jibson (1996) goes onto emphasize that investigations of any geomorphic paleo-indicators must use multiple lines of evidence which individually may be ambiguous but when combined help to constrain a seismic source.

One aspect supporting the coseismic relationship is the studies by Keefer (1984) who identified links between earthquake magnitude and spatial landslide frequency. Keefer (1984) formulated threshold levels of ground shaking necessary to trigger a particular style and number of landslides over a probable area. Keefer (1984) was able to quantify that landslide numbers decreased over distance a fact demonstrated by the recent Mw >7 Fiordland earthquake (IGNS website, 2003). These spatial relationships re-established the significance of paleolandslides. Keefer could demonstrate that for rock avalanches, Mw >6 is the lower threshold for failure. Certain broad inferences could then be made about earthquake motion properties, such as a very large coherent deep-seated rock mass (>1-50 x 10^6 m^3) may require stronger and probably longer duration of shaking. Rock avalanches, Keefer (1984) noted have the highest threshold. This is a point supported by Hancox et al. (1994) who indicates that the larger slides and rock avalanches are more likely to be triggered by longer-duration shaking associated with larger earthquakes (> M.6.5).

These observations of historical landslide frequency and distribution could also enable earthquake magnitude to be estimated from the comparison of historical to paleolandslide distribution. By correctly assigning landslides to earthquake events a minimum magnitude estimate can be made (Keefer, 1984). Hancox et al. (1994) also showed this for landslides during historic seismic events in New Zealand but noted that they occurred at higher magnitudes over smaller distances than that outlined by Keefer (1984). This was attributed to distinct topography and geology of the Southern Alps (Hancox et al. 1994). Using historical events Hancox et al. (1994) attempted to further correlate landslides to earthquakes by including site specific factors. This involved the correlation of slope angle, failure direction, rock type and slope type (Pearce and O'Loughlin, 1985; Hancox et al. 1994). Hancox et al. (1994) found that failures were typically oblique to directly away from the seismic centre which could delineate the source of shaking. This effect was demonstrated by the 1929 Arthur's Pass earthquake in greywacke terrain which included the Falling Mountain rock avalanche deposit (50 x10^6 m3) (see Fig.4.1; Appendix B Table 1).

Falling Mountain is located approximately 20.5 km from the epicentre and was one of six greywacke derived landslides of which all but one exceeded 1 x 10^6 m^3 of material. Failures occurred on slopes steeper than 25°-30° in a direction away from the source of motion. This may reflect site specific topography influencing seismic motion and the impact of motion normal to the planes of failure. Hancox et al. (1994) suggested that typical slopes forming

rock avalanches failures occurred on slopes >30° or dip slopes of 15°-40°. Landslide distribution therefore can provide an indication of epicentre location and extent of the fault rupture zone based on after shocks from historical events, but may be controlled by topographic properties so differs both in distance and magnitude of landsliding (Hancox et al. 1994).

Typical distance to intensity and magnitude comparisons are (MM VII) M 6 30km, 100km for M 7 (MMVIII) and almost 300km for (MM IX) M 8.2 (Hancox et al. 1994). The implications for this is that between 50-100km of the Red Hill valley exist many poorly constrained, but substantial fault structures other than the Porters Pass Fault including the Alpine Fault, which could release a shaking event causing the Acheron rock avalanche (Howard, 2001). Interestingly, Solonenko (1977) made observations that if a landslide is isolated then it is described as probably caused by a localised strong shaking event but if the deposits appear numerous and wide spread then they are probably from a strong shaking event exceeding MM 8-9.

Investigations of topographic amplification found that amplification generally increases with slope angle and proximity to the crest of the slope (Geli et al. 1988). This effect can trigger the failure of large rock masses forming rock avalanches and cause features such as ridge cracking and ridge rents all of which are present in the Red Hill valley area (Jibson, 1996). Crowns of the source scar are typically close to the top of the ridge or slope where the topographic amplification effect would be greatest (Sepulveda, 2003).

The influence of topographic amplification was demonstrated in recent studies of the 1999 Chi-Chi (Mw 7.6) earthquakes in Taiwan which identified a quantifiable link between slope form and landslide occurrence using a finite element model (Sepulveda et al. 2003). Approximately 22 000 landslides were triggered during Chi-Chi event however the spatial distribution was erratic with some valleys suffering concentrated landsliding while adjacent valleys were almost untouched (Sepulveda et al. 2003). The study found that slope instability analysis of landslides required accelerations 2-3 times the peak ground acceleration recorded in a nearby free-field strong motion station to initiate failure (Sepulveda et al. 2003). This result was considered to represent the effect of topographic amplification. Sepulveda et al. (2003) identified that specific geomorphological configurations increase the local ground accelerations, resulting in the trigger of an otherwise stable slope. This also corresponds to

Hancox et al. (1994) observations of landslide frequency distance to historical earthquake magnitude distributions in the Southern Alps where landsliding occurred at higher magnitudes over smaller distances than that outlined by Keefer (1984).

Crozier (1992) devised a check list of six requirements to support a landslide formed from a seismic origin:

- Ongoing seismicity in the area.
- Coincidence of landslide distribution with an active fault or seismic zone.
- Geotechnical slope stability analyses showing that earthquake would have been required to induce failure.
- Large size of landslide.
- Presence of liquefaction features.
- Landslide distribution that can not be explained by solely geological or geomorphic conditions.

This means the more of the criteria that can be met, the more compelling the link to a seismic event (Crozier, 1992; Jibson, 1996). The Acheron rock avalanche only meets two criteria of the six requirements as outlined above. The deposit is located in an area of ongoing seismicity, though clarity of landslide distribution with an active fault or seismic zone is uncertain. The geotechnical modelling of the parameters was outside the scope of this study due to a lack of detailed dimensional data of the defect source scar. This study chose to look at the local fault properties to establish a link between the faults and the rock avalanche.

Other parameters suggested by Solonenko (1977) that need to be considered were the weight of the active and passive parts of the landslide, the long term strength and strength at the time of movement, angle and direction of seismic motion, shock continuation, the degree of stress relief and the amount of defect fatiguing from previous seismic events on the rock mass.

6.3. THE PREVIOUS STUDIES OF THE AGE OF THE ACHERON ROCK AVALANCHE AND THE PORTERS PASS FAULT

6.3.1. THE ACHERON ROCK AVALANCHE DEPOSIT

The Acheron rock avalanche was first investigated in the early 1950s by Burrows (1975), looking for evidence of pre-European fires. He recognized the hummocky surface of the rock avalanche as a landslide deposit and concluded that most likely it was triggered by a rupture on a local fault most probably the Porters Pass Fault. This was due to the fault being buried beneath the mid section of the deposit. During his study, a well defined contact between an underlying terrace set and the rock avalanche deposit was recorded as exposing several species of buried plant material indicating a buried forest horizon. Burrows (1975) states that from this site wood was radiocarbon dated to 500 ± 69 years B.P. (NZ547 see Fig. 6.1). This date subsequently became the unofficial bench mark age for prehistoric coseismic landslide analysis for the eastern central Southern Alps, representing the probable youngest date of Holocene rupture on the Porters Pass Fault.

Bull and Brandon (1998) used the NZ547 (500 ± 69 years B.P.) age to support their lichen modal age for the Acheron deposit of 460 ± 10 years B.P. (≤ 84.3mm diameter lichens) as part of their substantial calibration set for the statistical analysis of maximum diameter lichen populations on rock fall deposits proposed to correspond to earthquake events on the Alpine Fault (Bull and Brandon, 1998).

SUMMARY

- Burrows (1975) located a wood sample radiocarbon dated at 500 ± 69 years B.P. (NZ547 see Fig. 6.1) derived from a river cut exposure through the Acheron rock avalanche deposit called site three in this study).

- Bull and Brandon's (1996 in Howard, 2001; 1998) 460 ± 10 year B.P. age was produced from modal lichen diameter population found at the Acheron deposit, supported by the radiocarbon age NZ547 (500 ± 69 years B.P.). This was used as a calibration site for their study of lichen size populations corresponding to earthquake events on the Alpine Fault.

6.3.2. THE PORTERS PASS-AMBERLEY FAULT ZONE

A study of the PP-AFZ conducted by Cowan (1992, et al. 1996) used landslides interpreted as being co-seismically triggered for additional information on the identification of earthquake magnitudes and timing along the fault zone. Applying ages from ten large landslides from a population of twenty, Cowan was able to distinguish a cluster of six landslides including the Acheron deposit around the 700–500 yrs B.P age spread along the length of the PP-AFZ. This concentration of landslide ages located in close proximity to the PP-AFZ implied one or more rupture events occurred between 700–500 yrs B.P., triggering slope instability along the fault zone.

Cowan et al. (1996) also discussed inherent unknowns associated with landslide history, such as geomorphic modification and invalidated trigger mechanisms which made a coseismic interpretation very tentative. They consequently were reluctant to assign the 500-700 year B.P. age as a probable time of the most recent rupture along the PP-AFZ (Cowan et al. 1996).

Looking beyond the PP-AFZ, Cowan recalibrated the weathering rind ages of rock avalanches in the central Southern Alps to the 1992 calibration curve of McSaveney (1992) using Whitehouse and Griffith (1983) data set. This enabled Cowan to identify any regional patterns of large scale instability between the 700-500 year B.P. period (see Fig. 6.2). Two modes of ages were identified; the younger circa 1050–1400 years B.P. (350 years range) and the older circa 1700–2100 years B.P. (400 years range Cowan et al. 1996).

Only two central Southern Alps rock avalanches matched the 500–700 years B.P. for the PP-AFZ landslides (Cowan et al. 1996). Cowan et al. (1996) interpreted the lack of overlap with those identified along the PP-AFZ at 500 -700 years B.P. to indicate a localised event, most probably along the PP-AFZ. In contrast, Cowan et al. (1996) noted that only three rock avalanche deposits correlated with those of the PP-AFZ between 2200-2450 years B.P. This was correlated with stratigraphic evidence for a rupture at around that time confirmed by Howard in trench four as event two (refer Table 1 in Cowan et al. 1996; Howard, 2001).

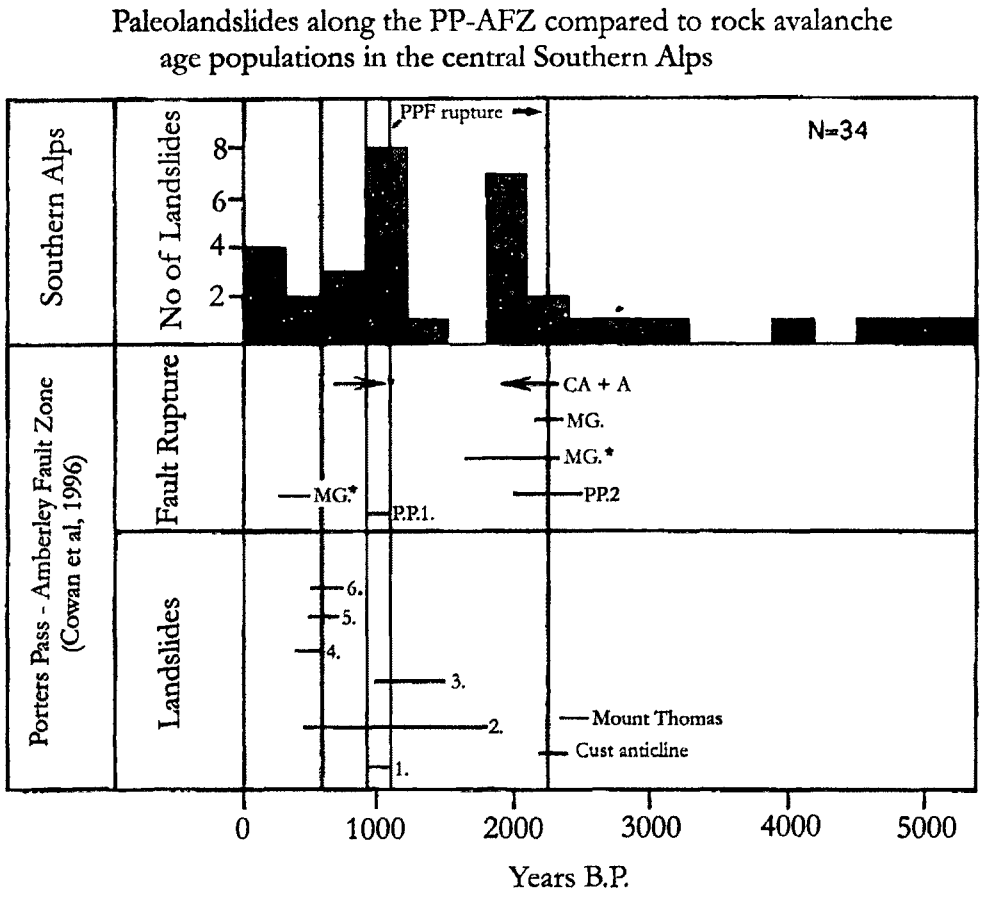

Figure 6.2: Weathering-rind ages(Re-calibrated to McSaveney 1992)from rock avalanches deposits in the Southern Alps displayed as a frequency histogram compared to the age distribution of landslides on the PP-AFZ (in Cowan et al. 1996). Landslide numbers correspond to a revised list below. (Abbreviations A. Ashley Fault, CA, Cust anticline, MG, Mount Grey, PP1. event one Porters Pass, PP.2 Event 2 Porters Pass. For more detail refer Table 2. Fig. 2, Fig.6 Cowan et al. 1996 p 6029-6030).

1. Acheron Rock Avalanche (closely postdates 1200-1100 years BP Radiocarbon age) (cal 1 s 1165 ± 5 and 1015 ± 55 years B.P.)(This study)	
2. Kowai Rock avalanche	(1700-400 years B.P. Weathering-rind thickness)(Howard, 2001)
3. Gentui River Slide 1.	(1210 ± 190 years B.P. Weathering-rind thickness)(Cowan et al, 1996)
4. Ashley Gorge	(490 ± 70 years B.P. Weathering-rind thickness)(Cowan et al, 1996)
5. Lees Valley	(580 ± 90 years B.P. Weathering-rind thickness)(Cowan et al, 1996)
6. Glentui River Slide 2.	(600± 100 years B.P. Weathering rind-thickness)(Cowan et al, 1996)

SUMMARY

- Cowan et al. (1996) identified a cluster of six landslides (including the Acheron deposit) around the 700–500 yrs B.P age spread along the length of the PP-AFZ. This concentration of landslide ages located in close proximity to the PP-AFZ implied that heightened seismic activity or at least one rupture event occurred between 700–500 yrs B.P.

- Comparing regional patterns of rock avalanche instability over the central Southern alps, Cowan et al. (1996) found instability to be absent between the 700-500 year B.P. period. Instead, two moderate modes of ages were identified, the youngest circa 1050–1400 years B.P. and the older circa 1700–2100 years B.P. (Cowan et al. 1996)

- Cowan et al. (1996) interpreted the lack of overlap with those identified along the PP-AFZ to show that between 700-500 years B.P. a local landslide-triggering seismic event occurred most probably along the PP-AFZ.

6.3.3. THE PORTERS PASS FAULT

The most comprehensive study of Holocene ruptures on the Porters Pass Fault was undertaken by Howard in 2001. This focused on a 40 km length of the Porters Pass Fault and included trenching, and an age investigation of both the Acheron and Kowai rock avalanches which Howard considered to post-date fault rupture. He also identified the Red Lakes terraces which were actively deformed by the Porters Pass Fault as representing a surface predating faulting (see Fig.6.3). At the Acheron deposit, a series of studies conducted over the previous twenty five years using weathering rind dates, lichen and radiocarbon dating had narrowed the age of deposition to 570-430 years B.P. (NZ547 Burrows, 1975; Whitehouse and Griffith, 1983; Bull and Brandon, 1998). Howard conducted weathering-rind measurement to check the authenticity of these ages and found a modal peak of rind thickness of 0.83mm producing an age of 490 ± 55 years B.P. (Howard, 2001).

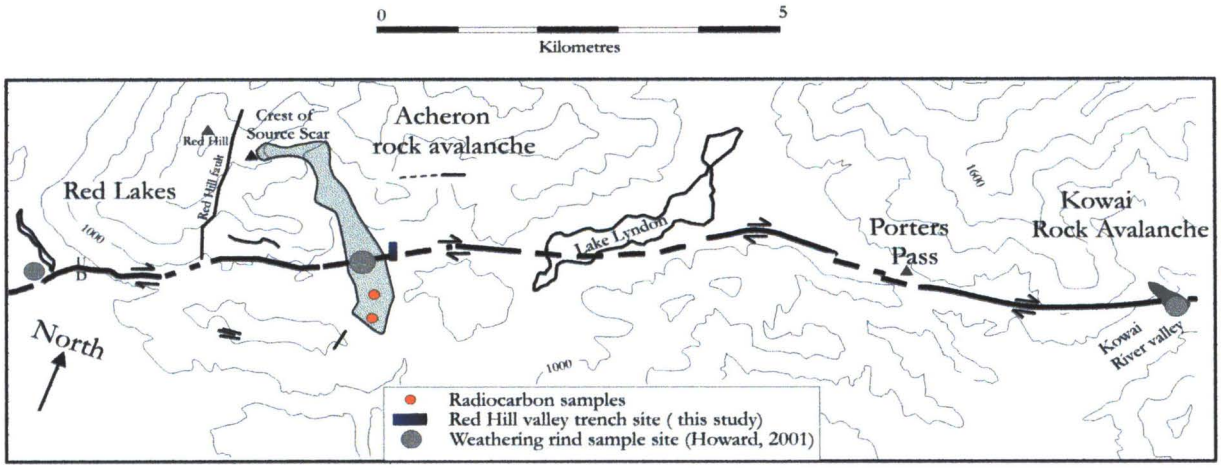

Figure 6.3: 1000m contour interval map of the Porters Pass Fault (heavy black line) between Red Lakes and the Kowai River. The weathering-rind sample sites from Howard, 2001 are shown as grey circles while the Radiocarbon sample site can be seen as orange circles. The Red Hill valley trench is depicted by the blue box. Map adapted from Nicol et al. (2001) and Howard, (2001).

Previous rind measurements from Whitehouse, (1983) of 0.66 mm were 0.17 mm too low, but still within the expectable error of weathering rind dating (Howard, 2001). Populations of lichen sizes obtained by Bull (Bull and Brandon, 1998, Bull 1996 in Howard, 2001) produced a modal peak age of 460 ±10 years B.P (84mm diameter) supporting the general age range at this time. Howard, realizing the limitations of the different dating methods, correlated the two previous dates from Burrows, (1975) and Bull and Brandon (1996) with his own and calculated a mean age of 464 ± 79 years B.P. for the surface of the rock avalanche (Howard, 2001).

The smaller Kowai rock avalanche, which also overlies the Porters Pass Fault trace, is located several km east of the Porters Pass in the Kowai valley (see Fig. 6.3). Howard (2001) noted that the Kowai deposit was not faulted, and therefore post-dated fault activity, offering what he considered to be a minimum age for the youngest earthquake event. Previous dating by Coyle inferred an age of 600 years B.P (Coyle, 1988). Howard redated the landslide using a larger but small population of 86 rind measurements, and found a wide spread of ages extending back between 1679 ± 260 years to 474 ± 45 years B.P., with a moderate peak at ca 1000 years B.P. (Howard, 2001). Howard (2001) concluded that these ages were reflecting an onset of instability at ca 1700 years B.P., with episodic periods of instability occurring until ca 500 years B.P.).

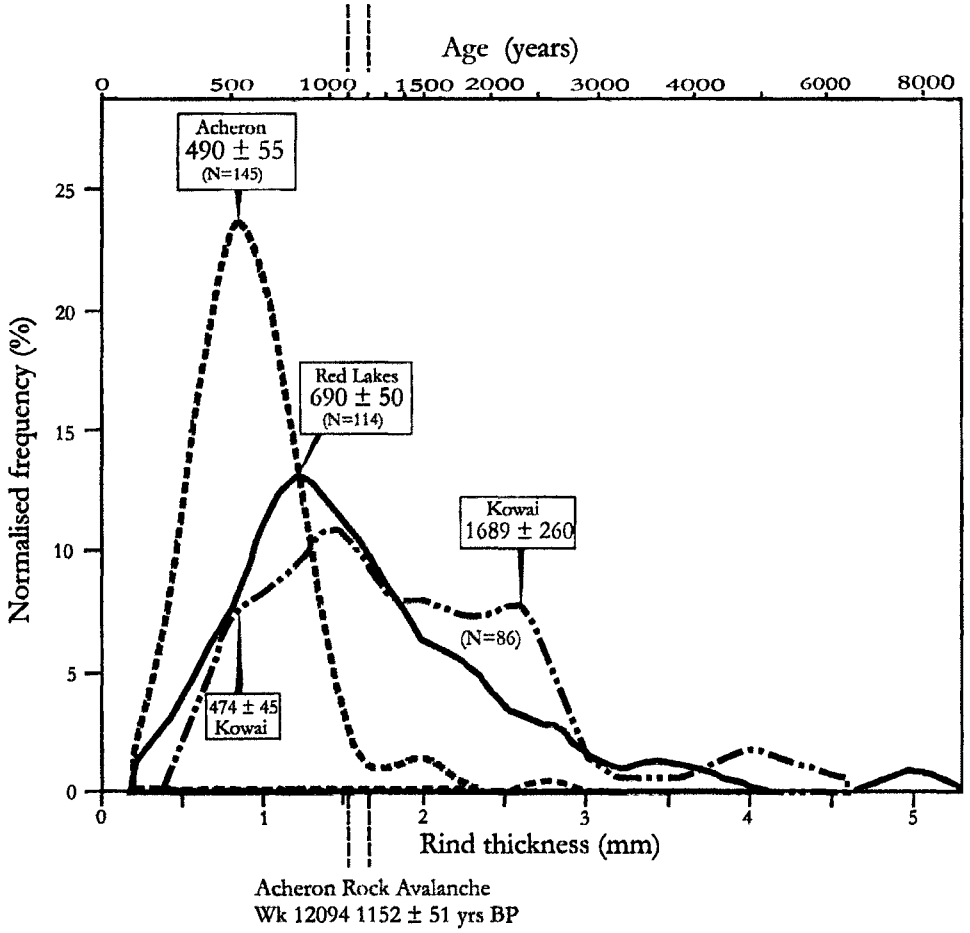

Figure 6.4: Weathering-rind thickness frequency histograms from the surface of the Acheron rock avalanche (heavy dotted line), the Kowai rock avalanche (stippled line) and from the T1 terrace surface at Red Lakes (heavy line). Labels display ages in years B.P. with error and number of rinds measured. The vertical dashed line represents the revised age for the Acheron rock avalanche.

A third site weathering-rind dated by Howard (2001) was the Red Lake terraces below the western limb of Red Hill (Fig. 6.3; Fig. 6.4). The site contained a set of five fluvial terrace surfaces unrelated to the local recessional glacial outwash surfaces of the Rakaia Acheron III (< 14 ka) advance that was clearly deformed by the Porters Pass Fault. This presented an opportunity to date a surface prior to the earthquake event (Campbell, et al. 2003). The impetus for the base level incision is thought to be the product of regional faulting lowering the base level (Howard, 2001; J.K. Campbell, pers comm. 2003). Weathering-rind ages from the extensive oldest terrace surface (T1) produced a modal peak thickness of 1.2mm, equating to a maximum age of 690 ± 50 years B.P using the McSaveney (1992) calibration curve and a 2 mm running average (see Fig. 6.4 Howard, 2001). This is older, but still similar to the weathering-rind and lichen modal peaks at the Acheron site only several kilometres to the east.

To collect stratigraphic information on Holocene movements along the Porters Pass Fault, Howard excavated four trenches across the fault between the Rakaia River and Porters Pass (see Fig. 6.5). Using this information in conjunction with previous studies, Howard was able to interpret four and potentially five large magnitude earthquakes events which ruptured the ground surface (Howard, 2001).

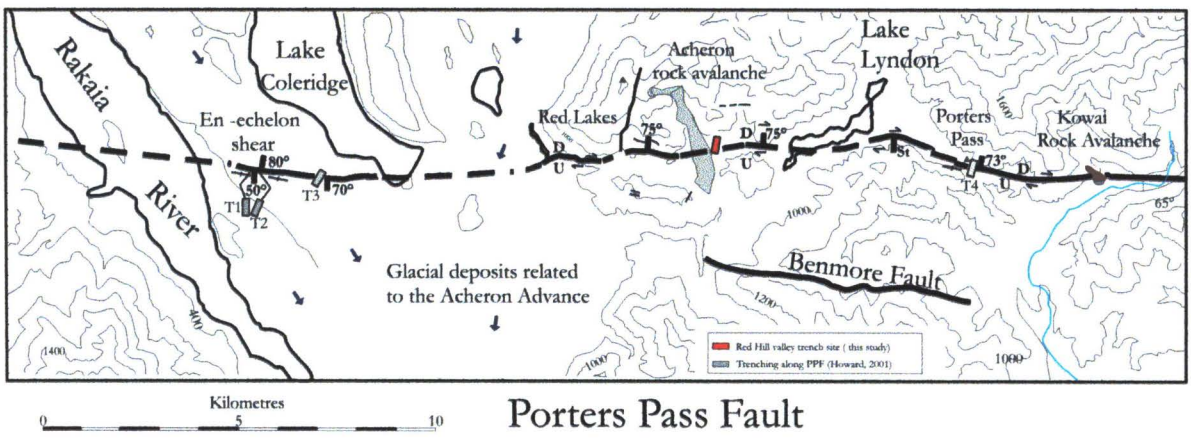

Figure 6.5: 1000m contour interval map illustrating the Porters Pass Fault between the Rakaia River and the Kowai rock avalanche. Trench sites T1, T2, T3 and T4 of Howard's (2001) study are shown by boxes of grey. The location of the Red Hill valley trench is shown by the red filled box (this study). Map adapted from Nicol et al. (2001) and Howard, (2001).

Trenches one-three were located in glacial gravels derived from the most recent glacial period of the Acheron III, between the Rakaia River and Lake Coleridge (see Fig. 6.5). A lack of recordable detail in trenches one and two hampered the identification of fault rupture events (Howard, 2001). Faulting evidence was recorded in trench three for a single surface-rupturing earthquake between c. 2000 years B.P. and 6000 years B.P. (Howard, 2001). Howard concluded that no evidence exists for fault rupture beyond trench three, suggesting that faulting does not rupture along the total length of the fault and typically ceases west beyond the Red Lakes (Howard, 2001).

Rupture ages identified in at Trench four Porters Pass using peat layers as dateable boundaries of fault displacement, gave the following ages:

- Earthquake 4. 8500 ± 200 yrs B.P.,
- *Possible event 6200 ± 500 yrs B.P*
- Earthquake 3. 5300 ± 700 yrs B.P.,
- Earthquake 2. 2500 ± 200 yrs B.P.
- Earthquake 1. 1000 ± 100 years B.P

The most comprehensive stratigraphic sequence was recorded during the excavation of trench four located across the Porters Pass fault, 200m east of Porters Pass SH 73 in swampy land resulting from fault scarp development (Howard, 2001). No faulting evidence was reported between 700-500 years B.P. (Fig.6.6.), with the youngest earthquake age of 1000 ± 100 years B.P. similar to the new dates for the Acheron rock avalanche. Howard identified a small scarp-derived colluvial wedge inferred to represent a rupture event, post-dating the earthquake two age of 2100 ± 600 B.P. (Howard, 2001). The colluvial wedge was considered to be disrupted by a shear, indicating a rupture event and bracketed by peat at an age of cal 1604 ± 82 years B.P. (Wk 9241) at the top of the earthquake two horizon below the colluvial wedge and 870 ± 76 years B.P (Wk 9236) above the colluvial wedge (See Fig. 6.6). This age was further constrained by a test pit dug into a scarp 3 km west of the trench site which identified a peat layer overlain by an inferred seismically-induced colluvium deposit which was overlain by the swamp material present today. The peat was radiocarbon dated to an age of cal 949 ± 22 years B.P. (Wk 9234) which was comparatively close to the cal 870 ± 76 years B.P. (Wk 9236) found in trench four (Howard, 2001).

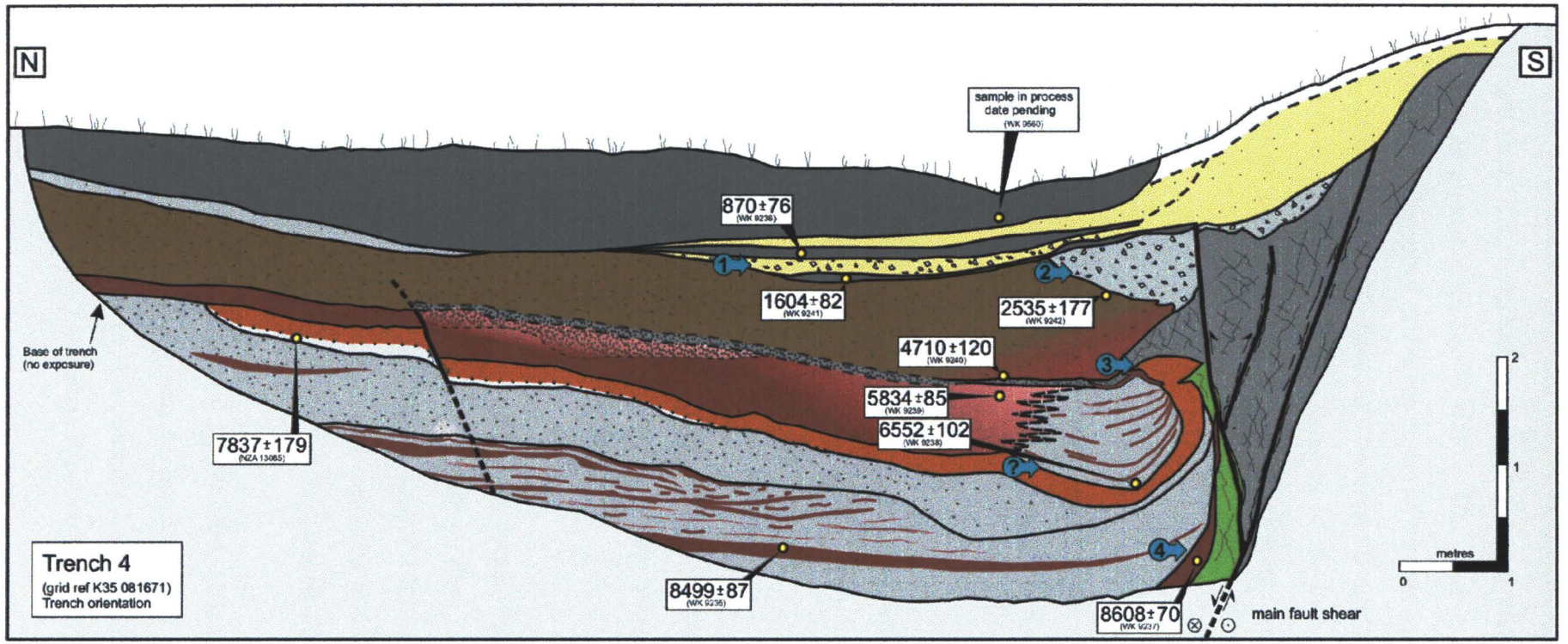

Figure 6.6: Log of the Porters Pass trench excavated across the Porters Pass Fault 75m east of Porters Pass. The yellow circles indicate radiocarbon samples with annotated calibrated ages (yrs BP) and laboratory reference number. Blue arrows show event horizons which are numbered from the most recent (top of log) to oldest (bottom of log), with a possible event marked by a question mark. Used with permission from Howard, (2001).

Howard (2001) therefore proposed that the youngest rupture event most likely ranged between 1700-800 years B.P, obtained using the minimum and maximum ages defined by the error bars, with an approximate age of 1000 ± 100 years B.P. The absence of colluvial material from the scarp, deposited above the colluvial wedges in the test pit site is inferred by Howard to rule out any later event. Howard's conclusions rightly disregarded the prehistoric landslide dates of 700-500 years B.P. on the basis of the lack of stratigraphic relationship, but his inferred age for earthquake one of 1000 ± 100 years is poorly constrained.

SUMMARY

- Howard (2001) calculated a mean age of 464 ± 79 years B.P. for the surface of the Acheron rock avalanche from averaging, lichenometry, radiocarbon (NZ 547), and weathering-rind ages.

- Dating of the Kowai rock avalanche using weathering-rind thicknesses identified a period of instability beginning at ca 1700 years B.P., with episodic periods of instability occurring until ca 500 years B.P.

- Weathering-rind thickness ages for the oldest terrace surface T1 at Red Lakes deformed by the PPF produced a modal peak thickness of 1.2mm, equating to a maximum age of 690 ± 50 years B.P.

- The youngest rupture event along the Porters Pass Fault identified by Howard (2001) within trench four excavated at Porters Pass most likely ranged between 1700-800 years B.P., with an approximate age of 1000 ± 100 years B.P. This resembles the youngest age from buried wood excavated at the base of the Acheron rock avalanche of (Wk 12094) 1152 ± 51 years B.P. obtained during this study.

- Although not stated clearly by Howard, (2001), it appears from his dates that the Porters Pass Fault segment to the southwest of Lake Lyndon (Red Lakes area) ruptured at or close to 700 years B.P. There is no evidence for the segment northeast of Lake Lyndon in the Porters Pass sub-section rupturing later than c.1000 years B.P.

6.4. THE ALPINE FAULT

6.4.1. BACKGROUND

The largest fault structure in the South Island is the Alpine Fault, extending 650 km in length between Blenheim and beyond Milford Sound (Yetton, 2002). Studies of the central fault section used tree stand ages, tree ring abnormality, dating of geomorphic surfaces (including landslides), and stratigraphic trench data to delineate prehistoric ruptures along the fault. Yetton (2002) was able to identify a series of earthquake events with moment magnitudes ranging as high as Mw 7.8-8.2, making the structure one of the principal candidates for triggering the Acheron rock avalanche. This is supported by independent paleoseismic studies along the fault line and lichenometry of rock fall deposits within the Southern Alps, which found overlapping ages for rupture events as shown in Fig. 6.7 (Bull, 1996, 1998; Berryman et al, 1998 Wright, 1994 in Yetton 2002; Wright, et al 1998; in Yetton 2002).

EARTHQUAKE CHRONOLOGY COMPARISON			
Yetton (1996) & (2000); Yetton et Al. (1998)	**Wright (1998) Waitaha River**	**Bull (revised in Yetton, 2002)**	**Berryman et al. (1998)**
233 yrs B.P.* Toaroha event	230 ± 10 yrs B.P.	232 ± 10 yrs B.P.	> 285, ? 233 yrs B.P.*
330 ± 10 yrs B.P.* Crane Creek event		334 ± 15 yrs B.P.	
	370 ± 10 yrs B.P.	372 ± 10 yrs B.P.	
525 ± 15 yrs B.P. Geologist Creek event	510 ± 10 yrs B.P.	522 ± 10 yrs B.P.	550 - 350 yrs B.P.
730 ± 50 yrs B.P. Muriel Creek event	740 ± 30 yrs B.P.	726 ± 10 yrs B.P.	845 - 730 yrs B.P.
1010 ± 50 yrs B.P. Round Top event	1050 ± 100 yrs B.P.*	989 ± 10 yrs B.P.	1070 ± 110 yrs B.P.

Figure 6.7: Comparison of available prehistoric earthquake chronologies for the Alpine Fault area south of the Ahaura River as in Yetton (2002)Ages in B.P. (Before Present 1950) * represents trench evidence

6.4.2. THE PROPOSED EARTHQUAKE EVENT ON THE ALPINE FAULT

6.4.2.1. ROUND TOP EARTHQUAKE EVENT

The Round Top event (1010 ± 50yrs B.P. in Yetton 2002) derives its name from a rock avalanche deposit in mylonitic rock immediately west of the Alpine Fault near Lake Kaniere

(Wright, 1998). Two dates from a Kahikatea tree buried at the base of the rock avalanche, were sampled 95 ± 5 tree rings apart (Wk 4877, 1100 ± 45 B.P. and Wk 4914, 1300 ± 40 B.P.), which enabled concise radiocarbon ages to be calculated of cal 1010 ± 50 years B.P. (Wright, 1998 in Yetton, 1998). Wright also collected a wood sample from the base of a sag pond 35 km southwest of the landslide near the Waitaha River, which was radiocarbon dated to 1160 ± 50 yrs B.P. (Wright 1998). This was inferred to have co-dated or post-dated the same event (Wright, 1998). Further evidence was presented by Yetton et al. (1998) from buried wood in a large debris flow on the bank of the Karangarua River, from which the sapwood was radiocarbon dated to 1210 ±50 years B.P. Bull and Brandon (1998) lichen mode size of 166.26mm suggests that an Alpine Fault event occurred approximately 990 ± 20 years B.P. along the Cook segment. Bull also estimated an age based on weathering rind thicknesses of 990 ± 50 B.P. for eight rock avalanches in the central Southern Alps from the correlation of deposits in Whitehouse and Griffith (1983 in Yetton 1998 see Fig 5.8). These ages appear consistent to the 1152 ± 52 year B.P. age proposed for the Acheron deposit.

6.4.2.2. THE PROPOSED MURIEL CREEK EVENT

The Muriel Creek event (730 ± 50 years B.P.) is less certain, with most of the evidence described by Yetton as based on tree ages which appears to be around 750 years BP (Yetton, 1998). Bull (in Yetton, 1998) lichenometry studies produced an age of 724 ± 10 years which is consistent with the tree stand age.

6.4.2.3. THE PROPOSED GEOLOGIST CREEK EVENT

The Geologists Creek earthquake event is also based on a forest age (525 ± 15) and a radiocarbon date from a log buried in a landslide deposit between 500-530years B.P (NZ 6471) (Yetton, 1998). No stratigraphic evidence has been obtained, and Yetton (1998) acknowledges that it is the most poorly defined of the three youngest earthquake events (1998). Nonetheless Yetton (1998) does suggest that based on forest ages the rupture length would have extended for a minimum of 250 km, with a probable moment magnitude of M > 7.8 ± 0.1. At this stage little is known of the event, therefore it is unrealistic to assign a trigger source until further investigation of the event as been undertaken. Bull's (Bull and Brandon 1998) lichen set produces an age of 522 ± 10 years B.P. and Wright also identified tilt abnormalities in tree rings from logged trees which approximate 500 years (in Yetton, 1998).

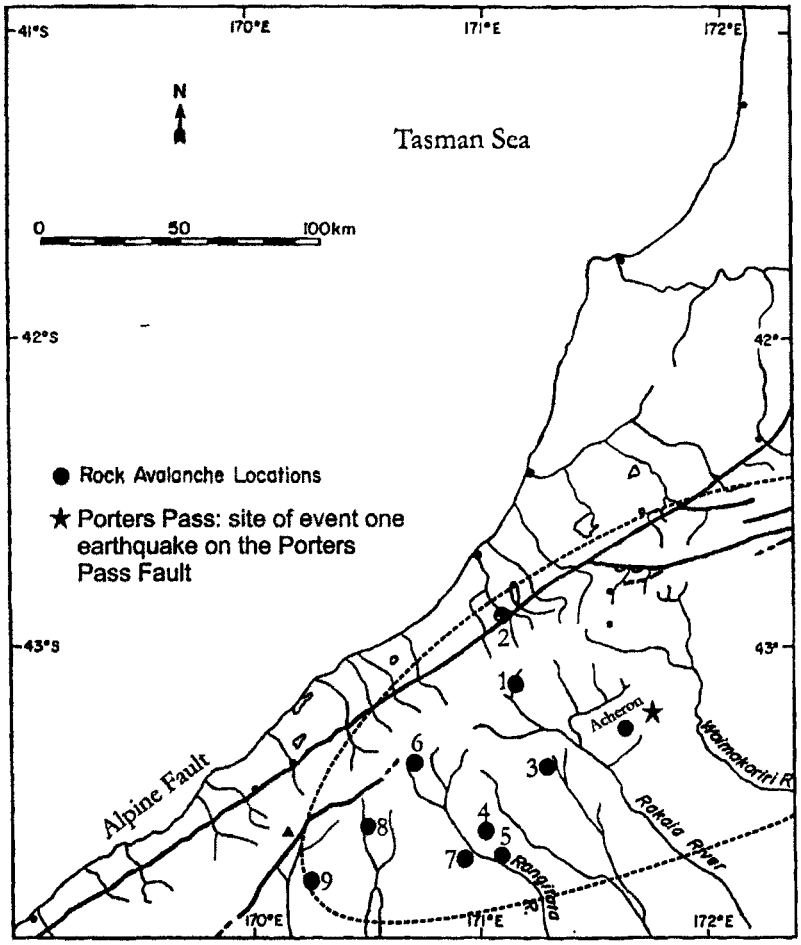

Locality	Recalculated age in years B.P. (In Yetton, 1998)	Alpine Fault:
• Acheron Rock Avalanche	1200-1100	Round Top event Porters Pass - event one
1. Mathias River (Boundary Ck)	950 ± 270	Round Top event
2. Roundtop Rock Avalanche	1020 ± 52	Round Top event
3. N. Ashburton River	990 ± 270	Round Top event
4. Rangitata River (Lake Camp)	1020 ± 270	Round Top event
5. Rangitata River (Pudding Stream)	1070 ± 270	Round Top event
6. Havelock River (Fan Stream)	990 ± 270	Round Top event
7. Rangitata River (Forest Creek)	990 ± 270	Round Top event
8. Godley River (Bloody Point)	1070 ± 270	Round Top event
9. Jollie River (Gammack Rg)	1070 ± 270	Round Top event

Figure 6.8: Locations of known rock avalanches including the revised age of the Acheron rock avalanche deposit (recalculated rock avalanche ages from Whitehouse & Griffith,1983 from Bull in Yetton, 1998) with ages coinciding with the inferred Round Top Alpine Fault earthquake event of around 1000 years B.P. Possible correlation is also suggested between the rock avalanche ages and an earthquake (event one) identified on the Porters Pass Fault (Howard, 2001).

The dashed line shows a landslide distribution ellipse with a maximum radius length of 100km (as defined by Keefer (1984) for a Mw > 7) correlating with the positions of the rock avalanche deposits. The star represents a hypothetical epicentre associated with a fault rupture at Porters Pass along the Porters Pass Fault and delineates the centre of the ellipse

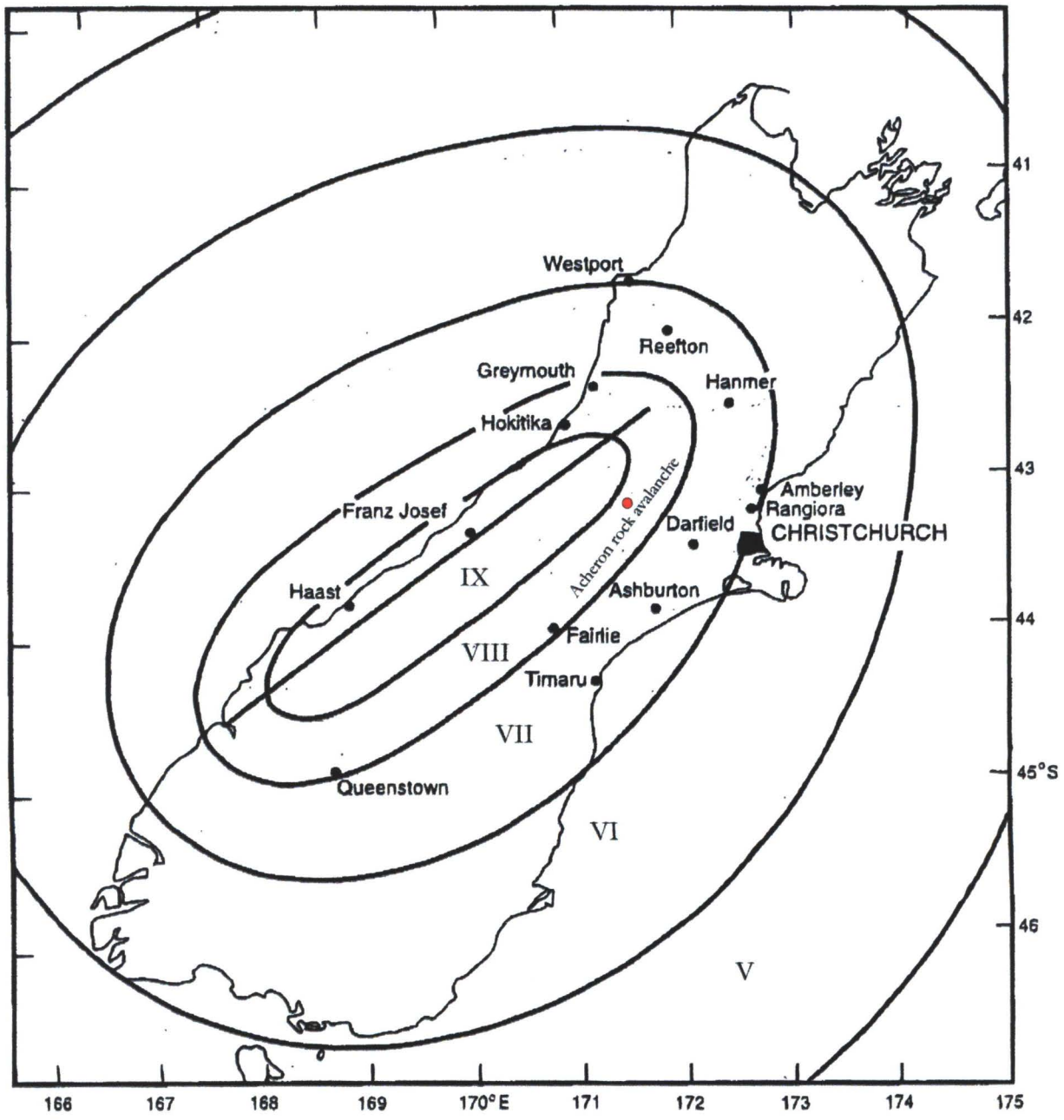

Figure 6.9: A comparison of the synthetic isoseismals for the well-constrained Toaroha River Alpine Fault event of 233 years BP (using the intensity formula and computational methods of Smith (1995a, 1995b) from Yetton (1998) p 103) with the position of the Acheron rock avalanche. The Acheron deposit is identifiable by the red circle in a MM VIII (Mw >7) zone which represents a shaking intensity clearly able to trigger the rock avalanche if a similar sized shaking event occurred between 1200-900 years BP.

SUMMARY OF ALPINE FAULT EVENTS

- The inferred Round Top event (1010 ± 50 years B.P. Yetton , 2002) is similar to event one (1000 ± 100 years B.P.) on the Porters Pass Fault as proposed by Howard (2001), and is close to the new radiocarbon age from buried wood of (Wk 12094) 1152 ± 51 years B.P. from this study. The wood sample from the base of a sag pond near the Waitaha River, radiocarbon dated to (Wk 5426) 1160 ± 50 years B.P. and the age for the sapwood from the buried tree at the base of Round Top rock avalanche (Wk 4877) 1100 ± 45 years B.P. from Wright, (1998) also show good comparison to the new ages for the Acheron rock avalanche.

- The combined weathering-rind ages for eight rock avalanches derived from Whitehouse and Griffith (1983) had a highest probability of an age of 987 ± 50 years B.P.(from Bull in Wright, 1998) which correlated to the Round Top event and to the youngest conventional radiocarbon age of the Acheron Rock avalanche (Wk 12094 1152 ± 51 years B.P.). However the large error of ± 270 years associated with the individual deposit ages reduces their reliability of being triggered by the same event.

- Two later successive events (the Muriel Creek and Geologist Creek events) appear to coincide with surface ages of the Kowai and Acheron rock avalanches and the Red Lakes terrace surfaces in the eastern Southern Alps (see Fig. 6.1), but are acknowledged as very poorly constrained.

- The Acheron rock avalanche is well within the 200-500 km zone defined by Keefer, (1984), for earthquake magnitude and distance from the epicentre for earthquake-generated landslides (see Fig. 6.9). Events along the Alpine Fault would be expected to act as both a fatigue mechanism and a trigger for failure at the Red Hill valley Acheron rock avalanche site.

6.5. DISCUSSION

6.5.1. IMPLICATIONS OF NEW AGES FOR THE ACHERON ROCK AVALANCHE

The new radiocarbon ages (from this study see below) identify a substantial difference in age from the radiocarbon sample NZ 547 (500 ± 69 years B.P., Burrows, 1975)

CONVENTIONAL RADIOCARBON AGES (from this study)
*Sample interpreted to best represent the emplacement age of the Acheron rock avalanche

SITE ONE Distal deposit

- Wk 12093 1319 ± 51 years B.P.

SITE FOUR Northeastern end of river cut exposure at site 3

- Wk 12094* 1152 ± 51 years B.P.
- Wk12095 1232 ± 52 years B.P.
- Wk12096 1327 ± 52 years B.P.

Burrows (1975) states that the (NZ547) wood sample was derived from the 40m long river cut exposure (Fig. 2 in Burrows 1975) referred to as site three and four in this study. This is the same site sampled for Wk 12074, Wk 12075, and Wk 12076 which produced ages with a range of 1380 to 1100 years B.P. Sampling during this study was conducted at two sites, and the overlap of ages between the wood samples strongly suggests that the NZ547 sample dated something other than that of the rock avalanche emplacement. This may have resulted from a disturbance of the site sampled or that the sample originated from some unknown source. This emphasises the need to recheck age evidence in geological studies, especially considering both Bull and Brandon (1998) and McSaveney (1992) used the NZ547 date (500 ± 69 years B.P.) as part of their extensive calibration data sets and the date is often referenced in literature, relating to weathering-rind dates in the Southern Alps and rock avalanches (Whitehouse, 1983; Whitehouse and Griffith, 1983; McSaveney, 1992; Cowan et al, 1996, Bull and Brandon, 1998; Orwin, 1998; Howard, 2001).

As previously discussed the most contemporaneous wood sample (Wk 12094 1152 ± 51 years) from the base of the deposit also differs considerably from dating techniques such as

lichenometry and rock weathering rind thickness which sampled the rock avalanche surface (Fig 6.1 see also Whitehouse and Griffith, 1983; Bull and Brandon, 1998; Bull and Brandon, 1996 in Howard, 2001). This could indicate problems in the collection and / or measurement process of either dating technique or more probably highlight the occurrence of an unconnected post-deposition earthquake event or other surface disturbance not affecting the base of the deposit. If the weathering-rind and lichen dating techniques can be shown to be erroneous then this could have implications for previously dated surfaces such as the 29 weathering rind thickness ages from Whitehouse and Griffith's (1983) rock avalanche compilation. However, the consistency of age produced by the different dating techniques suggests an event such as fire seismic shaking, or aggradation resulted in a reset of both the rinds and the lichen populations. This would have to cause movement or partially disturbance of surface gravels and boulders, causing a fresh rock surface to be exposed to surface. Interestingly, the large clasts present on the rock avalanche surface range in size from 40cm up to 5m in length with the larger elements displaying a long axis which presents a problem for ubiquitous disturbance of the surface boulders.

Effects such as fires appear to have been present over the Cass-Porters Pass area around 750-400 years B.P. and could have destroyed much of the pre 500 year B.P. lichen evidence on the lower altitude sections of the Acheron deposit. McSaveney noted charcoal (NZ5407C 660 ± 65) immediately below the base of the Craigieburn rock avalanche several km north of the Red Hill valley, which he interpreted to represent destruction of a beech forest by fire at around this time (McSaveney, 1992). This corresponds to charcoal (Wk 13112 653 ± 54years B.P) located in a buried soil during trenching of the fault line in the Red Hill valley (see Chapter Five). Bull and Brandon (1998) acknowledges the impact of fire on the populations of lichen, referred to as fire kill, which suggests that the presence of fire in the Cass-Porters Pass area may have had an effect.

The weathering-rind measurements from the Red Lakes terraces of 690 ± 50 years lies between the average age for the surface of the Acheron deposit from Howard (2001), Bull and Brandon (1998) of 464 ± 79 years BP and the new ages for the rock avalanche of 1152 ± 51 years B.P. (see Fig. 6.1). Base level incision forming the terraces at Red Lakes may have been initially caused by a seismic episode from faults in the Craigieburn–Porters Pass area (J.K. Campbell, pers comm. 2003). With corresponding ages between the rock avalanche and

the event one at Porters Pass overlapping around 1000 ± 100 year B.P, it implies that the source of disturbance resulted from the earthquake one event on the Porters Pass Fault.

The possibility of several deposition events associated with the Acheron rock avalanche has been considered; a fact first suggested by Bull based on the presence of tiny lichen populations extending up to 172mm in diameter (approx age 1030 years B.P.) on the forested true left side of the deposit mid zone (Map 1). That could reasonably explain the age differences between the base of the deposit and the surface ages. This author feels while the presence of multiple events can not be dismissed unequivocally it seems unlikely based on the rock avalanche morphology such as elevated trim lines, run up heights and the remnant mounds of rock material in the upper runout zone. The smaller second event would have had to comprise of a volume enabling it to travel more than 1.8 km along a path impeded by the debris of the first rock avalanche event before appearing to terminate metres from the site four radiocarbon sample site. The deposit does demonstrate evidence for pulses of activity and lobate behaviour which is a typical rock avalanche phenomenon rather than separate events also the distinct depression broadly appearing to divide the deposit in two (mid zone) is almost certainly caused by the burial of a terrace during deposition rather than two distinct rock avalanche episodes. Evidence from the site three river cut exposure shows a homogeneous mass with no lithological or structural differences to support secondary deposition. Based on these observations it is unlikely that two distinct landslides occurred with the valley. However unexplained differences exist between the ages at the buried contact and the rock avalanche surface.

The paleoseismic investigation of the Porters Pass Fault in the Red Hill valley identified a vertical offset of 40cm most likely from an earthquake event post-dating the new age of 1152 ± 51 years B.P. for the rock avalanche deposition. The lower of two buried soils interpreted to represent brackets of the event was dated at (Wk 13112) 653 ± 54 years B.P. It is proposed that a faulting event took place along the Porters Pass Fault west of Porters Pass post-dating the age and deposition of the Acheron Rock avalanche. This is considered to have taken place after 700 years B.P., causing the lineaments on the surface of the rock avalanche and possibly resetting the weathering rinds and lichen samples. A rupture on the Alpine Fault described as the Geologist Creek event (525 ± 15 years B.P.) also is thought to have occurred at this time which could offer another source of seismic shaking. This could also cause resetting of the

surface ages of the Acheron rock avalanche and trigger the instability along the PP-AFZ however the author is unaware of stratigraphic evidence supporting a rupture at this time.

6.5.2. SOURCES OF COSEISMIC TRIGGERING

The new dates presented in this study show a correlation between the youngest age of the Acheron rock avalanche deposit (Wk 12094 1152 ± 52 yrs B.P.) and the earthquake one event (1000 ± 100 yrs B.P.) recorded in trench four at Porters Pass by Howard (2001, refer Fig. 6.1). This reaffirms the possible coseismic relationship with the Porters Pass Fault, but it has to be acknowledged that it presents no convincing evidence for such a tightly constrained range.

The new Acheron rock avalanche age also corresponds to the moderate peak of circa 1050-1400 years B.P. identified in the frequency histogram for recalibrated rock avalanche weathering rind ages in the central Southern Alps (see Fig. 6.2, Whitehouse and Griffith, 1983; in Cowan et al. 1996). The peak includes the same eight rock avalanches identified by Bull in Yetton, 1998) displayed as evidence for the Round Top event on the Alpine Fault (see Fig 6.8). This is further supported by the addition of the Round Top rock avalanche with its radiocarbon age estimate of (Wk4877) 1100 ± 45 years for the sapwood from a buried tree and wood from a sag pond near the Waitaha River along the Alpine Fault radiocarbon dated to (Wk 5426) 1160 ± 50 years B.P. (Wright, 1998; Yetton, 1998). Cowan et al. (1996) interpreted the lack of a modal rock avalanche age peak at 700-500 year B.P. to represent more localised faulting in the Porters Pass area, so equally the presence of an age peak at 1200-900 years B.P. could be interpreted to represent large magnitude Mw 7-8 earthquakes over the central Southern Alps.

The rock avalanche localities are spread from the Jollie and Godley Rivers to the Havelock River in the Rangitata watershed, consecutively 100km and 60 km west of Porters Pass extending northwest to the Mathias River and Lake Kaniare on the West Coast less than 70km from the Porter Pass. Howard (2001) calculated moment magnitudes (Mw) from fault displacement and rupture area of 7.1 to 7.4 for the Porters Pass Fault and 7.5-7.7 for the entire PP-AFZ. The zone expected for landsliding for a magnitude 7.4 event, proposed for rupture along the 40km length of the Porters Pass Fault, would extend to a maximum of 100 km. This would place all ten deposits well within the minimum shaking zone of Mw 6 or MM VII (see Fig. 6.8) (Dowrick, 1994; Keefer, 1984; Howard, 2001).

Howard, (2001) highlighted the potential for other seismic sources to trigger rock avalanches. Within 100km of the Red Hill valley many poorly known fault structures exist, such as the Harper, Torlesse and Craigieburn Faults which could provide the energy necessary to trigger rock avalanches (> Mw 6). A fairly intensive study of the Alpine Fault has identified strong lines of evidence based mainly on paleolandslides as earthquake indicators for a rupture of a central section of the Alpine Fault at this time. A wood sample retrieved from the base of a sag pond 35 km southwest of the Round Top landslide interpreted as coseismic or post-seismic, was radiocarbon dated to 1160 ± 50 yrs B.P. This is the only stratigraphic evidence to support an Alpine Fault event at this time (Wright, 1998). The spread of rock avalanches identified in the previous paragraph is also proximal (< 20km) to the Alpine Fault and equally suggests a trigger derived from that source (see Fig. 6.8).

It could also be considered that any motion able to dislodge the rock mass forming the Acheron rock avalanche could also initiate widespread instability along the eastern foothills including forming a colluvium wedge at the Porters Pass trench site and concentration of landslides along the PP-AFZ. Only one landslide (Glentui 2 based on weathering rind thicknesses in Cowan et al. 1996) exists along the PP-AFZ dated at around 1000 ± 100 years B.P. which suggests minimal activity occurred along the extent of the fault zone. Cowan et al. (1996) however, noted that only half of the population of landslides along the fault had been dated. This would therefore exclude a large component of the paleolandslide record for the PP-AFZ. The lack of landslides along the PP-AFZ coinciding with the 1000 years ± 100 years is difficult to explain. Conversely, an event at 1000 ± 100 years B.P. may have indirectly acted as a fatiguing mechanism to the shear strength of the rock mass along the PP-AFZ resulting in the concentrated populations of landslide present around to the 700-500 years B.P. age during another earthquake.

The origin of the seismic source cannot be stated unequivocally, it is however, sometime at around 900-1200 years B.P. The central Southern Alps has been exposed to a period of concentrated instability causing the formation of ten catastrophic rock avalanche events spread over its length and width. At present the only ruptures shown to exist at this time capable of forming a > M 7 earthquake is the poorly constrained event one on the Porters Pass Fault and the sag-pond radiocarbon age along the Alpine Fault.

The close relationship between the ages for the Porters Pass Fault event one and inferred Round Top earthquake on the Alpine fault may reveal a structural relationship between the two faults. This could manifest as rupture events which reply to each other over time periods of less than several hundred years as defined by the spread of landslide ages (J.K. Campbell pers comm. 2003) and would have hazard implications if several high magnitude earthquakes occur over short time periods (J.K. Campbell pers comm. 2003). This highlights the question of dating sensitivity as discussed by Cowan, (et al. 1996) for multiple seismic events over short time periods.

Critical factors that need to be considered for coseismicity of rock avalanches:

- Clusters of landslides at the time of an event.
- Triggering of landslides can occur from multiple seismic sources over short time periods therefore do not need to be derived from a single earthquake event.
- Must be able to demonstrate a reliable (stratigraphic) rupture history that can be directly related to the formation of the rock avalanche deposit.
- Landslide and earthquake relationship is not valid unless reliable dating can be shown to coincide with a dated earthquake event therefore need to show the evidence.
- Segmentation along faults must be considered; where rupture evidence along one segment may not show up on another segment of the same fault.
- The reliability of the source of the dates needs to be demonstrated.
- Weathering-rinds thickness and lichen ages are a first approximation but can be affected by aggradation, fire and shaking or other surface disturbances causing resetting.
- Clear understanding of the geomorphological interpretations must be shown so that the surface is dated at relevant ages.

6.6 SUMMARY

The new age of (Wk 12094) 1152 ± 51years B.P interpreted to closely pre-date the deposition of the Acheron rock avalanche shows the previous NZ547 radiocarbon age of 500 ± 69 years B.P. (Burrows, 1975) to be dating something other than the Acheron rock avalanche emplacement. This may have resulted from a disturbance of the sample site, causing the sample to be derived from some other unknown source. This emphasises the need to recheck age evidence in geological studies.

The weathering-rind thickness and lichen ages produced for the surface of the rock avalanche (Bull and Brandon, 1998; Howard, 2001) are considerably younger than the new age for the Acheron rock avalanche. This could indicate problems in the collection and / or measurement process of either dating technique, but more likely highlights the occurrence of a surface disturbance such as aggradation, earthquakes or fire resetting the rock avalanche surface and affecting the longevity ability of lichens.

The new ages appear similar to the most recent earthquake event one (1000 ± 100 years B.P.) identified by Howard (2001) in the excavation of trench four at Porters Pass. This implies that that a coseismic relation could exist between the Acheron rock avalanche and the Porters Pass Fault. The narrow 1000 ± 100 year age does not represent the actual larger 1700-800 period between the bracketing peat horizons therefore is not that well constrained.

Nine rock avalanche deposits (recalibrated weathering-rind thickness ages from McSaveney, 1992; from Bull in Yetton, 1998) resemble the age of the Acheron rock avalanche and the event one on the Porters Pass Fault. These extend to a distance of 100km from the Porters Pass. This is considered to represent an episode of seismic shaking around 1000 ± 200 years B.P. resulting in widespread failures of large rock masses forming rock avalanches. Errors of ± 270 years were associated with eight of the rock avalanches which could represent multiple earthquake ruptures within the time span of several hundred years resulting in the landslides.

Another potential and more likely earthquake source is the Alpine Fault. Yetton (1998) proposed an event at this time called the Round Top event (1010 ± 50 years B.P.) based on geomorphic and stratigraphic evidence which appears more tightly constrained than that presented for event one on the Porters Pass Fault. However stratigraphic evidence of rupture

that is present along both faults indicates that either the Alpine Fault or the Porters Pass Fault are probable sources of the instability. A seismic event of a Moment Magnitude of Mw >7.0 along the Porters Pass Fault (estimated from Howard's 2001 study of Holocene rupture events along the fault) would be required to generate the spread (100km) of instability.

It is proposed in this study that faulting occurred along the Porters Pass Fault west of Porters Pass (probably extending to the Red lakes terraces) post dating the 1200-1100 years B.P. age of the Acheron Rock avalanche. It is probable this took place around 650 ± 70 years B.P. (700-500 years BP) causing the lineaments on the surface of the rock avalanche and potentially attributing to the reset of the weathering-rinds and lichen samples within the Red Hill valley.

A rupture on the Alpine Fault described as the Geologist Creek event is thought to have occurred 525 ± 15 years B.P. which could offer another source of seismic shaking. This could be another potential cause in the resetting of the surface ages of the Acheron rock avalanche and source for triggering the instability along the PP-AFZ. However, there is no apparent stratigraphic evidence supporting a rupture at this time

Certain critical factors must be considered when applying coseismicity to rock avalanches. These include; the identification of clusters of deposits at the time, reliable rupture history that can be shown to exist, known origin of dates and clear understanding of the geomorphological interpretations in order for the feature to be dated at relevant ages. It is essential therefore to obtain independent lines of evidence that may appear different but converge on a common age.

CHAPTER SEVEN

SUMMARY AND CONCLUSIONS

7.1 INTRODUCTION

The Acheron rock avalanche is one of 42 greywacke derived rock avalanches in the central Southern Alps identified in Whitehouse and Griffith's, (1983) rock avalanche compilation. Located in the Red Hill valley, 1 km west of Lake Lyndon near Porters pass, the deposit overlies the inferred position of the Porters Pass Fault; a prominent segment of the Porters Pass-Amberley Fault Zone. The Porters Pass Fault extends ca 40 km between the Rakaia River and Waimakariri River as a series of discontinuous scarps and has been shown by Howard (2001) to be active during the Holocene. The exact position of the fault is not known in the Red Hill valley but dating of the deposit by Burrows (1975), Whitehouse (1983) inferred that a co-seismic relation may exist with the buried Porters Pass Fault between 700-500 years B.P (Cowan et al. 1996). Recent paleoseismic investigations of the fault at Porters Pass and Lake Coleridge found the youngest rupture event to be between 1700-800 years B.P. which Howard (2001) suggests represents 1000 ± 100 years B.P and concluded that no coseismic relationship to the Acheron rock avalanche was found.

Basement rock in the Red Hill valley is Torlesse Supergroup greywacke ubiquitously covered by a thin layer of colluvium and solifluction materials with a small outlier of Tertiary marine sediments in the west and extensive terrace sets in the lower section of the valley. The largest basement outcrop is found in the source scar of the Acheron rock avalanche which displays steep north dipping massive sandstone and thinly bedded mudstone and sandstone sequences with a single massive mudstone unit. A defect analysis suggests that failure occurred along the weaker argillite and sandstone bedding contacts in combination with persistent steep south dipping and shallow north angled defects.

7.2. TRIGGERING MECHANISM

Large bedrock collapses which form rock avalanches are considered to be derived from the effects of constant gravity loading and fatiguing caused by regular seismic activity. The continual exposure to loading would likely result in the initiating and development of defects and fractures, which over time result in progressive destabilisation of the rock mass. Observations by McSaveney (2002) suggest that the balance between tectonic uplift and valley bed level drop force the condition that large bedrock failures are the only effective method for shedding of large amounts of rock material to keep up. Seismic motion is thought to accelerate the destabilisation process by causing dilation and weakening of cohesive bonds, a process known as fatiguing (Erismann and Abele, 2001). Fatiguing could be expected in areas where smaller seismic events are common such as in the Southern Alps. Larger episodes of seismicity may create a single stroke failure mechanism, which rapidly overcomes the shear strength within defects, causing sudden instability and collapse.

7.3. MORPHOLOGICAL PROPERTIES OF THE ACHERON ROCK AVALANCHE DEPOSIT

The Acheron rock avalanche displays properties typical of rock avalanche; long run out, elevated trim lines and highly fragmented internal material. Investigation during this study examined the interaction of the debris run out with the valley topography which included run-up heights and stalling of debris.

The source scar area of 1.12×10^5 m^3 was estimated from a GPS surveys and is considered to represent a volume of approximately 7.5×10^6 m^3 based on a dilation correction of 20 % applied to the deposition volume estimate described below. The failure appears to have occurred along the well developed north and south dipping defects and steep north dipping bedding contacts. A possible failure sequence is considered to resemble that of the Key Block theory where loss of a key supporting rock unit causes instability and collapse over a larger area than the site of the initial instability.

Run out of the rock avalanche extended almost 3.5 km covering an area of 7.2×10^5 m^3 consisting of a volume of 8.9×10^6 m^3 . Estimated velocity of 140 km / hr was calculated

from debris elevated run up heights based on the simple factor $(2gH)^{0.5}$ (where g is gravitational acceleration and H is the height of the run up of the debris). The rock avalanche is considered to displayed moderate to high mobility and interacted with the valley morphology forming two run ups of the valley walls, and a caroming or trim line feature. The debris show evidence for lobe partitioning probably associated with interaction with the valley geomorphology. The upper 1500m of the run out is considered to have confined the debris causing higher mobility and higher velocities while spreading, thickening and distal thinning was initiated at a valley junction containing the Porters Pass Fault.

The DAN long run out simulation successfully reproduced the 3.5 km run out of the Acheron rock avalanche using a Friction model rheology with a friction angle of 27° and earth pressure coefficients of ko 5.5, ka 5.2, kp 9.9 used to represent fragmentation-induced dispersive pressure. This produced velocities of 160 km / hr which are similar to the 140 km / hr calculated from the simple field investigations of run up heights. This supports Davies and McSaveney (2002) results for the large historical Falling Mountain rock avalanche and the theory for Dynamic Fragmentation.

Radiocarbon dating of four wood samples buried at the base of the Acheron deposit identified new ages for the deposition of the rock avalanche ranging between 1380-1100 years B.P. These are older than the radiocarbon age presented in Burrows (1975) of 500 ± 69 years B.P. and the weathering-rind thickness ages and modal lichen size population of 490 ± 55 years and 460 ± 10 years B.P. consecutively, assigned as the deposits age.

7.4. PALEOSEISMIC INVESTIGATION OF PORTERS PASS FAULT IN THE RED HILL VALLEY

Radiocarbon ages for the Acheron rock avalanche emplacement appear dissimilarity to previous inferred emplacement ages. The new preferred age of 1152 ± 51 years B.P. suggests a possible source of seismic activity occurred between 1200-900 years B.P. The age for the youngest event along the Porters Pass Fault identified by Howard, of 1000 ± 100 years B.P. is similar to the new age of the rock avalanche of 1152 ± 51 years B.P. A fault scarp and minor lineaments identified during detailed geomorphic mapping of the site suggested that the scarp predated while the lineaments may post-date the rock avalanche emplacement.

To show a definitive coseismic relationship to the Porters Pass Fault a paleoseismic investigation of the fault within the Red Hill valley inferred to strike below the deposit was undertaken.

The Main objectives were to

- clarify the position of the Porters Pass Fault within the Red Hill Valley

- identify datable evidence of rupture to delineate a coseismic relationship to the Acheron rock avalanche, suggested by the similar age for the youngest rupture event of 1000 ± 100 years B.P. from trench excavation at Porters Pass.

A 60m long scarp partially buried by the rock avalanche was surveyed using Ground Penetrating Radar to determine the position of the fault. This showed good evidence for faulting through the scarp confirming mapping observations and identified distinctive packages of sedimentation, confirmed from auguring of the scarp, which may record the faulting history.

Trenching confirmed the position of fault beneath the rock avalanche deposit and exposed a sag pond interpreted to be a sequence of ponded sediments inter-lain by two buried soils. The vertically offset lower soil horizons (2A) was radiocarbon dated to 650 ± 50 years B.P. suggesting a rupture of the fault occurred post-dating 700 years B.P. The evidence within the trench showed no co-seismic relationship to exist between the Red Hill valley section of the Porters Pass Fault and the Acheron rock avalanche age of emplacement age of 1152 ± 51 years B.P. The buried soil age reconfirms that the Acheron rock avalanche deposit is considerably older than interpretations assumed from previous dating (NZ547 500 ± 69 years B.P.). The trench data does confirm the observations of Cowan et al. (1996) and (J.K. Campbell. pers comm. 2003) that a small rupture event occurred on the segment south west of Lake Lyndon-Porters Pass resulting in a vertical displacement of Unit 1 (angular gravels) and Unit 2A (lower buried soil) of 40cm post-dating 700 years B.P. This event probably resulted in the disturbance of the surface of the rock avalanche resetting the weathering-rinds of Howard (2001) and the modal lichen age of Bull and Brandon (1996 in Howard, 1998). The lack of evidence post-dating 1000 ± 100 years B.P. within the previous trench excavation at Porters Pass supports Howard's hypothesis of segmentation of the Porters Pass Fault resulting

in rupture occurring on one fault segment but not visible on another. This study excavated only one trench within the site and it is considered that further evidence of faulting may exist within the valley but was beyond the scale of the project

7.5. THE COSEISMICITY OF THE ACHERON ROCK AVALANCHE

The Acheron rock avalanche has been shown to substantially predate previous ages assigned for the emplacement age therefore this study can not establish a clear coseismic link to the Porters Pass Fault in the Red Hill valley.

The earlier age of 1000 ± 100 years from the trench excavated by Howard (2001) at Porters Pass appears to resemble the age of the rock avalanche however the narrow age span of the error bars of ± 100 years implies a more tightly constrained age than was actually reflected in the trench. The time between the upper and the younger bracketing peat horizons ranges between 1700-800 years B.P reflecting a time gap of 900 years. While it is probable that the rupture event is reflected by the younger ages it can not be shown to clearly delineate a time of faulting of 1000 ± 100 years B.P. Subsequently it is unwise to state that a clear coseismic link exists between the Porters Pass Fault northeast of the Red Hill valley and the emplacement age of the Acheron rock avalanche.

Another potential earthquake source is the Alpine Fault. Yetton (2001) proposed a seismic event comparable to this time called the Round Top event of 1010 ± 50 years B.P. based on geomorphic evidence and wood from excavated from the bottom of a sag pond. The age of the wood (Wk 5426) 1160 ± 50 years B.P. was interpreted to co-date or post-date rupture along the Alpine Fault. Sapwood dated from a buried tree from the Round Top rock avalanche deposit adjacent to the Alpine Fault and 35 km northeast of the sag pond produced an age of (Wk 4877) 1100 ± 45 years B.P. These ages appear to show similarity to the Acheron Rock avalanche age of 1152 ± 51 years B.P. forming a cluster of age evidence for an earthquake event or events between 1200-900 years B.P.

Eight rock avalanche deposits excluding the Round Top rock avalanche (recalibrated weathering rind thicknesses from McSaveney, 1992; Bull in Yetton, 1998) resemble the age of the Acheron rock avalanche and the event one on the Porters Pass Fault extending to a

maximum distance of 100km from Porters Pass. This is considered to represent an episode of seismic shaking around 1200-900 years B.P resulting in widespread failures of large rock masses forming rock avalanches. However the ± 270 years associated with the error bars is too poorly constrained to identify any specific events directly relating to there formation.

Clustering of ages suggest that the Southern Alps experienced Mw > 7 earthquakes between 1200-900 years B.P. This probably reflects multiple earthquake events rather than a single event implied by correlations of rock avalanche and geomorphic ages in Fig. 6.1. The presence of a rock avalanche deposit does not signify an earthquake as the historical rock avalanche chronologies show. It is therefore critical to know the origin of dates used in literature and the useful range of their application.

7.6. FURTHER WORK

- Additional investigation of both the Alpine Fault and the Porters Pass Fault (including within Red Hill valley) is required to further constrain rupture ages and delineate seismic activity between 1200-900 years B.P.

- A detailed investigation of the eight rock avalanches described in Yetton (1998) similar to this study should be undertaken to determine what relationships these deposits have to the 1200-900 years B.P age to rupture activity. This includes a close examination of the morphology and emplacement history so reliable geomorphic interpretations can be made.

- A study of the application of lichen and weathering-rind ages needs to be undertaken to check its reliability as a site specific age dating tool in complex geomorphic conditions. Investigations need to be done into the practicalities of the resetting of weathering rinds during surface disturbance such as earthquakes and the effect of fire on populations of lichen.

- Lichen longevity should be investigated to identify if tiny populations of large lichens (160-175mm) represent the actual remnant of the original populations.

REFERENCES

Atkinson B. K., (1984), Subcritical crack growth in geological materials. Journal of Geophysical Research. 89: 4077-4114.

Bagnold R. A., (1954), Experiments on a gravity free dispersion of large solid particles in a Newtonian fluid under shear. Proc Royal Soc London A, 225: 49-63.

Berryman, K., Cooper, A., Norris, R. J., Sutherland, R., Villamor, P. (1998), Paleoseismic investigation of the Alpine Fault at Haast and Okuru: Geological Society of NZ and NZ Geophysical Society, Joint Annual Conference, Christchurch, New Zealand.

Bradshaw, J. D., (1971), Stratigraphy and structure of the Torlesse Supergroup (Triassic-Jurassic) in the foot-hills of the Southern Alps near Hawarden, Canterbury: New Zealand Journal of Geology and Geophysics. v. 15, p. 71-87.

Bradshaw, (1989), Cretaceous geotectonic patterns in the New Zealand Region: Tectonics, v. 8, p. 803-820.

Brundsen, D., Prior, D., (1984), Slope Instability, in Kirkby, M.J., ed., Landscape System, Volume 1: London, John Wiley & Sons, p. 620.

Bowman, S., (1990), Radiocarbon Dating: Interpreting The Past: Los Angeles, University of California Press, 64 p.

Bull, W. B. (1996) Prehistoric earthquakes on the Alpine Fault, New Zealand. Journal of Geophysical Research, 101 B3, 6037-6050

Bull, W. B. and Brandon, M. T. (1998) Lichen dating of earthquake-generated regional rock-fall events, Southern Alps, New Zealand. GSA Bulletin, 110 (1), 60-84

Burrows, C. J., (1975), A 500 - Year - Old Landslide in the Acheron River Valley, Canterbury: New Zealand Journal of Geology and Geophysics. v. 18, p. 357 - 360.

Burrows, C. J., Soons, J.S. (1978), Dates for Otiran deposits, including plant microfossils and macrofossils, from the Rakaia Valley: New Zealand Journal of Geology and Geophysics., v. 21, p. 607-15.

Campbell, J. K., Nicol, A., Howard, M. E., (2003), Long term changes to river regimes prior to late Holocene coseismic faulting, Canterbury, New Zealand: Journal of Geodynamics. v 36, 147-168.

Coates, G., (2002), The rise and fall of the Southern Alps: Christchurch, Canterbury University Press, 80 p.

Colye, S. A., (1988), *The Porters Pass Fault.* Unpublished M.Sc thesis: University of Canterbury, Christchurch, New Zealand.

Corominas, J., (1996), The angle of reach as a mobility index for small and large landslides: Canadian Geotechnical Journal, v. 33, p. 260-271.

Cowan, H., Nicol, A., & Tonkin, P., (1996), A comparison of historical and paleoseismicity in a newly formed fault zone and a mature fault zone, North Canterbury, New Zealand: Journal of Geophysical Research, v. 101, p. 6021-6036.

Crozier, M. J., (1986), Landslides: causes, consequences and environment. London: Croom Helm. p 252

Cruden, D. M., Van Gassen, W., (1989), Momentum transfer and friction in the debris of rock avalanches: Canadian Geotechnical Journal, v. 26, p. 623-628.

Davies, T. R., McSaveney, M. J., (2002a), Dynamic simulations of the motion of fragmenting rock avalanches: Canadian Geotechnical Journal, v. 39, p. 789 - 798.

Davies, T.R.H., McSaveney, M.J., (2002b), Rapid rock-mass flow with dynamic fragmentation, Proceedings of the NATO Advanced Research Workshop: Celano, Italy, p. 17.

Davies, T.R.H., (1982), Spreading of rock avalanche debris by mechanical fluidisation: Rock Mechanics, v. 15, p. 9 - 24.

Davies, T.R.H., McSaveney, M. J., (1999a), Runout of dry granular avalanches: Canadian Geotechnical Journal, v. 36, p. 313 - 320.

Davies, T.R.H., McSaveney, M. J., and Hodgson, K. A., (1999b), A fragmentation - spreading model for long runout rock avalanches: Canadian Geotechnical Journal, v. 36, p. 1096 - 1110.

DeMets, C., Gordon, R.G., Argus, D.F., Stein, S., (1994), Effect of recent revisions to the geomagnetic time scale on estimates of current plate motions: Geophysical Research Letters, 21. 2191 - 2194.

Dowrick, D. J., (1994), Damage and intensities in the Magnitude 7.8 1929 Murchison, New Zealand earthquake. Bulletin of the New Zealand National Society for Earthquake Engineering v27, 190-204.

Eiby, G., (1990), The Lake Coleridge earthquake of 1946: Bulletin of New Zealand National Society for Earthquake Engineering, v. 23, p. 150-158.

Eisbacher, G.H., (1978), Cliff collapse and rock avalanches (sturzstroms) in the Mackenzie Mountains, northwestern Canada: Canadian Geotechnical Journal, v. 16, p. 309-334.

Eisbacher, G.H., and Clague, J. J., (1984), Destructive mass movement in high mountains: Hazard and Management: Ottawa, Geological Survey of Canada, p. 16.

Erismann, T. H., (1979), Mechanics of large landslides. Rock Mechanics, V 12, 15-46.

Erismann, T. H., and Abele, G., (2001), Dynamics of rockslides and rockfalls: Berlin; New York: Springer. 316 p.

Eusdan, J. D.; Pettinga, J. R., Campbell, J.K., (2000), Structural evolution and landscape development of a transpressive duplex on the Hope fault, North Canterbury, New Zealand. New Zealand Journal of Geology and Geophysics v 43, 391-404.

Evans, S.G., Hungr, O., and Enegren, E.G., (1994), The Avalanche Lake rock avalanche, Mackenzie Mountains, Northwest Territories, Canada: description, dating and dynamics: Canadian Geotechnical Journal, v. 31, p. 749 - 768.

Evans, S.G. and Hungr, O., (1989), The Pandemonium Creek rock avalanche, British Columbia.: Canadian Geotechnical Journal, v. 26, p. 427 - 446.

Evans, S., Hungr, O., Clague J J., (2001), Dynamics of the 1984 rock avalanche and associated distal debris flow on Mount Cayley, British Columbia, Canada; implications for landslide hazard assessment on dissected volcanoes: Engineering Geology, v. 61, p. 29-51.

Fell, R.H., O. Leroueil, S. Riemer, W., (2001), The stability of natural slopes, and cuts and fills in soil: Geotechnical Engineering of Embankment dams.

Fougere, S., (2002), Paleoseismicity and active earth deformation, Lake Rotoiti to west Wairau valley section of the Alpine Fault. Unpublished M.Sc. thesis: University of Canterbury, Christchurch, New Zealand.

Goodman, R.E., Shi, G, (1985), Block theory and its application to rock engineering, Prentice-Hall International, Inc. p338

Govi, M.G., G. Nicoletti, P.G., (2002), Val Pola rock avalanche of July 28, 1987, in Valtellina (Central Italian Alps: Reviews in Engineering Geology: Catastrophic Landslides: effects, occurrence, and mechanisms. v. 15, p. 71-90.

Gregg, D.R., (1964), Geological Map of New Zealand 1:250, 000. Sheet 18, "Hurunui": N.Z. DSIR, Wellington.

Hancox, G.T., Perrin, N.D. and Dellow, G.D., (1997), Earthquake-Induced Landsliding in New Zealand and Implications for MM Intensity and Seismic Hazard Assessment: Lower Hutt, Institute of Geological and Nuclear Sciences Limited, p. 85.

Hermanns, R.L., Strecker, M.R., (1999), Structural and lithological controls on Quaternary rock avalanches (sturzstroms) in arid northwestern Argentina: Geological Society of America Bulletin, v. 111, p. 934-948.

Hewitt, K., (1998), Catastrophic landslides and their effects on the Upper Indus streams, Karakoram Himalaya, northern Pakistan: Geomorphology, v. 26, p. 47-80.

Hewitt, K., (2002), Styles of rock-avalanche depositional complexes conditioned by very rugged terrain, Karakoram Himalaya, Pakistan: Reviews in Engineering Geology: Catastrophic Landslides: effects, occurrence, and mechanisms. v. 15, p. 345-378.

Hogg, A.G., (1982), Radiocarbon Dating At University of Waikato, New Zealand: Hamilton, University of Waikato, p. 51.

Howard, M.E., (2001), *Holocene surface-rupturing earthquakes on the Porters Pass Fault.* Unpublished M.Sc thesis: University of Canterbury, Christchurch, New Zealand..

Hsu, K.J., (1975), Catastrophic debris streams (struztroms) generated by rockfalls: Geological Society of America Bulletin, v. 86, p. 129-140.

Hsu, K. J., (1978), Albert Heim: Observations on landslides and relevance to modern interpretations. In Voight B (ed) Rockslides and avalanches. 1. Natural phenomena, 71-93. Elsevier, New York.

Hungr, O., (1995), A model for the runout analysis of rapid flow slides, debris flows, and avalanches: Canadian Geotechnical Journal, v. 32, p. 610 - 623.

Hungr, O., and Evans, S.G., (1996), Rock avalanche runout prediction using a dynamic model., In Landslides, Proceedings of the 7th International Symposium on landslides, Trondheim, Norway, Edited by K. Senneset. A.A Balkema, Rotterdam, Vol 1, pp. 233 -238.

Hungr, O., Evans S.G., Bovis, M. J., Hutchinson, J.N., 2001, A review of the classification of landslides of the flow type: Environmental & Engineering Geoscience, v. 7, p. 221-238.

Hutchinson, J.N., (1988), General Report: Morphological and geotechnical parameters of landslides in relation to geology and hydrology, in Bonnard, ed., Landslides, Proceedings, 5th International Symposium on Landslides, Lausanne,, Volume 1, p. 3-35.

Jibson, R.W., (1996), Use of landslides for paleoseismic analysis: Engineering Geology, v. 43, p. 291-323.

Jibson, R.W., Prentice, B.A., Borissoff, E.A., Rogozhin, & Langer, C.J., (1994), Some observations of landslides triggered by the 29 April 1991 Racha earthquake, Republic of Georgia: Bulletin of the Seismological Society of America, v. 84, p. 963-973.

Keefer, D.K., (1984), Rock avalanches caused by earthquakes: source characteristics: Science, v. 223, p. 1288-1289.

Kilburn, C.R.J., and Pasuto, A., (2003), Major risk from rapid, large volume landslides in Europe (EU Project RUNOUT): Geomorphology, v. 54, p. 3-9.

Kilburn, C.R.J., and Sorensen, S.A., (1998), Runout lengths of sturzstroms: the control of intial conditions and of fragment dynamics: Journal of Geophysical Research, v. 103, p. 17877-17884.

McFadgen, B.G., (1982), Dating New Zealand archaeology by radiocarbon. New Zealand Journal of Science; 25, 379-392.

McNeil, J., (2001), History of slope instability at Castle Hill quarry, Castle Hill Basin, New Zealand. Unpublished B.Sc. Honours thesis: University of Canterbury, Christchurch, New Zealand.

McSaveney, M.J., (1978), Sherman Glacier rock avalanche, Alaska, U.S.A., in Voight, B., ed., Rockslides and avalanches, 1., Volume 14A, Dev. Geotech. Eng, p. 197 - 258.

McSaveney, M.J., (1992), A manual for weathering-rind dating of grey sandstones of the Torlesse Supergroup, New Zealand. Institute of Geological and Nuclear Sciences, Wellington.

McSaveney, M.J., (2002), Recent rockfalls and rock avalanches in Mount Cook National Park, New Zealand: Reviews in Engineering Geology: Catastrophic Landslides: effects, occurrence, and mechanisms. v. 15, p. 35-71.

Melosh, H. J., (1987), The mechanics of large rock avalanches. Rev Eng Geol VII, 41-49.

Mitchell, W. A., Dunning, S., Taylor, P. J., McSaveney, M. J., Strom, A,. (2001), Investigation of rock avalanches in high mountains: Earth system processes; programmes with abstracts; Geological society of America and Geological Society of London

Molloy, B.P.J., (1963), Soil genesis and plant succession in the sub-alpine and alpine zones of Torlesse Range, Canterbury, New Zealand: New Zealand Journal of Botany, v. 1, p. 137-148.

Nicol, A., Howard, M., Campbell, J., Pettinga, J., (2001), Paleoearthquakes on the Porters Pass Fault: Christchurch, IGNS, p. 28.

Nicoletti, P.G., (1991a), Rock - avalanche risk at Plati, Southern Italy, in Bell, D.H., ed., Landslides, Bel l(ed.), Balkema, Rotterdam.

Nicoletti, P.G.a.S.-V., M., (1991b), Geomorphic controls of the shape and mobility of rock avalanches: Geological Society of America Bulletin, v. 103, p. 1365-1373.

Nobes, D.C., (1996), Troubled Waters: environmental applications of electrical and electromagnetic methods: Surveys in Geophysics, v. 17, p. 393-454.

Nobes, D.C., Ferguson, R.J., and Brierley, G.J., (2001), Ground-penetrating radar and sedimentological analysis of Holocene floodplains: insight from the Tuross valley, New South Wales: Australian Journal of Earth Sciences, v. 48, p. 347-355.

Okura, Y., Kitahara, H. Sammori, T. Kawanami, A, (2000), The effects of rock fall volume on runout distance: Engineering Geology, v. 58, p. 109-124.

Orwin, J.F., (1998), The application and implications of rock weathering-rind dating to a large rock avalanche, Craigeburn Range, Canterbury, New Zealand: New Zealand Journal of Geology and Geophysics., v. 41, p. 219-223.

Pearce, A.J., O'Loughlin, C.L., (1985), Landsliding during a M 7.7 earthquake: Influence of geology and topography: Geology, v. 13, p. 855-858.

Pettinga, J.R., Yetton, M.D., Van Dissen, R.J. and Downes, G., (2001), Earthquake source identification and characterisation for the Canterbury region, South Island, New Zealand: Bulletin of the New Zealand Society for Earthquake Engineering, v. 34, p. 282-317.

Prebble, W.M., (2001), Hazardous terrain-An engineering geological perspective, Engineering and Development in Hazardous Terrain, IPENZ, p. 3-34.

Scheidegger, A., (1973), On the prediction of the reach and velocity of catastrophic landslides: Rock Mechanics, v. 5, p. 231-236.

Sepulveda, S., Murphy, W., Petley, D.N., (2002), Rock slope failures during the 1999 Chi-Chi earthquake, Taiwan: an example of topographic amplification effects?: Geological Society of America Bulletin.

Shreve R. L., (1968), The Blackhawk landslide. Spec Paper Geol Soc Am, 108: 1-47

Solonenko, V.P., (1977), Landslide and collapses in seismic zones and their prediction: Bulletin of International Association of Engineering Geology, v. 15, p. 4-8.

Soons, J.M., (1963), The glacial sequence in part of the Rakaia valley, Canterbury, New Zealand: New Zealand Journal of Geology and Geophysics. v. 6, p. 735-756.

Sousa, J., and Voight, B., (1991), Continuum simulation of flow failures: Geotechnique, v. 41, p. 515 - 538.

Strom, A.L.,(1996), Some morphological types of long - runout rockslides: Effect of relief on their mechanism and on the rockslide deposits distribution, in (ed.), S., ed., Landslides, Balkema, Rotterdam, p. 1977 - 1982.

Suggate, R.P., (1990), Late Pliocene and Quaternary Glaciations of New Zealand: Quaternary Science Reviews, v. 9, p. 175-197.

Taylor, R.E., Stuiver, M., Reimer, P.J., (1996), Development and extension of the calibration of the radiocarbon time scale: Archaeological applications: Quaternary Science Reviews, v. 15, p. 655-668.

Varnes, D. J., Cruden. D. M., (1996), Landslides: investigation and mitigation. Turner, K., Schuster, R. L., (ed) Special report (National Research Council (U.S.) Transportation Research Board 673

Voight, B., (1978), Rockslides and Avalanches: an introduction, in Voight, B., ed., Rockslides and Avalanches .1. Natural Phenomena, Volume 1, Elsevier, Amsterdam, p. 833.

Whitehouse, I.E., (1981), A large rock avalanche in the Craigeburn Range, Canterbury.: New Zealand Journal of Geology and Geophysics., v. 24, p. 415 - 421.

Whitehouse, I.E., (1983a), Distribution of large rock avalanche deposits in the central Southern Alps, New Zealand.: New Zealand Journal of Geology and Geophysics. v. 26, p. 271 - 279.

Whitehouse, I.E., Griffiths, G. A., (1983b), Frequency and hazard of large rock avalanches in the central Southern Alps, New Zealand.: Geology, v. 11, p. 331 - 334.

Whitehouse, I.E., and Bradshaw, J.D., (1988), Reconnaissance bedrock geology of upper Rakaia River, Canterbury: Upper Hutt, Institute of Geological & Nuclear Sciences Ltd, p. 18.

Wright, C.A., (1998a), The A.D. 930 long - runout Round Top debris avalanche, Westland, New Zealand: New Zealand Journal of Geology and Geophysics. v. 41, p. 493 - 497.

Wright, C.A., Norris, R.J. Cooper, A.F., (1998b), Paleoseismic history of the central Alpine Fault-Abstracts, in Nobes, D.C., Basset, K. N., ed., Geological Society of New Zealand and New Zealand Geophysical Society joint annual conference: Christchurch, Geological society of New Zealand.

Yetton, M.D., (1998a), Progress in understanding the paleoseismicity of the central and northern Alpine Fault, Westland, New Zealand.: New Zealand Journal of Geology and Geophysics., v. 41, p. 475-483.

Yetton, M.D., Wells, A., and Traylen, N. J., (1998b), The probablity and consequences of the next Alpine Fault earthquake., EQC research report 95/193, p. 1 -159.

Yetton, M.D., (2002), Paleoseismic investigation of the north and west Wairau sections of the Alpine Fault, South Island, New Zealand: Christchurch, Earthquake Commission Research Foundation, p. 96.

Young, D.A., (1997) Segmentation of the Craigeburn Fault Zone, Castle Hill Basin, Canterbury Unpublished B.Sc (honours) thesis: University of Canterbury, Christchurch, New Zealand.

APPENDICES

APPENDIX A
STRUCTURAL DATA FOR THE SOURCE SCAR OF THE ACHERON ROCK AVALANCHE

Aerial photograph of the source scar of the Acheron rock avalanche:

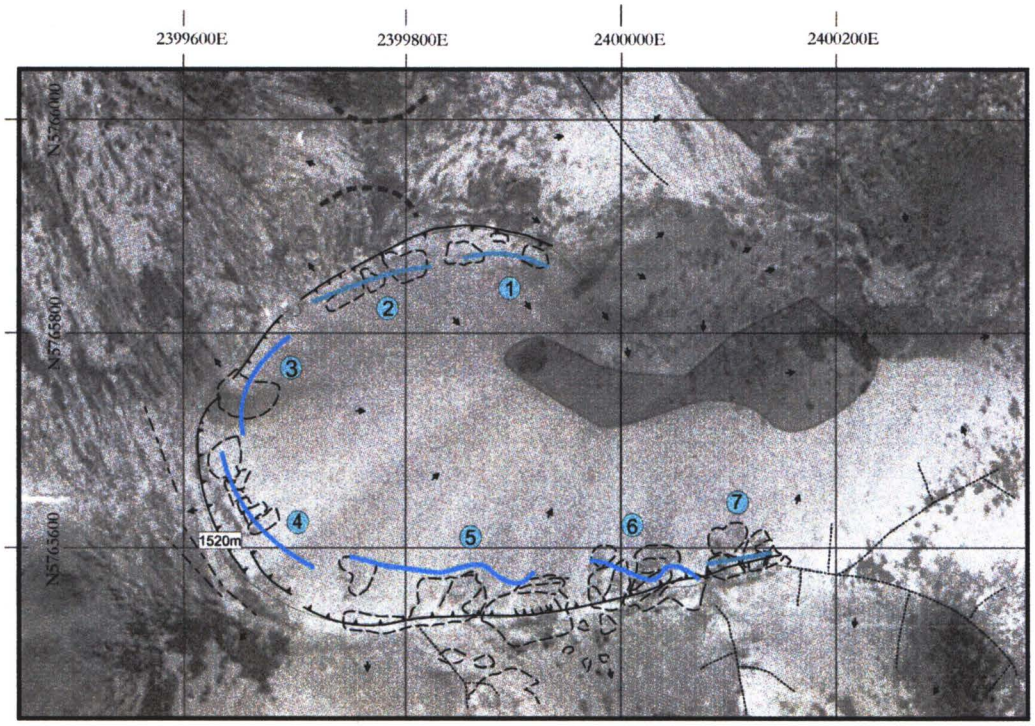

Aerial Photo of the Source Scar

The partitioning of the outcrop (outlined by the dashed lines) is identified by the numbered blue circles. In both text and tables the splitting up of the outcrop is described as either Traverse 1-7, Slope 1-7 or Section 1-7 however these all signify the same divisions as defined by the number. Tension cracks visible at the scar crest can be identified by the dash-dot lines trending NW-SE while the thin dotted lines represent ridge line topography. The black arrows show the direction of slope and the dark fill identifies the source basin floor.

APPENDIX A 1: RAW DATA COLLECTED IN SOURCE SCAR

RAW BEDDING AND JOINT DATA FROM THE SOURCE SCAR OF THE ACHERON ROCK AVALANCHE, RED HILL VALLEY							
ID	ORIENT 1	ORIENT 2	QUANTITY	TRAVERSE	SET	TYPE	SURFACE
1	52	3	1	1	1	bedding	rough
2	40	154	1	1	3	joint	rough
3	86	82	1	1	5	joint	rough
4	30	246	1	1		joint	rough
5	40	50	1	1		joint	rough
6	50	140	1	1	3	joint	rough
7	52	30	1	1	1	joint	rough
8	64	358	1	2	1	bedding	rough
9	30	180	1	2		joint	rough
10	70	98	1	2	4	joint	rough
11	36	200	1	2		joint	rough
12	90	290	1	2	4	joint	rough
13	44	0	1	2	1	joint	rough
14	70	14	1	2	1	bedding	rough
15	86	340	1	3	1	bedding	rough
16	40	128	1	3	3	joint	rough
17	82	210	1	3	1	joint	rough
18	85	194	1	3	1	bedding	rough
19	50	82	1	3	2	joint	rough
20	72	110	1	3	4	joint	rough
21	85	180	1	3	1	joint	rough
22	70	260	1	3		joint	rough
23	10	70	1	3		joint	rough
24	80	2	1	3	1	bedding	rough
25	90	34	1	3	1	bedding	rough
26	75	160		3		joint	rough
27	80	50		3		joint	rough
28	85	194	1	3	1	joint	rough
29	82	80		3	5	joint	rough
30	78	9		3	1	bedding	rough
31	82	72	1	4	5	joint	rough
32	50	22	1	4	1	joint	rough
33	60	130	1	4	3	joint	rough
34	66	144	1	4	3	joint	rough
35	76	330	1	4		joint	rough
36	68	20	1	4	1	bedding	smooth
37	90	355		4	1	bedding	rough
38	56	355		4	1	joint	rough
39	34	230		4		joint	rough
40	90	60		4		joint	rough
41	67	34		4	1	joint	rough
42	54	68	1	4	2	joint	rough

ID	ORIENT 1	ORIENT 2	QUANTITY	TRAVERSE	SET	TYPE	SURFACE
44	56	16	1	5	1	bedding	rough
45	82	2	1	5	1	bedding	rough
46	70	348	1	5	1	bedding	rough
47	56	348	1	5	1	joint	rough
48	84	226	1	5		joint	rough
49	40	40	1	5		joint	rough
50	45	315		5		joint	rough
51	39	1		5	1	joint	rough
52	81	355		5	1	joint	rough
53	86	20	1	5	1	bedding	rough
54	80	0	1	6	1	bedding	rough
55	36	6	1	6	1	joint	rough
56	52	80	1	6	2	joint	rough
57	60	212	1	6		joint	rough
58	40	19	1	6	1	joint	rough
59	40	18	1	6	1	joint	rough
60	70	6	1	6	1	bedding	rough
61	40	332	1	6		joint	rough
62	30	78	1	6		joint	rough
63	62	16	1	6	1	joint	rough
64	50	250	1	6		joint	rough
65	45	232		6		joint	rough
66	74	343		6	1	joint	rough
67	82	110	1	6	4	joint	rough
68	46	0	1	7	1	bedding	rough
69	64	18	1	7	1	bedding	rough
70	64	5		7	1	bedding	rough
71	48	314		7		joint	rough
72	75	352		7	1	joint	rough
73	48	352	1	7	1	joint	rough
74	80	352	1	7	1	bedding	rough

APPENDIX A.2: CONTOUR - POLE PLOT OF RAW DATA

Appendix A 2:

Contour and Pole plot of Bedding and Defect Data collected within the Source Scar of the Acheron Rock Avalanche Deposit

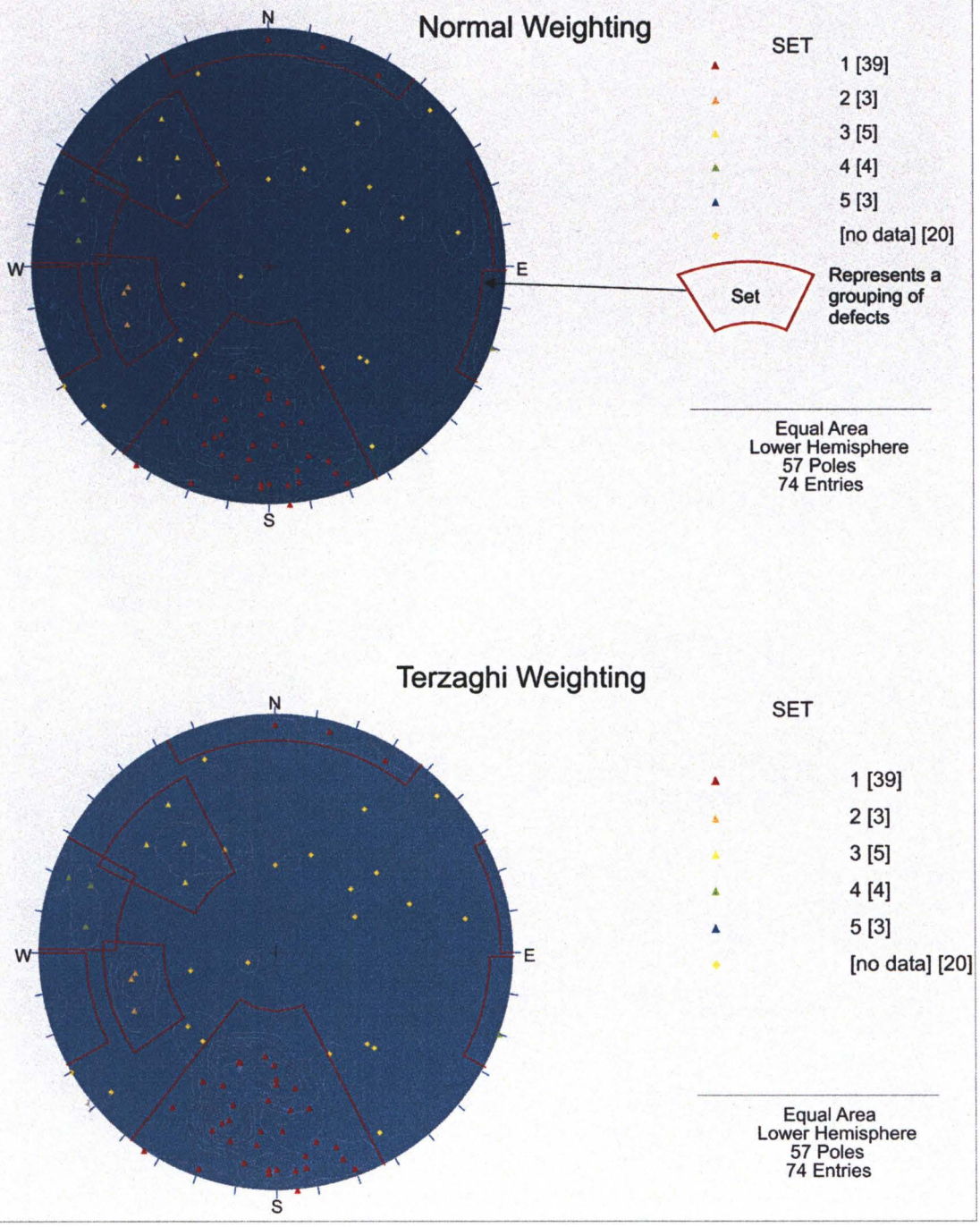

APPENDIX A.3 (A) KINEMATIC ANALYSIS OF SLOPES 1-7

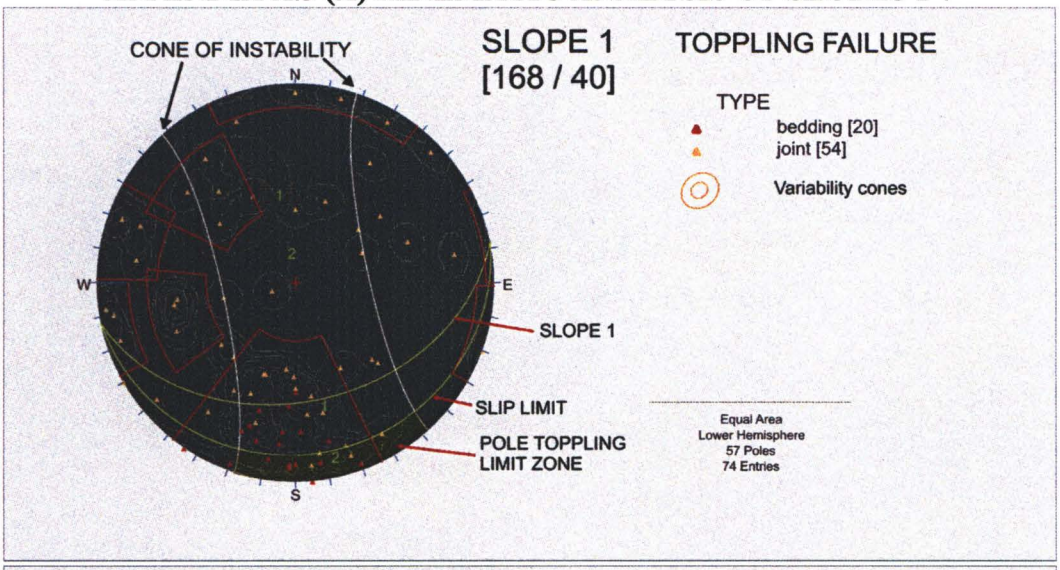

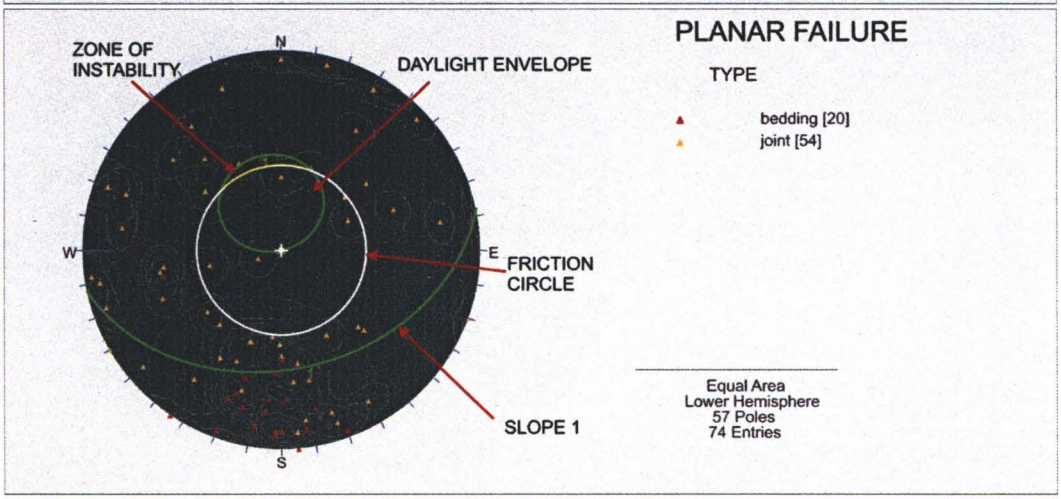

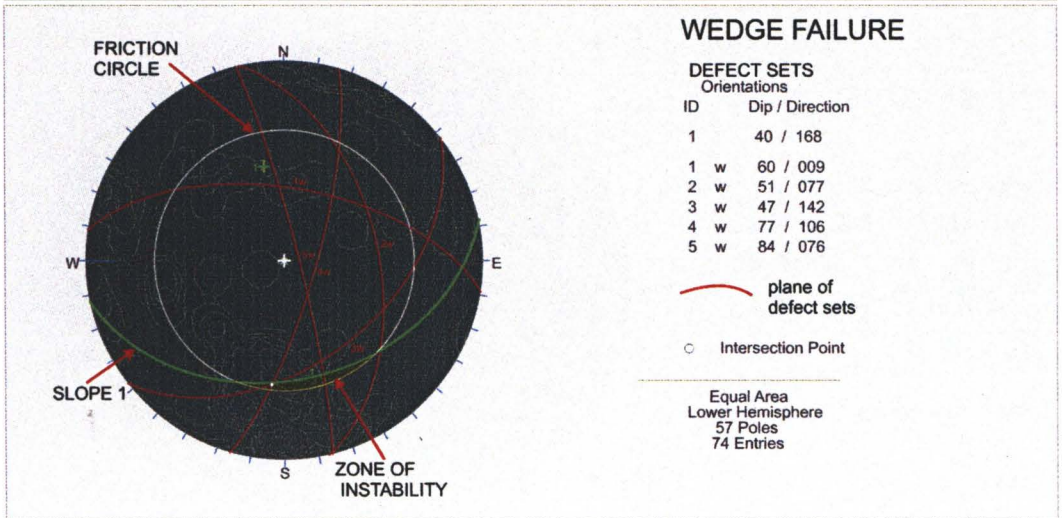

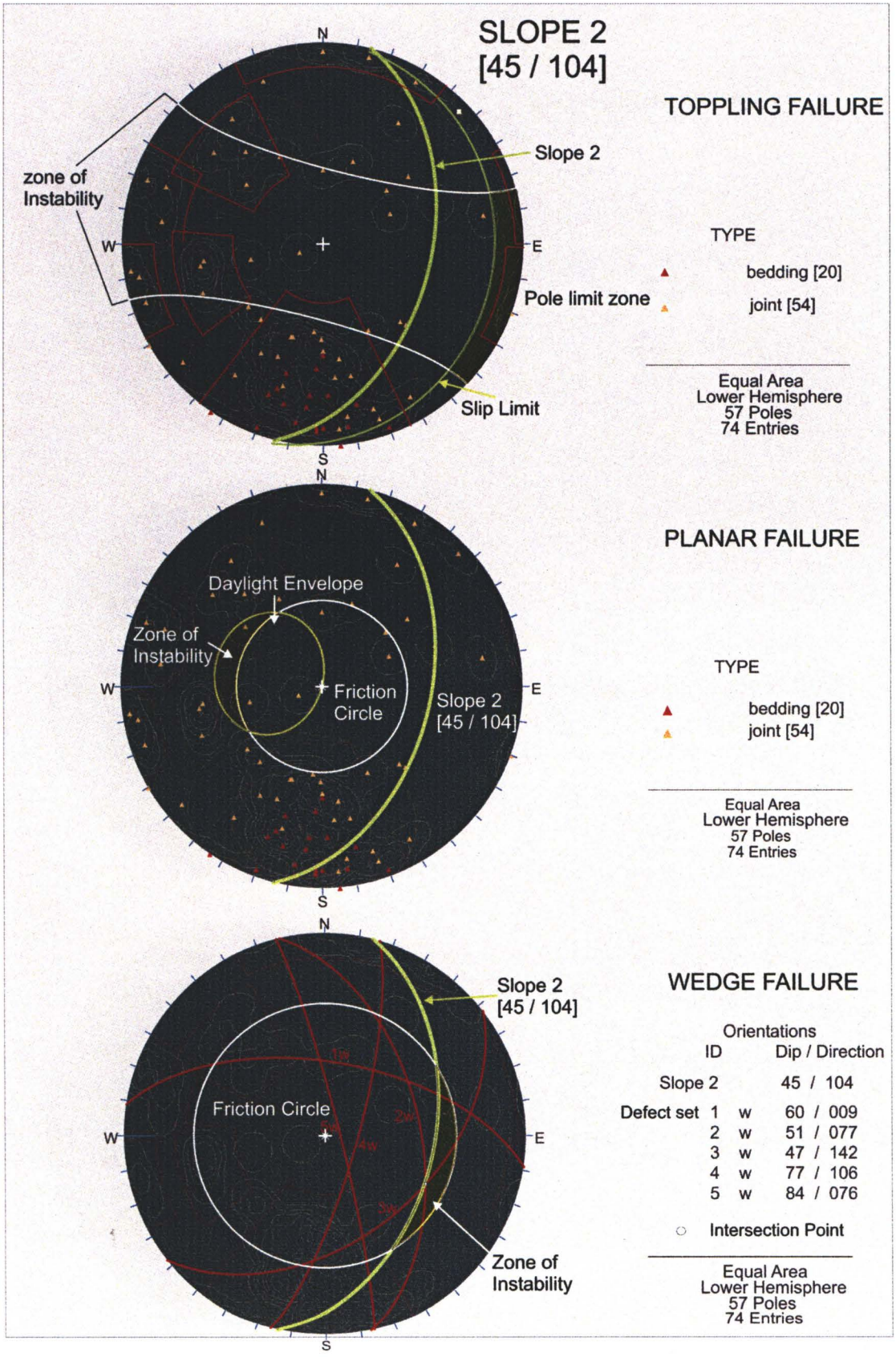
SLOPE 2
[45 / 104]
TOPPLING FAILURE
N
E
S
W
Slope 2
zone of
Instability
Pole limit zone
Slip Limit
TYPE
bedding [20]
joint [54]
Equal Area
Lower Hemisphere
57 Poles
74 Entries
PLANAR FAILURE
Daylight Envelope
Zone of
Instability
Friction
Circle
Slope 2
[45 / 104]
TYPE
bedding [20]
joint [54]
Equal Area
Lower Hemisphere
57 Poles
74 Entries
WEDGE FAILURE
Slope 2
[45 / 104]
Friction Circle
Zone of
Instability
Orientations
ID Dip / Direction
Slope 2 45 / 104
Defect set 1 w 60 / 009
2 w 51 / 077
3 w 47 / 142
4 w 77 / 106
5 w 84 / 076
Intersection Point
Equal Area
Lower Hemisphere
57 Poles
74 Entries

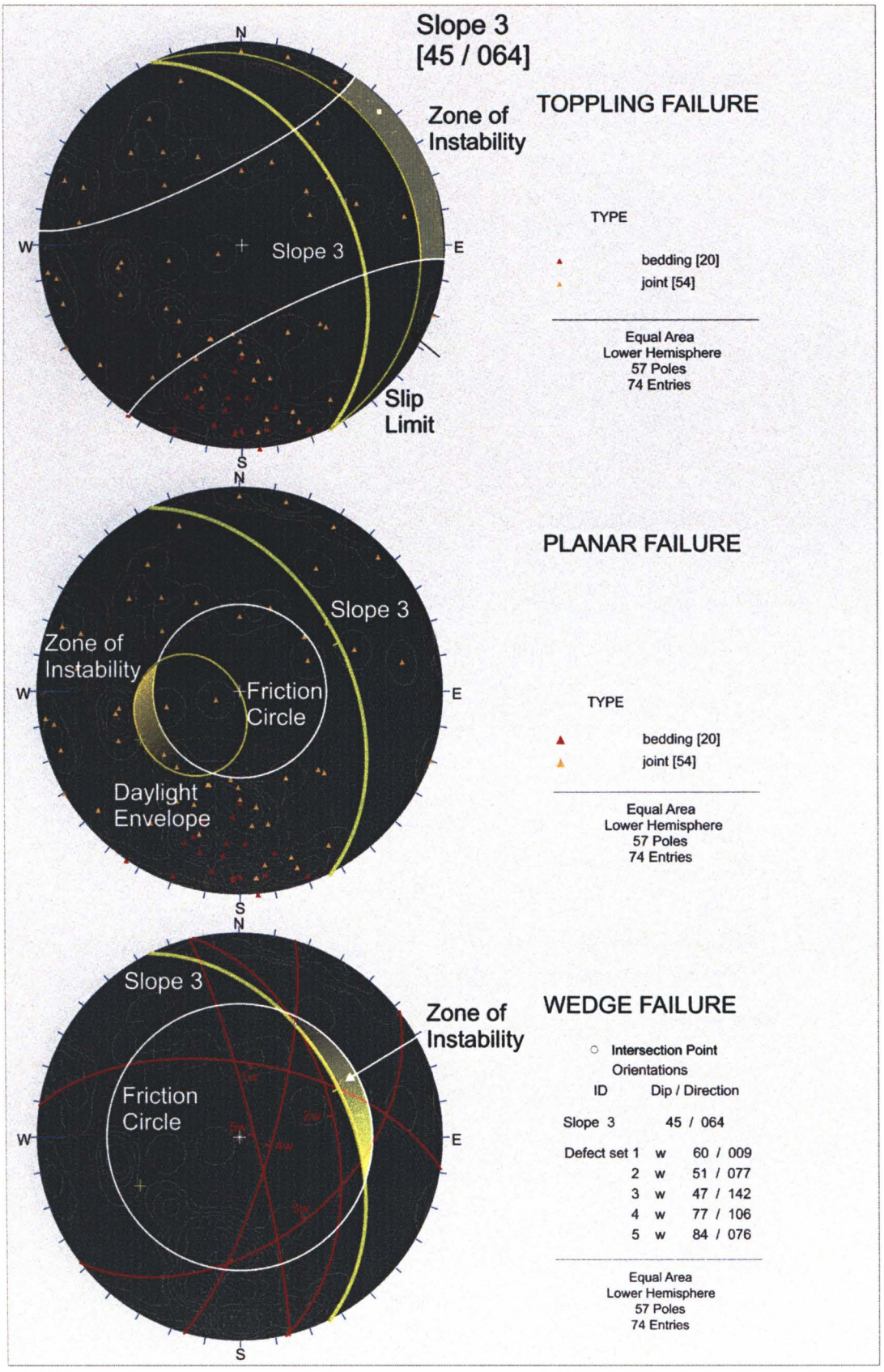
Slope 3
[45 / 064]
TOPPLING FAILURE
Zone of
Instability
N
W
E
S
Slope 3
Slip
Limit
TYPE
bedding [20]
joint [54]
Equal Area
Lower Hemisphere
57 Poles
74 Entries
PLANAR FAILURE
Slope 3
Zone of
Instability
Friction
Circle
Daylight
Envelope
TYPE
bedding [20]
joint [54]
Equal Area
Lower Hemisphere
57 Poles
74 Entries
Slope 3
Zone of
Instability
WEDGE FAILURE
Friction
Circle
Intersection Point
Orientations
ID Dip / Direction
Slope 3 45 / 064
Defect set 1 w 60 / 009
2 w 51 / 077
3 w 47 / 142
4 w 77 / 106
5 w 84 / 076
Equal Area
Lower Hemisphere
57 Poles
74 Entries

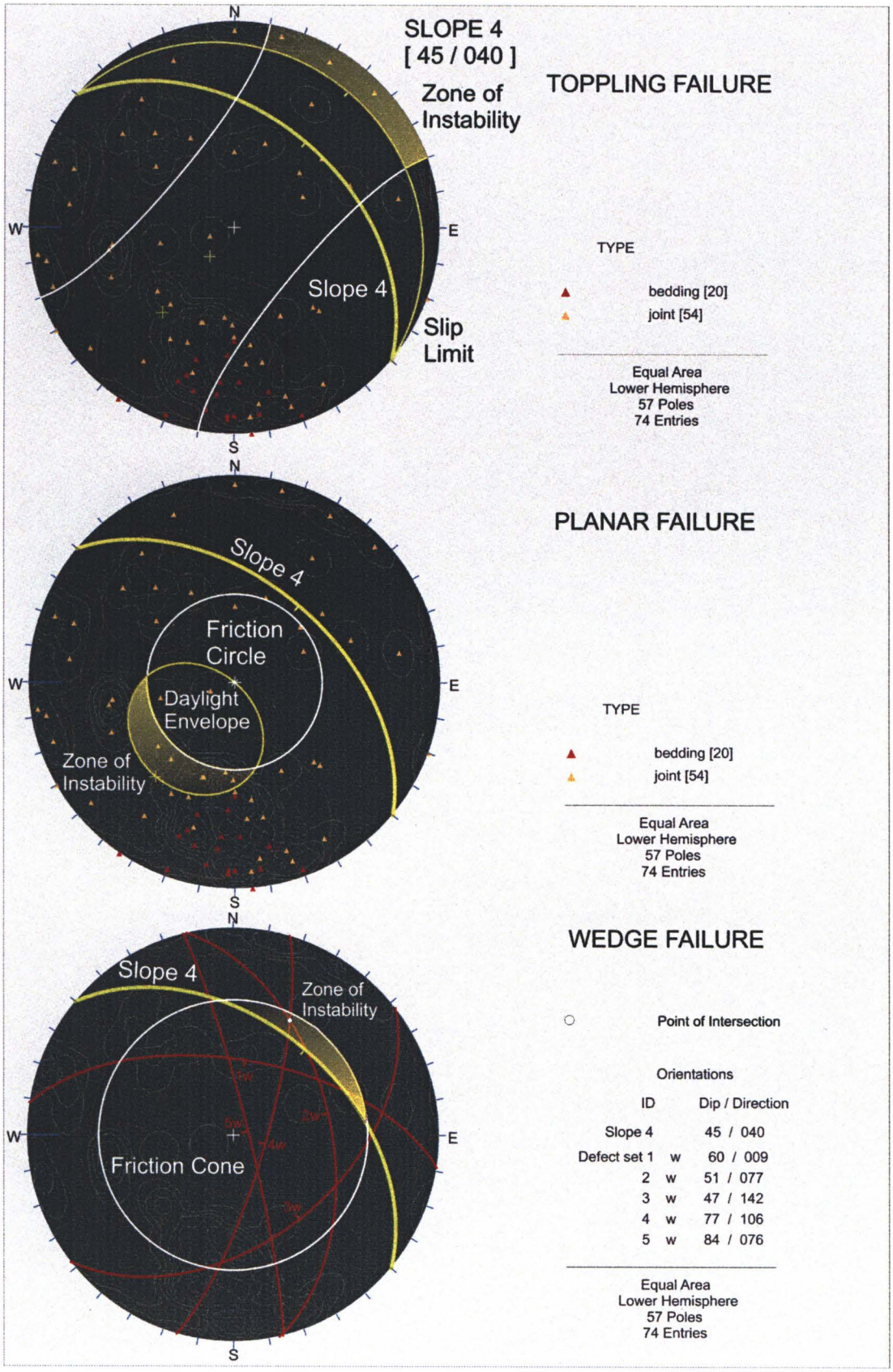
SLOPE 4
[45 / 040]
Zone of
Instability
Slope 4
Slip
Limit
N
S
W
E
TOPPLING FAILURE
TYPE
bedding [20]
joint [54]
Equal Area
Lower Hemisphere
57 Poles
74 Entries
Slope 4
Friction
Circle
Daylight
Envelope
Zone of
Instability
PLANAR FAILURE
TYPE
bedding [20]
joint [54]
Equal Area
Lower Hemisphere
57 Poles
74 Entries
Slope 4
Zone of
Instability
Friction Cone
WEDGE FAILURE
Point of Intersection
Orientations
ID Dip / Direction
Slope 4 45 / 040
Defect set 1 w 60 / 009
2 w 51 / 077
3 w 47 / 142
4 w 77 / 106
5 w 84 / 076
Equal Area
Lower Hemisphere
57 Poles
74 Entries

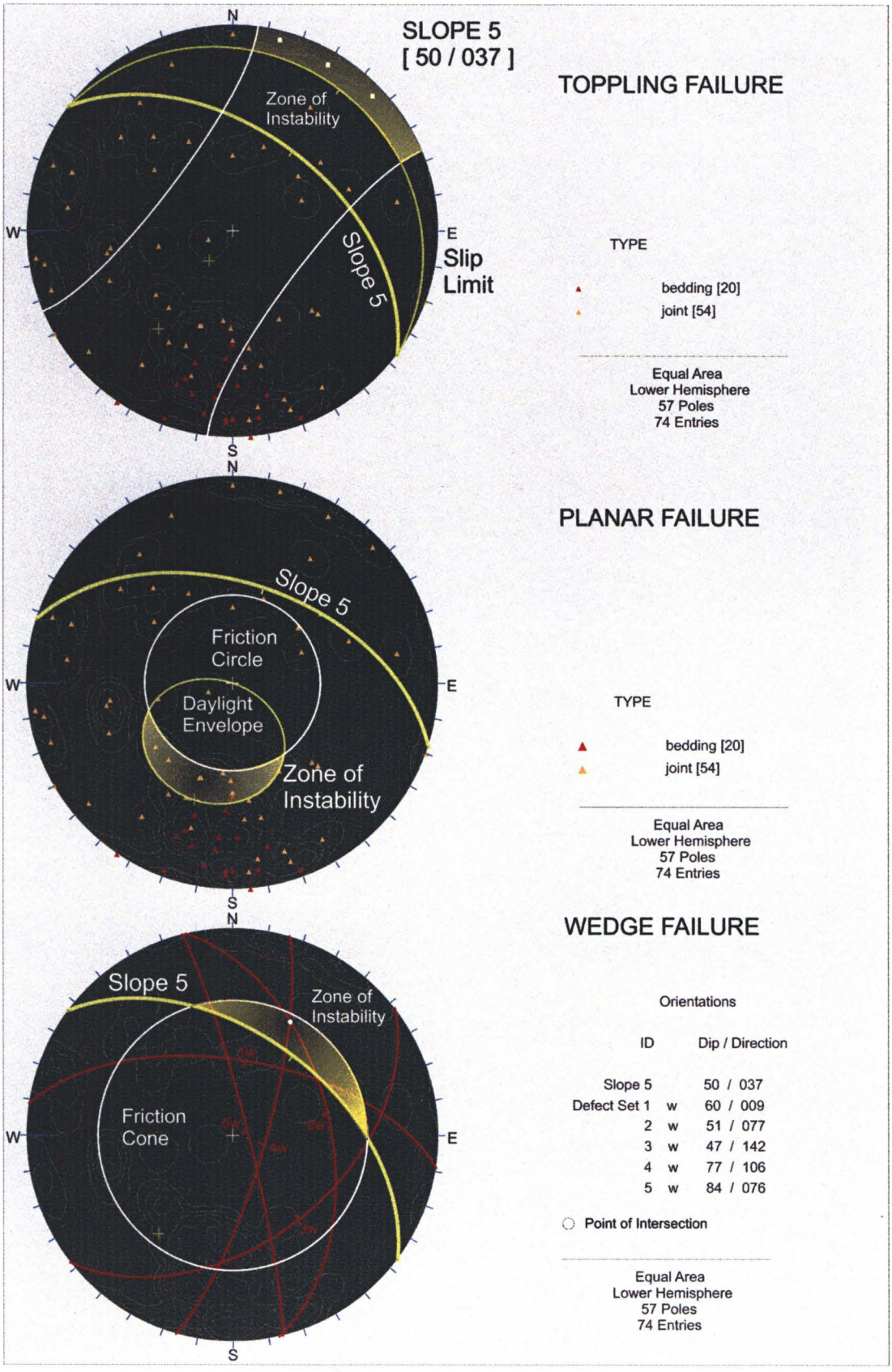
SLOPE 5
[50 / 037]
TOPPLING FAILURE
Zone of Instability
Slope 5
Slip Limit
N
S
E
W
TYPE
bedding [20]
joint [54]
Equal Area
Lower Hemisphere
57 Poles
74 Entries
PLANAR FAILURE
Slope 5
Friction Circle
Daylight Envelope
Zone of Instability
TYPE
bedding [20]
joint [54]
Equal Area
Lower Hemisphere
57 Poles
74 Entries
WEDGE FAILURE
Slope 5
Zone of Instability
Friction Cone
Orientations
ID Dip / Direction
Slope 5 50 / 037
Defect Set 1 w 60 / 009
2 w 51 / 077
3 w 47 / 142
4 w 77 / 106
5 w 84 / 076
Point of Intersection
Equal Area
Lower Hemisphere
57 Poles
74 Entries

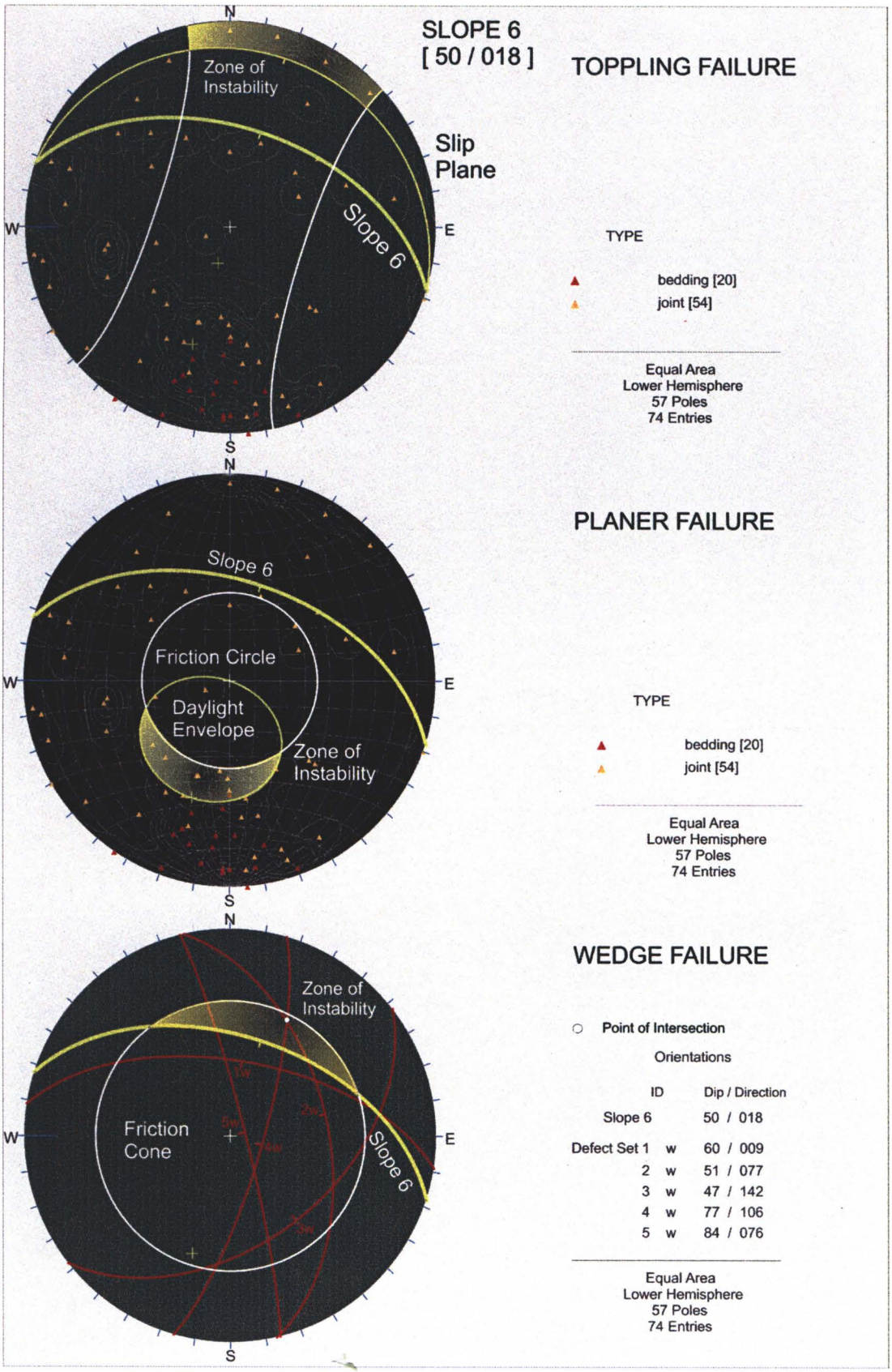
SLOPE 6
[50 / 018]
TOPPLING FAILURE
Zone of Instability
Slip Plane
Slope 6
N
S
W
E
TYPE
bedding [20]
joint [54]
Equal Area
Lower Hemisphere
57 Poles
74 Entries
PLANER FAILURE
Slope 6
Friction Circle
Daylight Envelope
Zone of Instability
TYPE
bedding [20]
joint [54]
Equal Area
Lower Hemisphere
57 Poles
74 Entries
WEDGE FAILURE
Zone of Instability
Friction Cone
Slope 6
Point of Intersection
Orientations
ID Dip / Direction
Slope 6 50 / 018
Defect Set 1 w 60 / 009
2 w 51 / 077
3 w 47 / 142
4 w 77 / 106
5 w 84 / 076
Equal Area
Lower Hemisphere
57 Poles
74 Entries

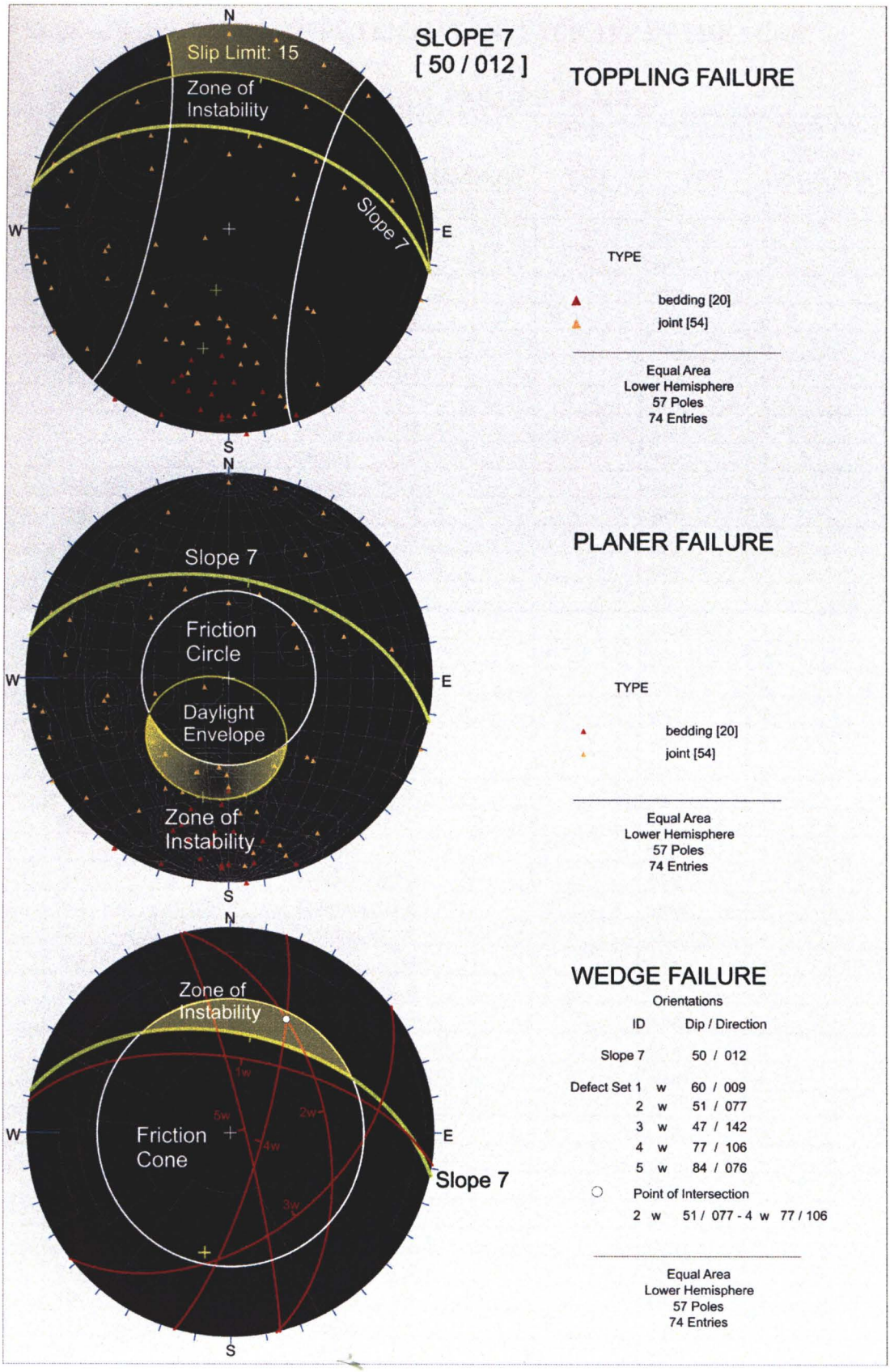
SLOPE 7
[50 / 012]
TOPPLING FAILURE
N
Slip Limit: 15
Zone of Instability
Slope 7
W
E
S
TYPE
bedding [20]
joint [54]
Equal Area
Lower Hemisphere
57 Poles
74 Entries
PLANER FAILURE
Slope 7
Friction Circle
Daylight Envelope
Zone of Instability
WEDGE FAILURE
Orientations
ID Dip / Direction
Slope 7 50 / 012
Defect Set 1 w 60 / 009
2 w 51 / 077
3 w 47 / 142
4 w 77 / 106
5 w 84 / 076
Point of Intersection
2 w 51 / 077 - 4 w 77 / 106
Friction Cone
1w
2w
3w
4w
5w

APPENDIX A. 3 (B): TABLE OF POTENTIAL INSTABILITY IN THE SCAR

TABLE OF POTENTIAL DEFECT FAILURE PLANES

DIP	DIP DIRECTION	REF. NO.	FAILURE TYPE	TRAVERSE	DEFECT SET	DEFECT TYPE	DEFECT ORIGIN TRAVERSE
40	332	61	Planar	7	1	joint	6
46	0	68	Planar	7	1	bedding	7
44	0	13	Planar	7	1	joint	2
39	1	51	Planar	7	1	joint	5
36	6	55	Planar	7	1	joint	6
40	18	59	Planar	7	1	joint	6
40	19	58	Planar	7	1	joint	6
40	40	49	Planar	7		joint	5
40	50	5	Planar	7		joint	1
51	77	2	Wedge	7	3	joint	1
77	106	4	Wedge	7		joint	1
82	210	17	Toppling	7	1	joint	3
85	194	18	Toppling	7	1	joint	3
85	180	21	Toppling	7	1	joint	3
85	194	28	Toppling	7	1	joint	3
46	0	68	Planar	6	1	bedding	7
44	0	13	Planar	6	1	joint	2
39	1	51	Planar	6	1	joint	5
36	6	55	Planar	6	1	joint	6
40	18	59	Planar	6	1	joint	6
40	19	58	Planar	6	1	joint	6
40	40	49	Planar	6		joint	5
40	50	5	Planar	6		joint	1
51	77	2	Wedge	6	3	joint	1
77	106	4	Wedge	6		joint	1
82	210	17	Toppling	6	1	joint	3
85	194	18	Toppling	6	1	joint	3
85	180	21	Toppling	6	1	joint	3
85	194	28	Toppling	6	1	joint	3
84	226	48	Toppling	6		joint	5
39	1	51	Planar	5	1	joint	5
36	6	55	Planar	5	1	joint	6
40	18	59	Planar	5	1	joint	6
40	19	58	Planar	5	1	joint	6
40	40	49	Planar	5		joint	5
40	50	5	Planar	5		joint	1
51	77	2	Wedge	5	3	joint	1
77	106	4	Wedge	5		joint	1
82	210	17	Toppling	5	1	joint	3
85	194	18	Toppling	5	1	joint	3
85	194	28	Toppling	5	1	joint	3
70	98	10	Toppling	5	4	joint	2

DIP	DIP DIRECTION	REF. NO.	FAILURE TYPE	TRAVERSE	DEFECT SET	DEFECT TYPE	DEFECT ORIGIN TRAVERSE
39	1	51	Planar	4	1	joint	5
36	6	55	Planar	4	1	joint	6
40	18	59	Planar	4	1	joint	6
40	19	58	Planar	4	1	joint	6
40	40	49	Planar	4		joint	5
40	50	5	Planar	4		joint	1
51	77	2	Wedge	4	3	joint	5
77	106	4	Wedge	4		joint	1
82	210	17	Toppling	4	1	joint	3
85	194	18	Toppling	4	1	joint	3
85	194	28	Toppling	4	1	joint	3
84	226	48	Toppling	4		joint	5
40	40	49	Planar	3		joint	5
40	50	5	Planar	3		joint	1
77	106	4	Wedge	3		joint	1
51	77	2	Wedge	3	3	joint	1
84	226	48	Toppling	3		joint	5
40	128	16	Planar	2	3	joint	3
51	77	2	Wedge	2	3	joint	1
86	82	3	Wedge	2	5	joint	1
77	106	4	Wedge	1		joint	1
86	82	3	Wedge	1	5	joint	1
76	330	35	Toppling	1		joint	4
86	340	15	Toppling	1	1	bedding	1
80	342	43	Toppling	1	1	joint	5
80	352	74	Toppling	1	1	bedding	7
75	352	72	Toppling	1	1	joint	7
81	355	52	Toppling	1	1	joint	5
80	0	54	Toppling	1	1	bedding	6
82	2	45	Toppling	1	1	bedding	5
80	2	24	Toppling	1	1	bedding	3
78	9	30	Toppling	1	1	bedding	3

APPENDIX A.4: SIMPLIFIED KINEMATIC ANALYSIS OF SLOPE 1, 3-7

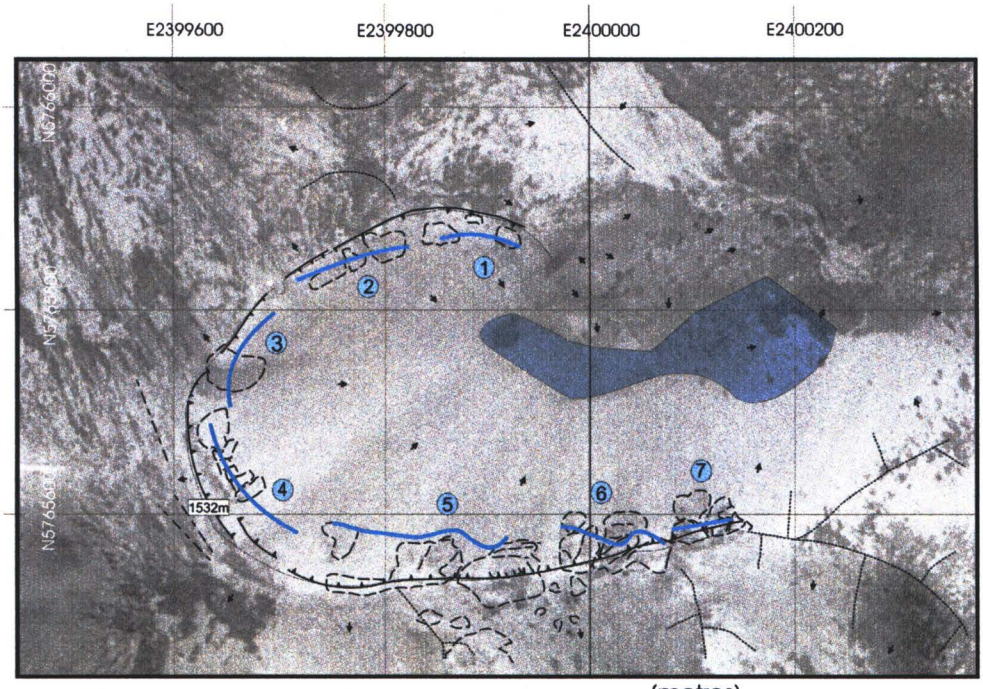

Aerial Photo of the Source Scar

(metres)
0 50 100 200

The traverses followed during data collection are identified by the blue line and slopes 1 to 7 can be distinguished by the numbered blue circles. The small arrows depict slope direction and the extent of the outcrop is outlined by the dashed line. The blue fill represents the floor of the source basin.

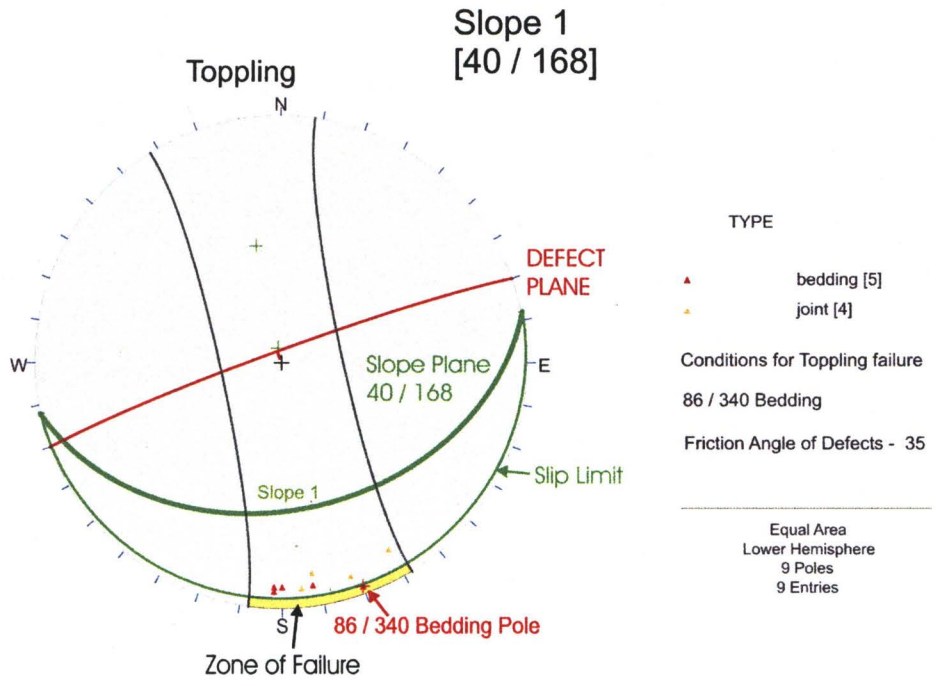

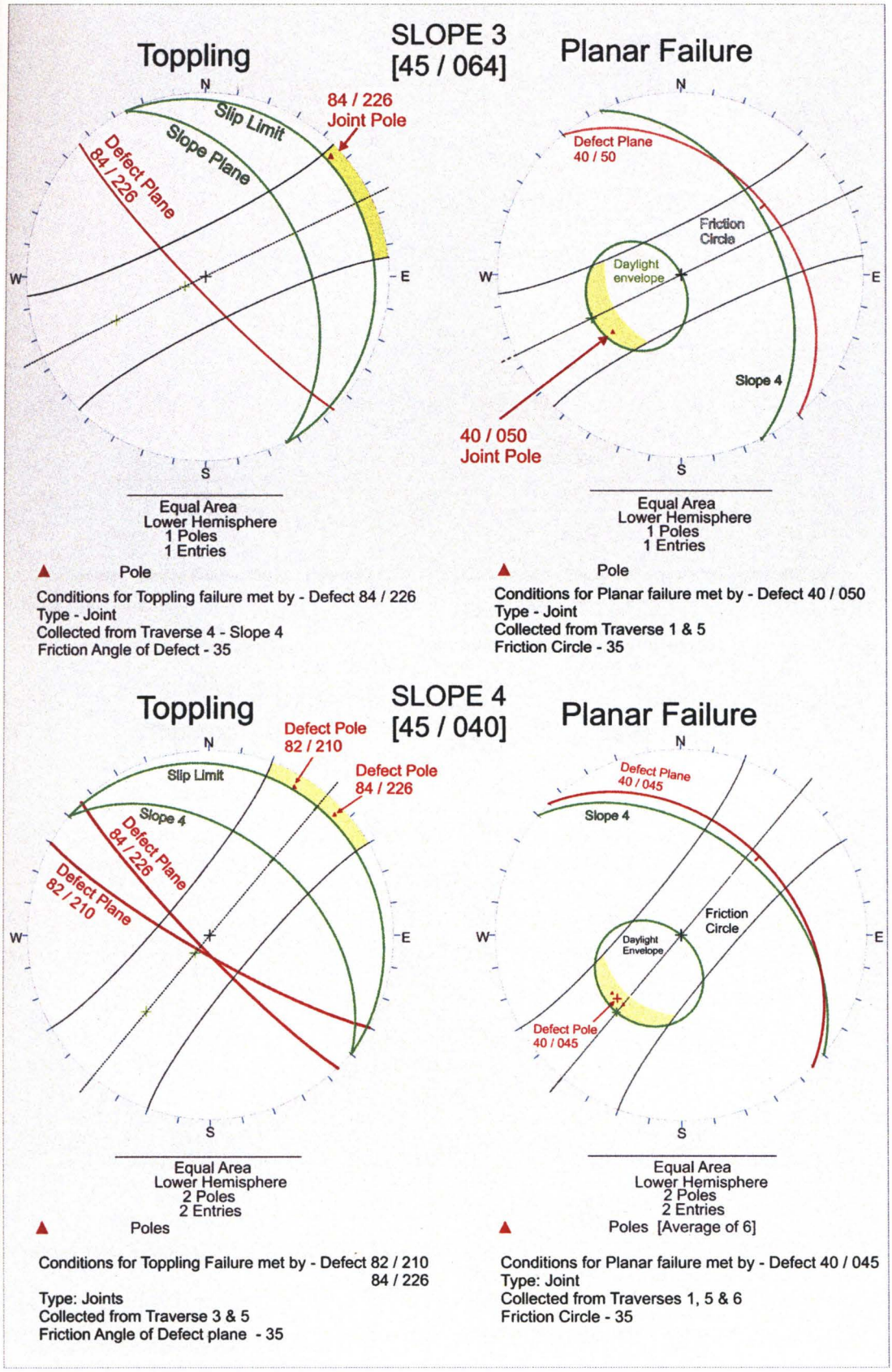
SLOPE 3
[45 / 064]
Toppling
Planar Failure
N
S
W
E
Slip Limit
Slope Plane
84 / 226
Joint Pole
Defect Plane
84 / 226
Defect Plane
40 / 50
Friction
Circle
Daylight
envelope
Slope 4
40 / 050
Joint Pole
Equal Area
Lower Hemisphere
1 Poles
1 Entries
Pole
Conditions for Toppling failure met by - Defect 84 / 226
Type - Joint
Collected from Traverse 4 - Slope 4
Friction Angle of Defect - 35
Equal Area
Lower Hemisphere
1 Poles
1 Entries
Pole
Conditions for Planar failure met by - Defect 40 / 050
Type - Joint
Collected from Traverse 1 & 5
Friction Circle - 35
SLOPE 4
[45 / 040]
Toppling
Planar Failure
Defect Pole
82 / 210
Defect Pole
84 / 226
Slip Limit
Slope 4
Defect Plane
84 / 226
Defect Plane
82 / 210
Defect Plane
40 / 045
Slope 4
Friction
Circle
Daylight
Envelope
Defect Pole
40 / 045
Equal Area
Lower Hemisphere
2 Poles
2 Entries
Poles
Conditions for Toppling Failure met by - Defect 82 / 210
84 / 226
Type: Joints
Collected from Traverse 3 & 5
Friction Angle of Defect plane - 35
Equal Area
Lower Hemisphere
2 Poles
2 Entries
Poles [Average of 6]
Conditions for Planar failure met by - Defect 40 / 045
Type: Joint
Collected from Traverses 1, 5 & 6
Friction Circle - 35

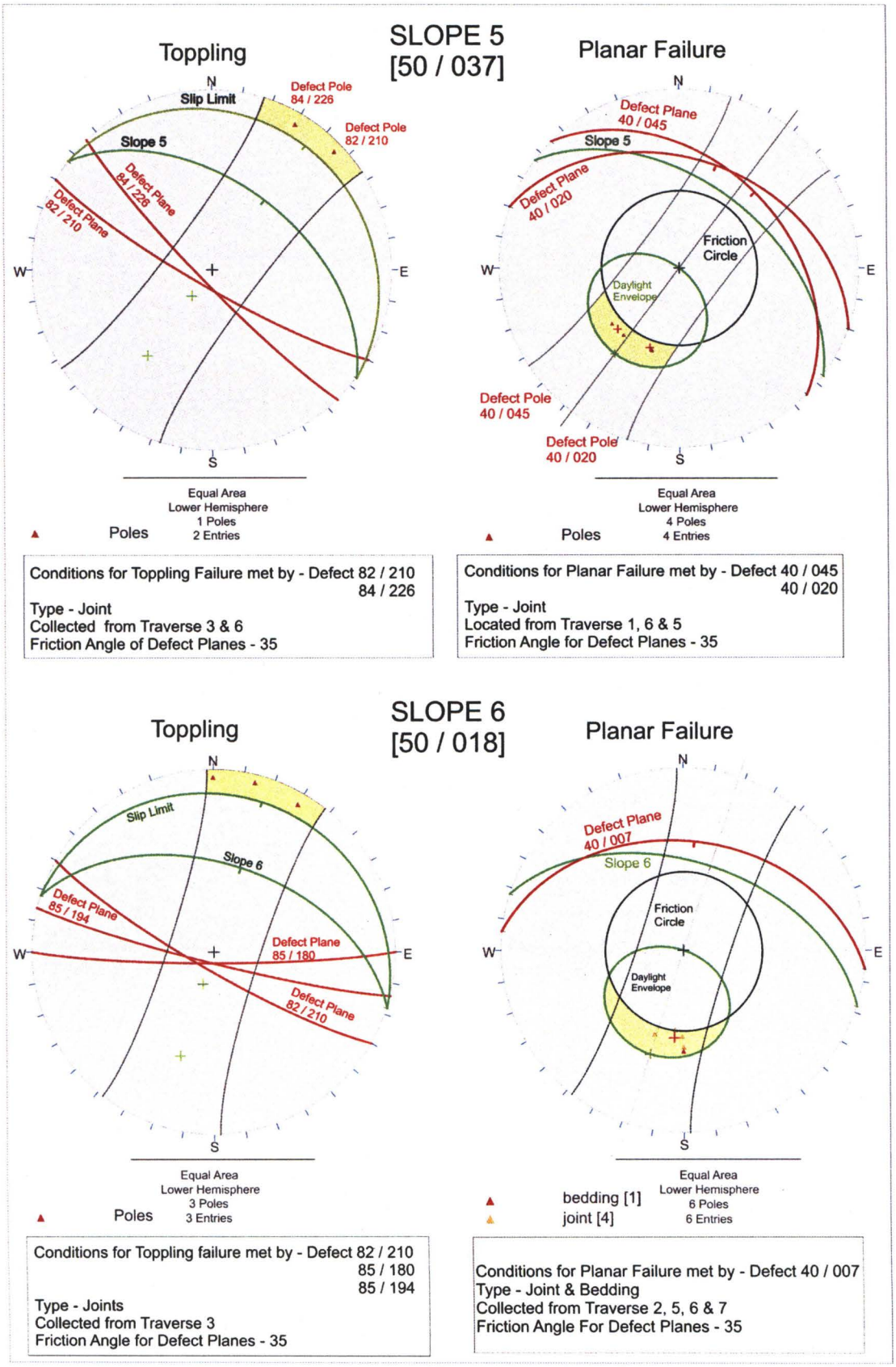
SLOPE 5
[50 / 037]
Toppling
N
Slip Limit
Defect Pole
84 / 226
Defect Pole
82 / 210
Slope 5
Defect Plane
84 / 226
Defect Plane
82 / 210
W
E
S
Equal Area
Lower Hemisphere
1 Poles
2 Entries
Poles
Planar Failure
N
Defect Plane
40 / 045
Slope 5
Defect Plane
40 / 020
Friction
Circle
Daylight
Envelope
W
E
Defect Pole
40 / 045
Defect Pole
40 / 020
S
Equal Area
Lower Hemisphere
4 Poles
4 Entries
Poles
Conditions for Toppling Failure met by - Defect 82 / 210
84 / 226
Type - Joint
Collected from Traverse 3 & 6
Friction Angle of Defect Planes - 35
Conditions for Planar Failure met by - Defect 40 / 045
40 / 020
Type - Joint
Located from Traverse 1, 6 & 5
Friction Angle for Defect Planes - 35
SLOPE 6
[50 / 018]
Toppling
N
Slip Limit
Slope 6
Defect Plane
85 / 194
Defect Plane
85 / 180
Defect Plane
82 / 210
W
E
S
Equal Area
Lower Hemisphere
3 Poles
3 Entries
Poles
Planar Failure
N
Defect Plane
40 / 007
Slope 6
Friction
Circle
Daylight
Envelope
W
E
S
Equal Area
Lower Hemisphere
6 Poles
6 Entries
bedding [1]
joint [4]
Conditions for Toppling failure met by - Defect 82 / 210
85 / 180
85 / 194
Type - Joints
Collected from Traverse 3
Friction Angle for Defect Planes - 35
Conditions for Planar Failure met by - Defect 40 / 007
Type - Joint & Bedding
Collected from Traverse 2, 5, 6 & 7
Friction Angle For Defect Planes - 35

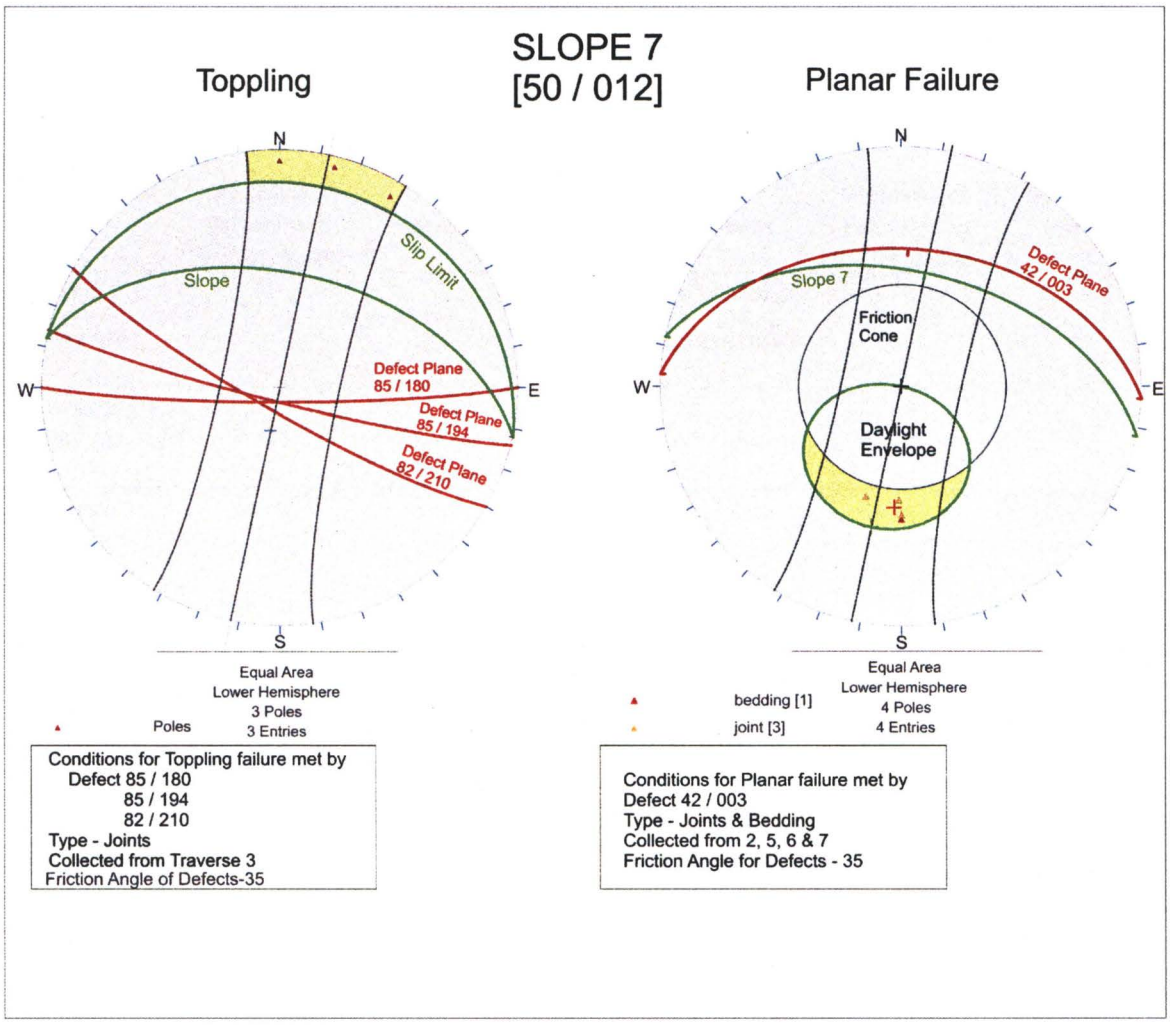
SLOPE 7
[50 / 012]
Toppling
Planar Failure
N
S
W
E
Slope
Slip Limit
Defect Plane
85 / 180
Defect Plane
85 / 194
Defect Plane
82 / 210
Equal Area
Lower Hemisphere
3 Poles
3 Entries
Poles
Conditions for Toppling failure met by
Defect 85 / 180
85 / 194
82 / 210
Type - Joints
Collected from Traverse 3
Friction Angle of Defects-35
Slope 7
Defect Plane
42 / 003
Friction
Cone
Daylight
Envelope
Equal Area
Lower Hemisphere
bedding [1]
4 Poles
joint [3]
4 Entries
Conditions for Planar failure met by
Defect 42 / 003
Type - Joints & Bedding
Collected from 2, 5, 6 & 7
Friction Angle for Defects - 35

APPENDIX A.5: SUMMARY TABLE OF MODES AND PLANES OF FAILURE WITHIN THE SOURCE SCAR OF THE ACHERON ROCK AVALANCHE DEPOSIT

Modes of Failure in the Source Scar

	Slope Traverse	Planar Orientation of Failure Plane *Dip / Dip direction*	Number of Planes	Toppling Orientation of Failure Plane *Dip / Dip direction*	Number of Planes	Wedge Orientation of Failure Plane *Dip / Dip direction*	Number of Planes
1	Slope 1	~		86 / 340	1 bedding	~	
	40 / 168	~	0	~	8 potential	~	0
		~		~		~	
2	Slope 2	~		~		~	
	45 / 104	~	0	~	0	~	0
		~		~		~	
3	Slope 3	40 / 50	1 joint	84 / 226	1 joint		
	45 / 064	~		~		51 / 077	1 joint
		~		~		77 / 106	1 joint
4	Slope 4	40 / 45	2 joint	82 / 210	1 joint		
	45 / 040	[average]		84 / 226	1 joint	Sliding intiates on line of intersection	
		~		~		*Trend*	*Plunge*
5	Slope 5	40 / 20	2 joint	82 / 210	1 joint	026°	38°
	50 / 037	40 / 45	2 joint	84 / 226	1 joint		
		[average]		~		Wedge failure may occur between	
6	Slope 6	40 / 007	5 joint	82 / 210	1 joint	the following orientations:	
	50 / 018	[average]	1 bedding	85 / 180	1 joint		
		~		85 / 194	1 joint	*Dip directions:*	012° - 075°
7	Slope 7	42 / 003	3 joint	82 / 210	1 joint	*Slope angles:*	55° - 90°
	50 / 012	[average]	1 bedding	85 / 194	1 joint		
		~		85 / 180	1 joint		

Friction Angle - 35° Ø

APPENDIX B

LOCATION OF GREYWACKE DERIVED ROCK AVALANCHES IN THE CENTRAL SOUTHERN ALPS

B.1: LOCATION MAP OF ROCK AVALANCHES IN THE CENTRAL SOUTHERN ALPS AS COMPILED FROM WHITEHOUSE AND GRIFFITH (1983)

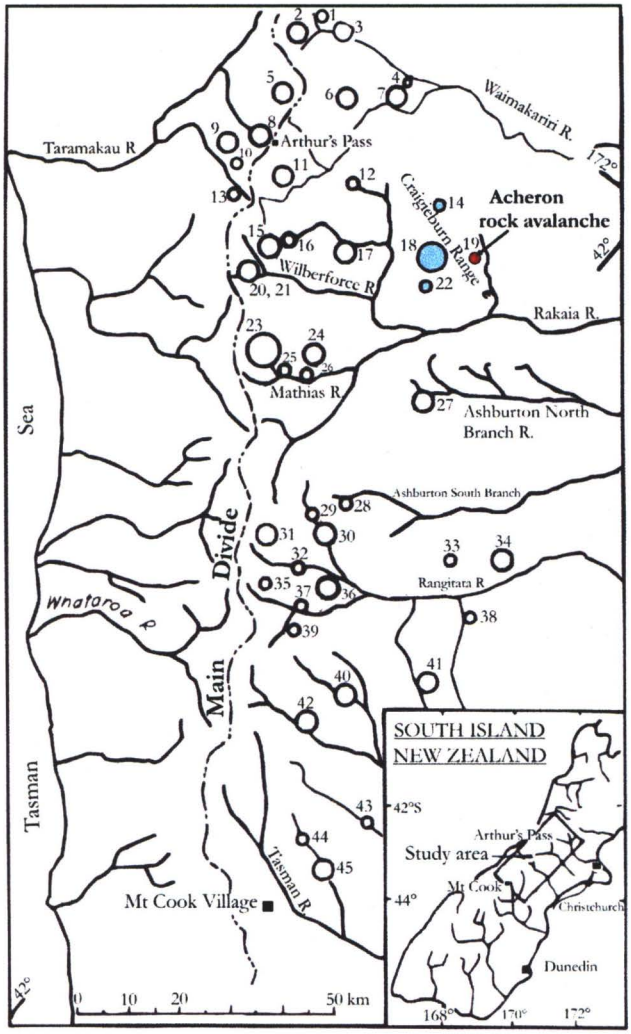

GREYWACKE ROCK AVALANCHES IN THE CENTRAL SOUTHERN ALPS

NOTE: Not including the Round Top rock avalanche deposit.

Table .1: Greywacke rock avalanches in the central Southern Alps (Whitehouse and Griffith, 1983)

	Locality	Deposit Area ($10^4 m^2$)	Thickness (m)	Volume $10^6 m^3$	Age Years B.P.	Dating Method (Whitehouse, 1983)
1	Poulter River (Thompson Stm	48	10 ± 1	4.8 ± 0.5	21	1
2	Poulter River L. Minchin	48	35 ± 3	27 ± 2	?	~
3	Poulter River (Casey Hut)	228	10 ± 1	23 ± 2	4020 +- 90	2
4	Poulter River (Mt Binser)	55	10 ± 2	5.5 ± 1	?	~
5	Falling Mountain (Otehake R.)	190	30 ± 3	57 ± 6	21	1
6	Waimakariri River (Hawdon R.	30	40 ± 3	12 ± 1	2750+-710	3
7	Waimakariri River (Mt Binser)	81	50 ± 5	40 ± 4	9000 ± 2340	3,4
8	Otira River	43	100 ± 5	43 ± 2	2000+-90	2 (4258)
9	Taipo River (Hunts Ck)	63	50 ± 3	35 ± 2	3600 +-940	3
10	Taipo River (Hunts Ck)	21	20 ± 3	4.1 ± 0.6	2750 +-710	3
11	Waimakariri River (Crow R.)	29	100 ± 10	29 ± 3	6100 ± 1580	3
12	Craigieburn Range (Cass Saddle	22	10 ± 2	2.2 ± 0.4	5750 ± 1490	3
13	Taipo River Julia Ck	22	15 ± 2	3.3 ± 0.4	2750 ± 710	3
14	Craigieburn Range	90	5 ± 1	4.5 ± 0.8	3800 ± 990	3, 5
15	Wilberforce River (Weka Stm)	38	50 ± 5	19 ± 2	2140 ± 560	3
16	Wilberforce River (Burnett Stm	36	20 ± 3	7.2 ± 1	7270 ± 90	6 (5509)
17	Avoca River	121	50 ± 3	60 ± 4	5500 ± 1430	3
18	Craigieburn Range Goldney Stm	387	130 ± 8	500 ± 30	350 ± 90	3, 7
19	Acheron River	61	10 ± 2	6.1 ± 1.2	532 ± 50	2, 8 (532)
	Red Hill stream	72	"	9 ± 1	1152 ± 51	This study
20	Wilberforce River (Griffith's Stm A)	95	10 ± 2	9.5 ± 2	7870 ± 120	2 (5009)
21	Wilberforce River (Griffiths Stm B)	~	25 ± 3	24 ± 3	10250 ± 150	2 (5010)
22	Lake Coleridge	23	20 ± 2	4.6 ± 0.4	150 ± 40	3

23	Mathias River (Boundary Ck)	280	100 ± 10	280 ± 28	1500 ± 390	9
24	Mathias River (Mistake Ck)	54	20 ± 2	11 ± 1	2750 ± 710	3
25	Mathias River (Moraine CK)	22	20 ± 3	4.2 ± 0.6	4400 ± 1140	3
26	Mathias River	37	10 ± 1	3.7 ± 0.4	3000 ± 780	9
27	North Ashburton	75	15 ± 2	11 ± 1.5	1560 ± 400	3
28	South Ashburton	70	10 ± 1	7.0 ± 0.7	5280 ± 105	2, 10 (1289)
29	Lawrence River	31	10 ± 1	3.1 ± 0.3	1000 ± 260	3
30	Lawrence River (Hermitage Hut)	70	15 ± 2	10 ± 1	800 ± 210	3
31	Clyde River (McCoy Stm)	31	50 ± 3	15 ± 1	4900 ± 1280	3, 11
32	Clyde River (Watchdog Hut)	50	20 ± 2	10 ± 1	354 ± 28	2 (4901)
33	Rangitata River (Lake Camp)	38	5 ± 1	1.9 ± 0.4	1600 ± 420	3
34	Rangitata River (Pudding Valley)	122	10 ± 1	10 ± 1	1700 ± 440	3
35	Havelock River (Fan Stm)	26	35 ± 3	9.1 ± 0.8	1560 ± 400	3
36	Havelock River (Cloudy Stm)	35	30 ± 3	10 ± 1	3370 ± 880	3
37	Havelock River (McDonald Hut)	38	20 ± 2	7.6 ± 0.8	?	–
38	Rangitata River (Forest Ck)	81	10 ± 1	8.1 ± 0.9	1560 ± 400	3
39	Havelock River (Forbes R.)	13	10 ± 1	1.3 ± 0.1	500 ± 140	3
40	Macaulay River	138	20 ± 2	27 ± 3	8460 ± 120	2, 10 (548)
41	Rangitata River (Bush Stm)	330	30 ± 3	99 ± 10	3370 ± 880	3
42	Godley River (Bloody Pt)	84	25 ± 3	21 ± 3	1700 ± 440	3
43	Cass River	36	10 ± 1	3.6 ± 0.4	1200 ± 310	3
44	Jollie River	23	20 ± 2	4.6 ± 0.5	2750 ± 710	3
45	Jollie River (Arthur's Point)	110	70 ± 4	77 ± 5	1700 ± 440	3

1 Historical Record- Failure during the 1929 Arthur's Pass earthquake
2 Radiocarbon dates using the new Half life (1 standard deviation)
3 Weathering Rind Dates using the method of Chinn (1981)
4 Close to maximum useable age of weathering rinds could be older
5 Minimum age: from talus on avalanche scar
6 Radiocarbon dates from wood samples in silt resulting from the event
7 Whitehouse (1981)
8 Burrows (1976)
9 Weathering Rinds measured to nearest 0.5mm instead of 0.2mm
10 Burrows (1972)
11 Minimum age Buried rinds

Refer to Whitehouse and Griffith (1983) for detailed background to data

APPENDIX C

RADIOCARBON DATING

C.1 EXPLANATORY BACKGROUND ON RADIOCARBON DATING

C.1.1 WHAT IS RADIOCARBON DATING

C.1.2 ORIGIN OF ^{14}CARBON

C.1.3. POTENTIAL ERRORS ASSOCIATED WITH RADIOCARBON DATING

3.1.3.2 ATMOSPHERIC ERRORS
3.1.3.3 INBUILT AGE
3.1.3.4 INFLUENCE OF STRATIGRAPHIC POSITION
3.1.3.5 CONTAMINATION

C.1.4 SAMPLE SELECTION FACTORS

C.1.5 SAMPLE PREPARATION

C.2 UNIVERSITY OF WAIKATO RADIOCARBON AGE DETERMINATION LABORATORY AGE REPORTS AND CALIBRATION DIAGRAMS FOR THE:

C.2.1 ACHERON ROCK AVALANCHE EMPLACEMENT

C.2.2 THE RED HILL VALLEY TRENCH EXCAVATION

C.3. TABLE OF RADIOCARBON AGES

C 1: BACKGROUND INFORMATION ON RADIOCARBON DATING AND SAMPLE SELECTION

C.1.1 WHAT IS RADIOCARBON DATING

Radiocarbon dating measures the half life of ^{14}C, an unstable radioactive isotope which ceases exchanging and begins to decay when a living organism, which is an absorber of ^{14}C, dies. The decay of ^{14}C is exponential following a constant and known rate based on the radioactive decay equation (Hogg, 1982).

During the decay process the ^{14}C atom decay to a ^{14}Nitrogen atom emitting a beta particle in the process which can be measured (Bowman 1990). The residual ^{14}C is then compared to that of modern material containing a known quantity of ^{14}C resulting in a measurable time elapse from the sample's death (Hogg, 1982).

This is calculated according to the Radioactive Decay Equation based on the half life of ^{14}C of 5730 ± 40 years. However, the actual half-life used in the dating procedure is 5568 ± 30 years and is referred to as the Libby half life. This is slightly less accurate but is the agreed standard for sample dating. The useful range for radiocarbon dating is from 200 years to 35, 000 years Before Present (Hogg, 1982).

C.1.2 ORIGIN OF ^{14}CARBON

^{14}Carbon is derived from the reaction between neutrons, generated by incoming cosmic rays, on atmospheric nitrogen atoms producing a proton and forming ^{14}C (Hogg, 1982). This carbon immediately oxidises forming CO^2 which joins the carbon cycle entering organic systems via nutrients or photosynthesis therefore making organic material ideal for dating. This application is based on the assumption that equilibrium exists between ^{14}C generation and radioactive decay through time. Wood in particular is considered an excellent type of sample to radiocarbon date, even when in poor condition. This is because it does not exchange easily with modern carbons (Hogg, 1982).

C.1.3.1 POTENTIAL SAMPLE ERRORS ASSOCIATED WITH RADIOCARBON DATING

Radiocarbon dating is inherently prone to atmospheric induced errors and unknown sample history as outlined below. It is also important that the observer understands that it does not provide an exact date, but rather ranges of age based on probability using Gaussian distribution curves.

C.1.3.2 ATMOSPHERIC ERRORS

Fluctuations of incoming solar radiation cause variations in the geomagnetic field which can alter the amount of ^{14}C production causing a series of highs and lows within a sample. Cosmic rays are charged particles so therefore can be deflected by a magnetic field (Bowman, 1990). When the magnetic field is increased less ^{14}C is produced and consequentially if there is a reduction in the magnetic intensity more ^{14}C is produced. This disparity is thought to be linked to sunspot behaviour (Bowman, 1990).

Atomic bomb detonations cause what is referred to as carbon bombs or abrupt increases in the level of ^{14}C in the atmosphere (Bowman, 1990). This is also seen with the onset of the industrial age with the combustion of fossil fuels which can be identified in the tree ring radiocarbon record.

C.1.3.3 INBUILT AGE

The field situation is pivotal in the choice of a sample and particularly its inbuilt age. This refers to the time lapse between the date of the life and death of the sample and the date of an event (McFadgen, 1982). Inbuilt age represents the growth age, or the living age of the tree and the storage age, or the time between death and the occurrence of the event (McFadgen, 1982). McFadgen (1982) considered that both the storage age and the tree age or growth age are required to gain the actual total inbuilt age. This could result in the sample being several hundred years older than the actual age of the event (McFadgen, 1982).

Table C.1: Kinds of radiocarbon samples listed according to the "inbuilt" age (from McFadgen, 1982).

Negligible Inbuilt Age	Unknown, possibly large Inbuilt Age
Wood and charcoal known to be from short-lived trees.	Unidentified wood and charcoal
Twigs and small sticks Outer rings of trees	Wood and charcoal known to be from long-lived trees
Bones and shells in middens	Non-midden disarticulated bones
Bones in position of articulation	Non-midden disarticulated bivalves
Bivalves in position of articulation	Non-midden gastropods

C.1.3.4 INFLUENCE OF STRATIGRAPHIC POSITION

Often in a stratigraphic situation, an event horizon is represented by a layer. It is important to correctly interpret the stratigraphic situation to reduce any disassociation of the sample to the event (Hogg, 1982). McFadgen (1982) identified three stratigraphic positions that can occur relative to the event layer; above, within or below. With the use of an inbuilt age, two variations of position emerge; no inbuilt age or an unknown - possibly high inbuilt age. The combination of both inbuilt age and stratigraphic position results in a date that can be classified as maximum, close, minimum or unknown (McFadgen, 1982). The ideal sample should have a known negligible inbuilt age, retrieved from a contemporaneous position giving a close result for the event.

Table C.2: Classification of Radiocarbon 'dates' for dating events (McFadgen, 1982)

	Stratigraphic relationship of sample to event		
Inbuilt Age	**Below Sample**	**Contemporary**	**Above Sample**
Negligible	Maximum Age	Close	Minimum Age
Unknown, Possibly Large	Maximum Age	Maximum Age	Unknown Age

C.1.3.5 CONTAMINATION

Radiocarbon dating follows the assumption that only radioactive decay alters the level of ^{14}C within a sample following its removal from the influence of the Biosphere (Bowman, 1990). However, outside influences may also alter the level of ^{14}Carbon in the sample completely. Buried wood can be exposed to residual inflow of organic carbons from an outside source through a process called organic carbon drift. This process produces younger dates than the actual wood age. Carbon drift is made up of three different types of Carbon and requires a harsh treatment of a sodium based chemical to isolate the original humid carbon for dating something not done in conventional sample preparation in most radiocarbon laboratories (pers. comm. Molloy, 2003). Contamination of the sample can also occur unknowingly during both collection and storage of the sample. These can include outside contaminants such as pollen, tobacco, ash, grease, petroleum based cleaning products on extraction and cutting equipment. Paper packaging, coffee, sugar and mould could also affect results (Hogg, 1884).

C.1.4 SAMPLE SELECTION FACTORS

The objective when using radiocarbon methods for dating an event is to find a sample that will reduce the time gap between the sample death and the event. With correctly interpreted stratigraphy this means finding a piece of wood best representing the time or age of the event with the smallest possible inbuilt age (McFadgen, 1982). This is based on the assumption that the time of death and cessation of radioactive exchange with the biosphere are contemporary. If this is not the case then the radiocarbon age is not zero (Bowman, 1990).

The youngest part of a tree is a layer located between the outer bark layer and the sapwood called the Cambium layer (Bowman, 1990). It is here that the growth region of a tree exists in a layer made up of a thin band of cells. Division of these cells causes new bark to be added to the outer of the Cambium and new sapwood to the inside (Bowman, 1990). It is this process that adds rings to a tree and generally occurs annually. Interestingly, once the rings are laid down they do not exchange with biosphere giving a variation of ^{14}Carbon across the tree diameter (Bowman, 1990).

The portion of a tree which gives the oldest age date is found in the lower trunk regions and in the central heart wood. Any radiocarbon dating of this region should be made in conjunction with an accurate count of the annual growth rings to correct for the growth age of the tree. If rings are disfigured or unreadable the sample will have unknown and potentially large inbuilt ages affecting the credibility of the date. Trees generally develop a growth ring annually however; this can vary due to other factors such as access to sunlight through the canopy. In beech forest, competing saplings waiting for a break in the canopy layer slow down their growth rate effectively stunting their development (Prof Butterfield pers comm., 2003). With the death of a tree and subsequent space availability, a period of rapid growth takes place causing inconsistencies to the assumed annual growth of the tree rings.

Comparably, wood fragments such as twigs and small branches are also considered good samples for dating because their life span is short and perhaps best represent the actual event by having reliable negligible inbuilt ages (McFadgen, 1982).

Knowledge of the tree is important for understanding life span and gives important information about a sample particularly its suitability. Mountain beech such as that retrieved from the Acheron rock avalanche lives approximately 300 years and has one of the lowest wood fibre densities in New Zealand allowing it to break down rapidly giving it a lower inbuilt age compared to a hard wood species (Prof Butterfield pers comm., 2003).

The use of buried soils for dating is far more susceptible to large errors in interpretation than wood samples mainly due to the uncertainty of the actual sample being dated (Trumbore, 2000). This is because soil is derived from a mixture of material of differing ages and origins. Consideration therefore must be given to the component of sample being dated (Trumbore, 2000).

Charcoal is often used in radiocarbon dating due to the high quantity of carbon and its ability to be well preserved however it is subject to several uncertainties (Trumbore, 2000). The primary problem is the unknown inbuilt age of the charcoal which could be derived from inherited

material transported from another source reflecting an age of the wood source rather than the time of burning or that of its position within the stratigraphy (Trumbore, 2000).

When collecting samples for Radiocarbon age estimates it is wise to consider that the evidence is only ever circumstantial and therefore as with the application of rock avalanches as paleoseismic indicators, independent lines of evidence must be compiled which converge toward an appropriate age.

C.1.5 SAMPLE PREPARATION

The preparation of the samples is well established and tested in today's labs. It involves the scraping clean of the surface of sample, chopping up of the entire sample into splinters which is washed in an ultra-sonic bath.

Because the sample is chopped up into splinters any date would have to be considered as an average range of the youngest and oldest parts of the sample therefore consideration must be given to choice of sample for example a cross-section of a tree would be sampled from the outer ten growth rings.

The samples are then subject to the ABA pre-treatment to remove outside impurities. This involves washing the wood in hot 10% HCL, followed by a rinsing and subsequent treatment with hot 1% NaOH. The sample is then rinsed and finally dried.

C 2: WAIKATO UNIVERSITY RADIOCARBON AGE REPORTS AND CALIBRATION DIAGRAMS

Conventional ages presented in the reports for radiometric age determinations, represent solely the amount of Carbon within a sample but fail to take into account the highly elastic variability of the ^{14}C content in the atmosphere which influences the age estimates (Taylor et al. 1996). The conventional radiocarbon ages (given in the age reports by Waikato Radiocarbon laboratory) are therefore calibrated against the international calibration curve for terrestrial samples, to produce the calibrated ages referred to in the graphs. They are also adjusted for New Zealand by applying the New Zealand correction of 27 ± 5 yrs.

The results are displayed in cal years Before Present - 1950 however they can also be in cal BC/AD nomenclature, but generally that terminology is used only by archaeologists. (A. Hogg, pers comm. 2003). These age results can be viewed in the calibration diagrams in the next section of Appendix C.2. and C.3.

For the purpose of this study all ages have been presented as conventional ages to maintain consistency when comparing other radiocarbon ages in literature which are also often presented in conventional format but also due to the inconsistencies in the calculation and presentation of calibrated age results.

It is important to note that conventional ages do not give a real-time age estimate however the inclusion of the calibration plots following the age reports and Tables 3.1-3.2 in Appendix 3.3 will enable the reader to obtain calibrated ages.

C.2. 1 INVESTIGATION OF THE EMPLACEMENT AGE FOR THE ACHERON ROCK AVLANCHE DEPOSIT

The University of Waikato
Radiocarbon Dating Laboratory

Private Bag 3105
Hamilton,
New Zealand.
Fax +64 7 838 4192
Ph +64 7 838 4278
email c14@waikato.ac.nz
Head: Dr Alan Hogg

Report on Radiocarbon Age Determination for Wk- 12093

Submitter	DH Bell
Submitter's Code	Acheron 1
Site & Location	Lowest extend of a rock avalanche deposit at the distal end of an incising fluvial system., New Zealand
Sample Material	Buried tree fragment cut in half
Physical Pretreatment	Surfaces scraped clean. The wood was chopped up into small splinters and washed in ultrasonic bath.
Chemical Pretreatment	Sample was washed in hot 10% HCl, rinsed and treated with hot 1% NaOH. The NaOH insoluble fraction was treated with hot 10% HCl, filtered, rinsed and dried.

$d^{14}C$	-154.8 ± 4.4	‰
$\delta^{13}C$	-27.0 ± 0.2	‰
$D^{14}C$	-151.4 ± 5.4	‰
% Modern	84.9 ± 0.5	%
Result	**1319 ± 51 BP**	

Comments

AGHogg
05/02/03

- Result is *Conventional Age or % Modern* as per Stuiver and Polach, 1977, Radiocarbon 19, 355-363. This is based on the Libby half-life of 5568 yr with correction for isotopic fractionation applied. This age is normally quoted in publications and must include the appropriate error term and Wk number.
- Quoted errors are 1 standard deviation due to counting statistics multiplied by an experimentally determined Laboratory Error Multiplier of 1.217 .
- The isotopic fractionation, $\delta^{13}C$, is expressed as ‰ wrt PDB.
- Results are reported as *% Modern* when the conventional age is younger than 200 yr BP.

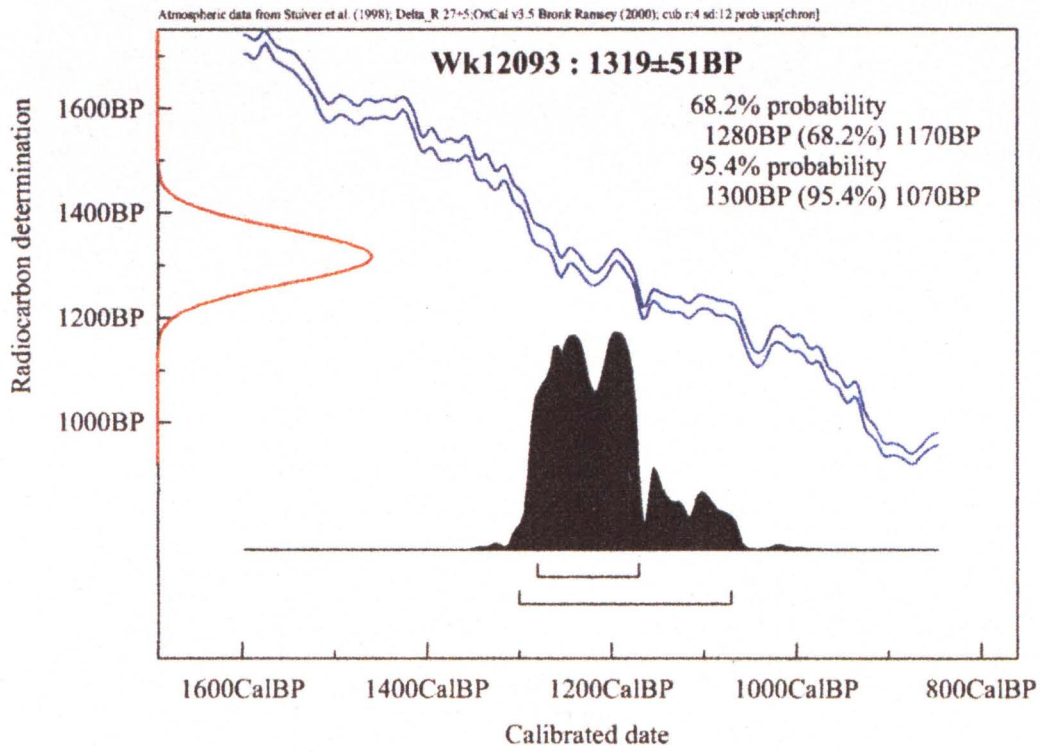

Calibration diagram of sample WK 12093: 1319 ± 51 yrs B.P. basal wood fragment from near distal limit of debris (site one)

The University of Waikato

Radiocarbon Dating Laboratory

Private Bag 3105
Hamilton,
New Zealand.
Fax +64 7 838 4192
Ph +64 7 838 4278
email c14@waikato.ac.nz
Head: Dr Alan Hogg

Report on Radiocarbon Age Determination for Wk- 12094

Submitter	DH Bell
Submitter's Code	Acheron 2
Site & Location	Lowest extend of a rock avalanche deposit at the distal end of an incising fluvial system., New Zealand
Sample Material	
Physical Pretreatment	Surfaces scraped clean. The wood was chopped up into small splinters and washed in ultrasonic bath.
Chemical Pretreatment	Sample was washed in hot 10% HCl, rinsed and treated with hot 0.5% NaOH. The NaOH insoluble fraction was treated with hot 10% HCl, filtered, rinsed and dried.

$d^{14}C$	-132.3 ± 4.5	‰
$\delta^{13}C$	-24.3 ± 0.2	‰
$D^{14}C$	-133.7 ± 5.5	‰
% Modern	86.6 ± 0.5	%
Result	**1152 ± 51 BP**	

Comments

AG Hogg

05/02/03

- Result is *Conventional Age or % Modern* as per Stuiver and Polach, 1977, Radiocarbon 19, 355-363. This is based on the Libby half-life of 5568 yr with correction for isotopic fractionation applied. This age is normally quoted in publications and must include the appropriate error term and Wk number.
- Quoted errors are 1 standard deviation due to counting statistics multiplied by an experimentally determined Laboratory Error Multiplier of 1.217 .
- The isotopic fractionation, $\delta^{13}C$, is expressed as ‰ wrt PDB.
- Results are reported as *% Modern* when the conventional age is younger than 200 yr BP.

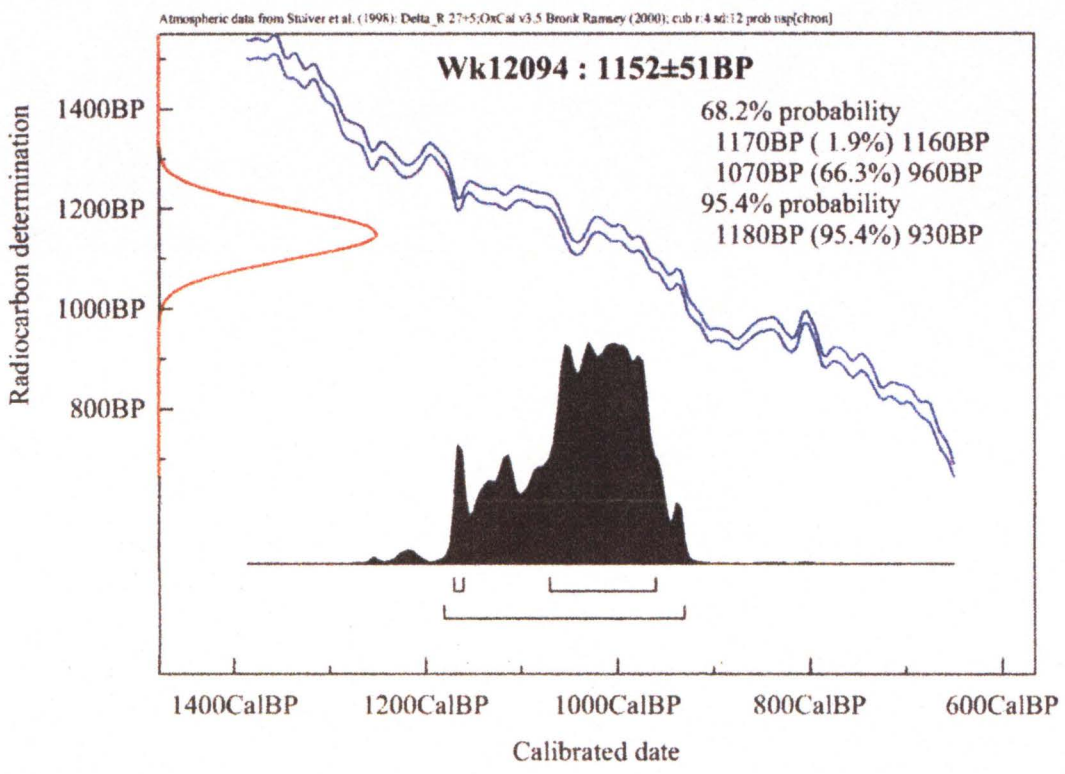

Calibration diagram for sample WK 12094: 1152 ± 51 yrs B.P. buried tree (site four)

The University of Waikato

Radiocarbon Dating Laboratory

Private Bag 3105
Hamilton,
New Zealand.
Fax +64 7 838 4192
Ph +64 7 838 4278
email o14@waikato.ac.nz
Head: Dr Alan Hogg

Report on Radiocarbon Age Determination for Wk- 12095

Submitter	DH Bell
Submitter's Code	Acheron 3
Site & Location	Lowest extend of a rock avalanche deposit at the distal end of an incising fluvial system., New Zealand
Sample Material	Wood
Physical Pretreatment	Surfaces scraped clean. The wood was chopped up into small splinters and washed in ultrasonic bath.
Chemical Pretreatment	Sample was washed in hot 10% HCl, rinsed and treated with hot 0.5% NaOH. The NaOH insoluble fraction was treated with hot 10% HCl, filtered, rinsed and dried.

$d^{14}C$	-143.8 ± 4.5	‰
$\delta^{13}C$	-25.9 ± 0.2	‰
$D^{14}C$	-142.2 ± 5.5	‰
% Modern	85.8 ± 0.6	%
Result	**1232 ± 52 BP**	

Comments

AGHogg

05/02/03

- Result is *Conventional Age or % Modern* as per Stuiver and Polach, 1977, Radiocarbon 19, 355-363. This is based on the Libby half-life of 5568 yr with correction for isotopic fractionation applied. This age is normally quoted in publications and must include the appropriate error term and Wk number.
- Quoted errors are 1 standard deviation due to counting statistics multiplied by an experimentally determined Laboratory Error Multiplier of 1.217 .
- The isotopic fractionation, $\delta^{13}C$, is expressed as ‰ wrt PDB.
- Results are reported as *% Modern* when the conventional age is younger than 200 yr BP.

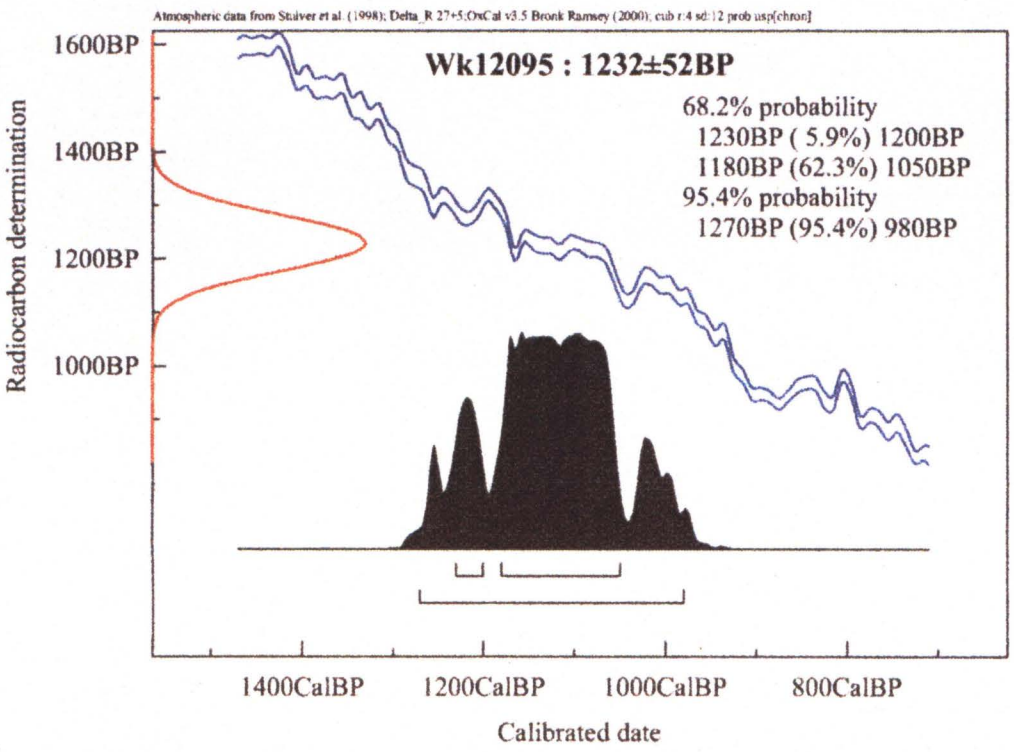

Calibration diagram for sample WK12095: 1232 ± 52 yrs B.P. twig sample (site four)

The University of Waikato

Radiocarbon Dating Laboratory

Private Bag 3105
Hamilton,
New Zealand.
Fax +64 7 838 4192
Ph +64 7 838 4278
email c14@waikato.ac.nz
Head: Dr Alan Hogg

Report on Radiocarbon Age Determination for Wk- 12096

Submitter	DH Bell
Submitter's Code	Acheron 4
Site & Location	Lowest extend of a rock avalanche deposit at the distal end of an incising fluvial system., New Zealand
Sample Material	Wood
Physical Pretreatment	Surfaces scraped clean. The wood was chopped up into small splinters and washed in ultrasonic bath.
Chemical Pretreatment	Sample was washed in hot 10% HCl, rinsed and treated with hot 0.5% NaOH. The NaOH insoluble fraction was treated with hot 10% HCl, filtered, rinsed and dried.

$d^{14}C$	-154.0 ± 4.5	‰
$\delta^{13}C$	-26.0 ± 0.2	‰
$D^{14}C$	-152.3 ± 5.5	‰
% Modern	84.8 ± 0.5	%
Result	**1327 ± 52 BP**	

Comments

AGHogg

05/02/03

- Result is *Conventional Age or % Modern* as per Stuiver and Polach, 1977, Radiocarbon 19, 355-363. This is based on the Libby half-life of 5568 yr with correction for isotopic fractionation applied. This age is normally quoted in publications and must include the appropriate error term and Wk number.
- Quoted errors are 1 standard deviation due to counting statistics multiplied by an experimentally determined Laboratory Error Multiplier of 1.217 .
- The isotopic fractionation, $\delta^{13}C$, is expressed as ‰ wrt PDB.
- Results are reported as *% Modern* when the conventional age is younger than 200 yr BP.

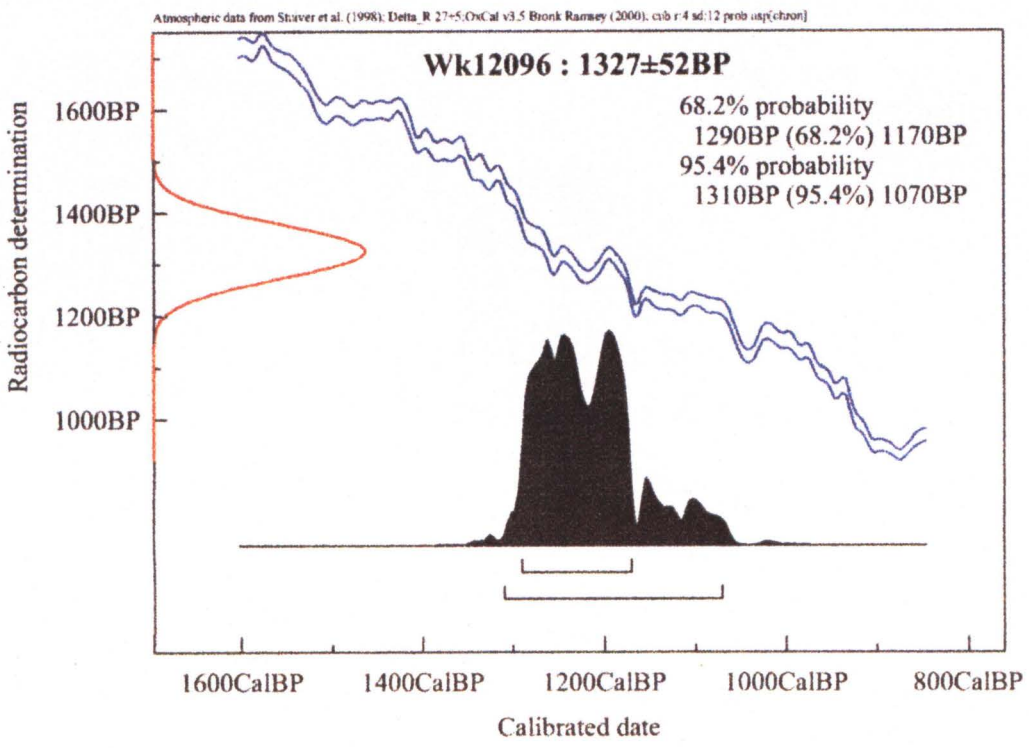

Calibration diagram for sample WK 12096: 1327 ± 52 yrs B.P. Bark Fragments (site four)

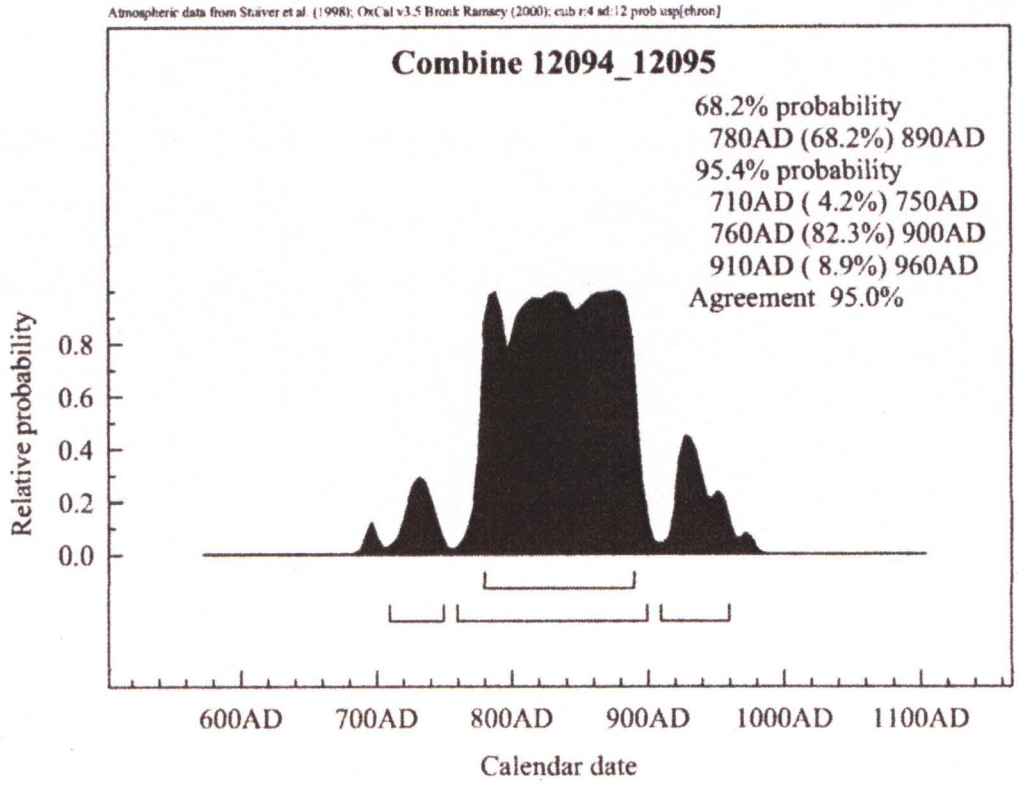

Combined calibration diagram (WK 12094 buried tree – WK 12095 twig) demonstrating the overlap of ages or statistical similarity between the two most contemporaneous samples retrieved from the base of the rock avalanche

C.2.2 AGE DETERMINATION AND CALIBRATION DAIGRAMS FOR THE BURIED SOIL HORIZONS EXPOSED IN THE RED HILL VALLEY TRENCH

UPPER PALEOSOL (2B) See Fig 5.8 Trench log for stratigraphic position

(a) WK 13033: 765 ± 42 YEARS B.P. SOIL AMS by Rafter Laboratory

LOWER PALEOSOL (2A) See Fig 5.8 Trench log for stratigraphic position

(b) WK 13034 661 ± 34 YEARS B.P. SOIL radiometric counting

(c) WK 13112 653 ± 54 YEARS B.P. CHARCOAL radiometric counting

Private Bag 3105
Hamilton,
New Zealand.
Fax +64 7 838 4192
Ph +64 7 838 4278
email c14@waikato.ac.nz
Head: Dr Alan Hogg

Report on Radiocarbon Age Determination for Wk- 13033

(AMS measurement by IGNS [NZA-18113])

Submitter	G Smith
Submitter's Code	ARADT1
Site & Location	Porters Pass Fault, New Zealand
Sample Material	Soil, organics
Physical Pretreatment	Visible contaminants removed.
Chemical Pretreatment	Washed in hot 10% HCl, rinsed and treated with hot 1% NaOH. The NaOH insoluble fraction was treated with hot 10% HCl, filtered, rinsed and dried.

$d^{14}C$	-93.9 ± 4.5	‰
$\delta^{13}C$	-28.7 ± 0.2	‰
$D^{14}C$	-90.8 ± 4.8	‰
% Modern	90.9 ± 0.5	%
Result	**765 ± 42 BP**	

Comments

AG Hogg
26/8/03

- Result is *Conventional Age or % Modern* as per Stuiver and Polach, 1977, Radiocarbon 19, 355-363. This is based on the Libby half-life of 5568 yr with correction for isotopic fractionation applied. This age is normally quoted in publications and must include the appropriate error term and Wk number.
- Quoted errors are 1 standard deviation due to counting statistics multiplied by an experimentally determined Laboratory Error Multiplier of 1 .
- The isotopic fractionation, $\delta^{13}C$, is expressed as ‰ wrt PDB.
- Results are reported as *% Modern* when the conventional age is younger than 200 yr BP.

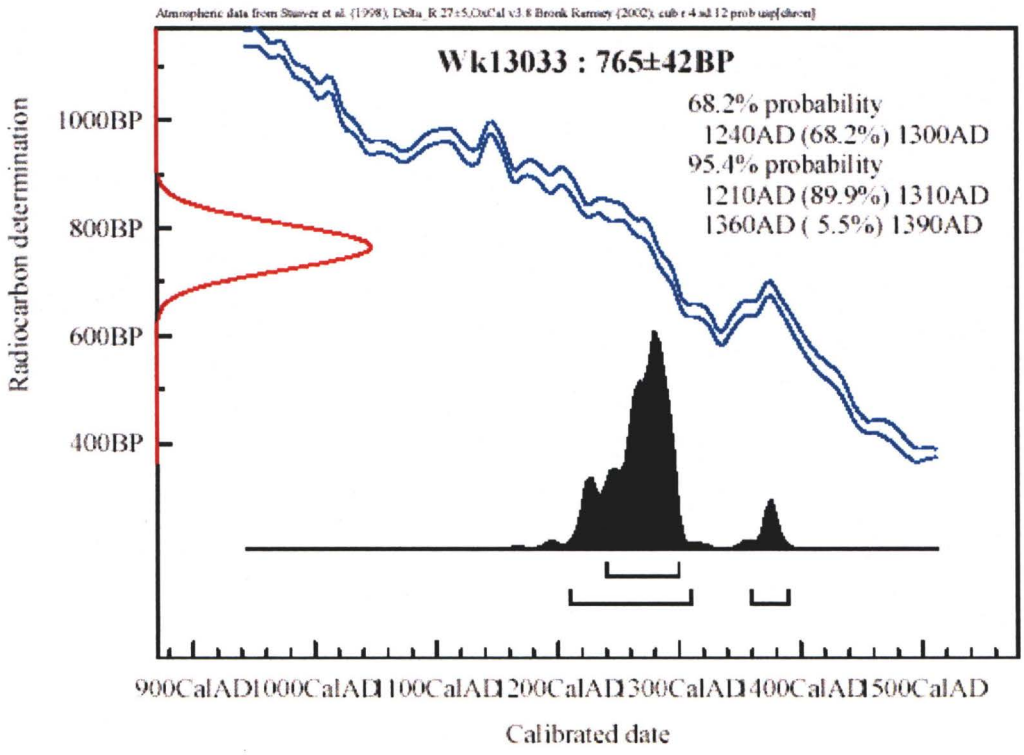

UPPER PALEOSOL (2B) See Fig 5.8 Trench log for stratigraphic position			
(a) WK 13033:	765 ± 42 YEARS B.P.	SOIL	AMS by Rafter Laboratory

The University of Waikato

Radiocarbon Dating Laboratory

Private Bag 3105
Hamilton,
New Zealand.
Fax +64 7 838 4192
Ph +64 7 838 4278
email c14@waikato.ac.nz
Head: Dr Alan Hogg

Report on Radiocarbon Age Determination for Wk- 13034

Submitter	G Smith
Submitter's Code	ARADT4
Site & Location	Porters Pass Fault, New Zealand
Sample Material	Soil, organics
Physical Pretreatment	Visible contaminants removed.
Chemical Pretreatment	Washed in hot 10% HCl, rinsed and treated with hot 1% NaOH. The NaOH insoluble fraction was treated with hot 10% HCl, filtered, rinsed and dried.

$d^{14}C$	-84.4 ± 3.9	‰
$\delta^{13}C$	-28.0 ± 0.2	‰
$D^{14}C$	-79.0 ± 3.9	‰
% Modern	92.1 ± 0.4	%
Result	**661 ± 34 BP**	

Comments

AG Hogg

26/8/03

- Result is *Conventional Age or % Modern* as per Stuiver and Polach, 1977, Radiocarbon 19, 355-363. This is based on the Libby half-life of 5568 yr with correction for isotopic fractionation applied. This age is normally quoted in publications and must include the appropriate error term and Wk number.
- Quoted errors are 1 standard deviation due to counting statistics multiplied by an experimentally determined Laboratory Error Multiplier of 1 .
- The isotopic fractionation, $\delta^{13}C$, is expressed as ‰ wrt PDB.
- Results are reported as % *Modern* when the conventional age is younger than 200 yr BP.

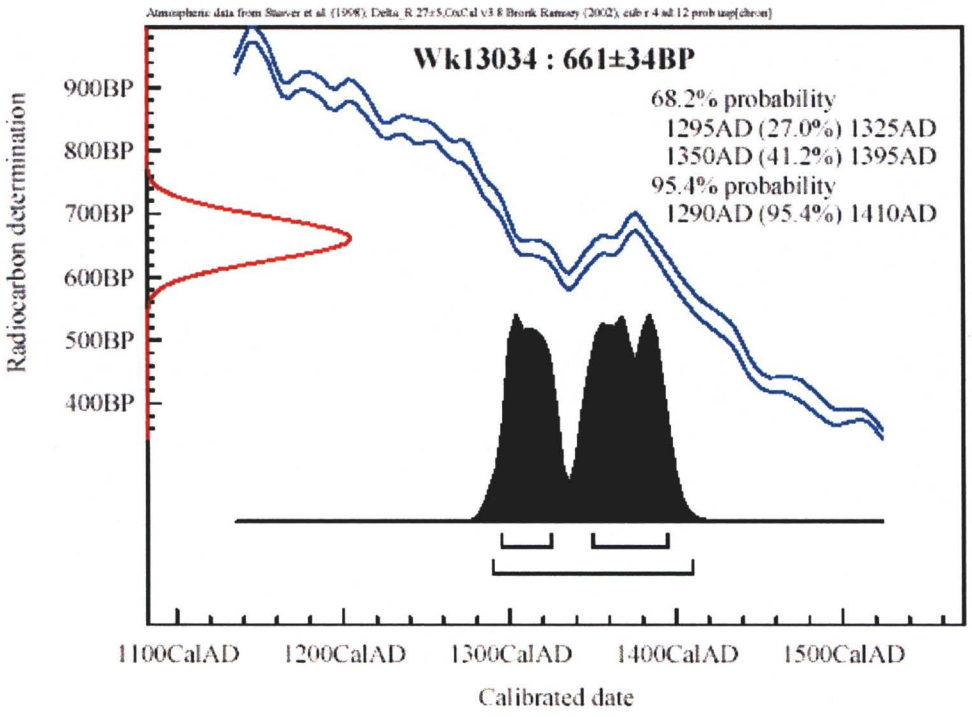

LOWER PALEOSOL (2A) See Fig 5.8 Trench log for stratigraphic position			
(b) WK 13034	661 ± 34 YEARS B.P.	SOIL	radiometric counting

The University of Waikato

Radiocarbon Dating Laboratory

Private Bag 3105
Hamilton,
New Zealand.
Fax +64 7 838 4192
Ph +64 7 838 4278
email c14@waikato.ac.nz
Head: Dr Alan Hogg

Report on Radiocarbon Age Determination for Wk- 13112

Submitter	G Smith
Submitter's Code	ARADT3
Site & Location	.
Sample Material	Charcoal
Physical Pretreatment	Possible contaminants were removed. Washed in ultrasonic bath.
Chemical Pretreatment	Sample washed in hot 10% HCl, rinsed and treated with hot 0.5% NaOH. The NaOH insoluble fraction was treated with hot 10% HCl, filtered, rinsed and dried.

$d^{14}C$	-77.3 ± 6.2	‰
$\delta^{13}C$	-24.6 ± 0.2	‰
$D^{14}C$	-78.0 ± 6.2	‰
% Modern	92.2 ± 0.6	%
Result	**653 ± 54 BP**	

Comments

AGHogg

26/8/03

- Result is *Conventional Age or % Modern* as per Stuiver and Polach, 1977, Radiocarbon 19, 355-363. This is based on the Libby half-life of 5568 yr with correction for isotopic fractionation applied. This age is normally quoted in publications and must include the appropriate error term and Wk number.
- Quoted errors are 1 standard deviation due to counting statistics multiplied by an experimentally determined Laboratory Error Multiplier of 1 .
- The isotopic fractionation, $\delta^{13}C$, is expressed as ‰ wrt PDB.
- Results are reported as *% Modern* when the conventional age is younger than 200 yr BP.

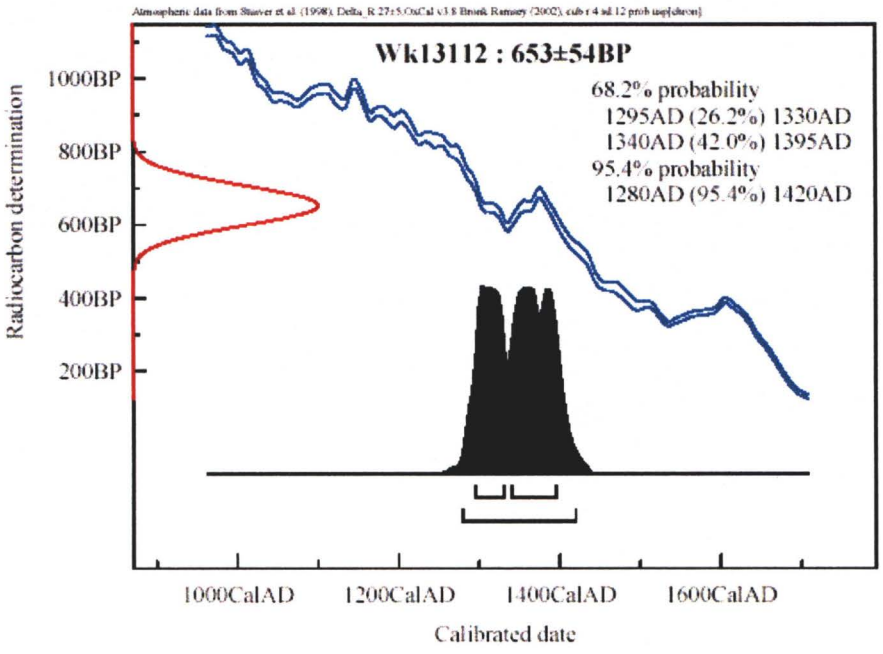

LOWER PALEOSOL (2A) See Fig 5.8 Trench log for stratigraphic position			
(c) WK 13112	653 ± 54 YEARS B.P.	CHARCOAL	radiometric counting

Table C.3: Radiocarbon dates for the new age of the Acheron rock avalanche and the buried soils in the trench excavated across the Porters Pass Fault in the Red Hill valley (this study).

SAMPLE NUMBER	SAMPLE LOCATION AND DESCRIPTION	GRID REFERENCE NZMS 260, 1988	CONVENTIONAL (YEARS B.P.)	RADIOCARBON AGE CALIBRATED (YEARS B.P.) 2 sigma	Confidence	1sigma	Confidence
	ACHERON ROCK AVALANCHE						
Wk 12093	Distal (basal material) wood fragment	2401840 E 5764010 N	1319 ± 51	1185 ± 115	95.40%	1225 ± 55	68.20%
Wk 12094	Contact (site 3) buried tree	2401725 E 5764420 N	1152 ± 51	1055 ± 125	95.40%	1015 ±55	66.30%
						1165 ± 5	1.90%
Wk 12095	Contact (site 3) twig	" " "	1232 ± 52	1125 ± 145	95.40%	1115 ± 65	62.30%
						1215 ± 15	5.90%
Wk 12096	Contact (site 3) bark fragments	" " "	1327 ± 52	1190 ± 120	95.40%	1230 ± 60	68.20%
	RED HILL VALLEY TRENCH						
Wk 13034	Lower buried soil horizon	2401700 E 5764870 N	661 ± 34	600 ± 60	95.40%	578 ± 23	41.20%
						640 ± 15	27.00%
Wk 13112	Lower buried soil charcoal fragments	" " "	653 ± 54	600 ± 70	95.40%	583 ± 28	42.00%
						638 ± 18	26.20%
Wk 13033	Upper buried soil (AMS)	" " "	765 ± 42	690 ± 50	89.90%	680 ± 30	68.20%
				575 ± 15	5.50%		

Table C.4: Summary of Radiocarbon ages for event one at Porters Pass in Howard (2001) and sample NZ547 in Burrows (1975)

SAMPLE NUMBER	SAMPLE LOCATION AND DESCRIPTION	GRID REFERENCE NZMS 260, 1988	CONVENTIONAL (YEARS B.P.)	RADIOCARBON AGE CALIBRATED (YEARS B.P.) 2 sigma	Confidence	1sigma	Confidence
	TRENCH 4 - Porters Pass Peat Samples						
Wk 9236	Upper Age Bracket	2408100E 5767100N	980 ± 50	865 ± 105	94.40%	945 ± 5	3.30%
						920 ± 15	20.30%
						845 ± 15	18.40%
						802 ± 8	10.80%
Wk 9241	Lower Age Bracket	" " "	1662 ± 53	1600 ± 145	97.70%	1680 ± 5	5.00%
						1570 ± 45	53.60%
Wk 9242	Event two lower bracket	" " "	2466 ± 55	2550 ± 200	99.60%	2540 ± 180	95.00%
Wk 9234	Test pit 3km west of Trench 4 - Buried peat	2406700E 5767200N	1042 ± 46	1040 ± 15	13.30%	949 ± 22	50.90%
				962 ± 50	73.50%		
				804 ± 5	1.30%		
NZ 547	Buried Tree (Burrows, 1975) in Howard, 2001	approx 2401840E 5764010N	500 ± 69	645 ± 60	22.20%	615 ± 1	0.80%
				520 ± 50	69.50%	530 ± 20	48.10%

REFER HOWARD 2001- APPENDIX C1 FOR CALIBRATION DIAGRAMS

APPENDIX D

D.1 RUN OUT PROFILE FORDAN LONG RUNOUT SIMULATION

Profile Data for the Acheron Rock Avalanche Runout

Applied to the DAN Runout Simulation to represent fragmentation induced long runout

Distance along profile (m)	Elevation of present day surface (m sl)	Elevation of inferred runout path (m sl)	Elevation of source rock mass (m sl)	Path Width (m)
0	1512	1515	1515	189
100	1428	1400	1512	265
200	1375	1325	1500	265
300	1310	1290	1480	189
400	1285	1285	1400	208
500	1260	1240	1240	208
600	1215	1195	~	208
700	1185	1165	~	170.6
800	1165	1165	~	151.7
900	1137	1127	~	265
1000	1110	1100	~	208
1100	1080	1070	~	170.6
1200	1057	1047	~	227
1300	1035	1025	~	360
1400	1015	1005	~	398
1500	997	987	~	322
1600	967	957	~	265
1700	955	945	~	208
1800	937	927	~	208
1900	928	921	~	265
2000	910	903	~	322
2100	900	893	~	379
2200	892	885	~	322
2300	887	880	~	322
2400	880	873	~	284
2500	879	872	~	417
2600	875	868	~	341
2700	865	858	~	322
2800	855	850	~	322
2900	850	845	~	436
3000	847	842	~	265
3100	840	835	~	265
3200	843	838	~	189

3300	825	823	~	94
3400	823	821	~	94
3500	818	816	~	94
3600	817	815	~	94
3700	817	815	~	94

NOTE: *(m above sea level - msl)*

D.2 DATA FROM SIMULATION TRIAL

NON-FRAGMENTING EARTHPRESSURE COEFFICIENTS

Earth pressure coefficients				K_o *0.5*	K_a *0.2*	K_p *4.9*		
16	*3657*	*14.91*	*10.77*	*0.27*	*81.28*	~	*9417854*	*959141*
18	2973.1	16.31	12.74	0.29	81.28	~	9417854	851188
20	2551.3	17.92	14.18	0.32	76.42	~	9417854	650370
22	2227.6	20.11	15.83	0.37	74..94	~	9417854	537389
24	1867.8	22.09	17.59	0.41	78.97	~	9417854	429741
26	1514.4	23.25	19.37	0.43	67.71	57.3	9417854	343,100.00
27	1451.3	24.18	19.65	0.45	67.8	51.16	9417854	323467
28	616.28	28.85	27.88	0.55	10.65	28.22	9417854	135096
30	630.79m	29.02	27.68	0.55	14.15	33.32	9417854	138231
34	525.25m	29.7	28.74	0.57	6.92	11.34	9417854	117007

OPTIMUM SIMULATION SETTING

Number of Blocks	*Shape Factor*	*Length of Simulation*	*Time Step*	*Bulk Density*	*Boundary Condition*	*Volume Change*
21	0.67	250 sec	0.02	20	0	0

FRAGMENTING EARTH PRESSURE COEFFICIENTS

Internal Friction Angle Ø	Runout Distance (m)	Travel Angle (o°)	Fahrböschung f (o°)	Ratio	Maximum Velocity Km\ hr	Runout Time (seconds)	Volume m^3	Final Area m^2
Earth	***pressure coefficients***			***K_o 5.5***	***K_a 5.2***	***K_p 9.9***		
24	3604.9	16.89	10.99	0.3	150.05	71.52	941, 7854	914, 326
25	3521.5	17.61	11.29	0.31	152.41	63.82	941, 7854	938, 767
26	3450.9	17.67	11.41	0.32	155.47	64.38	941, 7855	872, 498
27	*3475.9*	*18.05*	*11.35*	*0.33*	*164.46*	*55.48*	*941, 7856*	*877, 023*
28	3013.2	18.38	12.61	0.33	142.65	50.54	941, 7857	823, 182
29	2860.3	18.81	13.16	0.34	138.31	53.2	941, 7858	772, 664.
30	2804.3	19.13	13.35	0.35	140.01	47.78	941, 7859	743, 740
31	2505.9	19.49	14.4	0.35	120.16	42.72	941, 7860	663, 406
32	2436	19.79	14.79	0.36	118.32	34	941, 7861	624, 380
33	2543.4	20.13	14.21	0.37	138.24	37.02	941, 7862	690, 391
34	2481	20.47	14.54	0.37	137.15	34.74	941, 7863	659, 335
35	2218.7	20.77	15.88	0.38	118.25	33.06	941, 7864	555, 656
Earth pressure coefficients				***K_o 6.5***	***K_a 6.2***	***K_p 10.9***		
24	3652	16.28	10.79	0.29	139.11	71.32	941, 7854	896010
25	3529.4	16.69	11.23	0.3	148.94	68.66	941, 7854	896010
26	*3345.9*	*17.05*	*11.72*	*0.31*	*146.31*	*74.14*	*941, 7854*	*862243*
27	3290.3	17.43	11.87	0.31	151.23	60	941, 7854	891986
28	3020.2	17.83	12.58	0.32	138.88	54.16	941, 7854	804193
29	3053.5	18.09	12.48	0.33	150.77	47.94	941, 7854	837978
30	3016.5	18.43	12.6	0.33	155.29	48.72	941, 7854	819, 653
31	2850.2	18.73	13.07	0.34	148.42	48.42	941, 7854	776564
32	2749	19	13.53	0.34	146.7	42.6	941, 7854	731073
33	2647.5	19.28	13.83	0.35	145.05	36.46	941, 7854	705173
34	2572.3	19.55	14.09	0.35	144.61	36.76	941, 7854	679410
35	2508.8	19.86	14.38	0.36	144.27	35.56	941, 7854	680994

APPENDIX E
GROUND PENETRATING RADAR

E.1. INTRODUCTION AND PRINCIPLES OF GROUND PENETRATING RADAR (GPR)

Ground Penetrating Radar or GPR is a geophysical device used for shallow subsurface investigation and has been shown by Smith and Jol, (1995) and during this study to be an extremely useful technique to detect fault zones.

It records variations of the bulk electrical properties of subsurface lithologies enabling inferences of the subsurface stratigraphy to be made (Smith and Jol, 1995). This tool is primarily a shallow subsurface apparatus and can penetrate to a depth of 20m depending on the frequency of the signal, the type of lithology present and the required resolution of the profiles (Nobes, 1996). The GPR uses two antennas set a distance apart (1m apart in this study to enable more dense data collection). The first antenna sends an electromagnetic pulse or signal into the ground described as a propagating wave-front by Smith and Jol, (1995). The dielectric differences that exist within the various subsurface lithologies and structure i.e. clay, rock or water content, results in the changes in velocity and amount of energy or signal reflected back to the surface detected by the receiver antenna (Smith and Jol, 1995). The resulting series of reflections or EM echoes is then combined and represented by a wiggle plot or profile of a series of negative and positive signal returns, where shaded signals reflect positive echoes and unshaded reflect negative echoes (Howard, 2001). Water for example causes a decrease in velocity resulting in an unshaded negative echo or signal (Nobes et al 2001). The depth of a reflection is calculated by the time taken for the pulse to be reflected from the transmitting antenna to the receiving antenna called a two-way travel time.

Resolution of the GPR is dependent on the frequency of the signal, the required depth of penetration and the geological conditions present (Nobes 1996). High frequency signals

results in poor penetration but good resolution while low frequency signals shows good penetration and poor resolution. The quality of the signal is also influenced by the properties within the subsurface particularly by water quality, water quantity which can cause a negative echo or decrease in velocity. Clay content will also increase signal attenuation resulting in reduced signal depth penetration while scattering of the signal will occur in gravels using higher frequency (Nobes et al. 2001). The ideal geologic conditions for good signal response are dry or unsaturated material (Nobes et al. 2001). If pore-water is present then this should ideally be fresh-water (Nobes et al. 2001)

An important factor when interpreting the profile or wiggle traces is that they do not supply bed by bed stratigraphy, rather it shows the contrast in physical properties typically at a subsurface lithological boundary (Nobes et al. 2001). Nobes goes on to state that interpreting the displayed data therefore requires a systematic method of interpretation to avoid misleading interpretations and expectations (Nobes et al. 2001).

Interference of the signal may occur were EM pulses rebound against large surface objects such as trees, buildings, fences, or overheads wires (Howard, 2001). This may form an anomaly recorded in the profile as a series of diffractions concealing the underlying stratigraphy (Howard, 2001). No problem of this nature was encountered in the flat-lying grasslands of the fault zone during this study (see below).

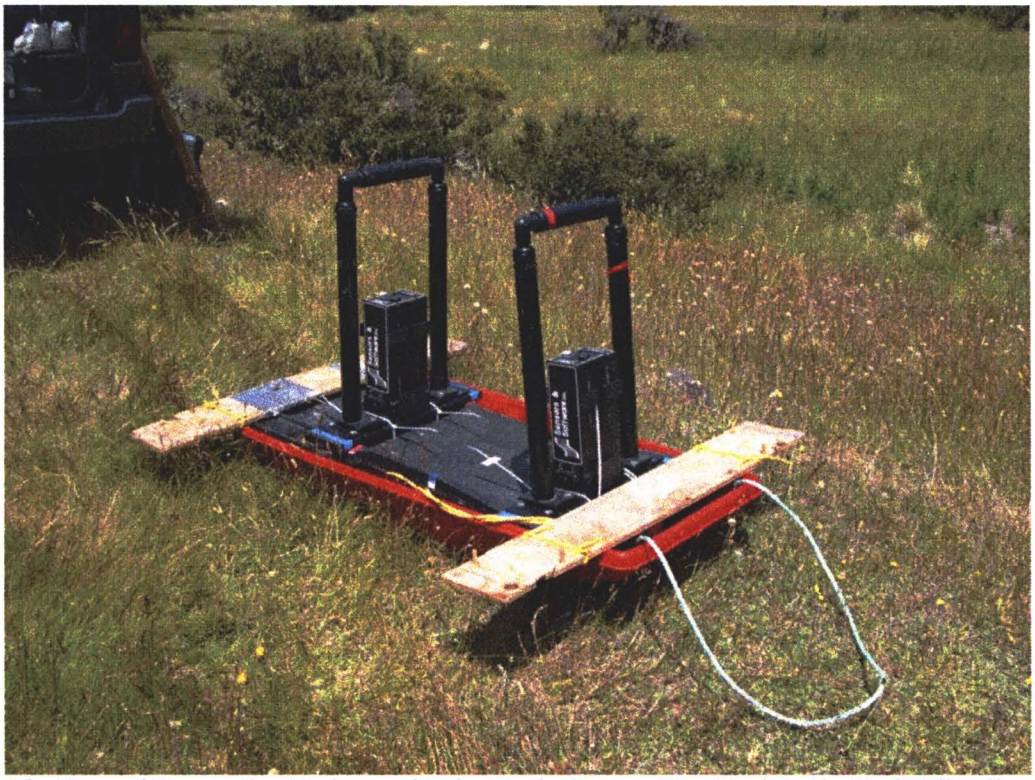

The Ground Penetrating Radar used to locate the Porters Pass Fault in the Red Hill valley

Photograph of the traverse taken for the GPR profile one survey heading south toward the raised expression of the Porters Pass Fault.

E.2. THE LOCATION OF THE PORTERS PASS FAULT WITHIN THE RED HILL VALLEY

Initially a brief site investigation was conducted using an electromagnetic survey to identify any anomalies thought to relate to the fault zone. These were marked and aided in the positioning of the traverses for the following GPR investigations

Two parallel 100m traverses using the GPR were undertaken separated by 10metres across an area of sedimentation thought to co-date or post-date faulting and perpendicular to the position of a raised expression interpreted to represent the Porters Pass Fault

The transmitter and receiver antenna were pulled on a sled across the marked traverse line of 100m as seen above. Packets of data were recorded at ten metre intervals over the 100 metre traverse. The antenna frequency was 200 MHz with an antenna spacing of 1m and a step size of 0.25metres. This was considered to show good resolution while maintaining the reasonable depth penetration.

DATA COLLECTION AND PRESENTATION

The software package used for the survey and processing of the data was PulseEKKO42. During processing each survey line was converted into a RUB file which stretches the data (f1-f10) into a single profile to match the distance of the runs as seen in the Table immediately below.

Traces	Distance (m)
f1	0.000
f2	10.000
f3	20.000
f4	30.000
f5	40.000
f6	50.000
f7	60.000
f8	70.000
f9	80.000
f10	90.000
f11	100.00

The resulting profiles were presented as flat-lying or horizontal in the RUB file format and needed to be adjusted for the topography over which the survey was conducted. The topographic data was obtained during this study by surveying the traverses using an EDM and prism. The data was then combined with the GPR profile data in RUB file format (as described above) then converted to "TOPO" files and corrected. Once corrected the dip and behaviour of the layers can be more correctly interpreted (see below).

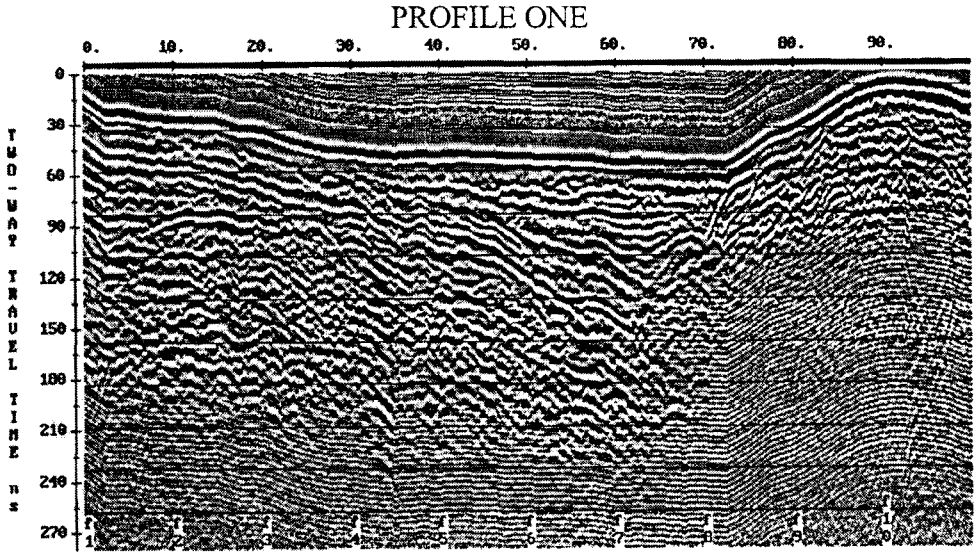

Profiles one and two corrected for topography but unfiltered for noise distortions
(Vertical exaggeration of 5m vertical: 1m horizontal)

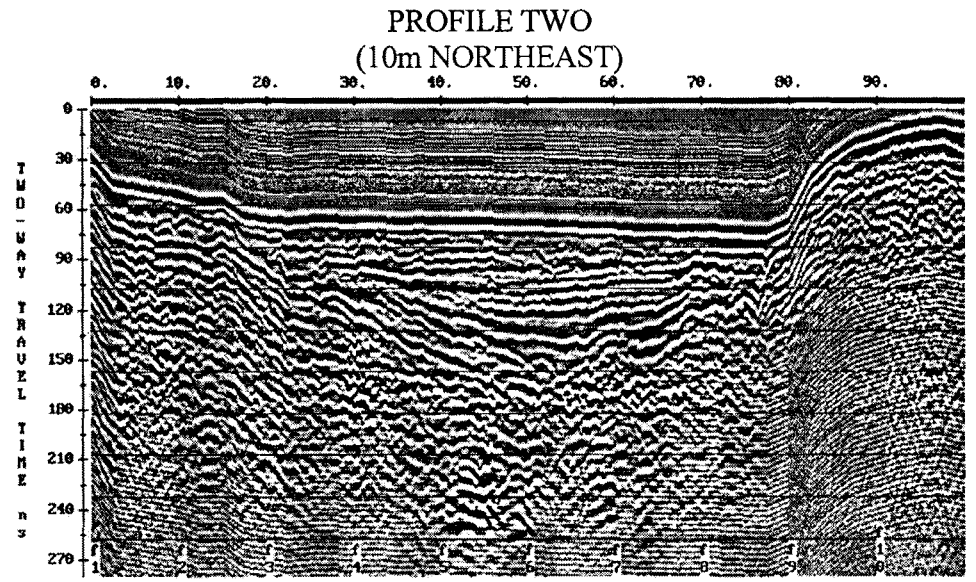

The plots as shown above have been corrected for topography but display unwanted frequency noise. The profiles were then processed using a "dewow" filter to remove the noise and migrated to focus and move reflected pulses to their correct positions while removing any diffractions. The resulting processed profiles can be viewed in Chapter 5 Fig. 5.6 and Fig. 5.7 and provided key information on the subsurface used to select the site for trenching. The position of the traverses in the field area can be seen in Chapter 5 Fig. 5.4.

APPENDIX F

SEDIMENTARY ANALYSIS OF UNIT 2 IN TRENCH

(Refer to the Trench Log Chapter Five, Figure 5.9 for sample stratigraphic positions)

F.1: GRAIN SIZE DISTRIBUTION CURVES

F.2. ATTERBURG LIMITS

F.3. X-RAY DIFFRACTION ANALYSIS

APPENDIX F.1 GRAINSIZE DISTRIBUTION

F.1: GRAIN SIZE DISTRIBUTION CURVES

SAMPLE CODE	DEPTH BELOW DATUM LINE 0m	
A) T-25cm	T-25cm	(Distance along trench 19m)
B) T-46cm	T-46cm	(Distance along trench 19m)
C) T- B2 65cm	T-65cm	(Distance along trench 19m)
D) T-B1 87cm	T-87cm	(Distance along trench 19m)

SAMPLE CODE	AUGUR DEPTH (metres)	
E) PAH 65-75cm	65-75cm	(Ephemeral Pond 150m north of Trench)

A).

GRAIN SIZE DISTRIBUTION CURVE FOR SAMPLE T-25cm

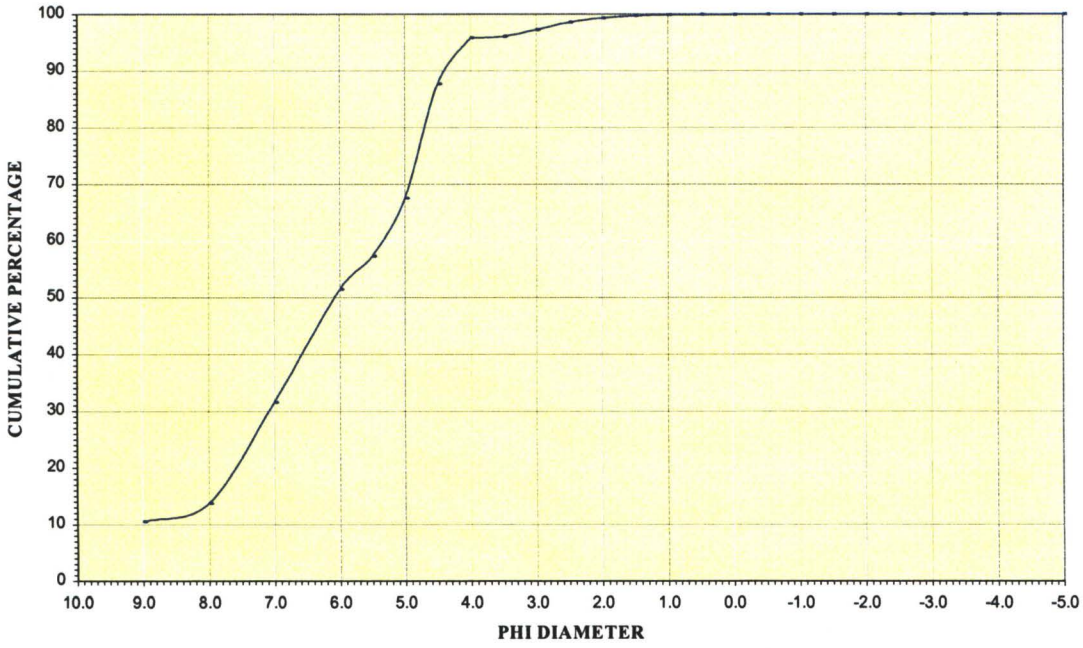

SAMPLE COMPOSITION

		Gravel	Sand	Silt	Clay	Total
8 phi:	g	0.000	0.716	14.050	2.350	17.116
Sed.	%	0.00	4.18	82.09	13.73	100.00
9 phi:	g	0.000	0.716	14.600	1.800	17.116
Eng.	%	0.00	4.18	85.30	10.52	100.00

B).

GRAIN SIZE DISTRIBUTION CURVE FOR SAMPLE T-46cm

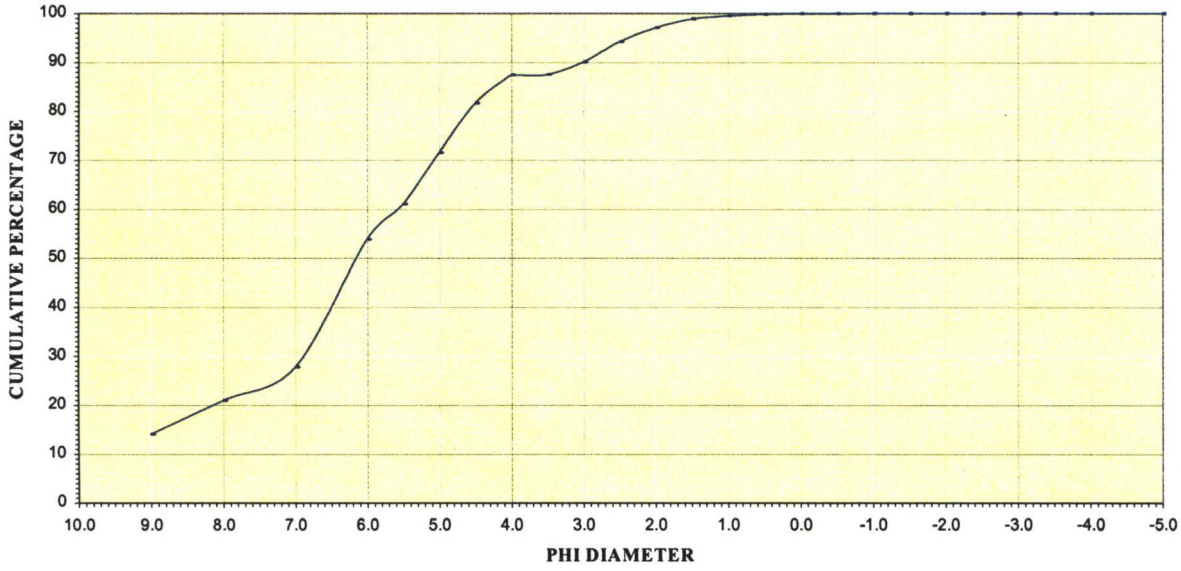

SAMPLE COMPOSITION

		Gravel	Sand	Silt	Clay	Total
8 phi:	g	0.000	1.739	9.200	2.900	13.839
Sed.	%	0.00	12.57	66.48	20.96	100.00
9 phi:	g	0.000	1.739	10.150	1.950	13.839
Eng.	%	0.00	12.57	73.34	14.09	100.00

C).

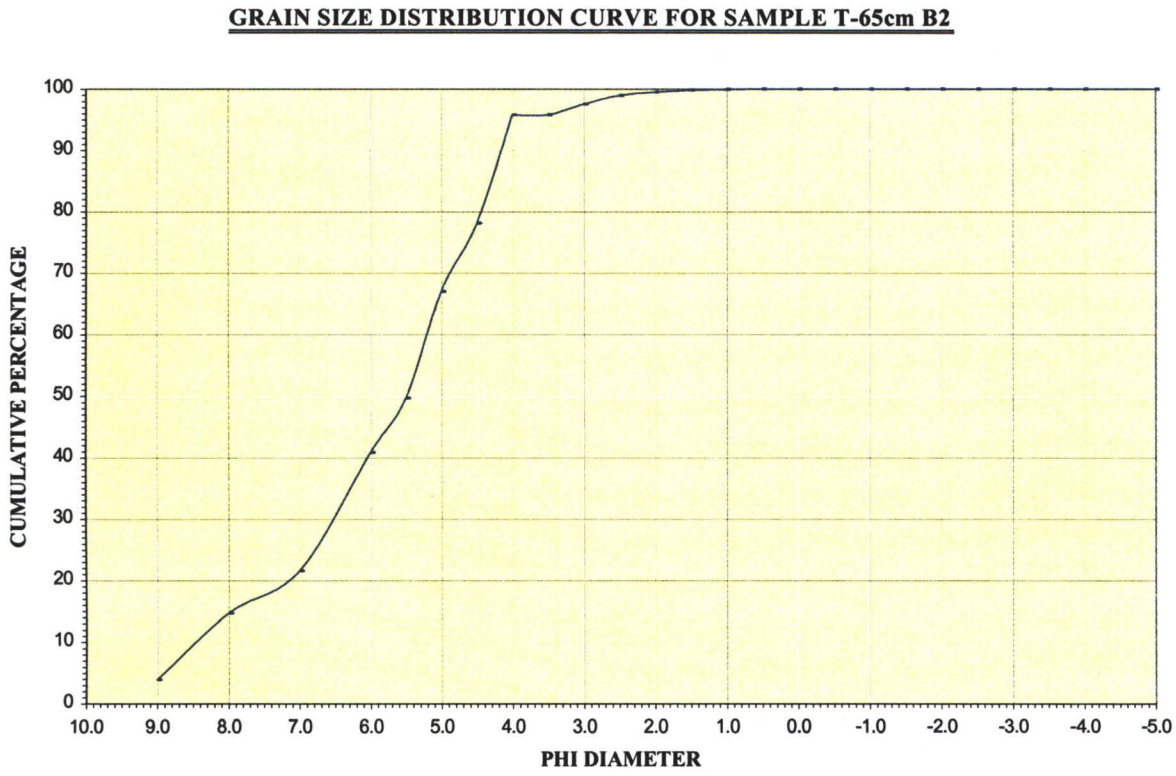

SAMPLE COMPOSITION

		Gravel	Sand	Silt	Clay	Total
8 phi:	g	0.000	0.644	12.400	2.250	15.294
Sed.	%	0.00	4.21	81.08	14.71	100.00
9 phi:	g	0.000	0.644	14.050	0.600	15.294
Eng.	%	0.00	4.21	91.87	3.92	100.00

D).

GRAIN SIZE DISTRIBUTION CURVE FOR SAMPLE T-87cm B1

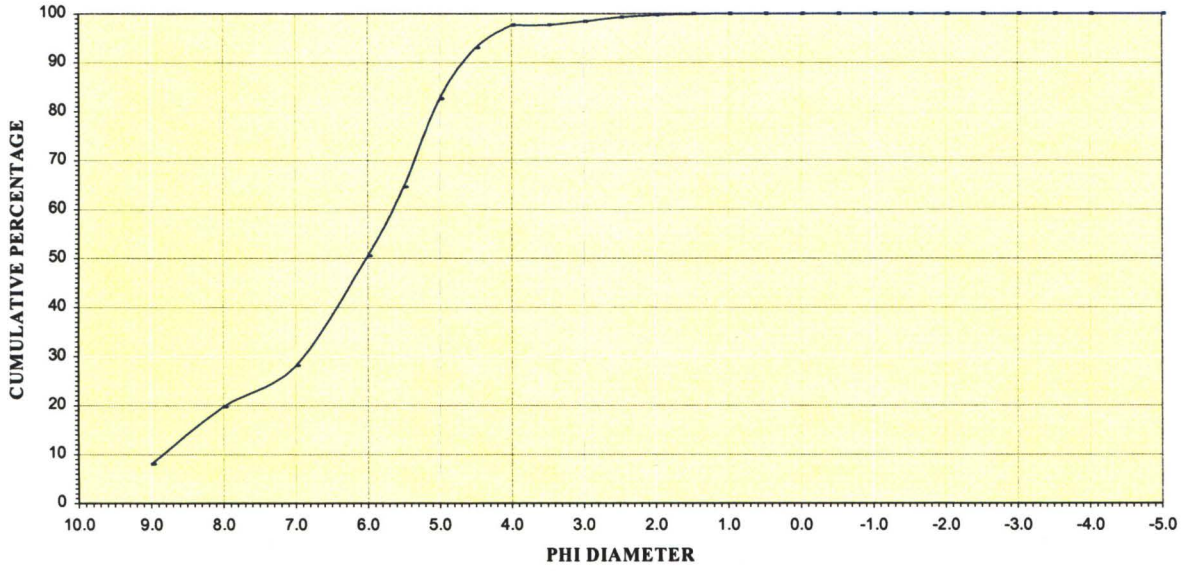

SAMPLE COMPOSITION

		Gravel	Sand	Silt	Clay	Total
8 phi:	g	0.000	0.350	11.650	2.950	14.950
Sed.	%	0.00	2.34	77.93	19.73	100.00
9 phi:	g	0.000	0.350	13.400	1.200	14.950
Eng.	%	0.00	2.34	89.63	8.03	100.00

E).

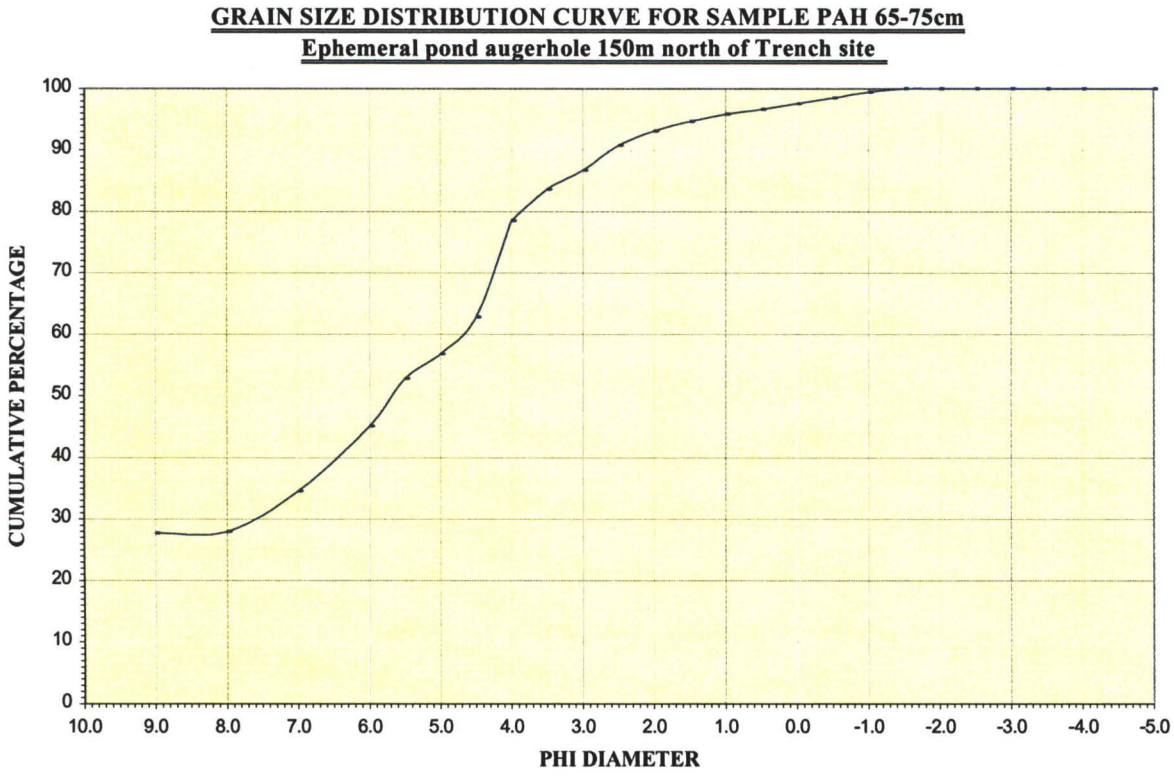

SAMPLE COMPOSITION

		Gravel	Sand	Silt	Clay	Total
8 phi:	g	0.100	3.666	8.850	4.900	17.516
Sed.	%	0.57	20.93	50.53	27.97	100.00
9 phi:	g	0.100	3.666	8.900	4.850	17.516
Eng.	%	0.57	20.93	50.81	27.69	100.00

F.2. ATTERBURG LIMITS

APPENDIX F.2 ATTERBURG LIMITS

Determination of Liquid and Plastic Limits, the Plastic Index and Water Content

		SAMPLES		METHODS:
	In Trench	T-25cm	Dist 19m	Casagrande
	(Depth below	T-46cm	Dist 19m	Worm Test
	datum 0m)	T-65cm	Dist 19m	Moisture Content
	Ephemeral Pond	Augerhole 2-Pond 65-75cm	150m north of trench	
In Trench	T-25cm	Min	Average	Max
	Water Content	65.90%	68.90%	71.80%
	Liquid Limit	65	65	65
	Plastic Limit	47.8	48.1	48.4
	Plastic Index	17.2	17	16.6
	DESCRIPTION:	Plastic	Silt	
In Trench	T-46cm	Min	Average	Max
	Water Content	77.30%	78.30%	79.50%
	Liquid Limit	78.7	78.7	78.7
	Plastic Limit	56.3	57.16	58
	Plastic Index	22.4	21.5	20.7
	DESCRIPTION:	Plastic	Silt	
In Trench	T-65cm	Min	Average	Max
	Water Content	68.90%	69.64%	70.30%
	Liquid Limit	70	70	70
	Plastic Limit	46.2	47.1	47.9
	Plastic Index	23.8	22.9	22.1
	DESCRIPTION:	Plastic	Silt	
Ephemeral Pond	Auger 65-75cm	Min	Average	Max
	Water Content	64.70%	68.90%	74.20%
	Liquid Limit	65	65	65
	Plastic Limit	41.2	41.7	42
	Plastic Index	23.8	23.3	23.8
	DESCRIPTION:	Plastic	Silt	

A) T-25cm		T-25cm	(Distance along trench 19m)
B) T-46cm		T-46cm	(Distance along trench 19m)
C) T- B2 65cm		T-65cm	(Distance along trench 19m)
D) PAH 65-75cm	65-75cm		(Ephemeral Pond 150m north of trench)

F.3. X-RAY DIFFRACTION ANALYSIS

SUMMARY RESULTS TABLE - A, B, C

SUMMARY RESULTS TABLE - D, E, F

RESULTS DIAGRAMS

SAMPLE CODE		DEPTH BELOW DATUM LINE 0m	
A) T Banded U	Clayey Silt	T-25cm	(Distance 19m)
B) TSHU (Wk 13033)	Buried Soil 2A	T-10cm	(Distance 17.5m)
C) TMI	Clayey Silt	T-46cm	(Distance 19m)
D) TSHcL	Buried Soil 2B	T-56cm	(Distance 19m)
E) TB2	Clayey Silt	T-65cm	(Distance 19m)
F) TBI	Clayey Silt	T-87cm	(Distance 19m)

APPENDIX F.3 X-RAY DIFFRACTION RESULTS

SUMMARY TABLE OF ESTIMATES FOR X-RAY DIFFRACTION ANALYSIS A, B, C

Name: Guyon Smith A). 25cm DEPTH BELOW DATUM
Sample: T Banded U 19m DISTANCE ALONG TRENCH

The crystalline material present in this sample has been identified as:

Component	Colour on scan	Percentage*
Quartz	blue	70
Albite	green	25
Kaolinite	yellow	5
Muscovite	red	trace

*Estimate only.

Name: Guyon Smith B). Wk 13033 10cm DEPTH BELOW DATUM
Sample: TSHU 17.5m DISTANCE ALONG TRENCH

The crystalline material present in this sample has been identified as:

Component	Colour on scan	Percentage*
Quartz	blue	65
Albite	green	30
Kaolinite	yellow	5

*Estimate only.

Name: Guyon Smith C). 46cm DEPTH BELOW DATUM
Sample: TM1 19m DISTANCE ALONG TRENCH

The crystalline material present in this sample has been identified as:

Component	Colour on scan	Percentage*
Quartz	blue	75
Albite	green	20
Kaolinite	yellow	5

*Estimate only.

SUMMARY TABLE OF ESTIMATES FOR X-RAY DIFFRACTION ANALYSIS D, E, F

Name: Guyon Smith

Sample: TSHcL D). 56cm DEPTH BELOW DATUM
19m DISTANCE ALONG TRENCH

The crystalline material present in this sample has been identified as:

Component	Colour on scan	Percentage*
Quartz	blue	65
Albite	green	30
Kaolinite	yellow	5

*Estimate only.

Name: Guyon Smith

Sample: TB2 E). 65cm DEPTH BELOW DATUM
19m DISTANCE ALONG TRENCH

The crystalline material present in this sample has been identified as:

Component	Colour on scan	Percentage*
Quartz	blue	65
Albite	green	30
Kaolinite	yellow	5

*Estimate only.

Name: Guyon Smith

Sample: TB1 F). 87cm DEPTH BELOW DATUM
19m DISTANCE ALONG TRENCH

The crystalline material present in this sample has been identified as:

Component	Colour on scan	Percentage*
Quartz	blue	60
Albite	green	35
Kaolinite	yellow	5
Muscovite	red	trace

*Estimate only.

Sampled at Depth Below Datum Line 0m at Distance of 19 m Along Trench Unless Otherwise Stipulated. (Refer to Chapter 5 Figure 5.9 for stratigraphic position of samples).

A. DEPTH 25cm BELOW DATUM - DISTANCE 19 m

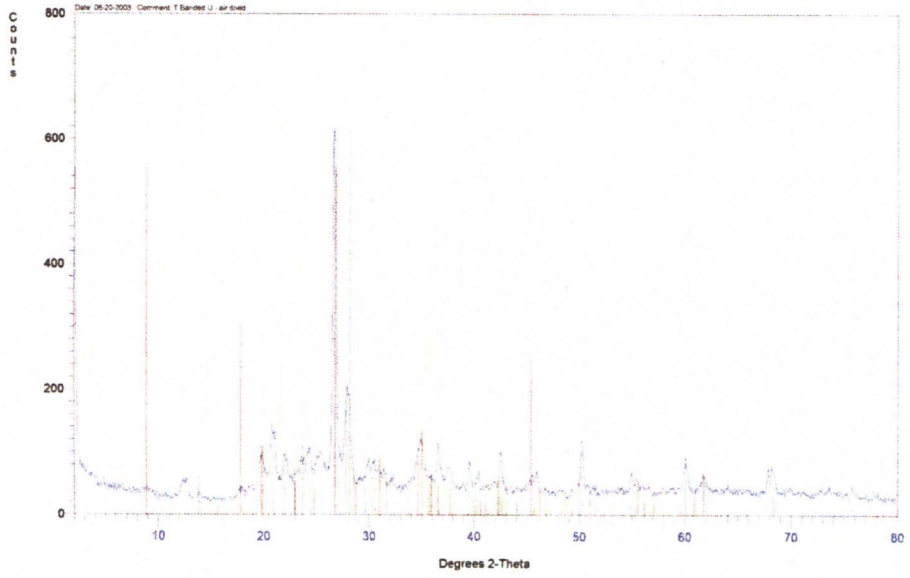

B. BURIED SOIL 2B - DEPTH 10 cm (SAMPLE Wk 13033) DISTANCE 17.5m

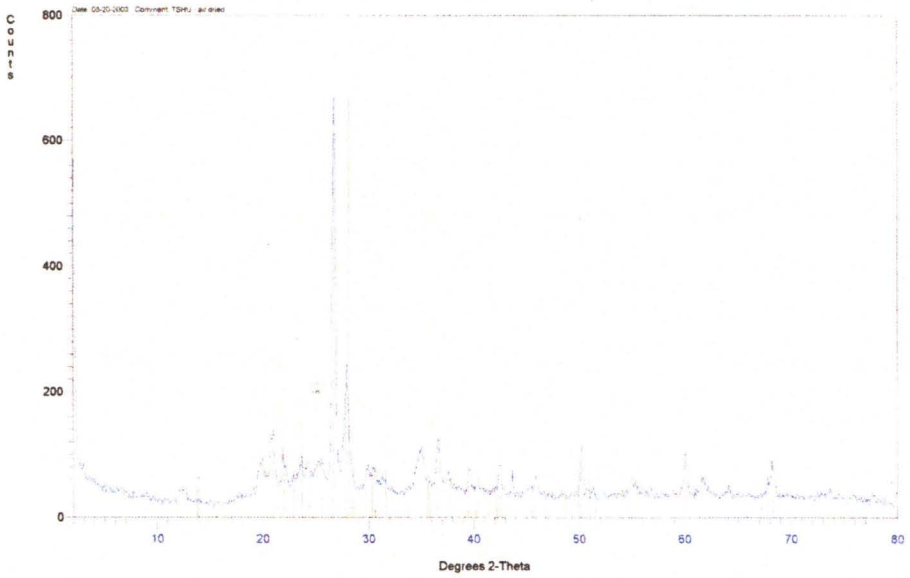

Sampled at Depth Below Datum Line 0m at Distance of 19 m Along Trench Unless Otherwise Stipulated. (Refer to Chapter 5 Figure 5.9 for stratigraphic position of samples).

C. DEPTH 46cm BELOW DATUM - DISTANCE 19 m

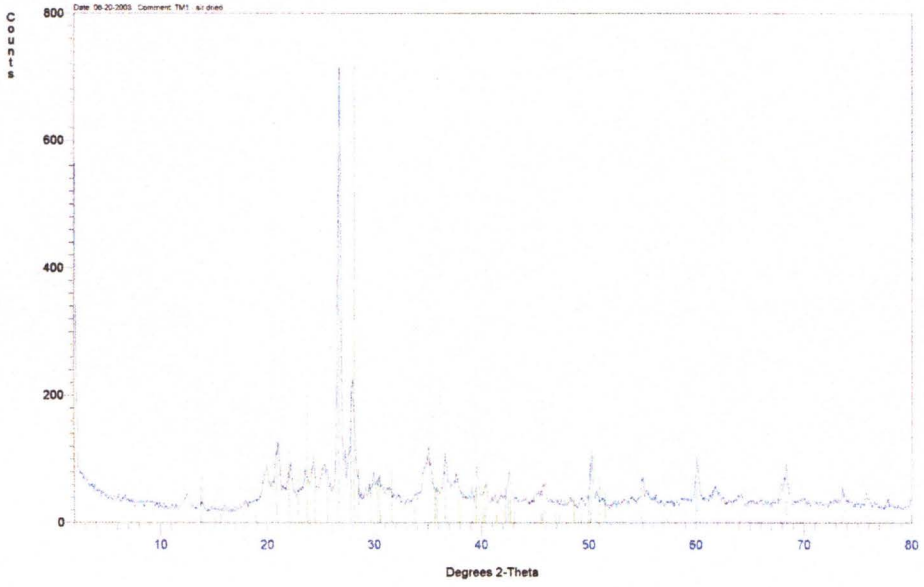

D. BURIED SOIL 2A
DEPTH 56cm BELOW DATUM - DISTANCE 19 m

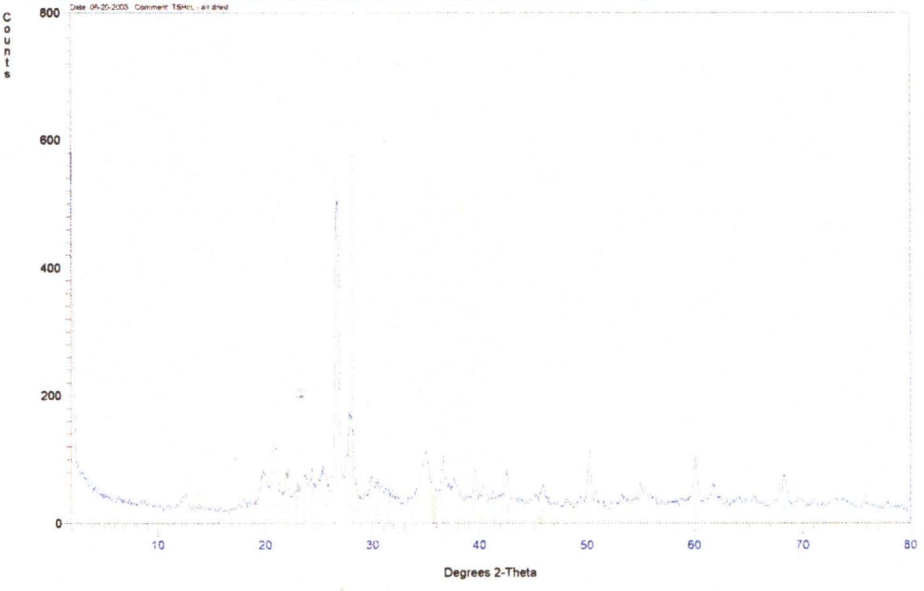

Sampled at Depth Below Datum Line 0m at Distance of 19 m Along Trench Unless Otherwise Stipulated. (Refer to Chapter 5 Figure 5.9 for stratigraphic position of samples).

E. DEPTH 65cm BELOW DATUM - DISTANCE 19 m

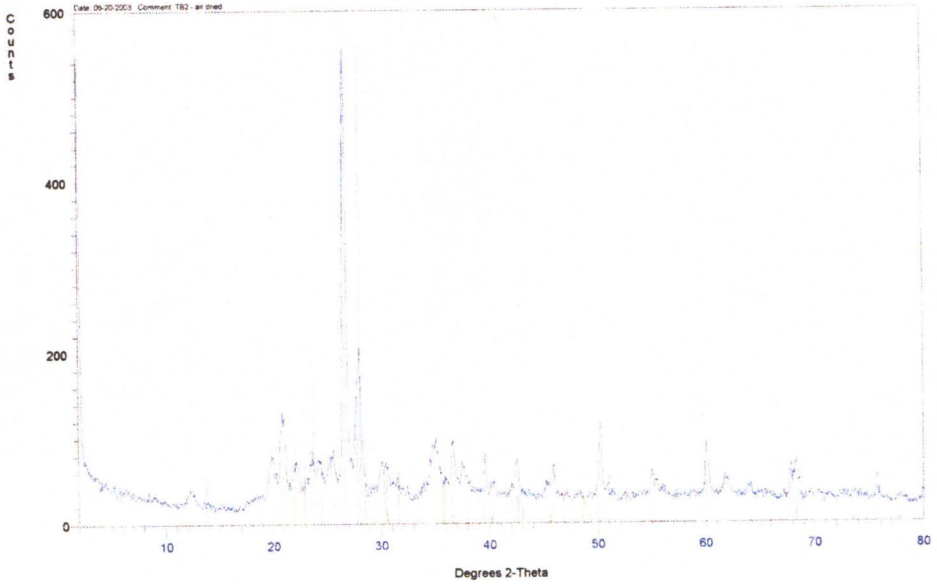

F. DEPTH 87cm BELOW DATUM - DISTANCE 19 m